A STUDY OF SECONDARY SUSPENSIONS AND HUMAN DRIVER RESPONSE TO WHOLE-BODY VEHICULAR VIBRATION AND SHOCK

Paul-Emile Boileau

A Thesis

in

The Department

of

Mechanical Engineering

Presented in Partial Fulfillment of the Requirements
for the Degree of Doctor of Philosophy at
Concordia University
Montreal, Quebec, Canada

March 1995

ISBN 0-612-01280-8

Canada

ABSTRACT

A Study of Secondary Suspensions and Human Driver Response to Whole-Body Vehicular Vibration and Shock

Paul-Emile Boileau, Ph.D.
Concordia University, 1995

Prolonged exposure to whole-body vehicular vibration and shock is known to contribute significantly to the degradation of health and comfort of seated drivers. Off-road vehicle drivers are considered particularly at risk in view of the severe nature of the vibration environment caused by the vehicle-terrain interactions. The effectiveness of secondary vehicle suspensions in reducing the vibration exposure levels is investigated through development and analyses of suspension seat and suspended cab models. The analytical models are validated through extensive laboratory tests of an off-road vehicle suspension seat and of a prototype suspended cab. A comprehensive whole-body vehicular vibration simulator (WBVVS) is developed to study the suspension seat and human driver response characteristics under deterministic and random vibration, and shocks. A methodology is developed for computing the shock response characteristics of a suspension seat, with and without travel limiting bump stop impacts.

A four-degree-of-freedom linear biodynamic model of the seated driver is developed to account for the influence of human body dynamics on the suspension seat vibration attenuation performance. The model parameters

for a seated driver maintaining a well defined posture are identified from measurements of the driving-point mechanical impedance and idealized values of seat-to-head transmissibility magnitude and phase characteristics, using optimization techniques. The biodynamic response characteristics are shown to be highly affected by the seated posture and the nature of the vibration excitation. The combined suspension seat-human driver model developed in this study correlates better with the measured response characteristics than the suspension seat model defined with a rigid driver mass representation.

Seat and cab suspension design guidelines are defined to minimize the vibration exposure levels of off-road vehicle drivers under different types of excitations. This is performed upon integrating the various proposed whole-body vibration and shock exposure assessment methods and health criteria into the response computations using the validated models. The vibration exposure levels differ considerably under random and shock excitations, particularly when bump stop interactions occur. Effective design and tuning of the secondary suspension systems can provide a significant reduction in vibration exposure levels. The design guidelines of such systems, however, must provide a distinction between the conditions involving high level shocks and those with low level shocks or continuous excitations.

ACKNOWLEDGEMENTS

I would like to express my sincere gratitude to my thesis supervisor, Dr. Subhash Rakheja, for his constant guidance and dedication throughout the realization of this work. I am also indebted to my employer, the *Institut de recherche en santé et en sécurité du travail (IRSST)*, who made it possible for me to conduct this research.

This work would not have been possible without the participation of many individuals at various stages of the research. I would like to acknowledge the support provided by Dale Rathwell, Danius Juras and John Feng in the realization of the experimental set-ups. The help provided by Mr. Liu Peijun and Mr. Cherian Thomas with the analytical modeling aspects, and by Dr. Raghu Gurram with the section dealing with biodynamics is gratefully appreciated. The constant and reliable support provided by Mr. Ajai Singh and Mr. Parmjit Kanth in manipulating large quantities of data and in performing their graphical presentation is gratefully acknowledged. Finally, my appreciation is extended to all the test subjects who voluntarily accepted to participate in the experiments.

This thesis would not have existed without the motivation and understanding of Carole and my daughter, Ève-Marie. I dedicate this thesis to them.

TABLE OF CONTENTS

CHAPTER 3
SUSPENSION SEAT: MODEL DEVELOPMENT, VALIDATION AND RESPONSE ANALYSES

CHAPTER 4
SUSPENSION SEAT RESPONSE ANALYSES UNDER SHOCK EXCITATIONS

CHAPTER 5
WHOLE-BODY BIODYNAMICS: A SYNTHESIS OF THE PUBLISHED DATA

CHAPTER 6
BIODYNAMIC MODEL DEVELOPMENT FOR OFF-ROAD VEHICLE DRIVERS

CHAPTER 7
VALIDATION AND RESPONSE ANALYSIS OF THE COMBINED SUSPENSION SEAT-HUMAN DRIVER MODEL

CHAPTER 8
CAB SUSPENSION ANALYSIS

CHAPTER 9
CONCLUSIONS AND RECOMMENDATIONS FOR FUTURE WORK

LIST OF FIGURES

LIST OF TABLES

LIST OF ABBREVIATIONS AND SYMBOLS

ABBREVIATIONS

c.g.	Centre of gravity
dc	Direct current
DADisp	Data Acquisition and Display
dB	Decibel
D/A	Digital to Analog
DIS	Draft International Standard
DOF	Degree-of-freedom
DRI	Dynamic Response Index
EBS	Erect back supported
ENS	Erect back not supported
FDP	Fatigue-decreased-proficiency
FFT	Fast Fourier Transform
HP	High-pass
ISO	International Standards Organization
LP	Low-pass
LVDT	Linear variable differential transformer
PSD	Power spectral density
rmq	root-mean-quad
rms	root-mean-square

S.E.A.T.	Seat Effective Amplitude Transmissibility
SDOF	Single-degree-of-freedom
SLO	Slouched
VDV	Vibration Dose Value
VRR	Vibration Ride Ratio
VRQI	Vibration Ride Quality Index
WBV	Whole-Body Vibration
WBVVS	Whole-Body Vehicular Vibration Simulator

SYMBOLS

a_i	Longitudinal distance from c.g. (m)
a_w	Frequency-weighted acceleration (ms^{-2})
a_{rmq}	Root-mean-quad acceleration (ms^{-2})
α	Angle of inclination (rad)
α_i	Weighting factor
b, b_i	Longitudinal distance from c.g. (m)
B	Frequency bandwidth (Hz)
β	Half the suspension travel (m)
c_i, C_i	Damping coefficient (Ns/m)
χ	Vector of model parameters
D	Width (m)
d, d_i	Longitudinal distance (m)

δ	Static deflection (m)
f	Frequency (Hz)
f_c	Crest factor
F	Force (N)
F_c	Cushion force (N)
F_C	Static friction force (N)
F_D, F_{di}	Damping force (N)
F_F	Coulomb friction force (N)
F_K, F_{Ki}	Restoring force (N)
F_{Oi}, p	Excitation force (N)
F_S	Bump stop restoring force (N)
F_{Tr}, F_{Tf}	Tire forces (N)
ϕ	Roll coordinate
ϕ_i	Phase angle (rad)
g	Acceleration due to gravity (ms^{-2})
G_{ii}	Auto-spectral density
G_{ij}	Cross-spectral density
h_i	Height (m)
H, h_{ij}	Frequency response or transfer function
I	Mass moment of inertia (kg m^2)
k_i, K_i	Stiffness coefficient (N/m)
ℓ	Longitudinal distance (m)

L	Wheelbase (m)
λ_i	Weighting factor
m, m_i, M	Mass (kg)
q	Response coordinate in time domain (m)
Q	Response coordinate in frequency domain (m)
Q_i	Quality factor
q_0	Excitation coordinate in time domain (m)
Q_0, P	Excitation coordinate in frequency domain (m)
θ	Pitch coordinate
s	Laplace Transform variable
S	Response Power Spectral Density
S_0	Excitation Power Spectral Density
t	Time (s)
T	Exposure duration (s)
$T(f)$	Transmissibility function
τ, τ_i	Period (s)
U, U_i	Objective function
V	Speed (m/s)
V_i	Transition velocity (m/s)
V_{ii}	Relative velocity (m/s)
w	Longitudinal distance (m)
W_d	Damping energy (J)

W_i	Weighting factor
W_k	Weighting filter
W_p	Processed energy (J)
W_z	Weighting filter
ω, ω_i	Angular frequency (rad/s)
x-	Longitudinal coordinate (fore-aft)
x_i	Relative displacement (m)
X_i	Displacement amplitude (m)
y-	Lateral coordinate
ψ_i	Phase angle (rad)
z-	Vertical coordinate
z_p	Peak vertical displacement (m)
z, z_i	Vertical displacement (m)
Z	Mechanical impedance (Ns/m)
ζ, ζ_i	Damping ratio

CHAPTER 1

INTRODUCTION AND SCOPE OF RESEARCH

Vehicle drivers are exposed to whole-body mechanical random and transient vibration arising primarily from the tire-terrain interactions. Exposure to such vehicular vibration is known to interfere with the driver's comfort and health. Whole-body vibration (WBV) exposure thus constitutes a physical stressor causing a complex distribution of oscillatory motions and forces within the body at frequencies below 80 Hz. Although motion sickness may constitute the most immediate direct effect of low frequency vibration in the 0.1 to 0.5 Hz frequency range, many chronic health effects have been associated with prolonged exposure to vibration in the range 1.0 to 80 Hz. These include disorders of the spine, of the nervous and of the circulatory systems, abdominal pain, digestive and vision problems, etc. [1,2].

Occupational exposure to whole-body vibration occurs widely in several transportation sectors, including road, off-road, rail and marine transport systems. Of particular concern are operators of off-road vehicles, such as agricultural tractors, forestry vehicles, earth moving vehicles, industrial tractors, scrapers, excavators, etc., who are constantly exposed to severe vibration and shock levels caused by the vehicle motion over rough terrains. Table 1.1 presents the relative importance of vibration levels reported at the seat-person

interface on off-road and other industrial vehicles along the vertical (z-axis) direction [3]. The range and mean values of frequency-weighted root-mean-square (rms) acceleration, a_w, representing whole-body vibration exposure in different vehicles are reported. The wide spread of reported values, observed particularly for off-road vehicles, provides an indication of the large variability which could be expected owing to the various vehicle characteristics, driving and seating conditions, and terrain profiles.

In view of the health and safety hazards posed by the low frequency ride vibration and shocks of vehicles, there has been an increased concern towards ride quality improvement via control of terrain-induced vibration. Primary and secondary suspension systems have been developed for heavy highway vehicles [4,5]. However, design of effective suspension systems to improve the off-road vehicle's ride quality has been the focus of only a limited number of studies. Moreover, these studies have very seldom considered the behaviour of suspension systems under the influence of shocks. In addition, the design criteria established for these suspensions have often overlooked the dynamics of the human body and the various assessment methods defined to characterize the driver's exposure levels when subjected to shock and vibration.

TABLE 1.1

Vertical Weighted Acceleration Levels Associated with Different Vehicles [3].

VEHICLES	Range of Weighted Acceleration a_w (ms^{-2})	Mean Weighted Acceleration a_w (ms^{-2})
OFF-ROAD VEHICLES		
Graders	0.3 - 1.6	0.65
Road Rollers	0.4 - 1.4	0.70
Dumpers	0.4 - 2.25	1.1
Scrapers	0.8 - 2.75	1.5
Wheel Loaders	0.4 - 2.25	1.1
Bulldozers	0.35 - 2.0	0.7
Excavators	0.2 - 1.9	0.55
Agricultural/Forestry Tractors	0.15 - 1.9	0.75
INDUSTRIAL VEHICLES		
Forklift Trucks	0.4 - 2.8	1.05
Trucks	0.4 - 1.15	0.60
Vans	0.35 - 0.8	0.60
Articulated Trucks	0.45 - 1.1	0.65
Locomotives	0.2 - 0.5	0.30

1.1 Effects of Vehicle Vibration

From the current state of knowledge, whole-body vibration exposure is known to be associated with the following effects [6]:

- Reduced comfort;
- Degraded health;
- Motion sickness.

The importance of vehicular vibration and shock on the driver's health and comfort, however, is influenced by several variables, such as posture, seated height, and placement of the controls [7,8]. The relationship between the driver's station design and the vibration effects is extremely complex and virtually not defined due to lack of knowledge on human response to shock and vibration. Furthermore, the variations in one of these variables to mitigate one effect might, at the same time, aggravate one or more of the other possible effects. Vibration effects constitute a complex phenomenon implying the interaction of several variables. Moreover, the vibration characteristics (frequency, magnitude, direction of application) represent additional variables presenting some degree of variation on the possible effects.

Vibration discomfort assessment is primarily based on laboratory evaluations of subjects' judgment when exposed to various vibration stimuli. Equivalent

comfort contours express the vibration magnitudes required to produce equivalent discomfort for each vibration frequency, axis and input position [9,10]. Although generally agreed that discomfort increases with vibration magnitude [11], the large variations in the experimental conditions, postures, feet support, subject population and analytical methods used in the experiments could explain the large variation in contours reported by various investigators. As for time dependency of vibration on comfort, the current state of knowledge does not support a well established relation between comfort rating and exposure duration [12].

Chronic health effects of whole-body vibration are estimated primarily from surveys of populations exposed to vibration during their work, although no dose-effect relationship is known to exist. Despite the fact that many confounding factors exist, the disorders most often reported are, in order of importance: back problems, digestive and reproductive system disorders and nervous system disorders [2]. Of these, low back pain has been the most widely investigated in an attempt to derive its relationship with whole-body vibration exposure [13]. However to date, it can only be concluded that driving is related to an excess risk of low back pain and that vehicular vibration and shock could be considered under strong suspicion. Evidences on the possible impact of shock and vibration are believed to outweigh the weak evidence of low back pain being possibly caused by prolonged sitting. The

uncertainty associated with the injury mechanism of low back pain or other health disorders believed to be caused by prolonged exposure to WBV makes it difficult to identify the most important vibration exposure characteristics amongst acceleration level, frequency, exposure duration, peak values and shocks which could account for the effects.

Exposure to low frequency vibration in the 0.1 to 0.5 Hz frequency range has been identified as one possible cause of motion sickness, characterized by breathing irregularities, sensation of warmth, palor, nausea and vomiting. The action of vibration on the vestibular system located within the inner ear and also on the visual system could explain this effect [14]. The current state of knowledge indicates that the probability of vomiting could increase with increasing vibration magnitude and exposure duration.

1.1.1 EPIDEMIOLOGY

Surveys of populations exposed to vibration compared with non-exposed control groups offer the possibility of estimating long-term effects of WBV exposure. Although these studies indicate an increased health risk of the spine and of the peripheral nervous system after intense long-term WBV exposure, the methodology used in attaining these results has often been criticized [15,16]. Questions on the adequacy of the control groups and of the type of questionnaire used in registering the symptoms associated with WBV exposure,

the presence of confounding factors and the lack of information on vibration exposure data have prevented the development of a clear dose-effect relationship.

From the earlier work by Rosegger and Rosegger [17] on a population of 328 professional tractor drivers, to the review of more than 78 published papers, involving a total population of over 40 000 workers, performed by Seidel and Heide [2], it may be concluded that on average, health risks increase with higher intensity or duration of vibration exposure. Well-defined exposure-effect relationships, however, cannot easily be detected in many of these studies. Seidel and Heide [2] suggest that exposure to whole-body vibration near or beyond the 4 to 8 hours "exposure limit", as defined in the current ISO 2631/1 standard [18], involves a greater health risk and, in that respect, should in no case be exceeded at workplaces.

1.1.2 BIODYNAMIC RESPONSE OF THE HUMAN BODY

In the search for explaining the damage mechanisms associated with WBV exposure, studies related to the biodynamic response of the human body have concentrated mostly on the spinal column. Ideally, these studies should provide indications on the spinal stress resulting from WBV exposure. This would lead to the identification of the failure mechanisms leading to structural spinal damage. However, the invasive techniques required for direct in-vivo

measurements of intra-discal pressure pose a risk, especially with exposure to WBV [1]. Estimation of the loads acting on the spine of a seated subject under the influence of vibration may be obtained by alternate methods: the evaluation of the seat-to-head transmissibility of the seated body (ratio of head to seat acceleration); and the driving-point mechanical impedance (ratio of force at the seat to the resulting velocity). The analysis of the test data derived from these methods provides an identification of the resonant frequency of the trunk. The greatest strain on the spinal column may then be expected to occur at the identified resonant frequency. Information on the relative displacement and phase difference between two spinal segments can further lead to an estimate of the loads on the spine.

Several seat-to-head transmissibility and driving-point mechanical impedance characteristics have been reported by various investigators under different experimental conditions. Laboratory measurements have been performed for different intensities and frequencies of sinusoidal and random vibration, postures, and seating configurations [6] Although a detailed discussion of these results is presented in Chapter 5, it may be stated that the extensive variations in experimental conditions employed in different studies could account for many of the differences in results reported in the literature. Despite the extensive differences in the measured response characteristics, most studies have consistently concluded that the resonance of the seated upper

body lies between 4 to 5 Hz, although only few of these experiments are known to reflect the true driving environments and seating configurations encountered in practice.

The studies on the vibration transmissibility of specific spinal segments and electromyographic measurements of the back muscles permit a gross estimate of the magnitude of the maximum load under vertical sinusoidal vibration exposure. In the most sensitive frequency range, the maximum load is observed to lie between 0.5 and 3 kN, representing 20 to 30% of the ultimate strength of a vertebral segment[13]. Depending on the number of cycles, the risk of fracture could increase even further. Additional loads resulting from rotational and shear forces caused by bending of the spine also add to the risk of fracture. Despite these findings, there is little conclusive evidence on the WBV induced fatigue failure of the vertebral column, although the risk of fracture due to cyclic loading under the action of vibration cannot be excluded.

A number of biodynamic models, many of them reviewed by Griffin and Bongers et al.[6,13], have been proposed in the literature to simulate human response to shock and vibration, and to provide insight on potential injury mechanisms under vibration exposure. The validation of these models, as will be demonstrated in Chapter 5, has relied on either data derived from cadaveric material, or on matching the driving-point mechanical impedance or the seat-to-

head vibration transmissibility. These models are considered valid only under certain laboratory test conditions which, in many cases, do not represent the true driving situations. On this basis, the applicability of the models and their uniqueness may very well be questionned.

1.2 Whole-Body Vibration Standards

To this day, the most widely used standard for evaluating human exposure to whole-body vibration and shock has been the International Standard ISO 2631/1 [18] developed by the International Standards Organization (ISO). This standard describes the measurement procedures for evaluating exposure to whole-body vibration, and also presents vibration limits based on root-mean-square (rms) acceleration, specified in one-third octave bands from 1.0 to 80 Hz, as a function of the daily exposure duration, varying from 1 minute to 24 hours. Two sets of limits are defined: one for vertical (z-axis) vibration, the other for fore-aft (x-axis) and lateral (y-axis) vibration.

In the current ISO 2631/1 standard, vibration limits are specified for assessing vibration effects on comfort, "reduced comfort limit", on work performance, "fatigue-decreased-proficiency (FDP) limit", and on health, "exposure limit". The fatigue-decreased proficiency (FDP) limits under exposure to vertical vibration are shown in Figure 1.1. The reduced comfort limits are obtained by dividing the FDP limits by 3.15 (10 dB lower, dB re. 1 μms^{-2}), while the

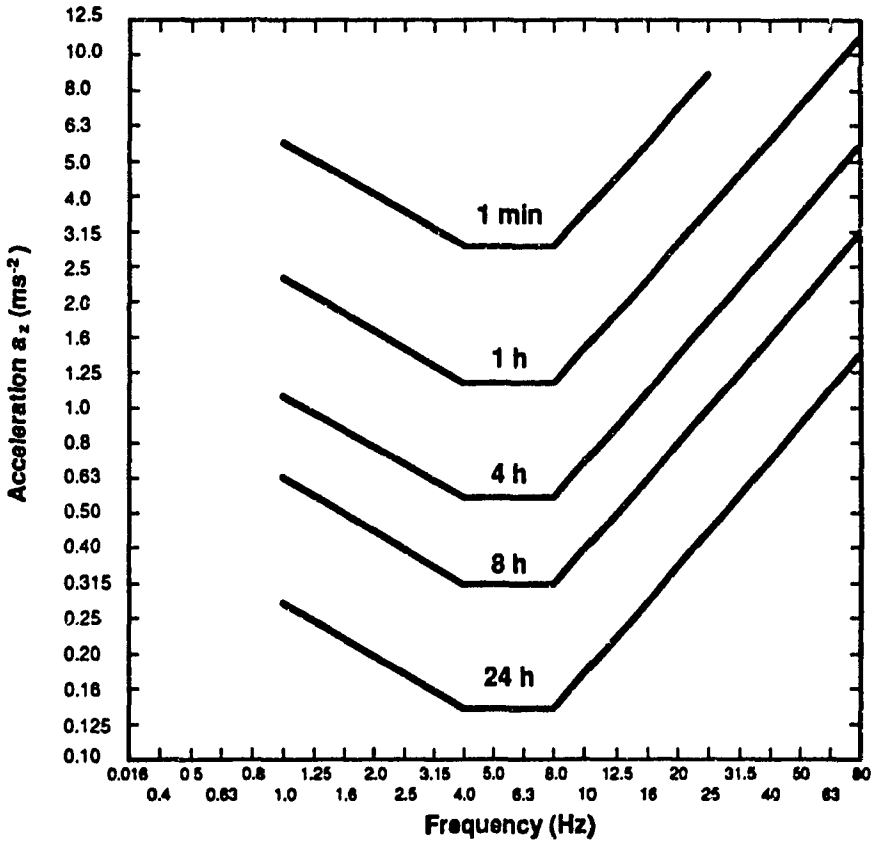

Figure 1.1 Fatigue-decreased proficiency limits as defined in the current ISO 2631/1 standard for vertical (z-axis) vibration [18].

exposure limits are obtained by multiplying the FDP limits by 2 (6 dB higher). These limits are specifically defined for assessing the effects of continuous vibration with very little transients or shocks, applicable when the crest factor (f_c), defined as the ratio of weighted instantaneous peak to rms acceleration, measured at the driver-seat interface, is less than 6. Inversion of the curves shown in Figure 1.1, defines the frequency weighting, W_z, expressing a 3 dB/octave decrease in vertical vibration sensitivity below 4 Hz and a 6 dB/octave decrease in sensitivity above 8 Hz. Application of the limits to situations for which the crest factor is greater than 6 is not recommended, although no alternative guideline is proposed in the standard.

1.2.1 NEW PROPOSED STANDARD

A new proposed version of the current ISO 2631/1 standard , presently at the stage of a Draft International Standard (DIS) [12], is currently being evaluated by the responsible Committee. This revised version proposes quite significant changes to the current standard. The most important changes include: the elimination of limits defined exclusively in terms of vibration frequency for specified daily exposure duration; the elimination of the concept of fatigue-decreased-proficiency in the evaluation of the vibration effects; the definition of new frequency weightings which differ not only with the direction of measurement but also with the measurement location (i.e. seat, feet, back) and with the effect being evaluated (i.e. health, comfort, perception, motion

sickness); and the definition of additional evaluation methods applicable to high crest factor motions.

For the assessment of health and comfort effects due to vertical vibration, a new frequency weighting curve, W_k, is defined in the 0.5 to 80 Hz frequency range. Figure 1.2 presents a comparison of this frequency weighting with the W_z weighting defined in the current standard. Unlike vibration limits, the newly proposed version defines a "health guidance caution zone" indicated by the shaded area in Figure 1.3. For vertical vibration, this zone specifies the range of W_k-frequency-weighted acceleration within which caution should be exercised with respect to potential health risks for a daily exposure duration varying between 4 and 8 hours. For alternate exposure durations, these may be referred to the 4 to 8 hours exposure duration using one of the following time-dependence relationships:

$$a_{w1} t_1^{1/2} = a_{w2} t_2^{1/2} \qquad (1.1)$$

or:

$$a_{w1} t_1^{1/4} = a_{w2} t_2^{1/4} \qquad (1.2)$$

where: a_{w1} is the weighted acceleration measured for exposure period t_1;

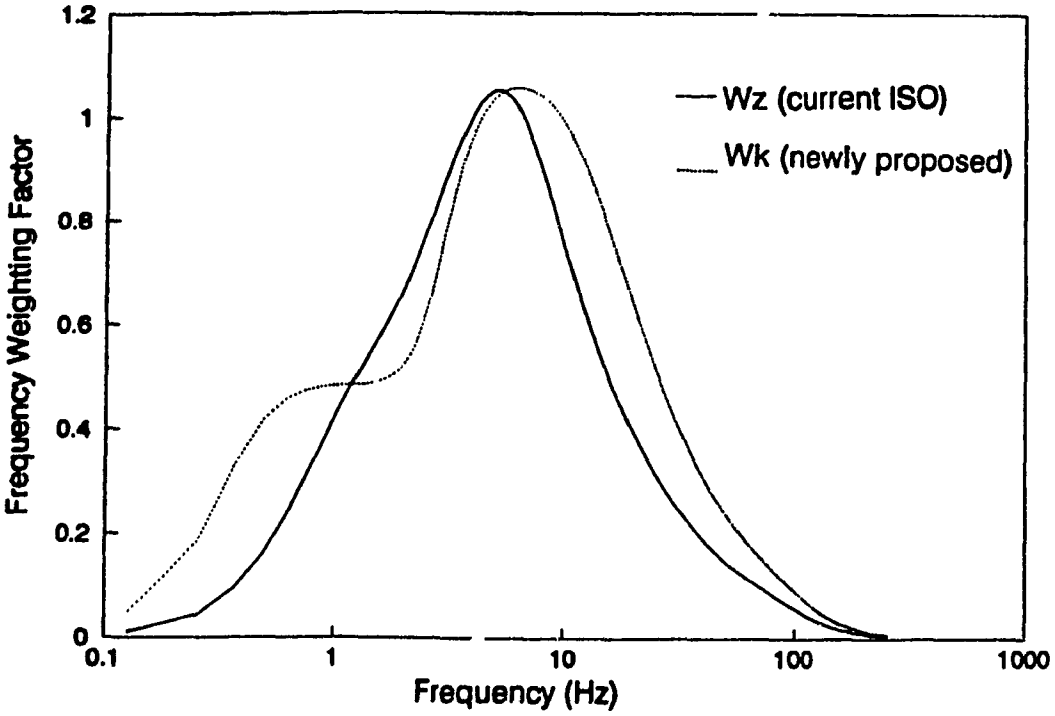

Figure 1.2 Frequency response characteristics of the band-limiting weighting filters.

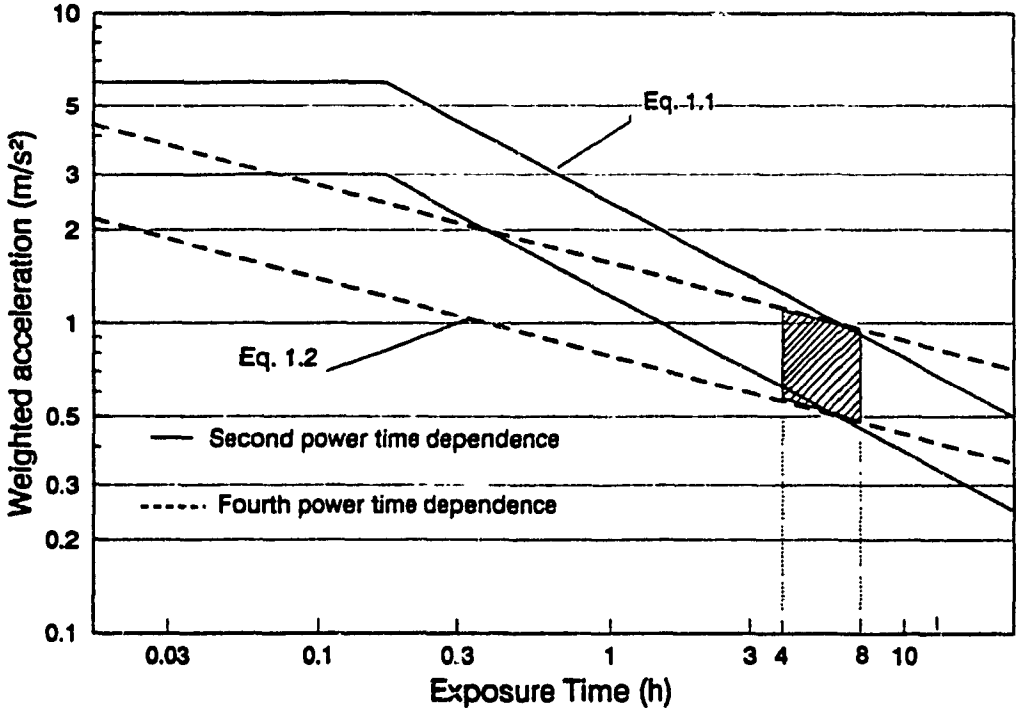

Figure 1.3 Health guidance caution zone as defined in the proposed revised version of ISO 2631/1 [12].

a_{w2} is the corresponding weighted acceleration computed for an alternate exposure period t_2.

These are based on the energy conservation principle; the former being used in the current ISO 2631/1 standard while the latter being promoted in the DIS proposal. For the evaluation of health effects, these two relations are found to yield relatively close results for exposure durations ranging from 4 to 8 hours, as shown in Figure 1.3.

The crest factor, defined as the weighted ratio of instantaneous peak to rms acceleration, is said to describe the shock contents of the vibration. In the new proposal, for crest factors below 9, the weighted rms acceleration may be computed in the time domain as in the current standard from:

$$a_w = \sqrt{\frac{1}{T}\int_0^T a_w^2(t)dt} \qquad (1.3)$$

where: $a_w(t)$ is the instantaneous frequency-weighted acceleration amplitude at time t;

T is the total integration time or exposure duration.

In the frequency domain, the weighted rms acceleration may be computed from:

$$a_w = \sqrt{\sum_{i=1}^{N} (W_i a_i)^2} \qquad (1.4)$$

where: W_i is the frequency weighting factor in the i^{th} one-third octave frequency band;

a_i is the rms acceleration in the i^{th} frequency band;

N is the total number of frequency bands considered.

A major addition in the proposed version is the introduction of a procedure for assessing health and comfort effects of vibration comprising shocks, for which the crest factor is larger than 9. In such cases, a root-mean-quad (rmq) frequency-weighted acceleration may be computed from:

$$a_{rmq} = \left[\frac{1}{T} \int_0^T a_w^4(t) dt \right]^{1/4} \qquad (1.5)$$

where the fourth power of acceleration is used to give greater emphasis on large instantaneous aceleration values characterizing the presence of shocks. A Vibration Dose Value (VDV) may then be defined as:

$$VDV = a_{rmq} T^{1/4} \qquad (1.6)$$

The lower and upper bounds of the health guidance caution zone, presented in Figure 1.3 and defined by equation 1.2, are selected such that the VDV is 8.5 and 17, respectively to account for epidemiological evidence suggesting increased health risks within such a range of values. The VDV, along with the frequency-weighted acceleration are required to be reported whenever the crest factor is found to be larger than 9 or that the ratio VDV/($a_w T^{1/4}$) is greater than 1.75.

1.3 Control of Vehicle Ride Vibration

The ride vibration environment of heavy vehicles, whether highway or off-highway, is strongly dependent upon vehicle-terrain interactions and the dynamics of the vehicle. Low-speed wheeled vehicles, such as construction, agricultural, forestry, mining, and industrial vehicles, are often unsuspended. The dynamic behaviour of such vehicles is, therefore, primarily a function of radial and lateral stiffness of the tires. Ride vibration of such vehicles can be characterized by lightly damped system resonance occurring at low frequencies due to the light damping properties of large and significantly soft tires. Ride vibration of heavy highway and off-highway vehicles (wheeled and tracked) predominates in the 0.5 to 10 Hz frequency range, enclosing the range within

which the human body is most sensitive, as illustrated by the weighting curves of Figure 1.2. Ride vibration of wheeled off-road vehicles predominates below 5 Hz in translational as well as in rotational modes, as presented in Table 1.2 [19].

TABLE 1.2

Predominant Frequency Range of Wheeled Off-Road Vehicle Vibration [19].

MODE OF VIBRATION	PREDOMINANT FREQUENCY RANGE (Hz)
Bounce	2.0-3.5
Lateral	≈1.0
Longitudinal	2.0-4.5
Roll	0.5-4.5
Pitch	2.0-4.5

The amplitude of vibration encountered by off-road vehicle operators, however, is significantly larger than that of the highway vehicles. A need to improve the ride vibration environment of these vehicles has long been recognized in view of three factors:

1. Large amplitude of ride vibration and shocks caused by the dynamic interactions of the unsuspended wheeled vehicles with irregular terrains;
2. Prolonged exposure time;
3. Dominant ride frequencies within the range of increased body response.

A number of approaches to improving off-road vehicle ride have been proposed, including suitable tires, primary suspension at front and rear axles, and secondary (cab and seat) suspension. These are briefly reviewed below.

1.3.1 RIDE IMPROVEMENT THROUGH TIRES

Off-road vehicle tires are primarily selected for maximum traction and roll stability. Large diameter and soft tires reduce the level of forces transmitted in the bounce and pitch modes, with an amplification of roll and lateral vibration due to higher location of the operator. Terrain-induced vibration of these vehicles predominates in the 0.5 to 5.0 Hz frequency range, implying even softer and consequently larger tires are required, so that the vehicle does not resonate in this range of ride frequencies. Thus, the ride improvement through tires alone is considered infeasible because of size limitations on the tires [20]. Moreover, tires offer only light damping, which is inadequate to attenuate terrain-induced vibration.

1.3.2 RIDE IMPROVEMENT THROUGH PRIMARY SUSPENSION

Alternatively, a primary suspension at the axles can improve vehicle ride by increasing the proportion of sprung mass to unsprung mass of the vehicle. A plane model of an off-road vehicle idealized by a suspended seat and suspended chassis has been analyzed by Matthews [21] and Patil et al [22]. Their studies concluded that a sprung front axle provides significant reduction

in fore-and-aft motion; however, the vertical ride remains unaffected. A number of wheel suspension configurations have been investigated by Claar II et al. [20], and the ride improvement potentials of a sprung front axle have been studied by Haack [23], and Cadou et al.[24]. Because of the restrictions placed on the suspension stiffness due to variations in vehicle loads and mounted implements, front and rear axle suspensions result in only a small ride improvement, at least for those investigated. The concept of primary suspension, however, requires complex alterations in wheeled vehicle design and would be impractical to implement in vehicles carrying frame-mounted equipment.

1.3.3 RIDE IMPROVEMENT THROUGH SECONDARY SUSPENSION

In view of the severe nature of wheeled off-road vehicle vibration and limitations of primary suspensions, the need to develop effective secondary (seat and cab) suspensions has long been identified by the manufacturers of these vehicles. A suspension at the seat offers perhaps the simplest option for ride improvement. Effective low-natural frequency bounce suspension seats have been commercially developed and are widely used in off-road vehicles to attenuate vertical vibration above 1.5 Hz. Although soft suspension seats reduce the vertical vibration transmitted to the driver, the resulting large relative motion of the driver with respect to the floor causes excessive leg pumping.

Developments in vertical suspension seats have been primarily attained through repetitive field and laboratory trials and subjective evaluations. Because the frequency contents and amplitude of ride vibration of vehicles vary considerably with many vehicle design and operating factors, the design practices based on expensive field trials are considered highly inefficient. Further, seat suspension designs, optimally suited to the ride vibration characteristics of a specific vehicle, cannot be effectively developed through such design practices. Alternatively, effective seat suspension designs with optimal vibration attenuation performance can be realized using the modeling and simulation techniques, and the ride vibration characteristics of a specific vehicle. The computer simulation of the analytical model can then provide an excellent aid to the designer to effectively evaluate the shock and vibration isolation performance of the suspension system and to develop optimal seat suspension designs for different types of vehicles. However, the seat suspension performance is affected not only by the suspension design but also by the dynamics of the driver. It is thus essential to develop an acceptable human body model in order to investigate the performance characteristics of the total driver-seat suspension system.

Developments in cab mounts/suspension for off-road vehicles have been quite limited, while extensive efforts have been mounted to develop effective cab suspensions for heavy highway vehicles, namely Ford's CL-9000 [25]. The

ride performance potentials of off-road vehicle cab suspensions have been investigated in a few studies using analytical and experimental means. Three- and four-mount cab suspension systems comprising coil springs, hydraulic shock absorbers, and elastic motion-limiting stops have been proposed for highway as well as off-highway vehicles [26]. Since the off-road vehicle vibration predominates in the 0.5 to 5.0 Hz frequency range, these suspensions need to be extremely soft to attain effective vibration isolation. Consequently, anti-roll bars may be required to enhance the roll stiffness. A cab suspension offers considerable potentials to improve vehicle ride quality and driver's comfort by providing a stable floor, reducing leg-pumping for the driver, and attenuating roll and pitch vibration in addition to bounce. Furthermore, a combined cab and seat suspension may perhaps yield additional improvement in bounce ride, although this may largely be dependent upon the characteristics of the vibration excitation present.

1.4 Scope and Objectives of the Proposed Research

Secondary seat and cab suspensions have long been recognized as potential solutions for reducing terrain-induced vibration, particularly in off-road vehicles with predominant ride vibration below 5 Hz. Bounce or vertical mechanical and pneumatic suspension seats have been commercially developed for many years. Some of these seats incorporate a longitudinal isolator for attenuating transverse vehicle vibration as well. Although cab suspensions have been

mostly associated with highway vehicles, their potential for improving the ride quality in off-road vehicles is recognized, specifically for reducing the magnitude of transmitted vibration in the pitch and roll modes. The need to maintain high roll stiffness and low relative travel of the suspension poses a rather severe design constraint in view of the low frequency vehicular vibration to attenuate.

Effective suspension design can be conveniently performed analytically using modeling and simulation techniques to predict the suspension's behaviour under known excitations. Using these models, optimal design parameters can be established to meet well-defined constraints. Previous studies [27] on suspension seats have led to the validation of a nonlinear analytical model under sinusoidal excitation and to the derivation of optimal suspension seat design parameters under a particular class of random vibration. The off-road vehicle environment comprising a mixture of random and transient vibration, the need to validate such a model under real environments, including shocks, has long been recognized in order to identify the most desirable characteristics of the suspension in real-life situations.

While most studies have represented the sitting human body as a rigid load, knowledge on the biodynamic response of the human body and of its influence on the response of the seat have indicated their need to be taken into account. Because of this interaction, prediction of the seat performance should ideally be

performed by analyzing the combined suspension seat-human body system. A human body model is therefore required capable of accounting for the measured behaviour of the body under different classes of off-road vehicle vibration and representative sitting postures likely to be encountered while driving.

With regard to current knowledge on comfort and health effects of vibration on the human body, the need to minimize the weighted rms acceleration at the driver-seat interface constitutes the primary design criterion to be met, using the vibration frequency weighting curves defined in the standards. Only on this basis can the ride improvement be effectively judged with respect to preservation of health and safety of vehicle drivers.

The shock response of suspension systems has been the subject of very few investigations. The evidence suggesting that shocks are perhaps more detrimental to health than constant, low level vibration [28] suggests the need to study suspension systems under typical shocks and to derive optimal design characteristics. Since the driving environment may be thought as being constituted of a mixture of shocks and random vibration, there is a need to bring these optimal design characteristics into perspective in order to achieve the best possible compromise.

1.4.1 OBJECTIVES OF THE RESEARCH

The objectives of the research are formulated upon review of published studies on the driver response to vehicular vibration and design of ride vibration control mechanisms. The review of measured ride vibration characteristics of different off-road vehicles has established the need to develop control mechanisms to reduce the intensity of transmitted vibration. From the study of field measured vibration environment of a class of forestry vehicles, it has been established that ride vibration characteristics exhibit strong presence of shocks, with crest factor ranging from 5 to 13 [29]. The need to incorporate the contribution of the seated human subject to the overall shock and vibration response of the control mechanisms is further recognized. Subsequently, it is necessary to explore the performance characteristics of vertical suspension seats in view of current guidelines on human response to vibration and shock. The need to incorporate these guidelines is further identified to design an effective cab and seat suspension system. The specific objectives of the research are thus formulated as follows:

(a) Study and validate a generalized vertical nonlinear suspension seat model of a representative off-road vehicle suspension seat under the influence of sinusoidal, random, and shock excitations.

(b) Design and develop a whole-body vehicular vibration simulator (WBVVS) capable of simulating the shock and vibration environment of particular categories of off-road vehicles to study the driver and combined driver and suspension seat responses in the laboratory.

(c) Derive idealized values of driving-point mechanical impedance and seat-to-head transmissibility characteristics of the seated off-road vehicle driver on the basis of a synthesis of selected data reported in the literature and of measurements of mechanical impedance performed under representative conditions, including variations in vibration excitations and sitting postures.

(d) Develop an analytical model of the seated off-road vehicle driver using the idealized driving-point mechanical impedance and seat-to-head transmissibility characteristics through the application of nonlinear programming based optimization methods.

(e) Develop and validate the combined suspension seat-human driver model, and derive the contribution of body dynamics to the vibration and shock attenuation performance of the suspension seat.

(f) Perform an extensive parametric sensitivity analysis to derive near optimal suspension seat design requirements under shock and random excitations.

(g) On the basis of the seat-driver model, estimate the driver's exposure levels under the influence of shock and vibration using current guidance on human response to vibration and the various proposed assessment methods.

(h) Develop a combined suspended cab-suspension seat model to investigate the roll, pitch and vertical vibration isolation characteristics. Design and develop a prototype cab suspension, and validate the combined cab and suspension seat model using the measured data.

(i) On the basis of the combined suspended cab-suspension seat model, derive near optimal cab suspension design parameters under a typical off-road vehicle vibration environment.

1.4.2 THESIS ORGANIZATION

This thesis is divided into nine chapters. Whenever relevant, the literature is discussed in appropriate chapters highlighting the research contributions on the various subjects. Chapter 2 presents the ride vibration excitations of various

classes of vehicles, including shock excitations caused by an ideal half-sine shaped obstacle. The design and operation of a whole-body vehicular vibration simulator (WBVVS) including various safety features are also described, along with the signal processing leading to the synthesis of field representative excitations. Chapter 3 presents a mathematical treatment of the nonlinear suspension seat model and its reponse under sinusoidal and random excitations characterizing various classes of off-road vehicles. Experimental results leading to the validation of the model are presented and the relative influence of the suspension seat design parameters is investigated. Chapter 4 presents the response of the nonlinear suspension seat model under shock excitations and the results of the model validation under such excitations. The relative importance of seat design parameters is discussed on the basis of results obtained for different shock characteristics.

A synthesis of selected data reported in the literature on human body driving-point mechanical impedance and seat-to-head transmissibility is presented in Chapter 5, and the apparent influence of the various experimental conditions used in deriving this data is estimated. Measurements of the driving-point mechanical impedance characterizing off-road vehicle drivers are reported in Chapter 6 under various classes of vibration excitations. These results are used along with the synthesis of published data to derive target values on whole-body driving-point mechanical impedance and seat-to-head transmissibility for

off-road vehicle drivers and to define a seated human driver model. In Chapter 7, the suspension seat model is combined with the human driver model and the results of the validation are presented under sine, random and shock exitations. Optimal suspension seat design parameters are defined on the basis of this model and the influence of body dynamics on seat vibration attenuation performance is estimated.

In Chapter 8, a prototype design of an off-road vehicle cab suspension is described. The combined cab and seat suspensions are analytically modeled and validated using laboratory test data measured under sinusoidal excitations. The response of the combined suspended cab-suspension seat model is evaluated under a typical off-road vehicle vibration environment, and the results are used to derive near optimal cab suspension design parameters. Finally, the conclusions and the recommendations for future investigations are presented in Chapter 9.

CHAPTER 2

OFF-ROAD VEHICLE VIBRATION ENVIRONMENT AND SIGNAL GENERATION

2.1 Introduction

The magnitude and frequency characteristics of the vibration environment of different off-road vehicles are known to vary considerably with vehicle weights and dimensions, vehicle design, tire properties, terrain roughness, vehicle speed, etc. [30]. Study of human response to whole-body vehicular vibration and control of vibration transmission thus involves the characterization of the vibration environment of different vehicles. The vertical ride vibration of various categories of vehicles have been described in International Standards in terms of power spectral density (PSD) of acceleration encountered at the seat location [31,32]. These ride vibration characteristics, however, do not describe the shock motions encountered while driving over discrete obstacles, a situation more likely to occur when off-road vehicles are involved.

The evaluation of the vibration attenuation performance of secondary suspensions is often carried out through field trials on specific vehicles equipped with such suspensions. Alternatively, laboratory evaluations may be performed for either deterministic or random vibration excitations with seats loaded with either a rigid load or a human subject. Since laboratory tests using low frequency and large amplitude vibration poses safety risks for the seated

human subjects, laboratory study of human response to vibration and performance evaluations of the driver-suspension seat systems raises many ethical and safety concerns. Previous work reported by Griffin [33] and Suggs et al. [34] have demonstrated that the performance evaluation of suspension seats cannot be effectively performed without considering the combined seat-human body interactions. Laboratory evaluations, however, may be considered provided a vibration simulator with enhanced safety control loops can be developed. The use of a laboratory vibration simulator to evaluate the effectiveness of secondary suspension systems offers many advantages over long and costly field trials, and greater convenience, versatility and better control of the test conditions. The design of a whole-body vehicular vibration simulator (WBVVS) capable of accommodating human subjects, however, necessitates several safety and performance considerations to be described in this chapter.

In view of the considerable interest for off-road vehicles, particular attention is given in this study to excitation classes, identified in International Standards, with vibration characteristics that closely resemble those of a log skidder, a widely used forestry vehicle. Since shocks resulting from the wheel travel over discrete obstacles constitute an important part of the vibration environment of such vehicles, representative shock excitations are needed to study the shock isolation properties of the suspension systems. The characteristics of transient

shock excitations are strongly related to vehicle speed, dynamics of the vehicle and the nature of the terrain abruptness or obstacle. In this study, the shock excitations encountered at the seat attachment location are derived from a simple two-degree-of-freedom pitch-plane model of a log skidder subject to an idealized half-sine displacement. The resulting shock excitations are synthesized using the vibration simulator designed and developed in the laboratory.

As a prerequisite to studying the vibration attenuation of suspension seats for use in off-road vehicles, this chapter is devoted to the design and development of a laboratory whole-body vehicular vibration simulator (WBVVS) incorporating safety features enabling the use of human subjects. The vibration simulator is designed to synthesize harmonic excitations in the 0.625 - 10 Hz frequency range, random vertical vibration of different classes of off-road vehicles, and shock excitations encountered in the 1 - 10 km/h speed range. The methodology used for synthesizing these signals and for driving the simulator is given in later sections.

2.2 Whole-Body Vehicular Vibration Simulator

A special purpose and dedicated WBVVS was designed to simulate whole-body vibration environment of a wide class of vehicles. In this study, the vehicles with ride vibration characteristics similar to those of forestry skidders are

specifically considered. The simulator comprises a vibration platform supported on two servo-hydraulic actuators, and a servo-control system interfaced with either an analog or a digital signal generator. Since the vertical vibration encountered in forestry vehicles is among the most severe, the WBVVS was configured to simulate vertical vibration alone. The two servo-actuator design, however, also permits generation of in-plane rotational vibration. The WBVVS was designed with the following considerations to ensure the safety of the test subjects and to meet appropriate vibration requirements for testing driver-suspension seat systems.

- The magnitude of the compressive and extensive forces generated by the WBVVS must be continuously monitored and limited, such that the rms acceleration levels are well below the exposure limit proposed in ISO 2631/1 [18]. Furthermore, the peak acceleration level at any time must not exceed 1.0 g.
- Slow ramp-up and ramp-down circuit must be incorporated to eliminate the undesired transient motions and forces that could arise during start-up, stoppage, and sudden power interruptions.
- Emergency safety switches must be provided to the subject and the operator.
- The WBVVS must support the load due to the platform, the steering column, the seat, and the driver.

- The WBVVS must be able to reproduce the vibration environment of different classes of vehicles, specifically in the 0.5 to 10 Hz frequency range.
- The fundamental frequency of the platform must be above 40 Hz, for the simulator to be used for off-road as well as for heavy highway vehicles.

Figure 2.1 presents a schematic diagram of the WBVVS including a seat and steering column assembly. General specifications of the simulator appear in Table 2.1, while the design details of the major systems are described in the following sections.

TABLE 2.1

General Specifications of the WBVVS

Maximum Payload	270 kg
Mass of the Platform	127 kg
Maximum Displacement	20 cm
Frequency Range	0 - 40 Hz
Dimensions of the Platform	1.37 m long 0.91 m wide 0.33 m deep

2.2.1 VIBRATION PLATFORM

The vibration platform was fabricated using tubular structural steel members to ensure maximum bending strength under vibratory loads. It was designed with minimal weight and low height to provide easy access for the test subjects. When installed on the servo-hydraulic actuators, the platform was at a height of

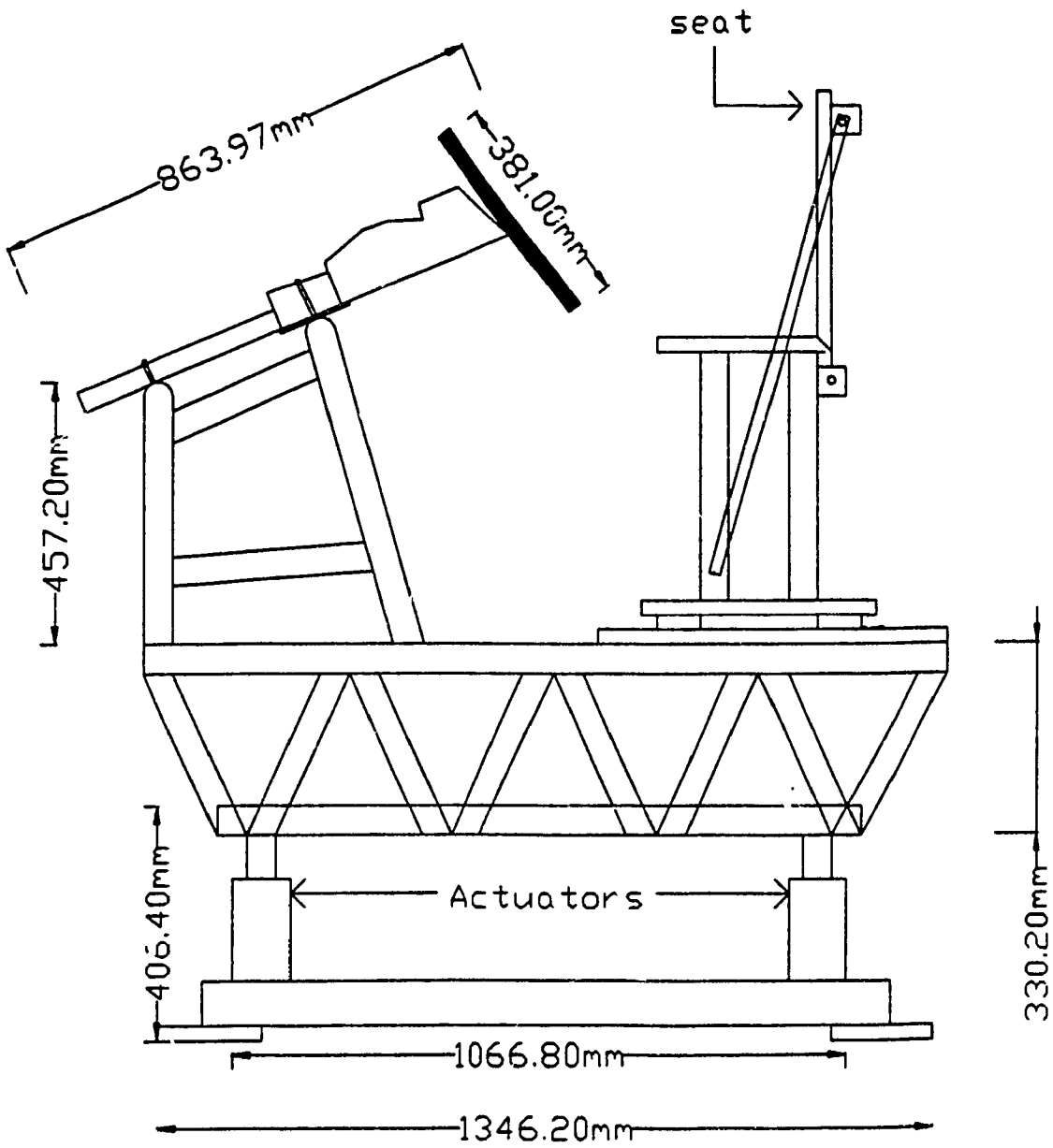

Figure 2.1 A schematic of the WBVVS.

0.70 m above the floor. The vibration platform was mounted on two servo-hydraulic actuators installed on a base frame. Safety position control switches were installed between the platform and the base frame to monitor and limit the vibratory motion in compression and rebound. The desired position limits could be conveniently selected by manually adjusting the safety switches.

A resonance search test was performed to identify the useful frequency range and fundamental resonant frequency of the WBVVS. The test was performed under white noise random excitation in the 0 - 50 Hz frequency range. The frequency response characteristics of the simulator, illustrated in Figure 2.2, reveal a nearly flat frequency response at excitation frequencies below 20 Hz. Since the tests were performed under very low displacement excitations, the response peak at low frequencies, below 1 Hz, is attributed to the large noise levels associated with acceleration being measured using a capacitive transducer. Since most vehicles exhibit ride vibrations in the 0.5 to 20 Hz frequency range, the WBVVS can effectively be used to assess the driver and combined driver-suspension seat responses to vehicular ride vibration.

2.2.2 THE HYDRAULIC SUB-SYSTEM

The hydraulic system comprises two double-ended servo-hydraulic actuators equipped with hydro-static bearings. Each actuator is equipped with a two-stage electro-hydraulic servo-valve, an LVDT ("linear variable differential

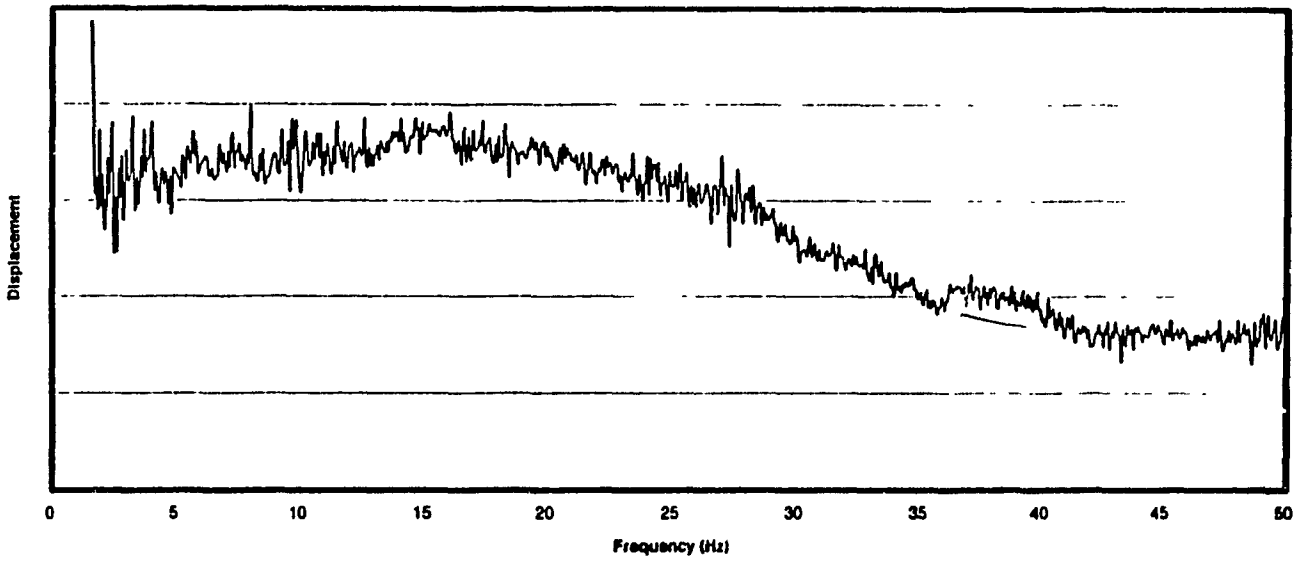

Figure 2.2 Frequency response characteristics of the WBVVS.

transformer") position sensor for the position feedback loop, and a differential pressure transducer providing the monitoring and feedback for the force limit control. The hydraulic actuators are connected to a hydraulic power supply composed of an electric motor, pump, reservoir, various hydraulic filters, valves, water cooler and a pump controller. The flow capacity of the hydraulic power supply is 19 l/min (5 gpm) at a pressure of 20.6 MPa (3000 psi). The hydraulic pressure of the power supply was reduced such that the operating pressure varied in the 10.3 to 13.7 MPa (1500 - 2000 psi) range. The reduction in hydraulic pressure resulted in reduced transient motions and forces, and enhanced flow capacity and thus increased actuator displacements to meet the desired levels of vehicular vibration motions. The measurements performed at different excitation frequencies in the 0.5 - 10 Hz range revealed that the flow capacity of the WBVVS servo-valves increased to approximately 30 l/min (8.5 gpm) at frequencies below 2.5 Hz, and to 25 l/min (6.6 gpm) at frequencies above 2.5 Hz.

The two hydraulic cylinders yield a maximum displacement of 19 cm between the stops and each actuator is equipped with a 20 cm LVDT position sensor that provides the displacement feedback to the servo-controller. The two hydraulic actuators are synchronized using the electronic control system, integrated within the servo-control, to achieve true vertical motion of the platform.

2.2.3 THE SERVO-CONTROL SYSTEM

The servo-control system is an integral part of the WBVVS that monitors and controls the platform motion. Although the control system was designed to operate the WBVVS using position, velocity or acceleration feedback, displacement feedback has been used in order to ensure safe and stable operation, since the LVDT sensors provide a direct measure of the actuator motion. Furthermore, the displacement feedback control facilitates the tuning and calibration of the WBVVS. The servo-control system, through its various control loops, monitors and displays the warning lights on a control panel to indicate the limit faults related to position, force, emergency stop, oil temperature, filter status, and hydraulic pressure.

The servo-control system incorporates different control loops to ensure safe levels of forces and accelerations transmitted to the test load or the subject. Figure 2.3 illustrates a schematic of the servo-control system and safety control loops. The primary control loop is based upon continuous monitoring and control of the motion of the platform using the feedback from the LVDT position sensor. The secondary control loop comprises: (i) monitoring and control of compression and rebound forces using the feedback from the differential pressure sensors mounted on each actuator; (ii) monitoring and control of displacement from the externally mounted and adjustable position limit switches; and (iii) emergency safety switches provided to the operator and

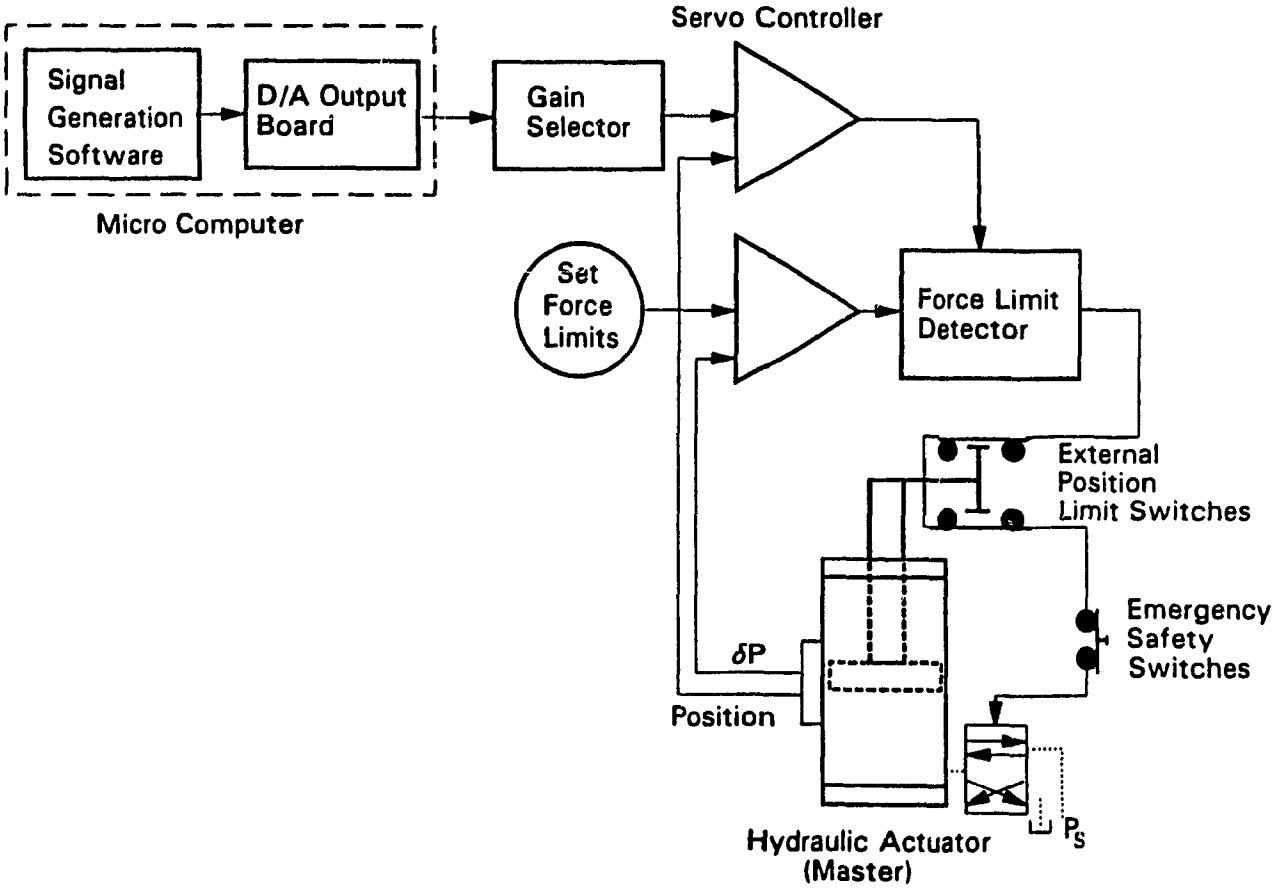

Figure 2.3 A schematic of the servo-control system.

the subject. The desired force limits are selected using the potentiometers located on the control panel. The externally mounted position limit switches can be easily adjusted to limit the maximum displacement to a desired value.

The servo-control system can be operated with an external signal generator or a computer based signal and data generation software. In this study, various vibration excitation signals are synthesized to evaluate the response characteristics of the driver and driver-suspension seat system. The synthesized displacement signal is provided to the servo-control system through a D/A output board integrated within the micro-computer. The signal gain is selected using a potentiometer to achieve the desired levels of WBVVS motion. A ramp-up and ramp-down control circuit is integrated within the servo-control system to ensure smooth start-up and stoppage with minimal transient motions.

2.3 Ethical Considerations

While every effort may have been expended to ensure the safe operation of the WBVVS, there are inherent risks in exposing experimental subjects to vibration. The risk may depend on the health of the experimental subject, whereas the necessity to be aware of any medical contraindications that would make the subject unfit for the experiments. Subjects should be made thoroughly aware of the risks and of all safety precautions and know that they are free to withdraw from the experiment at any time.

In this study, the subjects who agreed to take part in the vibration tests on the WBVVS were made thoroughly aware of the operating principles and of the various safety features of the simulator. Each subject was asked, prior to the tests, to sign a "Participant Consent Form", a copy of which appears in Appendix A. This form provides a brief description of the objectives and of the methodology to be used in the experiments and describes the various safety features of the simulator. Each class of vibration excitation to be used is identified, along with the approximate exposure duration expected for the tests. Emphasis is placed on the free-will of the participants and on their right to discontinue their participation at any time.

2.4 Random Vibration Environment of Wheeled Off-Road Vehicles

A review of whole-body vibration environment of different off-road vehicles is carried out to identify classes of vehicle vibration that resemble those of the forestry log skidder. Vertical vibration measured on the cab floor of unsuspended log skidder vehicles have shown the following characteristics [29]:

- predominance of vertical vibration in the 2.0 to 2.6 Hz frequency range;
- overall W_z-frequency-weighted vertical acceleration ranging from 0.7 to 1.1 ms^{-2};
- a crest factor usually greater than 6.0.

For laboratory measurement of transmitted vibration, four random excitation classes defined in the Standards [31,32] possess similar frequency characteristics as those measured for log skidders, although higher in intensity. For agricultural tractors, the preliminary version of ISO Standard 5007 [35] defines seat vibration excitations for two categories of vehicles: those with unladen mass lower than 3600 kg are grouped in a single class, specified as "ISO 1" vehicles; and those with unladen mass between 3600 and 5000 kg are referred to as "ISO 2" vehicles. For different types of earth-moving machinery, ISO standard 7096 [32] defines a Class I for tractor-scrapers without primary suspension or vibration absorber and a Class II for tractor-scrapers with either front axle suspension or vibration absorber hitch. The mathematical description of these excitations are given in the following sections.

2.4.1 ISO 1 AND ISO 2 EXCITATIONS

Based upon the ride vibration data of agricultural tractors measured on a simulated track, ISO 5007 has proposed two vehicle classifications and their respective vertical accelerations in terms of power spectral density (PSD). The two vehicle classes, ISO 1 and ISO 2, are based upon vehicle loads, tire inflation pressure, and wheelbase. The PSD of vertical acceleration measured at the seat attachment location are described as:

$$S(f) = S_{max} \exp\left[\frac{-(f - f_m)^2}{2B^2}\right] \qquad (2.1)$$

where: S(f) is the PSD of vertical acceleration at frequency f in $(ms^{-2})^2/Hz$;

S_{max} is the maximum or peak acceleration PSD;

f_m is the frequency at which the maximum PSD occurs, (Hz);

B is a constant related to the frequency bandwidth, (Hz).

For the ISO 1 excitation, S_{max} is equal to 6.0 $(m/s^2)^2/Hz$, f_m is 3.25 Hz and B is set equal to 0.33 Hz. For the ISO 2 excitation, S_{max} is 5.5 $(m/s^2)^2/Hz$, f_m is 2.65 Hz and B is 0.3 Hz. Figure 2.4 illustrates the acceleration PSD of the vertical vibration characteristics of ISO 1 and ISO 2 classes. The Technical Report [35], constituting the preliminary version of the ISO 5007 standard, further defines the time traces of vertical displacement at the seat attachment location, the true rms acceleration and the overall W_z-weighted rms acceleration.

2.4.2 CLASS I AND CLASS II EXCITATIONS

Alternately, four classes of vibration are defined for different types of earthmoving machinery in ISO standard 7096 [32], of which Classes I and II are comparable to those of the forestry skidder vehicles. The peak acceleration PSD measured at the seat location of Class I vehicles is 4.13 $(ms^{-2})^2/Hz$

occurring at a frequency of 1.85 Hz, while the peak acceleration PSD of Class II vehicles is 2.4 $(ms^{-2})^2$/Hz occurring at 2.1 Hz. Target values on true as well as overall W_z- frequency-weighted acceleration are also specified in the standard. The acceleration PSD characteristics of these classes of excitation are given in terms of transfer functions of low- and high-pass filters of the Butterworth type. The PSD of vertical acceleration measured at the seat attachment location are given by:

$$\underline{\text{CLASS I}} \qquad S(f) = 5.30(HP_{24})^2(LP_{24})^2$$

$$\underline{\text{CLASS II}} \qquad S(f) = 2.72(HP_{24})^2(LP_{24})^2 \qquad (2.2)$$

where $(LP)_{24}$ and $(HP)_{24}$ characterize low- and high-pass filters respectively with 24 dB/octave attenuation. The filter transfer functions are given by:

$$(LP)_{24} = \frac{1}{1 + 2.613s + 3.414s^2 + 2.613s^3 + s^4}$$

$$(HP)_{24} = \frac{s^4}{1 + 2.613s + 3.414s^2 + 2.613s^3 + s^4} \qquad (2.3)$$

where $s = jf/f_c$ is the imaginary frequency ratio, f is the excitation frequency and f_c is the filter cut-off frequency in Hz The cut-off frequency for the HP_{24} filter is 1.5 Hz for both classes of vehicles, while that for the LP_{24} filter is 2.5 Hz for

Class I and 3.0 Hz for Class II excitation. Figure 2.5 illustrates the acceleration PSD spectra of these two excitation classes.

2.5 Synthesis of Shock and Vibration Displacement Excitation Signals

In order to conform with the requirement that displacement signals are required to drive the WBVVS, appropriate displacement motions characterizing the various identified classes of vibration excitations had to be defined. For the ISO 1 and 2 classes, this was performed using the data files specified in the standard, while synthesis of the power spectral density of the acceleration defined for Classes I and II excitations was required. A swept sine displacement excitation was also defined in the 0.625 to 10 Hz frequency range. Finally, shock motions idealized by the passage of a vehicle over a half-sine shaped obstacle at various speeds were also defined. The methodology used in creating the desired motions is described in the following sections.

2.5.1 SINUSOIDAL EXCITATIONS

While the need to study suspension systems under realistic excitations may be well recognized, use of deterministic harmonic excitation offers the possibility of studying the behaviour of the systems at selected frequencies, which otherwise would not be possible. Complete control over the frequency and the amplitude of excitation provides a means of exciting the normal modes of the systems and of studying their steady-state response. Sinusoidal excitation may

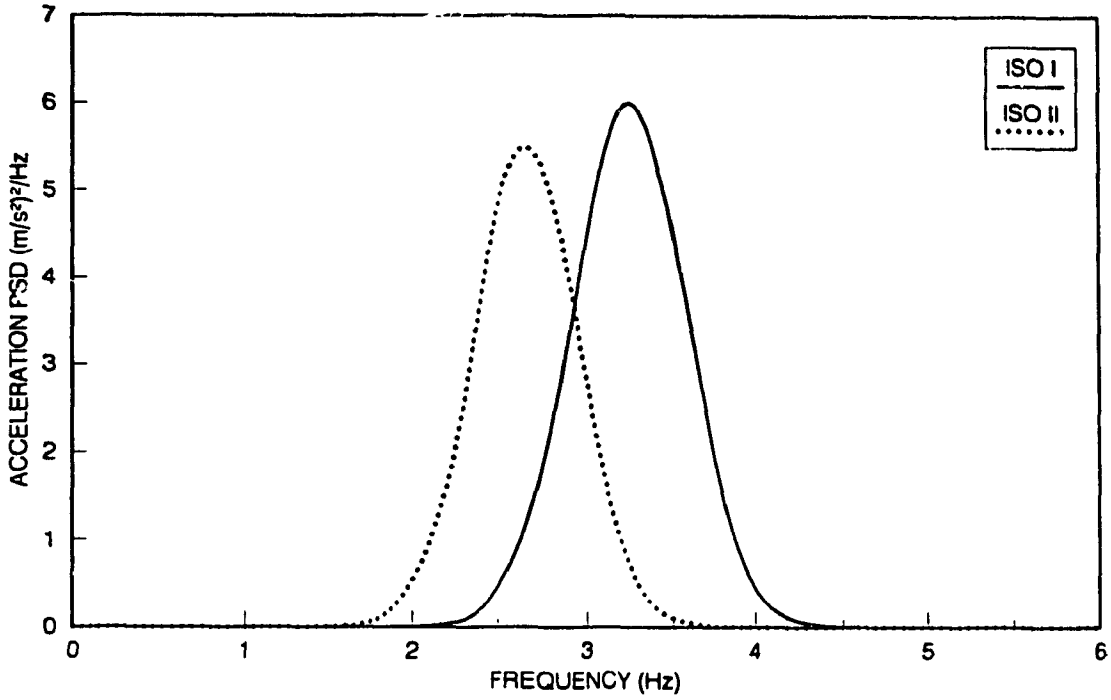

Figure 2.4 Acceleration PSD of the vertical vibration characteristics of ISO 1 and ISO 2 excitation classes defined in ISO 5007 [31].

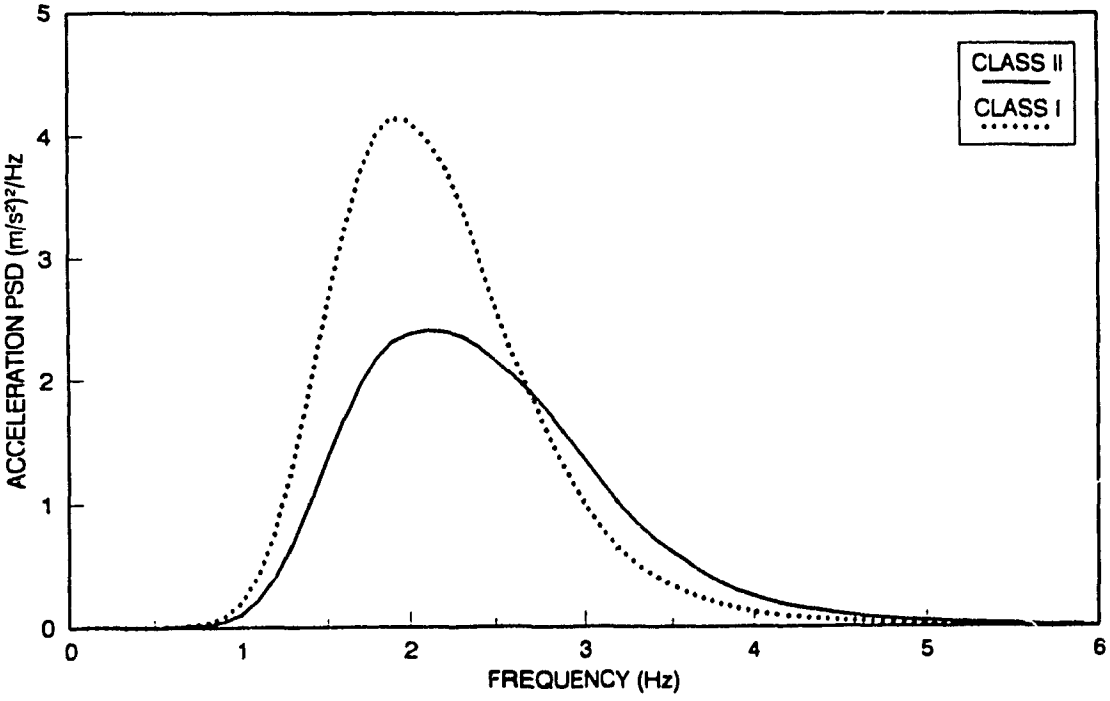

Figure 2.5 Acceleration PSD of the vertical vibration characteristics of Class I and Class II excitations defined in ISO 7096 [32].

be achieved manually at discrete frequencies or a frequency sweep may be used in which the instantaneous motion commences at a known frequency, and smoothly increases or decreases at a known rate to a final frequency. Although this method is much quicker than using discrete sinusoids, it does not provide phase information and only the ratio of input to output spectra has significance.

A swept sine signal was synthesized using the DSP software and hardware. The frequency range was selected as 0.625 to 10 Hz and the sweep rate as 1 octave/min. Based on the WBVVS capabilities, the signal was synthesized to yield a constant 25 mm peak displacement in the 0.5 to 2 Hz range, followed by a constant peak acceleration of 3.95 ms^{-2} between 2 and 10 Hz. The various steps involved in the synthesis of the sweep signal are summarized in Figure 2.6 which presents the transformation of acceleration sweep into a displacement sweep through double integration, filtering, scaling and concatination of samples.

2.5.2 ISO 1 AND ISO 2 RANDOM EXCITATIONS

To create the input vibration excitations corresponding to these two classes, data files are formed using the 700 time-displacement coordinates specified at 40 ms intervals for each class of vibration in an earlier version of the ISO 5007 Standard, at the stage of a Technical Report [35]. Through a suitable software

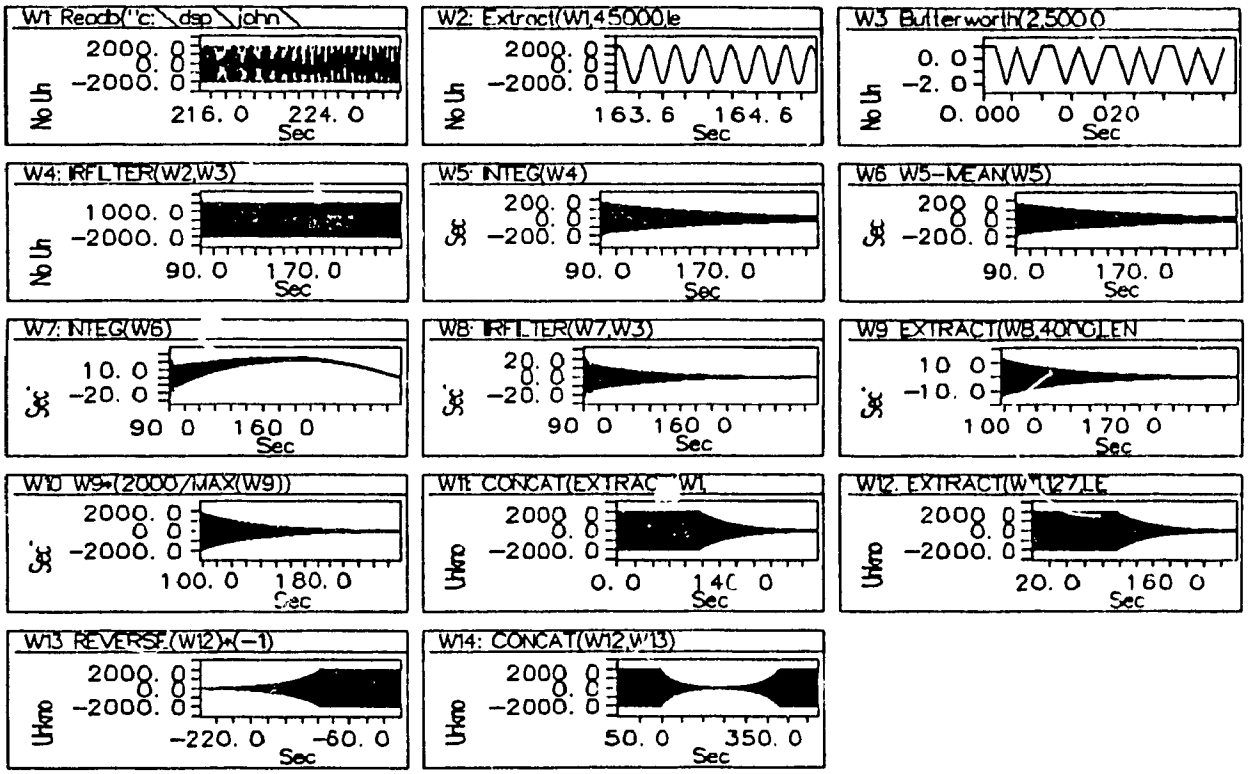

Figure 2.6 Synthesis of swept sinusoidal displacement excitations.

and digital to analog (D/A) output board, these signals are used to drive the WBVVS. The resulting acceleration spectra are smoothened and compared to those proposed in the standard, as shown in Figures 2.7 and 2.8. Although similar to the recommended PSD, the synthesized motions yield peak accelerations somewhat higher and frequency characteristics slightly different than those of the recommended data. It should be noted that the recommended acceleration PSD spectra are the mean values derived upon performing numerous averaging and smoothing. The spectra of the synthesized signals are thus considered acceptable for the study of driver-suspension seat system for these classes of vehicles. The overall W_z-weighted and unweighted (true) rms accelerations due to the synthesized motions of the WBVVS are computed and compared to those recommended, in Table 2.2.

2.5.3 CLASS I AND CLASS II RANDOM EXCITATIONS

To create the input vibration excitations corresponding to Class I and Class II signals, a software is developed to synthesize the vibration spectra using the DSP hardware and software. Digital low- and high-pass filters are designed using the filter module of the DADiSP software. A white noise random signal in the 0 - 12.5 Hz range is generated and processed through the filters described by equation (2.3). The filtered acceleration signal is integrated twice to achieve the displacement signals required to drive the WBVVS. The displacement signal is further filtered through a high-pass filter with cut-off frequency set at 0.1 Hz

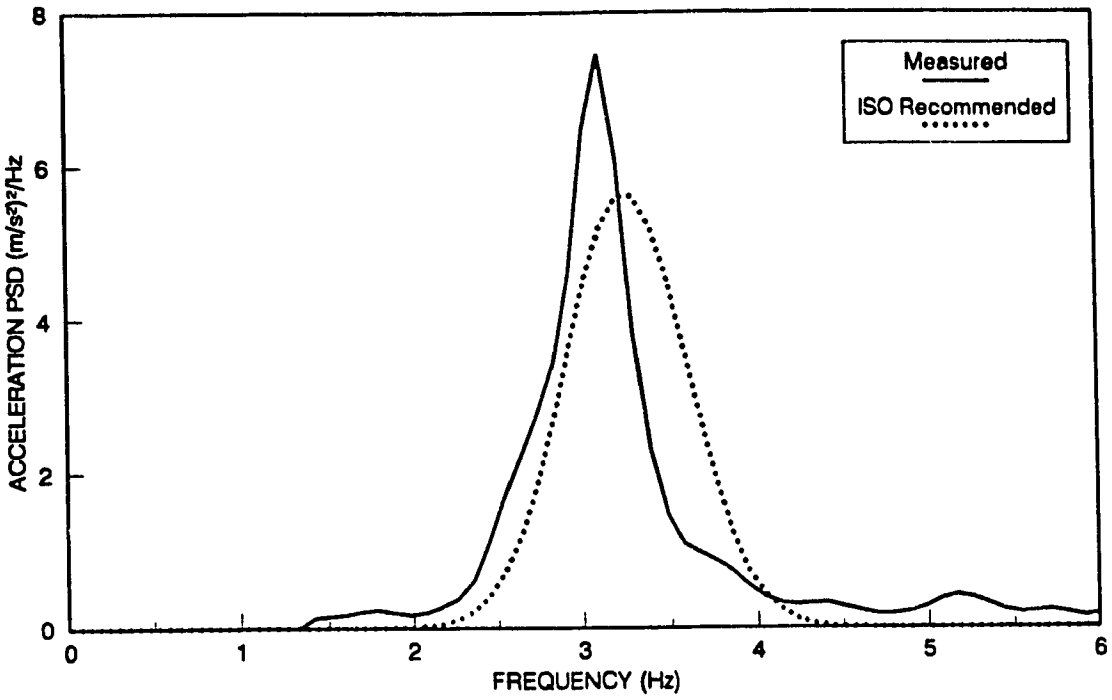

Figure 2.7: A comparison of PSD of measured acceleration to that recommended for ISO 1 vehicles.

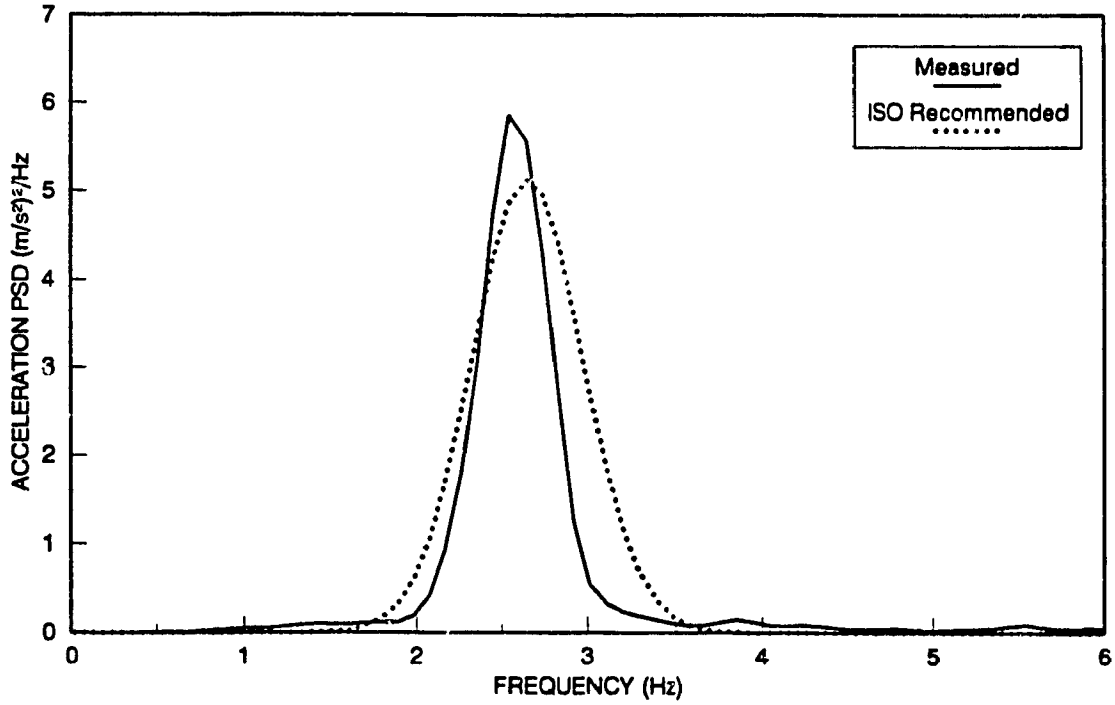

Figure 2.8: A comparison of PSD of measured acceleration to that recommended for ISO 2 vehicles.

in order to remove the dc components. Figure 2.9 summarizes the methodology used to synthesize the displacement signals for Classes I and II vehicles.

The acceleration PSD of the synthesized signals measured on the WBVVS for these two classes of excitation is compared to the recommended PSD, as illustrated in Figures 2.10 and 2.11. The results show a reasonably close agreement, taking into account the averaging and smoothing leading to the recommended curves. The W_z-frequency-weighted and true rms accelerations obtained for these vibration classes are further compared to the recommended levels in Table 2.2.

TABLE 2.2

Comparison of Synthesized Random Signal Acceleration Levels with Target Values

Excitation Class	Unweighted (true) RMS Acceleration (ms^{-2})			W_z Weighted RMS Acceleration (ms^{-2})		
	Target	Measured	Error (%)	Target	Measured	Error (%)
ISO 1	2.25	2.59	15	2.05	2.31	13
ISO 2	1.94	2.00	3	1.70	1.65	3
Class I	2.35	2.42	3	1.75	1.96	14
Class II	2.05	2.08	1.5	1.60	1.69	5.6

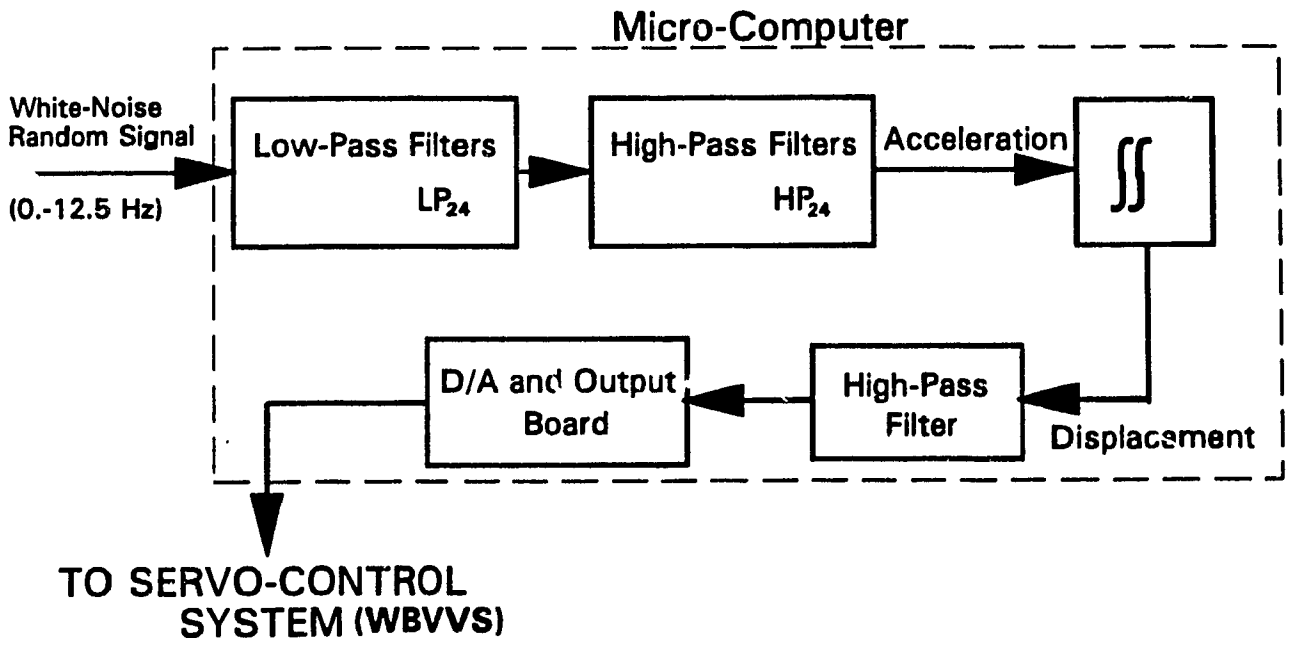

Figure 2.9 Synthesis of vibration displacement signals for Class I and Class II vehicles.

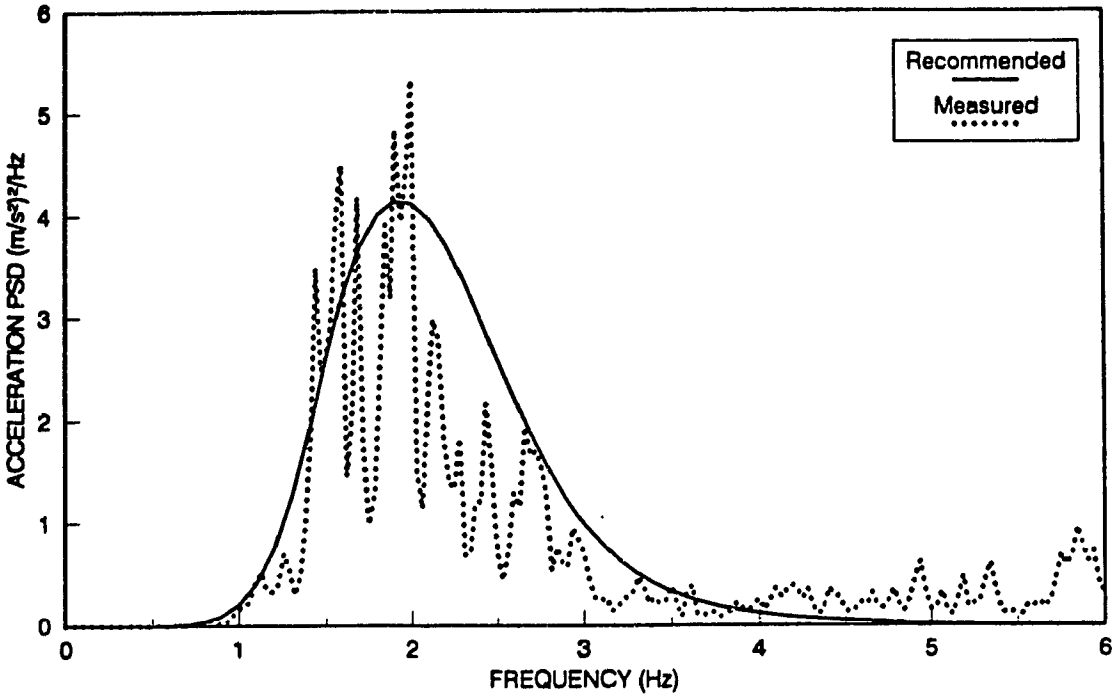

Figure 2.10 A comparison of PSD of measured acceleration to that recommended for Class I vehicles.

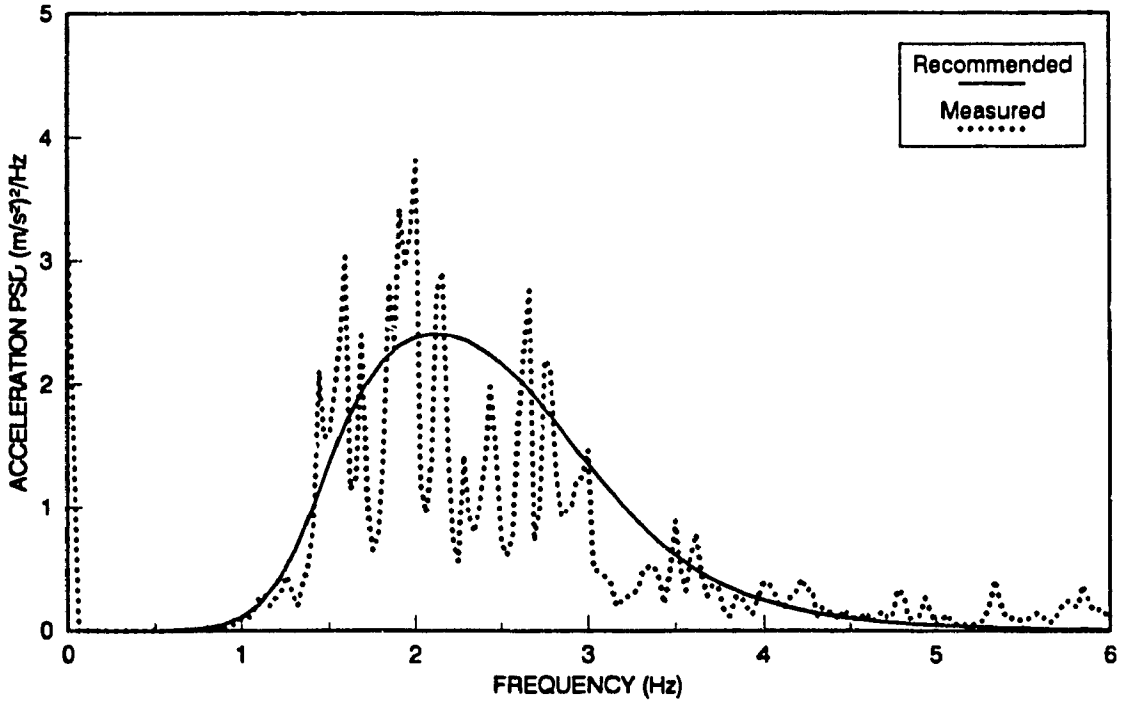

Figure 2.11 A comparison of PSD of measured acceleration to that recommended for Class II vehicles.

2.5.4 SHOCK EXCITATIONS

Off-road vehicles frequently encounter shock type excitations while driving over different obstacles in forestry, mining and construction environments. Forestry vehicles may encounter shock excitations while driving over logs, rocks and abrupt terrains. Shock excitations vary considerably in intensity and duration depending upon the nature of the obstacle, the vehicle speed and the dynamics of the vehicle. In this study, the shock excitation encountered by the vehicle tires is idealized by a half-sine pulse displacement in order to evaluate the human and secondary suspension response characteristics. The period, τ, of the transient displacement excitation is related to the vehicle speed, V, and to the width of the obstacle or shock input, D, by the relation, $\tau = 2D/V$. The shock input to the cabin floor of the vehicle may thus be represented by the half-sine displacement input filtered through the tires of a two-degree-of-freedom vehicle model. The two-axle off-road unsuspended vehicle shown in Figure 2.12 is modeled as a two-degree-of-freedom dynamic system, as shown in Figure 2.13. The pitch-plane vehicle model is derived assuming undeformable terrain, linear tire properties, negligible roll dynamics, and negligible contributions due to the seat-driver combination in view of its relatively small mass.

The displacement excitations at the two wheels caused by the idealized sine pulse are derived as:

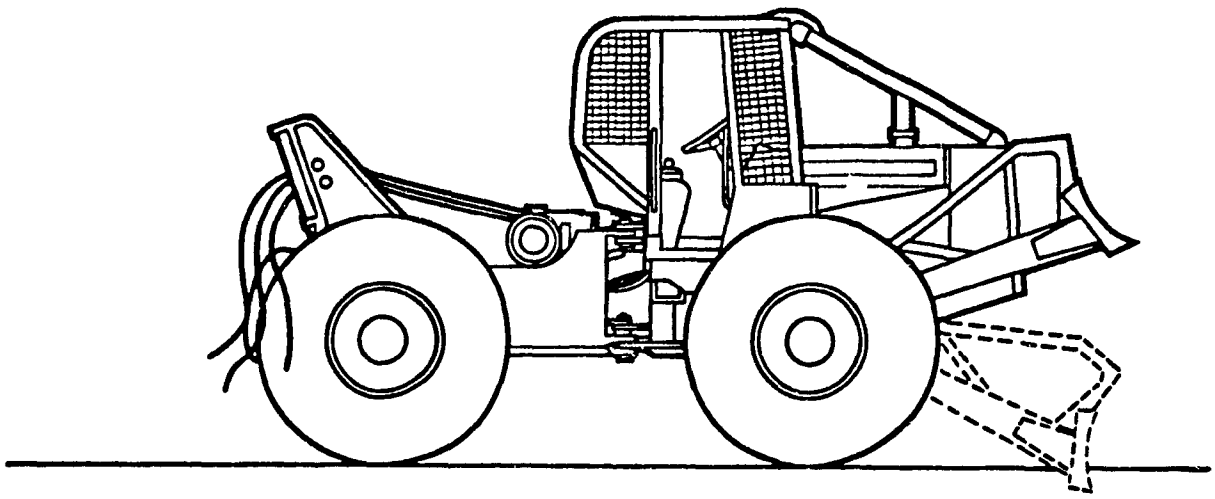

Figure 2.12 Schematic diagram of a log skidder.

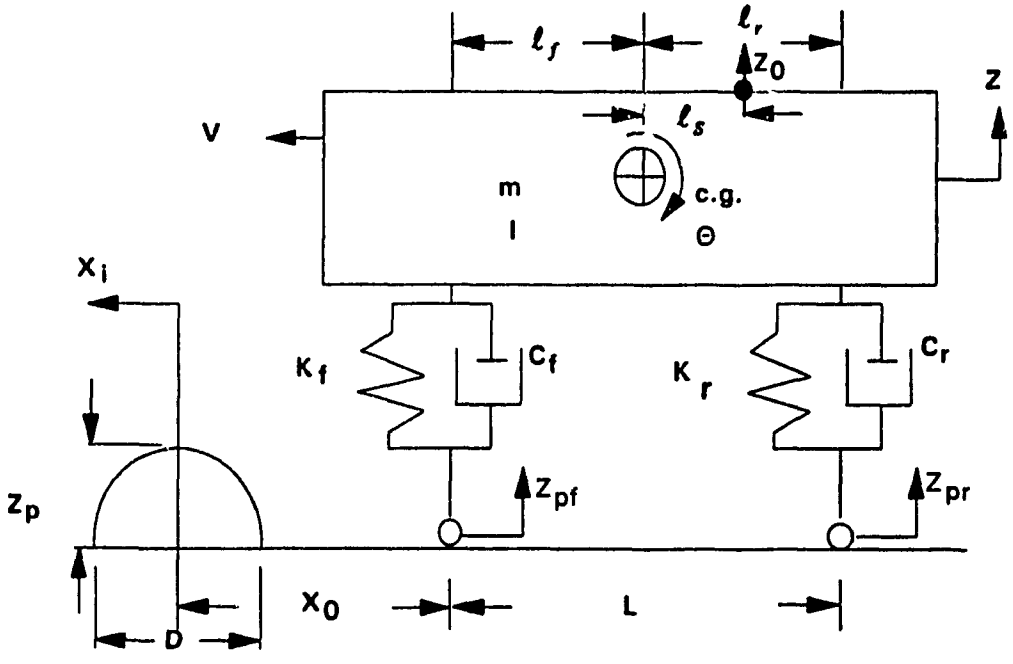

Figure 2.13 Model representation of a log skidder vehicle subject to a half-sine pulse displacement.

$$z_{pi} = 0; \quad |x_i| \geq D/2 \quad ; \qquad i = f,r$$

$$z_{pi} = z_p \sin\left(\pi Vt/D\right); \quad -D/2 \leq x_i \leq D/2 \; ; \qquad i = f,r \qquad (2.4)$$

where z_p represents the peak obstacle pulse height, z_{pi} is the excitation displacement at each wheel, and f and r denote the front and rear wheel, respectively. x_i is the horizontal coordinate of the wheel i with respect to the centre line of the bump. The wheel position is related to the vehicle speed in the following manner:

$$x_i = -x_0 + Vt; \qquad i = f$$

$$x_i = -(x_0 + L) + Vt; \qquad i = r \qquad (2.5)$$

where x_0 is the initial horizontal distance of the front wheel from the center line of the bump, and L is the vehicle wheelbase. Equations (2.4) and (2.5) reveal that the severity of shock excitation is strongly dependent upon the speed of the vehicle, V, and the peak displacement input or obstacle height, z_p. The characteristics of transient vertical excitations encountered at the seat attachment location, z_0, are related to the pitch-plane dynamics of the vehicle.

The equations of motion for vertical and pitch modes of the vehicle may be written in the following manner:

$$m\ddot{z} + F_{Tf}\left(z, z_{pf}, \theta, t\right) + F_{Tr}\left(z, z_{pr}, \theta, t\right) = 0.$$

$$I\ddot{\theta} + \ell_f F_{Tf}\left(z, z_{pf}, \theta, t\right) - \ell_r F_{Tr}\left(z, z_{pr}, \theta, t\right) = 0. \qquad (2.6)$$

where m is the vehicle mass supported by the tires, I is the pitch mass moment of inertia of the vehicle about its center of mass, ℓ_f and ℓ_r are the longitudinal distances from the center of gravity and the front and rear axles, respectively. F_{Tf} and F_{Tr} are the forces developed by the front and rear tires, respectively. Assuming linear stiffness constants (K_f and K_r) and viscous damping coefficients (C_f and C_r) of the tires, and negligible wheel hop of the soft tires used in these vehicles, the tire forces are derived as:

$$F_{Tf}\left(z, z_{pf}, \theta, t\right) = K_f\left(z + \ell_f\theta - z_{pf}\right) + C_f\left(\dot{z} + \ell_f\dot{\theta} - \dot{z}_{pf}\right)$$

$$F_{Tr}\left(z, z_{pr}, \theta, t\right) = K_r\left(z - \ell_r\theta - z_{pr}\right) + C_r\left(\dot{z} - \ell_r\dot{\theta} - \dot{z}_{pr}\right) \qquad (2.7)$$

Table 2.3 lists the model parameters for a log skidder. The coupled differential equations of motion, (2.6), are solved to yield the vertical and pitch displacement response of the vehicle centre of mass. The vertical displacement excitation at the seat attachment location is then computed from the foliowing constraint equation, assuming small pitch motion:

$$z_0 = z - \ell_s\theta \qquad (2.8)$$

where ℓ_s is the horizontal distance of the seat attachment with respect to the center of mass of the vehicle. A free vibration analysis of the vehicle model was performed to determine its pitch and vertical mode resonant frequencies which were found to be 1.5 and 2.6 Hz, respectively. The vertical mode resonant frequency agrees well with the dominant frequency described for ISO 2 class of excitation and with the field measured excitation for log skidder vehicles [36]. The pitch mode frequency also correlates well with the range of dominant frequencies observed in various measurements reported in the literature [37].

TABLE 2.3

Model Parameters for the Vehicle Driving over a Half-Sine Displacement Pulse.

Description	Symbol	Value
Tire Stiffness, front (N/m)	K_f	998910
Tire Damping, front (Ns/m)	C_f	6115
Tire Stiffness, rear (N/m)	K_r	998910
Tire Damping, rear (Ns/m)	C_r	6115
Total mass of vehicle (kg)	m	7486
Pitch mass moment of inertia of vehicle (kgm^2)	I	45384
Distance from c.g. to the seat base (m)	ℓ_s	0.25
Distance from c.g. to front axle (m)	ℓ_f	1.65
Distance from c.g. to rear axle (m)	ℓ_r	1.14

Solution of the linear second order differential equations described by (2.6) and (2.7) is accomplished in the time domain using a Runge-Kutta numerical integration algorithm [38].

A set of ten different shock excitation motions were defined at the seat attachment point for vehicle speeds ranging from 1 to 10 km/h. The obstacle width, D, was set equal to 200 mm while the height, z_p, was fixed at 75 mm. The total integration time was thus selected as a function of the vehicle wheelbase and the speed. The resulting acceleration signal had still further to be synthesized to provide the displacement signals necessary to drive the WBVVS. Figure 2.14 describes schematically the signal processing steps involved in the synthesis, including double integration of the acceleration signal and removal of the offsets created by the integrations through regression and proper filtering.

2.6 Summary

The ride vibration environment of four classes of wheeled off-road vehicles are identified and synthesized to study the response characteristics of the driver and driver-suspension seat system. The synthesized vibration spectra are generated using a dedicated whole-body vehicular vibration simulator (WBVVS). The simulator is designed to generate the vertical vibration spectra with enhanced safety control loops. Furthermore, the shock motions encountered

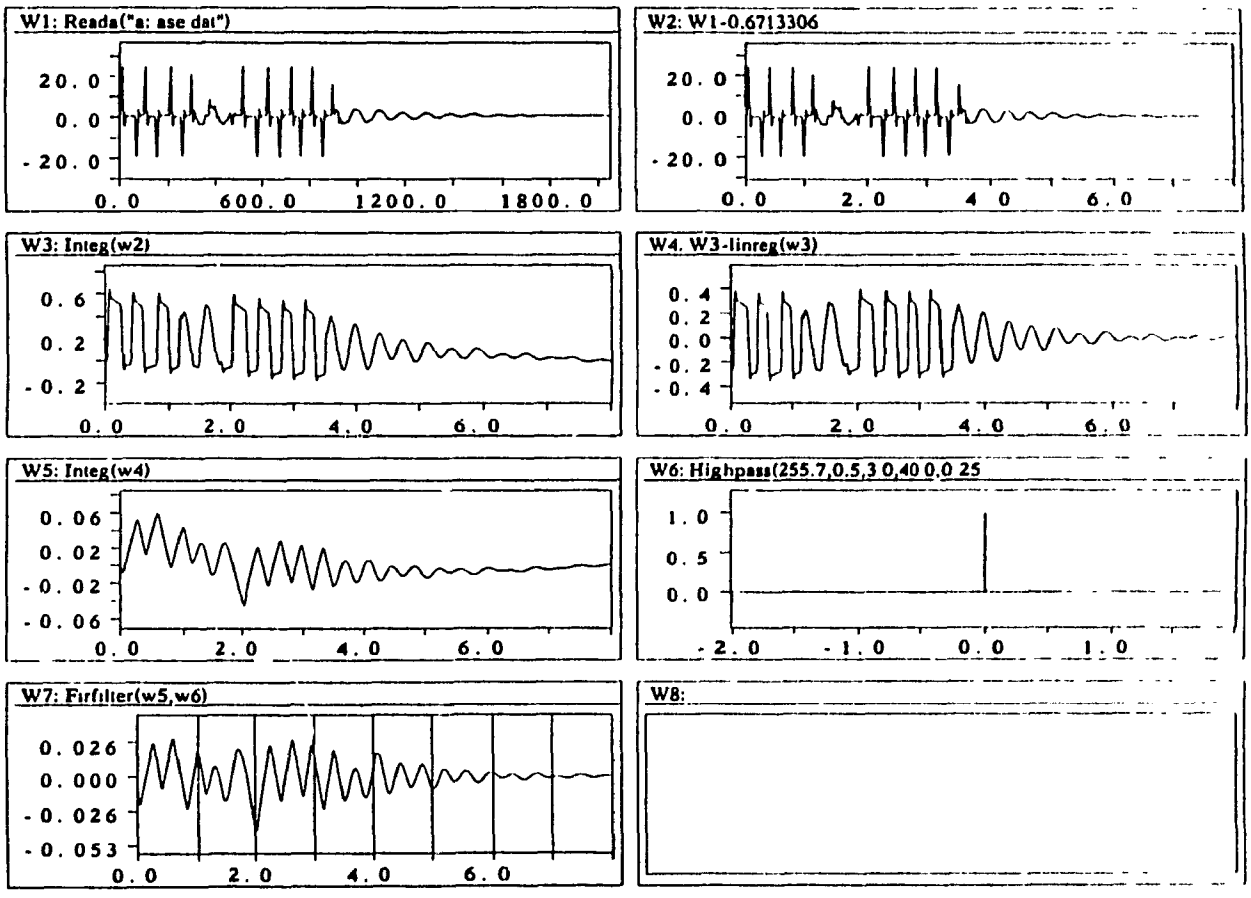

Figure 2.14 Signal synthesis steps involved in the transformation of acceleration to displacement shock excitations.

while driving a class of forestry vehicles over discrete obstacles are synthesized over a range of vehicle speeds to provide means of studying the shock isolation performance of the seats. Deterministic harmonic motion swept in the 0.625 to 10 Hz frequency range is also synthesized. The WBVVS serves as a unique tool that can effectively be used to study the combined driver-suspension seat response to whole-body vibration and shock under laboratory test conditions, while including enhanced safety features for the test subjects.

CHAPTER 3

SUSPENSION SEAT: MODEL DEVELOPMENT, VALIDATION AND RESPONSE ANALYSES

3.1 Introduction

Many vertical and longitudinal passive suspension seats have been commercially developed for off-road vehicles [39]. These include under-the-seat and behind-the-seat suspensions and may present differences owing to their construction (i.e. type of cushion, linkage, shock absorber), dimensions and basic accessories (i.e. backrest, armrest, lumbar support, etc.), type of suspension (i.e. mechanical or pneumatic) and the availability of various adjustments to modify such settings as the seating height, the cushion and backrest angles, the fore-aft position, and the static mid-ride position [40]. In view of the low natural frequency of off-road vehicle vibration (near 2.5 Hz), the vertical seat suspensions are designed with low natural frequency springs, light damping, and motion limiting compression and extension stops to limit the excessive suspension deflection. While longitudinal seat suspensions are frequently employed in road vehicles, these suspension systems are seldom applied to off-road vehicles due to large slopes encountered on the off-road terrain.

Development of an analytical suspension seat model necessitates adequate

consideration of the realistic static and dynamic characteristics of the basic components including the cushion, the suspension spring, the bump-stops and the shock absorber. Dynamic characteristics of the human driver also need to be considered in order to formulate an effective driver-suspension seat model. As a first approximation, however, a rigid body representation of the human driver may be considered appropriate in view of the fact that off-road vehicle vibration dominates around low frequencies. Mechanical impedance characteristics of the seated human body reveal in fact a behaviour similar to that of a rigid mass up to approximately 2 Hz [41].

Vertical suspension seats, irrespective of the linkage and suspension type can be characterized by a two-degree-of-freedom dynamic system, while neglecting body dynamics. An analytical model incorporating a rigid driver mass and nonlinearities due to shock absorber damping, Coulomb friction force and elastic limit stops has been proposed and studied by Rakheja [42,43]. The linearized suspension seat model, validated under constant displacement sinusoidal excitations, was used to predict the overall ride performance of the suspension seat under ISO 2 random excitations. One and two-degree-of-freedom models of the human body, as defined in the literature [34,41], were later incorporated to estimate the contributions due to driver dynamics.

In view of the strong nonlinearities of the seat suspension, and the ride

vibration environment comprising random and shock motions, the nonlinear analytical model of the suspension seat needs to be validated for realistic vibration and shock motions. The complexities associated with the dynamics of the seated driver further necessitate the analysis and validation of a reliable driver-suspension seat model under realistic vibration excitations. The need for the realization of reliable seat and driver models is further recognized to derive optimal suspension parameters under shock and random vibration environments. As a first step towards realizing this goal, this chapter is devoted to the validation and response analyses of a nonlinear suspension seat model under deterministic sinusoidal sweep motion and four classes of random vibration excitations defined in the preceeding chapter.

3.2 Analytical Model of the Suspension Seat

The vertical suspension seat system is characterized by a two-degree-of-freedom dynamic system, assuming negligible dynamics due to the seated human body as shown in Figure 3.1. Additional assumptions associated with the model are: i) transverse stiffness of the cushion is assumed to be very high such that the visco-elastic properties of the cushion along the vertical axis may be characterized by equivalent linear stiffness and damping coefficients within the operating range; ii) Coulomb friction due to shock absorber seals and various linkage joints is assumed to possess ideal characteristics; iii) the resilient means of the suspension system is modeled as a vertical spring with linear

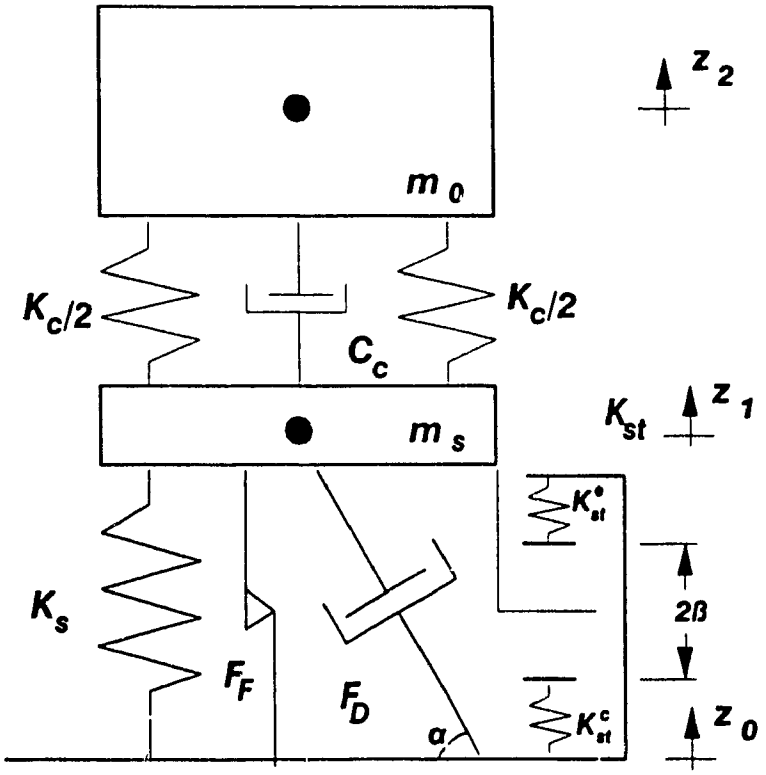

Figure 3.1 Nonlinear suspension seat model [27].

stiffness coefficient; iv) the shock absorber is modeled as a nonlinear damper incorporating bleed and blow-off stages; v) motions along the generalized coordinates are assumed to be small relative to overall dimensions of the seat; vi) the seat is considered to move in the vertical direction only; and vii) the dynamics due to the seated driver are considered negligible.

The equations of motion of the nonlinear suspension seat model are derived as:

$$m_s\ddot{z}_1 + F_s(x_1,\beta) + F_K(x_1) + F_F(\dot{x}_1) + F_D(\dot{x}_1,\alpha) - F_c(x_2,\dot{x}_2) = 0.$$

$$m_0\ddot{z}_2 + F_c(x_2,\dot{x}_2) = 0. \qquad (3.1)$$

where m_v is the effective mass of the seated driver, and m_s is the suspension mass. z_1 and z_2 represent vertical displacements of the suspension and operator masses, respectively. $x_1 = (z_1-z_0)$ and $x_2 = (z_2-z_1)$, represent the relative vertical displacements between the suspension mass and the base, and between the driver mass and the suspension. z_0 represents vertical displacement excitation at the base of the seat. The total suspension force developed by the cushion is expressed as:

$$F_c(x_2,\dot{x}_2) = K_c x_2 + C_c\dot{x}_2 \qquad (3.2)$$

where K_c and C_c are linear stiffness and damping coefficients of the cushion, respectively. F_K, F_F, and F_s are the suspension forces due to suspension spring, Coulomb friction, and bump stons, respectively, given by:

$$F_K(x_1) = K_s\, x_1 \tag{3.3}$$

$$F_F(\dot{x}_1) = F_C\, \mathrm{sgn}(\dot{x}_1) \tag{3.4}$$

$$F_S(x_1, \beta) = K_{st} S[x_1 - \beta\, \mathrm{sgn}(x_1)] \tag{3.5}$$

where K_s is the suspension spring rate, F_C is the magnitude of Coulomb friction, and K_{st} is the spring rate of the bump stops. The K_{st} may assume different values corresponding to compression and rebound. The nonlinear functions S and sgn(.) are given by :

$$S = 1; \quad \text{for} \quad |x_1| > \beta; \quad \text{and } S = 0; \quad \text{for} \quad ; |x_1| < \beta$$

$$\mathrm{sgn}(.) = +1 \; ; \quad \text{for } (.) > 0 \text{ and } -1 \; ; \quad \text{for } (.) < 0 \tag{3.6}$$

where β is the maximum permissible travel from mid-ride position. F_D is the suspension force due to the shock absorber, which provides high damping coefficient C_H due to bleed damping at low velocities and a low damping coefficient C_L due to blow-off valves at high velocities [44]. The transition from high to low damping occurs at a preset velocity V_s. Figure 3.2 illustrates

a schematic of a typical shock absorber with symmetric valving in compression and rebound, along with the corresponding force-velocity characteristics [27]. The damping force developed by the shock absorber is thus related to the relative velocity and its angle of inclination, α, assumed to be constant for the type of suspension considered:

$$F_D(\dot{x}_1,\alpha) = C_H \dot{x}_1 \sin^2\alpha \quad ; \quad |\dot{x}_1 \sin\alpha| \le V_s \tag{3.7}$$

$$F_D(\dot{x}_1,\alpha) = \left[C_H V_s \operatorname{sgn}(\dot{x}_1) + C_L \left\{ \dot{x}_1 \sin\alpha - V_s \operatorname{sgn}(\dot{x}_1) \right\} \right] \sin\alpha \quad ; \quad |\dot{x}_1 \sin\alpha| \ge V_s$$

Equations (3.1) to (3.7) describe the dynamics of the nonlinear suspension seat with negligible dynamics due to the seated driver.

3.3 Identification of Model Parameters

Since the vertical vibration environment of off-road vehicles is predominantly around low frequencies, the seat suspension must be relatively soft in order to achieve a resonant frequency below $1/\sqrt{2}$ times the dominant excitation frequency. The dynamic relative travel of the soft suspension system, however, must be limited such that the driver motion does not interfere with safe driving of the vehicle. Based on the vertical vibration characteristics of a log skidder and on basic ergonomic principles, a suitable suspension seat for such vehicles should possess [40]:

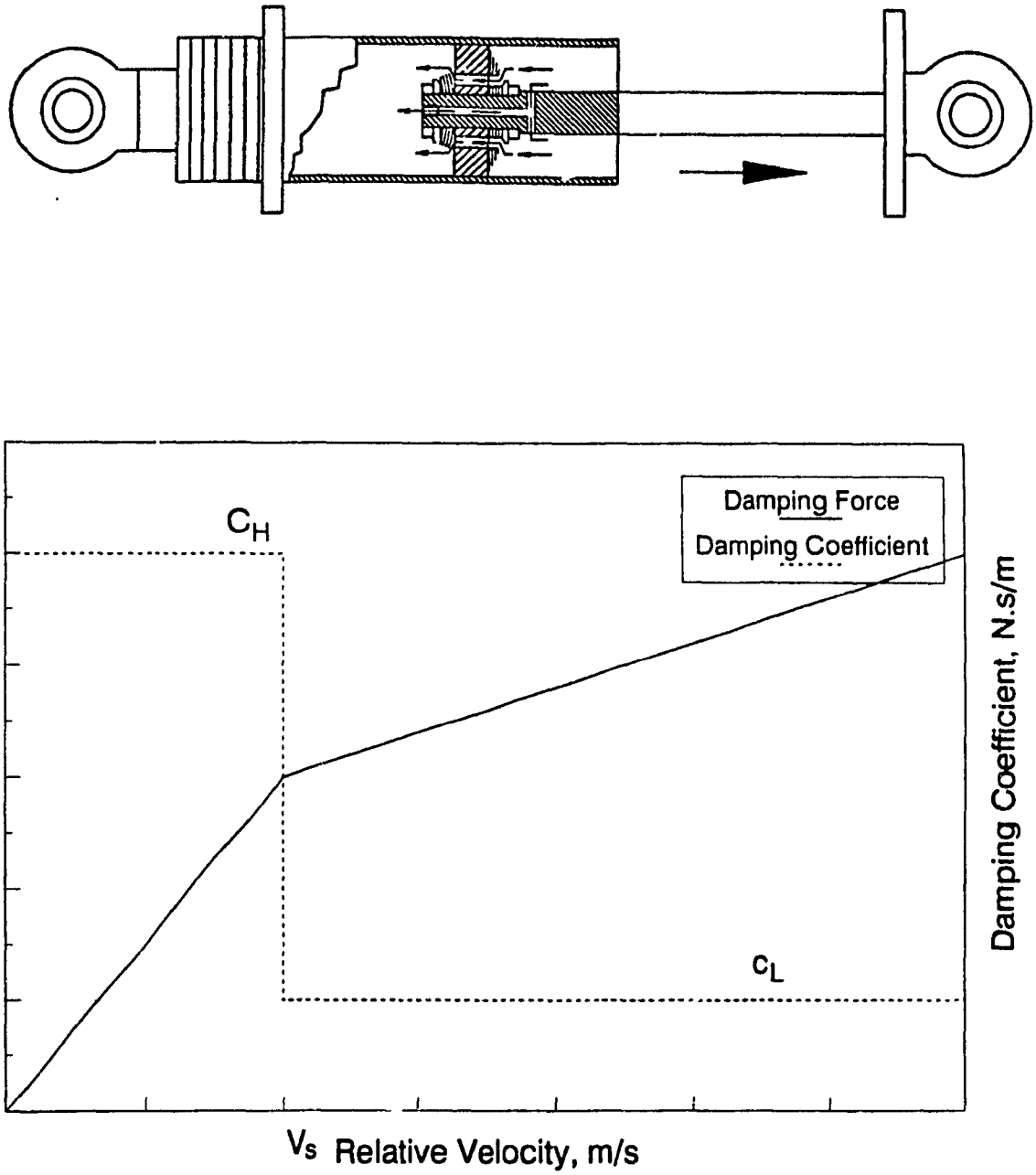

Figure 3.2 Schematic of a nonlinear shock absorber incorporating bleed and blow-off stages and associated force-velocity characteristics.

- a resonant frequency lower than 1.8 Hz;
- a cut-off frequency lower than 2.5 Hz;
- a weight compensation mechanism independent of height adjustment;
- a total relative travel lower than 100 mm;
- a transmissibility ratio not exceeding 2.0 at the seat's resonant frequency;
- a "Seat Effective Amplitude Transmissibility" (S.E.A.T.) value of less than 1.0.

Here the S.E.A.T. is defined as the ratio of overall frequency-weighted acceleration at the driver mass-seat interface to that at the floor:

$$S.E.A.T. = \frac{a_{w,seat}}{a_{w,floor}} \tag{3.8}$$

The seat vibration acceleration transmissibility, T(f), at an excitation frequency, f, is defined as:

$$T(f) = \frac{|\ddot{z}_2(f)|}{|\ddot{z}_0(f)|} \tag{3.9}$$

where the absolute values denote the magnitudes of the rms accelerations, $\ddot{z}_2(f)$ at the driver mass-seat interface, and $\ddot{z}_0(f)$ at the base of the seat.

A suspension seat (SIFRA) with behind-the-seat suspension, as depicted in Figure 3.3, was known to potentially meet these vibration requirements in addition to having the necessary dimensions to adapt to the relatively limited space available in the candidate vehicle cabin. The suspension seat parameters have been identified from the static and dynamic tests performed in the laboratory [45]. The stiffness and damping coefficients (K_c and C_c) due to the cushion were identified from the static and dynamic force-displacement characteristics of the cushion. Force-deflection properties of the suspension system were analyzed to derive the spring rate (K_s), the magnitude of static friction (F_C), and the stiffness coefficients of the elastic limit stops in compression and extension. The magnitude of dynamic friction was estimated from the vibration transmissibility tests performed in the laboratory. Damping properties of the shock absorber were estimated from the force-velocity characteristics supplied by the manufacturer. Various parameters of the suspension seat, identified from the laboratory tests and the manufacturer's specifications, are summarized in Table 3.1.

3.4 Suspension Seat Model Response Evaluations

The nonlinear differential equations of motion represented by (3.1) may be solved in the time domain using direct integration routines such as the fourth-order Runge-Kutta method to determine the analytical driver mass response or the base-to-seat acceleration transmissibility defined by equation (3.9).

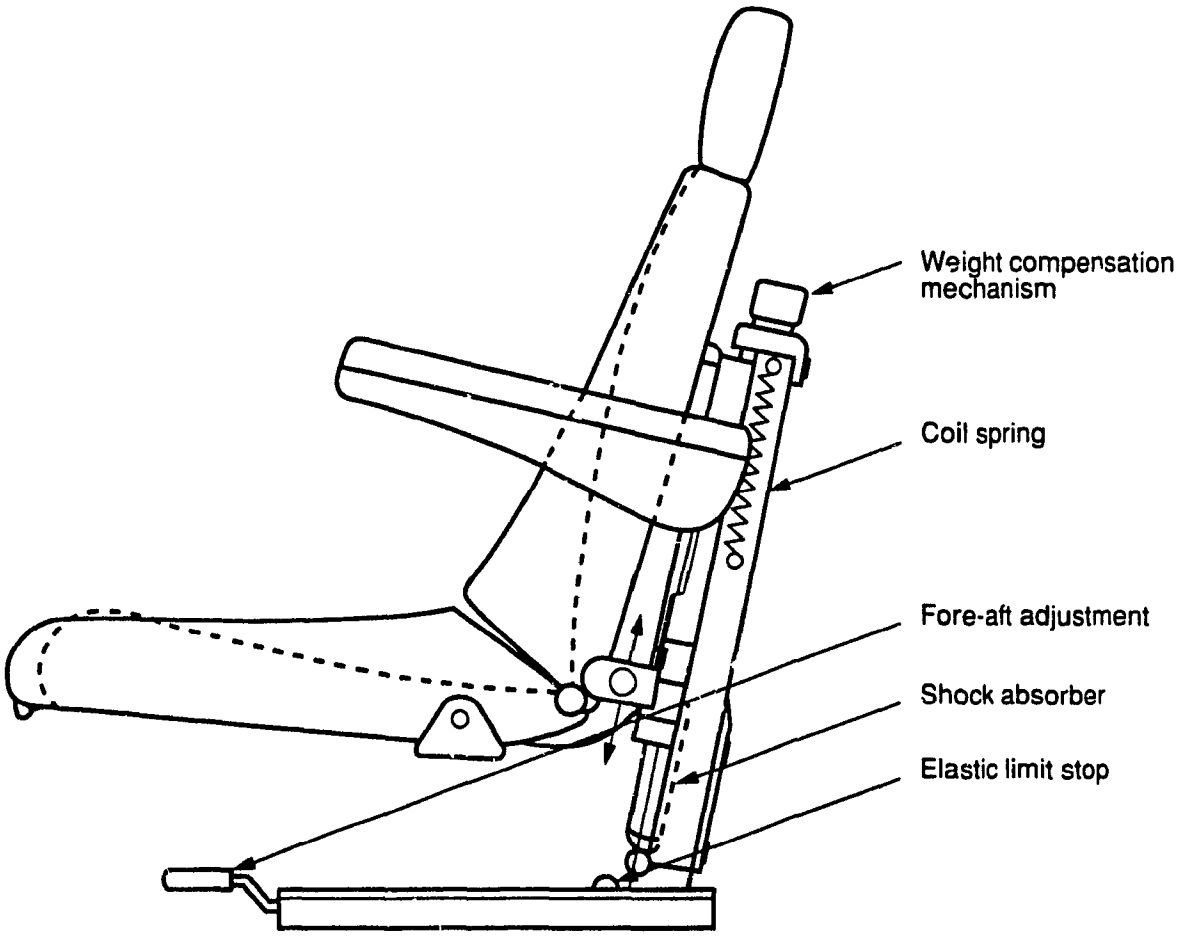

Figure 3.3 Schematic of the SIFRA suspension seat.

Alternatively, the solution may be sought by transforming the time-domain equations into frequency-domain equations using the Fourier Transform technique. However, the application of such technique requires that the equations be linear or at least, expressed in terms of an equivalent linear system. As a second prerequisite, the frequency spectrum of the excitation motion is required to be known for this technique to be applicable. These two methods of solution are presented below.

TABLE 3.1

Model Parameters for the Suspension Seat

Description	Symbol	Value
Mass of driver or rigid load (kg)	m_0	63.6
Cushion stiffness (N/m)	K_c	82300
Cushion damping (Ns/m)	C_c	300
Suspension mass (kg)	m_s	10
Suspension spring stiffness (N/m)	K_s	5330
Coulomb friction force (N)	F_C	15
Shock absorber damping coefficients (Ns/m)	C_H C_L	790 672
Damping transition velocity (m/s)	V_S	0.032
Shock absorber angle (radians)	α	1.22
Bump stop stiffness (kN/m) -compression -extension	K_s' K_s'	120 75
Total travel between bump stops (mm)	2β	100

3.4.1 TIME DOMAIN SOLUTION

The differential equations of motion for the nonlinear suspension seat are solved in the time domain using the fourth-order Runge-Kutta method. Under sinusoidal excitation, the equations are solved at selected frequencies of excitation to evaluate the base-to-seat acceleration transmissibility,T(f), as described in equation (3.9). Under random excitation, the differential equations of motion (3.1) are solved for synthesized time histories of vehicular vibration to evaluate the time response of the driver mass, $\ddot{z}_2(t)$. Fast Fourier Transform techniques are then applied to derive the vibration acceleration power spectral density (PSD), and root-mean-square (rms) acceleration of the driver mass response [38].

3.4.2 FREQUENCY DOMAIN SOLUTION

Frequency domain solutions are often of more interest than the time history and can usually be performed more conveniently than in the time domain. However, for the solutions to be applicable, the equations must either be linear, or linearized. Several analytical techniques have been developed to solve nonlinear systems [46]. Of these, a technique based on the principle of energy similarity may be applied to formulate local equivalent constants, where each local constant is considered valid in a narrow frequency band centered around a selected excitation frequency [4,47]. Equivalent linearization techniques may be applied to replace the nonlinear dissipative and restoring

functions, present in equations (3.1), by equivalent linear functions [48]. The gains of the linear functions are selected such that the linearized response does not deviate considerably from the nonlinear system's response.

It has been established that nonlinearities such as Coulomb friction, shock absorber damping force, and bump stops restoring force cannot be accurately characterized by equivalent global constants. Such nonlinearities may be characterized by an array of local constants as a function of the local excitation frequency and amplitude, using a local equivalent linearization technique [49]. Each local constant accurately characterizes the nonlinear system's response only in the vicinity of selected excitation frequencies and excitation amplitudes. The nonlinear system's response in the entire frequency range is characterized from the solution of an array of a local equivalent linear system.

In view of the suspension seat nonlinearities, the technique described above is applied to evaluate the local equivalent stiffness and damping coefficients due to nonlinear bump stops, Coulomb friction, and shock absorber damping upon equating the dissipated and processed energy of the nonlinear elements to those of the linear ones [27]. The nonlinear differential equations are then expressed by an array of linear equations, given by:

$$[M]\{\ddot{q}\}+[C_e]\{\dot{q}\}+[K_e]\{q\}=[C_f]\{\dot{q}_o\}+[K_f]\{q_o\} \qquad (3.10)$$

where [M], [C_e] and [K_e] are (2x2) matrices of mass, local equivalent damping and local equivalent stiffness coefficients, respectively. [C_f] and [K_f] are forcing matrices of local equivalent damping and stiffness coefficients, {q} and {q_o} are response and excitation vectors, respectively.

The local equivalent damping constants due to Coulomb friction and shock absorber damping are evaluated by equating the energy dissipated per cycle by the nonlinear elements to that of a linear damper, $\pi C_e(\omega_k, X_1)\omega_k X_1^2$, where $C_e(\omega_k, X_1)$ is the local equivalent damping coefficient as a function of local excitation frequency, ω_k, and response relative magnitude, X_1 [27]. The energy dissipated per cycle, W_d, can be derived from:

Coulomb Damping: $$W_d = 4F_C X_1 \tag{3.11}$$

Shock Absorber Damping: $$W_d = \pi\omega_k X_1^2 C_H \sin^2\alpha; \quad for\ \omega_k X_1 \sin\alpha \le V_S$$

$$W_d = 4\sin\alpha\left[\int_0^{t_1} C_H V_S \omega_k X_1 \cos\omega_k t\, dt + \int_{t_1}^{\pi/2\omega} C_L \omega_k (\omega_k X_1 \sin\alpha\cos\omega_k t - V_S) X_1 \cos\omega_k t\, dt\right];$$

$$for\ \ \omega_k X_1 \sin\alpha \ge V_S \tag{3.12}$$

where t_1 represents the time at which the shock absorber piston velocity approaches V_S, given by:

$$t_1 = \frac{1}{\omega_k}\cos^{-1}\left[\frac{V_s}{\omega_k X_1 \sin\alpha}\right] \qquad (3.13)$$

The equivalent stiffness coefficients due to bump stops are derived from the processed energy, W_p, in a similar manner:

$$W_p = 0.; \text{ for } x_1 \leq \beta \qquad (3.14)$$

$$W_p = 2\left[\int_{t_2}^{\pi/2\omega} \left|K_{st}^c(x_1 - \beta)\right| \dot{x}_1 dt + \int_{t_2}^{3\pi/2\omega} \left|K_{st}^e(x_1 - \beta)\right| \dot{x}_1 dt\right] ; \text{ for } x_1 > \beta$$

where t_2 is the time at which the suspension deflection approaches the permissible travel, β , given by:

$$t_2 = \frac{1}{\omega_k}\sin^{-1}\left|\frac{\beta}{X_1}\right| \qquad (3.15)$$

K_{st}^c and K_{st}^e represent the compression and extension bump stop stiffness constants, respectively. The local equivalent stiffness coefficient due to bump stops is determined by equating the processed energy to that of a linear spring, $2\, K_e(\omega_k, X_1)\, X_1^2$.

Determination of local equivalent constants from equations (3.11) to (3.15)

however, necessitates prior knowledge of the relative displacement response X_1. An iterative algorithm, described in [4], is applied to derive the local equivalent linear suspension seat model parameters. Using this scheme, initial values of equivalent viscous damping and stiffness coefficients, C_s^0 and K_s^0, are assumed at an excitation frequency, ω_k. The linearized equations of motion (3.10) are then solved for the displacement and velocity response vectors. The relative displacement response, X_1, is then derived using the coordinate transformation. The corresponding local equivalent damping and stiffness coefficients, C_s^l and K_s^l, are computed by applying the relations developed in (3.11) to (3.15). The magnitude of errors between the assumed and computed values is then evaluated and the entire procedure is repeated until convergence is achieved. This process is repeated at each successive excitation frequency, ω_k, to derive the local equivalent coefficients over the entire frequency range of interest.

The local equivalent system of equations thus derived, equation (3.10), is solved to yield the complex frequency response function matrix, $[H(j\omega_k)]$, using the Fourier Transform technique:

$$[H(j\omega_k)] = \left[\left[K_s(\omega_k, X_1)\right] - \omega_k^2[M] + j\omega_k\left[C_s(\omega_k, X_1)\right]\right]^{-1}\left[\left[K_f(\omega_k, X_1)\right] + j\omega_k\left[C_f(\omega_k, X_1)\right]\right] \quad (3.16)$$

The magnitude of vibration transmissibility at the driver mass, analogous to that given by equation (3.9), may then be obtained from:

$$|T(\omega_k)| = \sqrt{h_{21}(j\omega_k)h_{21}^*(j\omega_k)} \tag{3.17}$$

where $h_{21}(j\omega_k)$ represents the complex frequency response of mass m_0 due to the excitation acting at the base of the suspension-mass system, and "*" designates the complex conjugate.

3.4.3 RESPONSE UNDER RANDOM EXCITATION

Denoting the Fourier Transforms of the response and excitation vectors, {q} and $\{q_0\}$, respectively, by $\{Q(j\omega_k)\}$ and $\{Q_0(j\omega_k)\}$, the Fourier Transform of equation (3.10) may be written as:

$$\{Q(j\omega_k)\} = [H(j\omega_k)]\{Q_0(j\omega_k)\} \tag{3.18}$$

Alternately, the vector PSD of response coordinates, $\{S(j\omega_k\}$, may be derived from the frequency response function and PSD vector of the input excitation $\{S_0(j\omega_k)\}$:

$$\{S(j\omega_k)\} = [H(j\omega_k)][H^*(j\omega_k)]^T \{S_0(j\omega_k)\} \tag{3.19}$$

where "^{T}" denotes the transpose. Subsequently, the root-mean-square (rms) response at angular frequency, ω_k, may be determined by integrating the PSD response over a frequency band of width $\Delta\omega = \omega_2 - \omega_1$, centered at ω_k;

$$z_{i,rms}(\omega_k) = \sqrt{\int_{\omega_1}^{\omega_2} S_{ii}(j\omega_k) d\omega} \tag{3.20}$$

where $z_{i,rms}$ is the rms of the i^{th} response variable corresponding to the PSD, $S_{ii}(j\omega_k)$, at frequency ω_k.

3.4.4 VERIFICATION OF THE LINEARIZATION TECHNIQUE

The local equivalent linear model of the nonlinear suspension seat system is verified by comparing its vibration transmissibility response characteristics, equation (3.17), with the time domain solution derived from direct integration of the nonlinear differential equations. Figure 3.4 illustrates a comparison of the displacement transmissibility characteristics derived using the two methods for constant displacement sinusoidal excitations (0.03 m peak). Both time domain and frequency domain solutions are in excellent agreement except perhaps at frequencies below 0.5 Hz, where the largest discrepancies are attributed to high equivalent damping due to Coulomb friction associated with relatively small acceleration and relative displacement.

3.5 Model Validation under Sinusoidal and Random Excitations

The validation of the analytical suspension seat model is accomplished via laboratory experimentation of the physical system (i.e. SIFRA seat) under different types of excitations synthesized by the WBVVS. Subsequently, the nonlinear differential equations of motion of the model can be solved to determine the analytical base-to-seat transmissibility or acceleration response of the driver mass using the techniques discussed in the previous section. These may then be compared to the measured laboratory data to qualify the analytical model under various types of excitations. In this section, validation of the analytical model is realized under sinusoidal sweep motion and the four random classes of off-road vehicle vibration, defined in Chapter 2. The test methodology is briefly described and the measured acceleration response at the seat is compared with the response characteristics of the analytical model for each excitation class.

3.5.1 SUSPENSION SEAT TEST METHODOLOGY

The SIFRA suspension seat was mounted on the platform of the WBVVS described in section 2.2. The seat was loaded with two sandbags representing the rigid load. The lower sandbag had a mass of 35 kg, on top of which was mounted a second sandbag of mass 28.6 kg resting against the backrest. A triaxial seat accelerometer, B&K 4322, was installed at the interface of the seat and the lower sandbag, with only the vertical z-axis motion ($\ddot{z}_2$) being

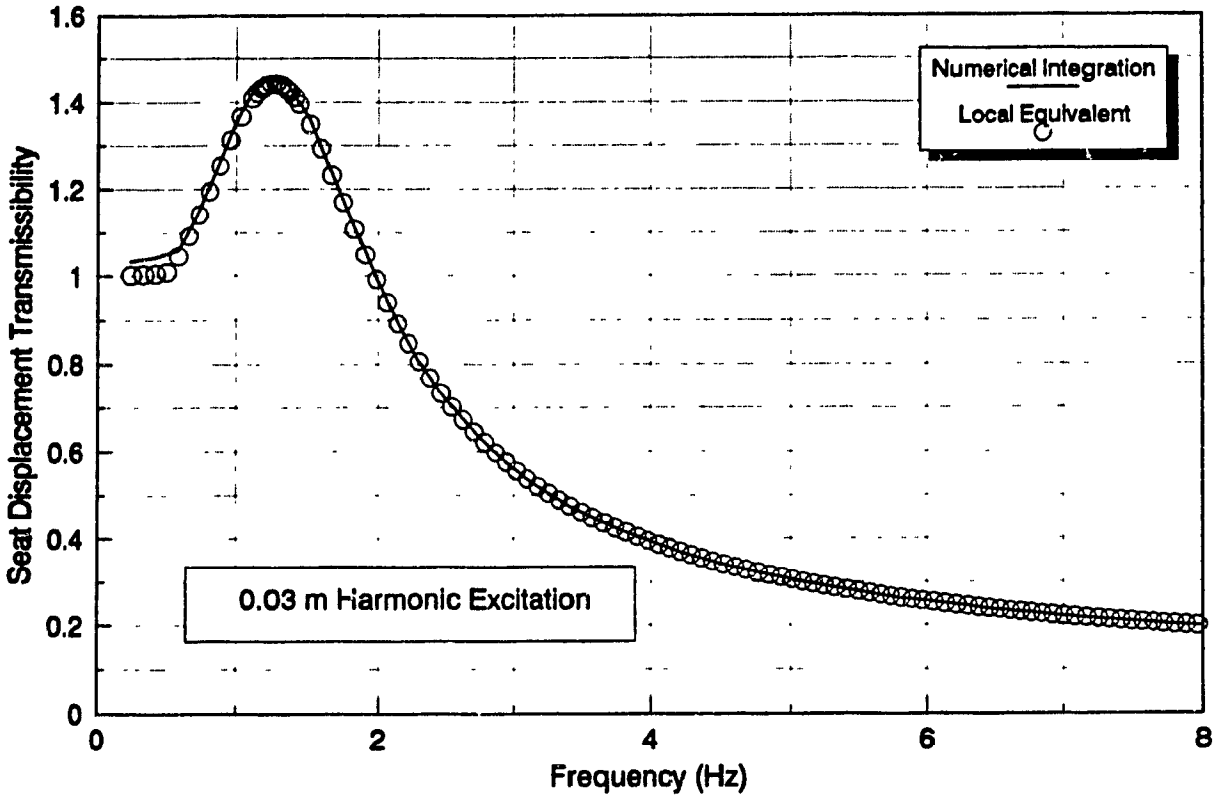

Figure 3.4 Comparison of the seat displacement transmissibility characteristics using different analytical methods.

monitored. Similarly, a single axis accelerometer was fixed on the simulator platform underneath the seat to monitor the input vibration to the suspension seat ($\ddot{z}_0$). The outputs of these accelerometers were linked to charge amplifiers followed by low-pass filters with variable cut-off frequencies. The resulting vibration signals were then monitored, analyzed and stored using a two-channel B&K 2035 signal analyzer The rms acceleration frequency spectra at the rigid mass-seat interface and at the base, and the vibration transmissibility characteristics could be directly produced from the acquired data, using the signal analyzer.

For the purpose of validating the analytical model, the SIFRA suspension seat was adjusted at mid-ride position by ensuring that the weight adjustment mechanism was set to 63.6 kg, representing the total mass on the seat. This adjustment was performed by setting the appropriate preload. When properly adjusted, this setting ensures equal suspension travel in compression and rebound with respect to the mid-ride position. As for the other available adjustments, the backrest angle was set at 90° to the horizontal and the cushion was positioned parallel to the floor. The seat height and fore-aft position were fixed and held constant during the entire test program.

The suspension seat with rigid load was tested using the following vibration excitations, defined in Chapter 2: sinusoidal sweep in the 0.625 to 10 Hz

frequency range, ISO 1, ISO 2, Class I and Class II random vibration defined for specific classes of off-road vehicles. Under sinusoidal excitation, the seat and rigid load were subjected to several sweeps of increasing and decreasing frequencies within the sweep range, and the resulting acceleration signals were filtered using a low-pass filter set at 20 Hz. Under the random excitation classes, the duration of the excitation was maintained sufficiently long to allow at least 1500 averages to be performed on the analyzer.

3.5.2 VERIFICATION OF THE SUSPENSION-SEAT MODEL

The vibration response characteristics of the suspension seat model are compared to those derived from the laboratory tests performed using the WBVVS, in order to demonstrate the validity of the analytical model. The nonlinear differential equations of motion are solved using the model parameters described in Table 3.1, to derive the acceleration response at the mass-seat interface. The acceleration response is presented in terms of acceleration transmissibility for harmonic sweep excitations, and in terms of rms acceleration for both harmonic and random excitations.

The response characteristics of the model are compared to those established from the laboratory measured data, as illustrated in Figures 3.5 to 3.9. Figure 3.5 illustrates a comparison of measured and model acceleration transmissibility and rms acceleration response under sinusoidal sweep excitation. Although the

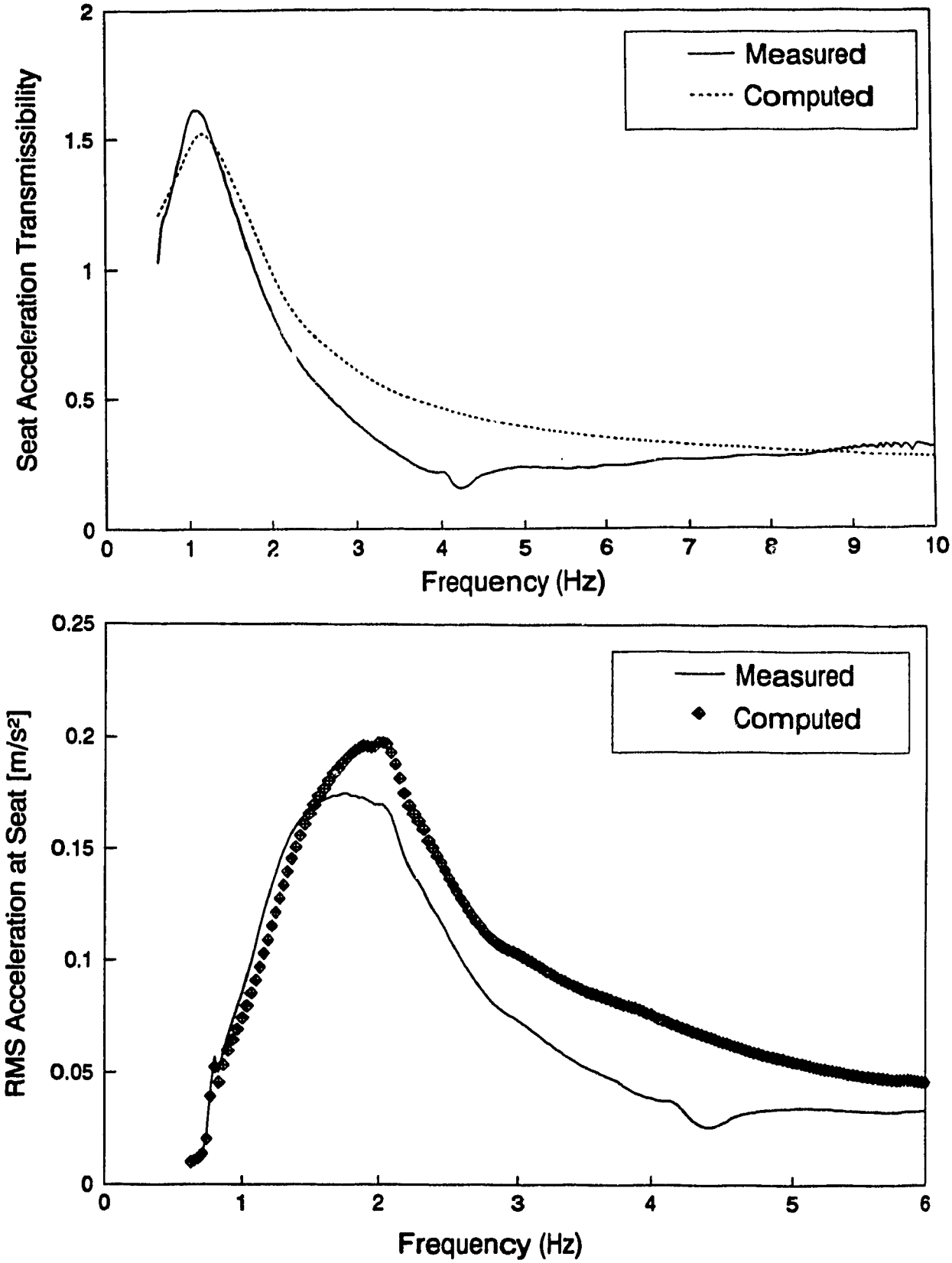

Figure 3.5 Comparison of measured and computed suspension seat response under sinusoidal sweep excitation.

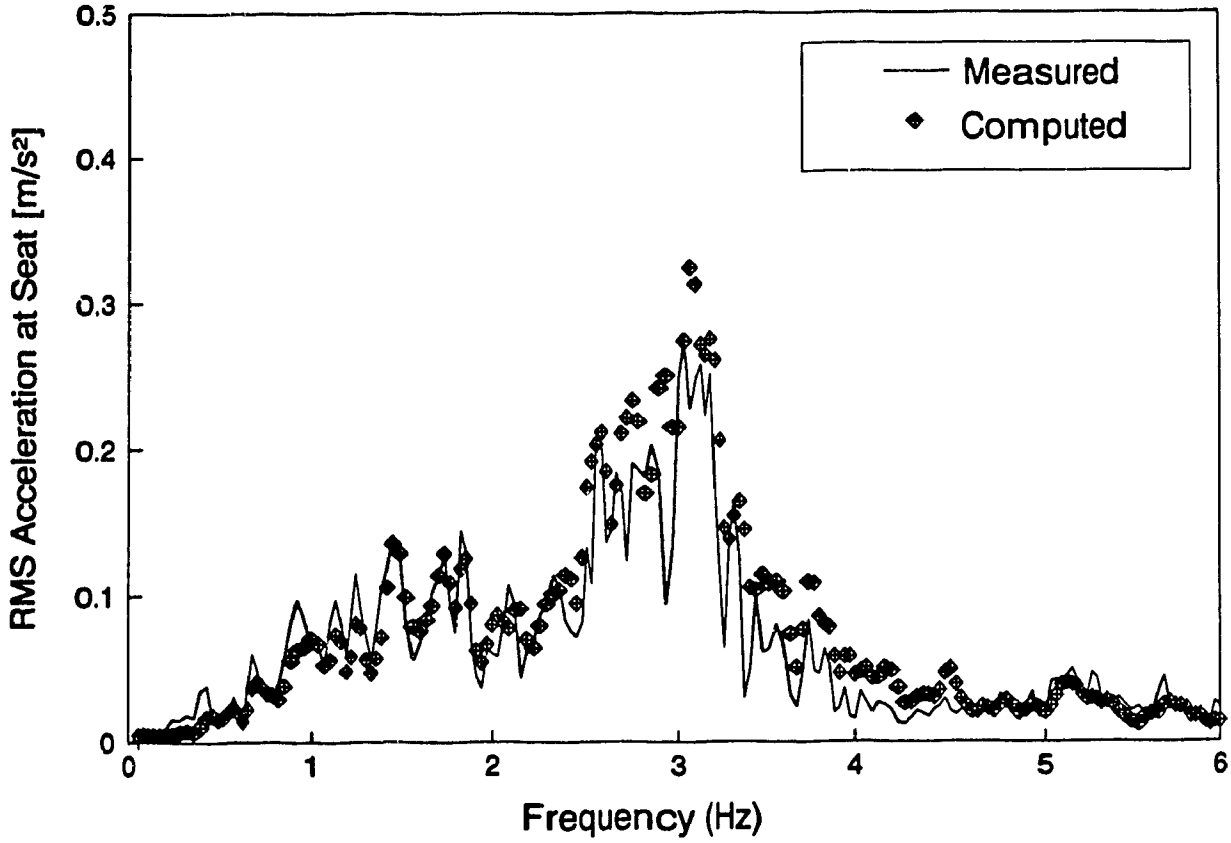

Figure 3.6 Comparison of measured and computed suspension seat response under ISO 1 class of random excitation.

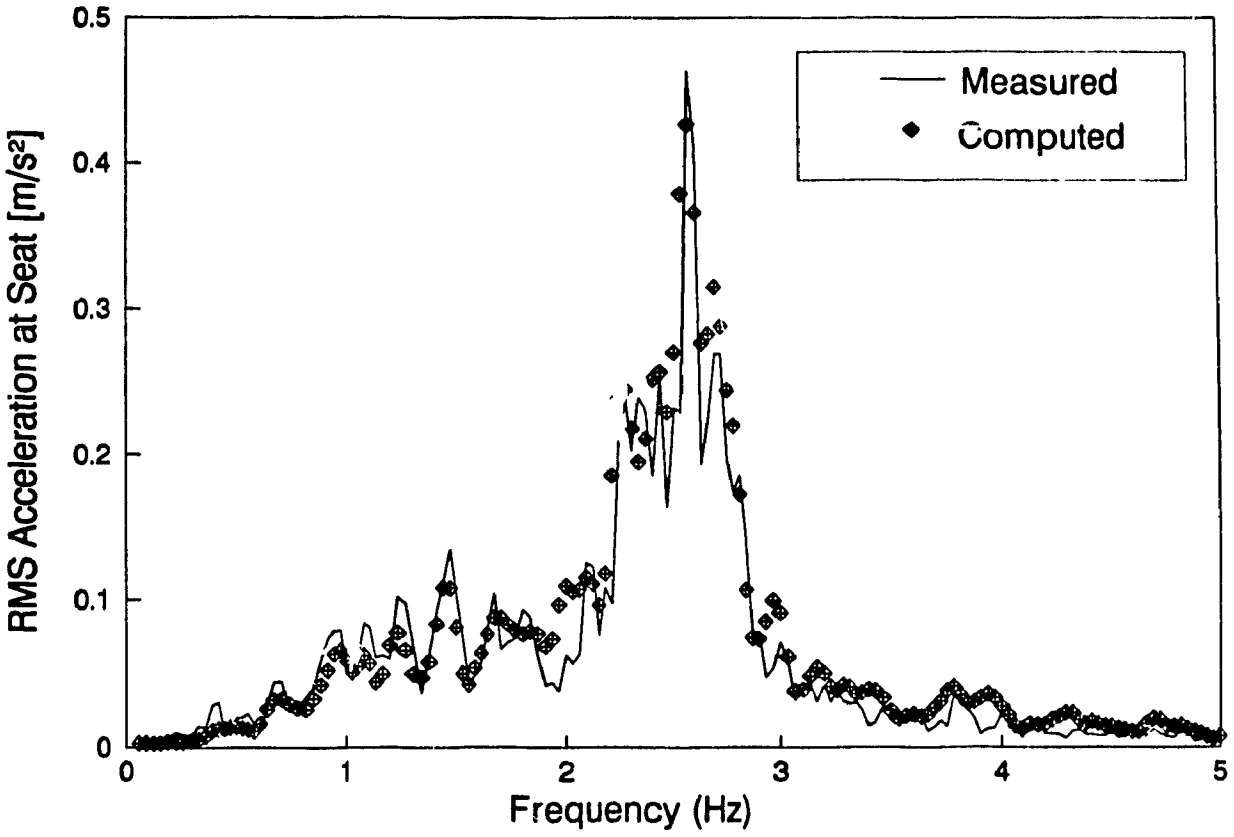

Figure 3.7 Comparison of measured and computed suspension seat response under ISO 2 class of random excitation.

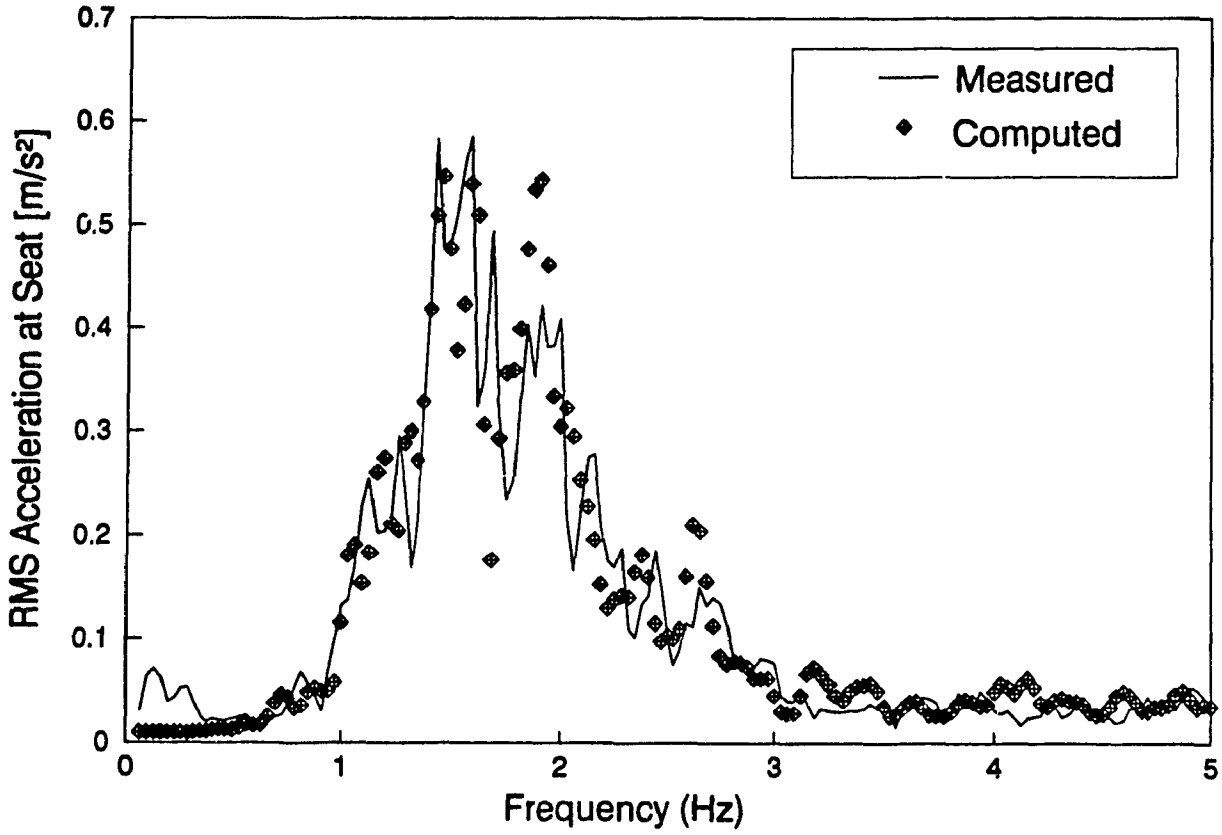

Figure 3.8 Comparison of measured and computed suspension seat response under Class I of random excitation.

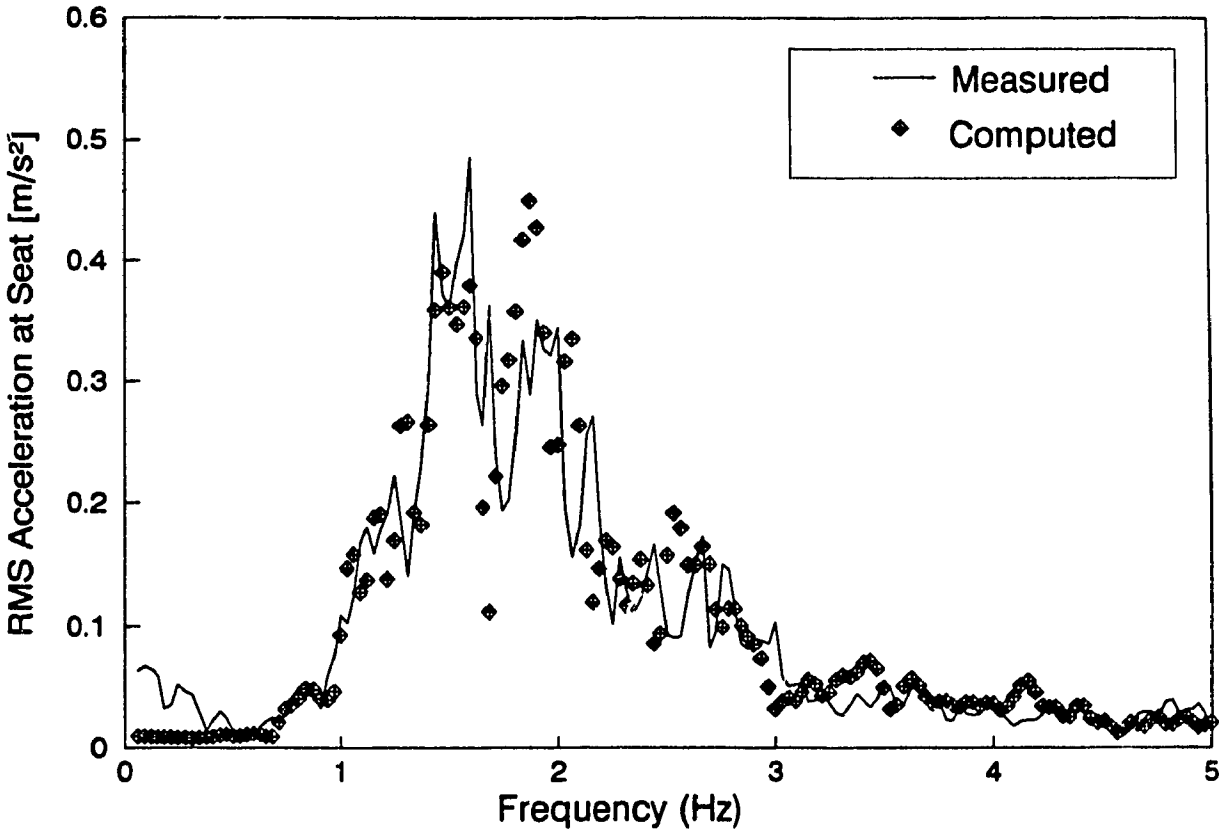

Figure 3.9 Comparison of measured and computed suspension seat response under Class II of random excitation.

model response exhibits trends similar to the measured response, the acceleration response of the model differs considerably from the measured response near the resonant frequency, and at frequencies above 1.5 Hz where the measured rms acceleration and base-to-seat acceleration transmissibility are lower than the computed values over most of the frequency range of interest. In the 2 to 3 Hz frequency range, the model overestimates the measured transmissibility by as much as 50%. Such discrepancies may be attributed to the averaging of the data during measurements, which resulted in a tendency to lower the measured values. It is to be noted that the model response is computed for a single frequency sweep unlike the repetitive sweeps and averaging used during laboratory tests. The averaging of the measured data may further result in an apparent excitation lower in amplitude than what is being assumed at each individual frequency when computing the model response. The acceleration transmissibility response depicted in Figure 3.5 also reveals the measured resonant frequency of the suspension seat-driver mass system slightly lower than that computed from the model, the latter being 1.3 Hz as opposed to 1.2 Hz derived from the measurements. The peak acceleration transmissibility measured at the resonant frequency is observed to be slightly higher at 1.7 than the 1.5 computed from the model.

Figures 3.6 to 3.9 indicate relatively good agreement between the measured and computed rms acceleration response at the driver mass-seat interface

derived under different random excitation classes, except in the neighbourhood of the predominant excitation frequency. Since the random excitations predominate in a relative narrow frequency band, depending upon the excitation class, the suspension seat response tends to be quite pronounced in that particular band. Outside this frequency band, the acceleration response tends to be masked by excessive noise due to very low level excitation. The acceleration transmissibility characteristics under such excitations have little significance, and are thus not presented.

Although under ISO 2 excitation, the computed model response is in close agreement with that measured (less than 10% difference), the model generally tends to overestimate the response by as much as 30% under the other classes of random excitations, particularly at the predominant excitation frequency. This tendency was also observed under sine sweep excitation in a similar frequency range, although the overestimation was more pronounced. In view of the high level of difficulty involved in determining the model parameters, the degree of correlation between computed and measured response is considered relatively good under the four classes of off-road vehicle vibration selected. Too large damping coefficient values might, however, have been assumed since the computed responses were usually larger than measured at frequencies above the seat resonant frequency. The error associated with the model may be considered within tolerable limits, thus providing a useful tool to further

study the response behaviour of coupled driver-suspension seat system, the influence of the suspension parameters on the vibration attenuation performance, and the optimal suspension design to minimize whole-body vibration exposure.

3.6 Parametric Analysis of the Suspension Seat Model

The effectiveness of a suspension seat in attenuating whole-body vibration is strongly dependent on the static and dynamic characteristics of the seat components such as cushion, suspension spring, shock absorber, suspension mass, Coulomb damping, and bump stops. A parametric sensitivity analysis in which a single parameter is changed at a time may provide a basis for deriving near optimal suspension seat parameters for specific excitations. Near optimal design parameters, however, are selected on the basis of a performance index or indices related to driver's response to whole-body vehicular vibration.

Since the preservation of health and safety of the driver under exposure to vehicular vibration is of primary concern, the performance indices are defined based on overall frequency-weighted and unweighted rms accelerations at the driver mass-seat interface. The parametric study is performed to study the influence of various suspension pararneters on the overall driver mass rms accelerations, and specifically for ISO 2 class of random excitation.

3.6.1 SELECTION OF PERFORMANCE INDICES

The current version of the ISO 2631/1 standard [18] proposes two different evaluation procedures for assessing exposure to broad-band whole-body random vibration. The first one, referred to as the "rating procedure", involves the derivation of the frequency spectrum of the vibration in one-third octave bands in the 1.0 - 80 Hz frequency range, and the estimation of the severity of the exposure from the frequency component having the most significant magnitude with respect to the specified limits for a set exposure duration (e.g. fatigue-decreased-proficiency limits defined in Figure 1.1). This method implies insignificant interactions between vibration effects of different frequencies and considers only the dominant frequency component as the primary indicator of vibration exposure. The proposed method further implies that the effect of broad-band vibration is considered analogous to that resulting from a pure sinusoidal motion with frequency and acceleration magnitude being equal to the dominant frequency component of the broad-band spectrum.

The second procedure, referred to as "weighting procedure", involves computation of the overall frequency-weighted acceleration over the 1.0 - 80 Hz frequency range, either in the time or frequency domain. The frequency response characteristics of the W_z weighting filter for vertical vibration have been illustrated in Figure 1.2. This procedure thus considers the contributions of all the different frequency components when assessing the severity of

vibration exposure. For vertical vibration, the standard suggests that the overall frequency-weighted acceleration be compared with the limits specified in the 4 - 8 Hz frequency range for estimating the severity of the exposure.

The two evaluation procedures, although equivalent under pure sinusoidal vibration, may lead to quite significantly different estimations of the exposure severity under broad-band random vibration, depending on the frequency spectrum distribution. The results of many experimental studies have supported the use of the weighting procedure, specifically for the assessment of broad-band random vibration [50]. Parsons and Griffin [51] assessed the ride comfort of individuals exposed to automobile vibration using the rating and weighting procedures, and concluded that the latter yields better correlation. Ever since the publication of ISO 2631, numerous studies have indicated the superiority of the weighting procedure over the rating or "worst component" method for estimating the discomfort produced by the motions. The revised ISO/DIS 2631-1 [12] retains the weighting procedure as the only assessment method, using either rms or rmq acceleration. However, a revised frequency weighting curve, W_k, which is slightly different from W_z, is identified for the assessment of vertical vibration at the driver-seat interface.

Since the primary objective of this part of the work is to provide suspension seat design criteria for reducing the severity of whole-body vibration exposure

of the driver, the performance indices selected must somehow be linked to the measure of vibration exposure itself. Based on the above, and in view of the frequency weighting networks defined in the current ISO standard (W_z) and its proposed revision (W_k), the following performance indices are selected:

- overall unweighted rms acceleration at the seat in the 1.0-20 Hz frequency range;
- overall W_z-frequency-weighted rms acceleration at the seat in the 1.0-20 Hz frequency range;
- overall W_k-frequency-weighted rms acceleration at the seat in the 0.5-20 Hz frequency range;
- overall rms relative displacement at the driver mass in the 1.0-20 Hz frequency range.

The performance index related to relative displacement expresses the need for limiting the overall travel of the driver mass with respect to the cab floor to reduce interference with the driver's interactions with the controls. The upper frequency of interest is limited to 20 Hz since off-road vehicle vibration predominates at low frequencies, and the attenuation of the vibration provided by the weighting filters is quite significant at frequencies above.

3.6.2 EVALUATION OF PERFORMANCE INDICES

All the performance indices identified in the previous section are derived through solution of the differential equations of motion, equations (3.1) to (3.7), for the specified random excitation class and the model parameters. The equations of motion are solved in the time domain to determine the unweighted acceleration response, $\ddot{z}_2(t)$, of mass m_0 and the relative displacement, $[x_2(t) + x_1(t)]$, of this mass with respect to the base. The overall unweighted rms acceleration and rms relative displacement response may then be computed in the time domain using the following basic definition:

$$u_{rms} = \sqrt{\frac{1}{T}\int_0^T u^2(t)dt} \qquad (3.21)$$

where u may represent $\ddot{z}_2$ or $[x_2 + x_1]$ depending on the performance index being evaluated, and T represents the integration period of the response time signal.

The performance indices related to W_z- and W_k-frequency-weighted overall rms accelerations are computed by applying the weighting network to the acceleration response, $\ddot{z}_2(t)$. This may be accomplished in the time domain using the filter equations characterizing each weighting curve plotted in Figure 1.2. Each weighting curve is obtained from a combination of a band-limiting

filter, $H_b(s)$, and a network weighting filter, $H_w(s)$, where $s = j2\pi f$ denotes the Laplace Transform variable. The transfer function of the total weighting filter is then obtained from:

$$H(s) = H_b(s)\, H_w(s) \tag{3.22}$$

where $H_w(s)$ may represent $H_{wz}(s)$ for the W_z weighting, or $H_{wk}(s)$ for the W_k weighting. The network filter for W_z weighting is expressed as:

$$H_{wz}(s) = \frac{\omega_4^2 (s + \omega_3)}{\left(s^2 + \frac{\omega_4}{Q_2} s + \omega_4^2\right) 2.38\omega_3} \tag{3.23}$$

where: $Q_2 = 0.68$, $f_3 = 1.5$ Hz and $f_4 = 5.3$ Hz.

The network filter corresponding to W_k weighting is described as:

$$H_{wk}(s) = \frac{(s + \omega_3)\omega_4^2 \left(s^2 + \frac{\omega_5}{Q_5} s + \omega_5^2\right)}{\omega_3 \left(s^2 + \frac{\omega_4}{Q_4} s + \omega_4^2\right)\left(s^2 + \frac{\omega_6}{Q_6} s + \omega_6^2\right)} \tag{3.24}$$

where: $Q_4 = 0.63$, $Q_5 = 0.91$, $Q_6 = 0.91$, $f_3 = f_4 = 12.5$ Hz, $f_5 = 2.37$ Hz and $f_6 = 3.35$ Hz.

Although the frequency response characteristics of the total weighting filters were presented previously in Figure 1.2, Figure 3.10 presents a comparison of the W_z and W_k weighting filter response characteristics defined by equations (3.23) and (3.24), respectively. In comparison with the W_z weighting, the W_k network provides greater emphasis on vibration frequency components below 0.9 Hz and above 5 Hz, but gives slightly lower weighting on those components in the intermediate frequency range. Thus for vertical off-road vehicular vibration predominating at frequencies in the 1.0 to 5.0 Hz frequency range, the weighted accelerations computed using the W_k network would be expected to be lower than those using the W_z weighting defined in the current ISO standard.

The band-limiting filters may be expressed in terms of the Laplace Transform variable s and the angular frequencies ω_1 and ω_2 by:

$$H_b(s) = \frac{s^2\omega_2^2}{\left(s^2 + \sqrt{2}\omega_1 s + \omega_1^2\right)\left(s^2 + \sqrt{2}\omega_2 s + \omega_2^2\right)} \qquad (3.25)$$

where $\omega_1 = 2\pi f_1$ and $\omega_2 = 2\pi f_2$ are the band-pass limiting angular frequencies.

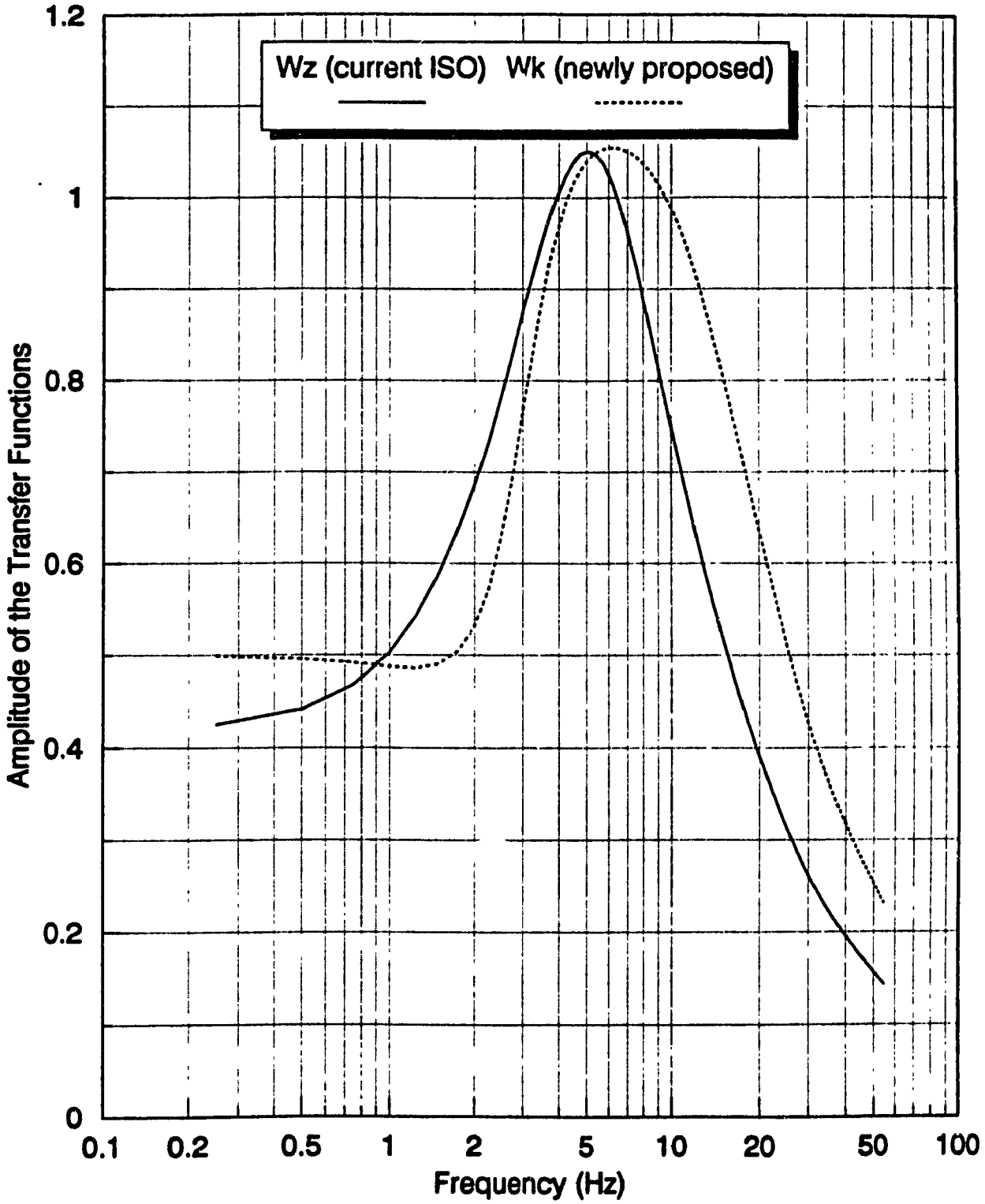

Figure 3.10 Characteristics of the frequency response functions of the weighting filters W_k and W_z (without band limitations).

The values of the limiting frequencies for the W_z-and W_k-weighting filters are listed in Table 3.2.

TABLE 3.2

Band-Pass Limiting Frequencies for the Weighting Filters W_z and W_k.

WEIGHTING	f_1 (Hz)	f_2 (Hz)
W_z	0.8	100
W_k	0.4	100

The weighted acceleration response, $\ddot{z}_{2\,w}(t)$, may be computed in the time domain by applying the solutions of the differential equations of the filters, derived from inverse Laplace Transform of equation (3.22). The W_z and W_k network filters yield additional 3 and 4 second-order differential equations, respectively, to be solved in the time domain. The overall weighted rms acceleration and relative displacement responses are then computed from direct integration of the differential equations for the filter and suspension seat model, using equation (3.21).

3.6.3 INFLUENCE OF SUSPENSION SEAT MODEL PARAMETERS

Sensitivity of the four performance indices defined above to variations in a single model parameter at a time is investigated under ISO 2 class of random excitations. This excitation was chosen since it corresponds more closely to

the vibration encountered by skidders, a vehicle on which the emphasis is placed in this study. Specifically, the influence of the suspension stiffness, K_S, suspension mass, m_S, shock absorber high and low damping coefficients, C_H and C_L, and transition velocity, V_S, cushion damping and stiffness coefficients, C_c and K_c, Coulomb friction, F_C, and compression and extension bump stop stiffnesses, K_{st}^c and K_{st}^e, are investigated. Values of these parameters are modified with respect to their baseline values identified in Table 3.1 in order to establish their influence on each of the four performance indices, under ISO 2 class of random excitations.

Figures 3.11 to 3.14 illustrate the influence of the suspension seat model parameters on the overall unweighted, and W_z and W_k frequency-weighted rms accelerations and relative rms displacement, respectively. The various model parameters are varied to assume values ranging between 0.4 and 1.6 times the baseline values, in increments of 20%.

Considering strictly the three performance indices involving rms accelerations, the parameters having the most influence on the driver mass exposure levels are, in order of importance, the suspension stiffness, K_S, the shock absorber low damping coefficient, C_L, the suspension mass, m_S, and the Coulomb damping force, F_C. Other parameters of lesser importance, creating less than 5% variation on the acceleration response levels are, in order of importance,

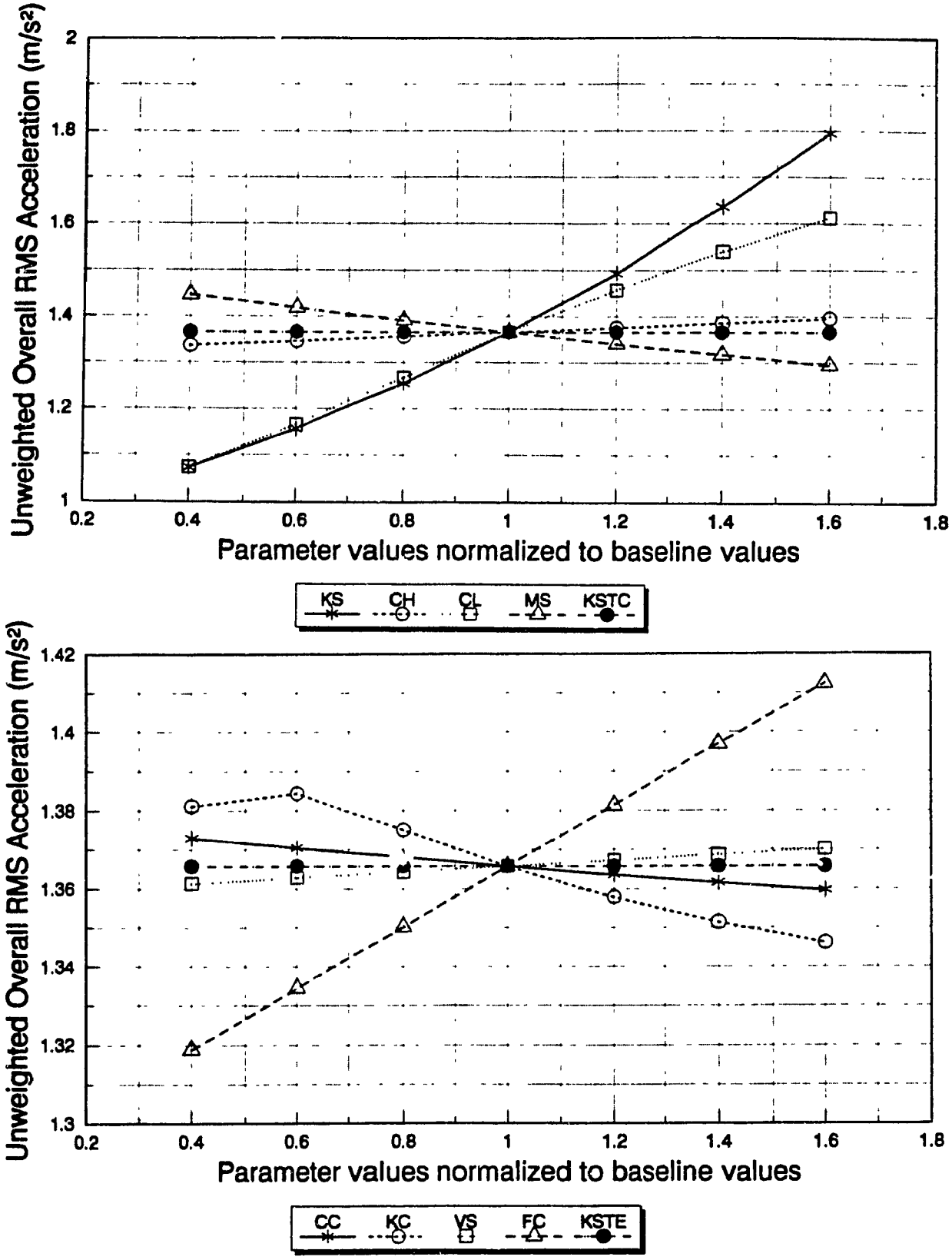

Figure 3.11 Influence of suspension seat model parameters on the overall unweighted rms acceleration response at the seat under ISO 2 excitation.

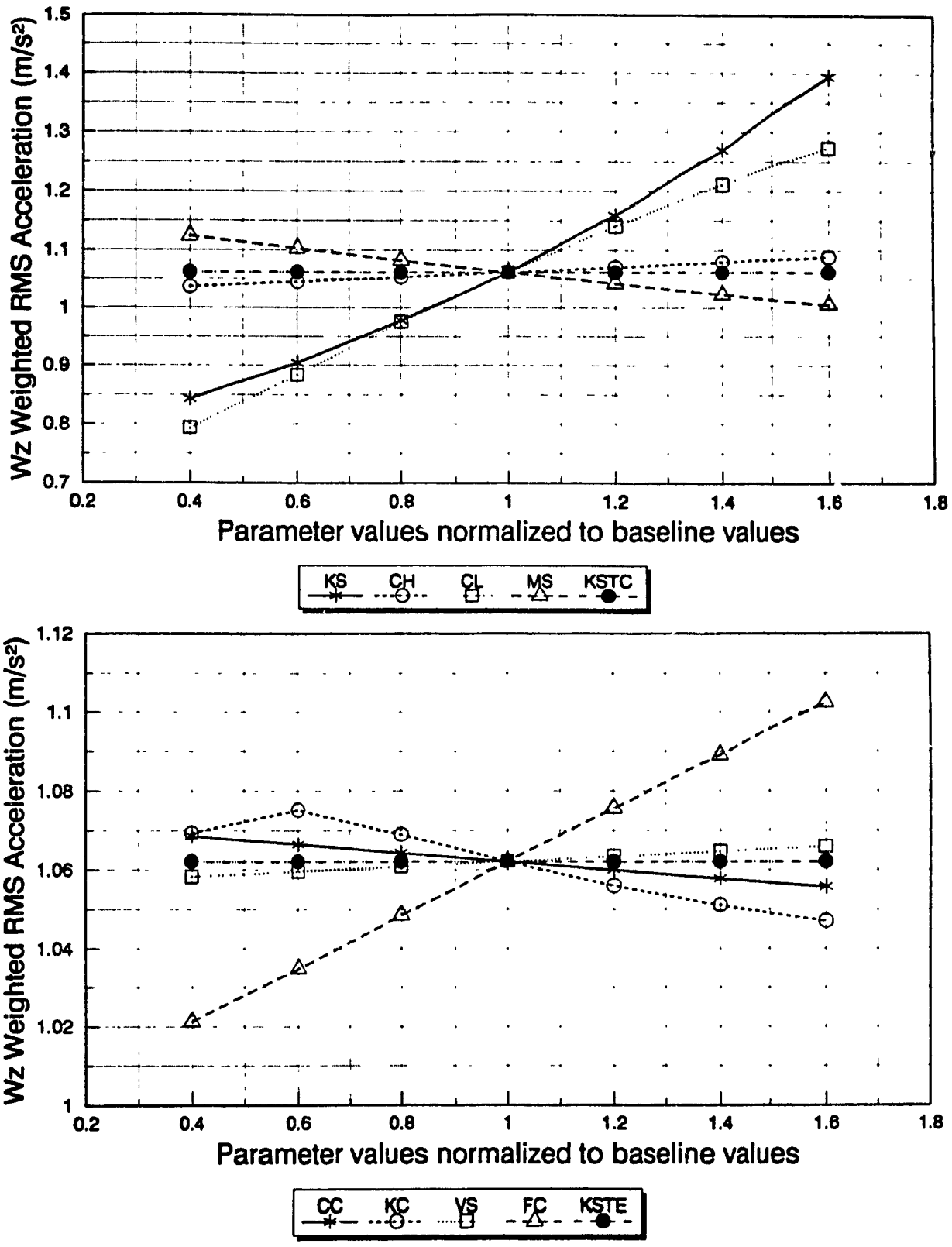

Figure 3.12 Influence of suspension seat model parameters on the overall W_z weighted rms acceleration response at the seat under ISO 2 excitation.

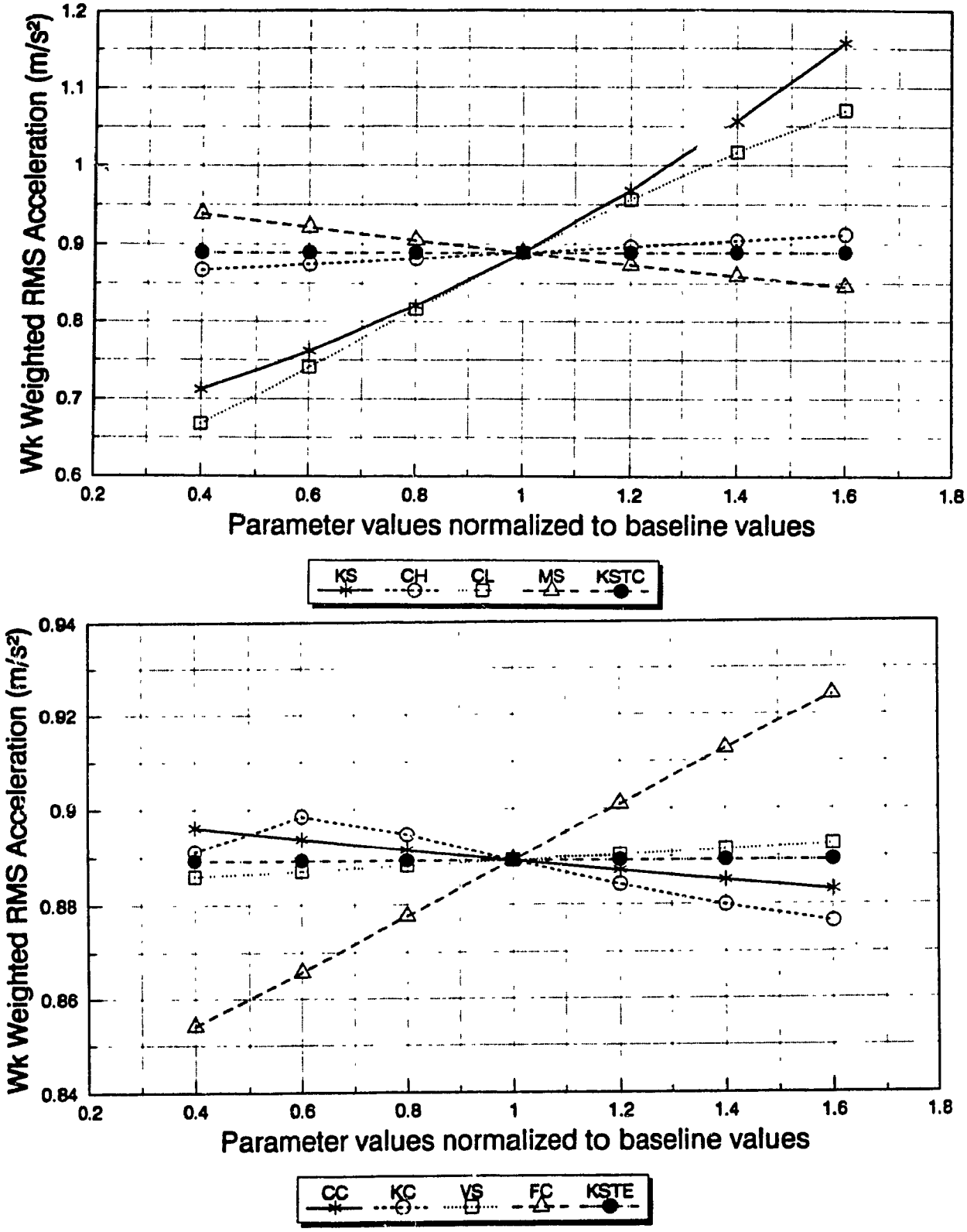

Figure 3.13 Influence of suspension seat model parameters on the overall W_k weighted rms acceleration response at the seat under ISO 2 excitation.

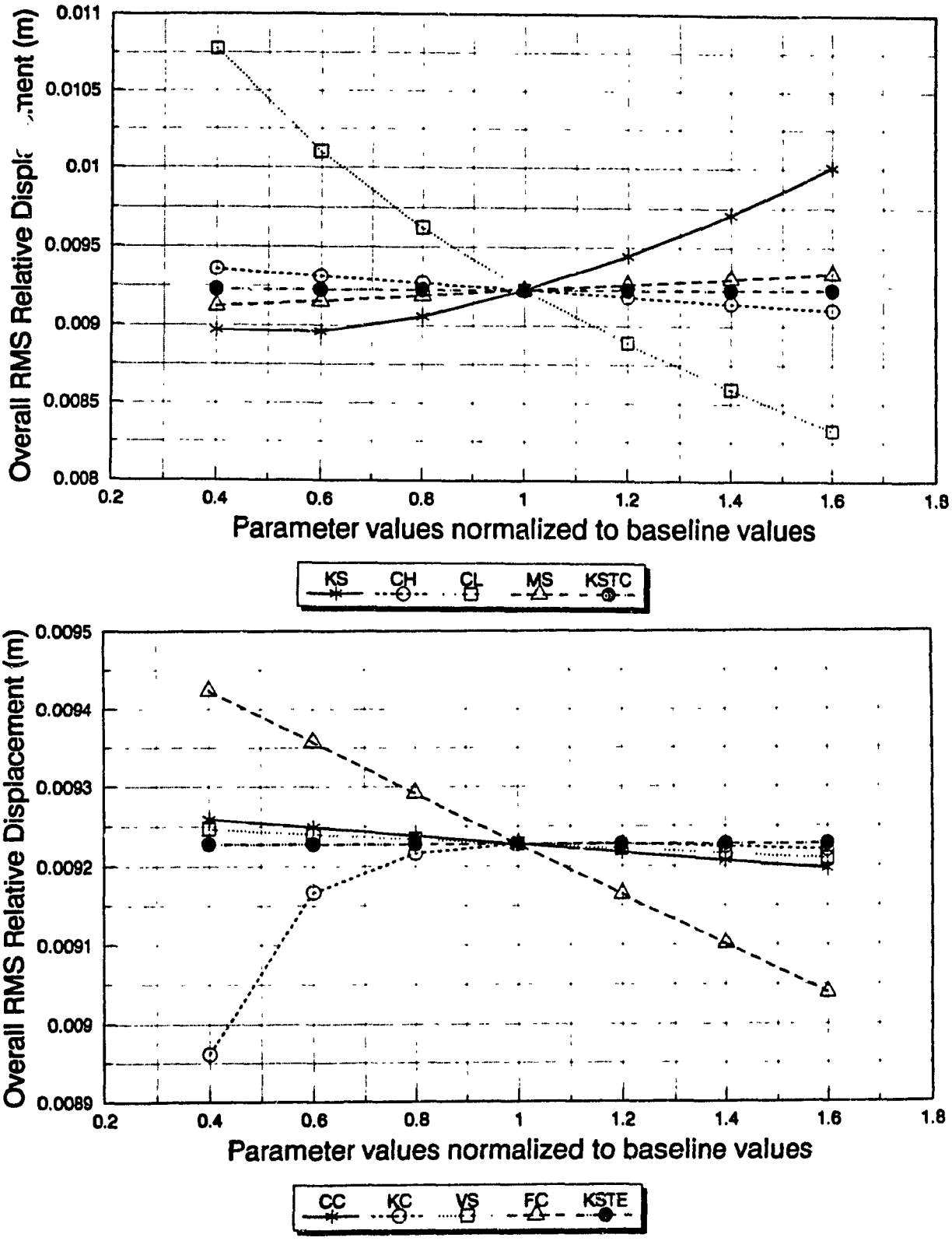

Figure 3.14 Influence of suspension seat model parameters on the overall rms relative displacement response at the seat under ISO 2 excitation.

the shock absorber high damping coefficient, C_H, the cushion stiffness, K_c, the cushion damping, C_c, and the shock absorber transition velocity, V_S. The bump stop stiffness coefficients in extension and compression show no influence since the stops are not sollicited under this type of excitation. With regard to the performance index involving rms relative displacements, the various suspension seat parameters are found to have only a minimal effect over the range of values investigated. While for most suspension seat parameters, the trend observed with relative displacement is just the opposite of that with the rms acceleration, the overall variation of relative displacement is seen to be less than 2 to 3 mm for any of the suspension parameters being varied over the entire range of values.

The following suspension seat design guidelines are found to provide the lowest vibration exposure for the driver under ISO 2 class of random excitation:

- a low suspension spring stiffness;
- a shock absorber with low damping coefficients and transition velocity;
- a large suspension mass;
- a low Coulomb damping force;
- a seat cushion with high stiffness and damping coefficients.

Of the various suspension seat design parameters, the lowest acceleration exposure level is achieved with a low value of shock absorber low damping

coefficient, while maintaining all the other parameters equal to their baseline values. In such a case, the acceleration exposure level may be reduced by as much as 25%, irrespective of the vibration assessment method used. All the other parameters lead to lesser reductions in exposure level when set according to the design guidelines.

The seat dominant excitation created by the ISO 2 vibration class is at 2.65 Hz. Thus, a reduction of the suspension stiffness coefficient has the effect of lowering the seat natural frequency and of providing increased vibration attenuation at the excitation frequency. Similarly, an increase of the suspension mass yields a lower seat natural frequency, originally estimated at 1.3 Hz, thus better vibration attenuation at the 2.65 Hz dominant excitation frequency.

An increase in shock absorber damping coefficients and Coulomb friction force tends to suppress the response corresponding to the resonant frequency, while impeding the suspension performance at higher excitation frequencies. Since the seat resonant frequency computed from the model is nearly 1.3 Hz, a reduction of the shock absorber high and low damping coefficients and Coulomb friction force yields improved vibration attenuation at the excitation frequency, estimated at 2.65 Hz for the ISO 2 class. However, the shock absorber low damping coefficient corresponding to blow-off stage, affects the

suspension performance more than the high damping coefficient. For this reason, a low shock absorber transition velocity is found to be beneficial by providing blow-off damping over an extended range of suspension operation.

An increase in cushion stiffness tends to reduce the resonant acceleration transmissibility, while leading to only slight improvement in the attenuation characteristics at higher frequencies. While the trend observed for cushion damping is similar to that of cushion stiffness, its influence is considerably less. High cushion stiffness and damping coefficients lead to improved attenuation of the vibration at the dominant excitation frequency defined by ISO 2 class.

A comparison of the acceleration exposure levels appearing in Figures 3.11 to 3.13 reveals that those computed using the W_k weighting network are consistently lower than the unweighted or W_z-weighted levels. For a suspension seat with baseline parameters, the rms acceleration exposure levels computed from the model using the various assessment methods are 1.37 ms^{-2} when no frequency weighting is applied, and 1.06 ms^{-2} and 0.89 ms^{-2} when weighted according to the W_z and W_k networks, respectively. Based on the current and new proposed guidelines on WBV exposure, the "exposure limit" defined in the current ISO 2631/1 standard would be reached after approximately 4 h (W_z-weighted level), while the W_k-weighted level falls within

the "health guidance caution zone" defined in the proposed revision (Figure 1.3) for a daily exposure duration between 4 and 8 hours.

Upon modifying the seat suspension to include a 60% reduction in low damping coefficient C_L, the corresponding unweighted rms and W_z- and W_k-weighted acceleration levels computed from the model reduce to 1.08 ms^{-2}, 0.79 ms^{-2} and 0.67 ms^{-2}, respectively. On the basis of these levels, the "exposure limit" would be reached after approximately 6 hours (W_z-weighted level), while the exposure would still be considered within the 4-8 hours "health guidance caution zone" (W_k-weighted level). The two assessment methods involving W_z and W_k weightings and their associated guidelines, thus lead to a similar estimate of the health hazard for the case considered. The results further reveal that the seat estimated S.E.A.T. under ISO 2 excitation would be on the order of 0.70 when designed with baseline parameters and 0.50 when selecting the parameters according to the guidelines.

3.7 Summary

A two-degree-of-freedom nonlinear suspension seat model incorporating a rigid mass as the driver is described analytically to represent a commercially available suspension seat (SIFRA) for off-road vehicles. The analytical model is validated experimentally for the sinusoidal and random excitation classes described in Chapter 2, and generated using the WBVVS. A comparison of model and measured response characteristics reveals a relatively good agreement for

deterministic as well as random excitations, although the model overestimates the seat response at the predominant random excitation frequencies. A parametric study is performed to identify the most desirable suspension seat characteristics for minimizing the severity of driver's exposure to vibration. This necessitates the identification of four performance indices based on the overall rms frequency-weighted and unweighted accelerations at the driver mass and on the rms relative displacement between the mass and the base. A methodology to derive the selected performance indices is developed and the parametric study is performed to evaluate the influence of the suspension seat design parameters on the severity of the exposure under the ISO 2 class of random excitation. For the seat considered, a reduction of the suspension low damping coefficient is observed to produce the most significant improvement on the degree of severity of the exposure as determined from the current and new proposed guidelines on WBV exposure.

CHAPTER 4

SUSPENSION SEAT RESPONSE ANALYSES UNDER SHOCK EXCITATIONS

4.1 Introduction

Off-road vehicles encounter not only terrain-induced vibration but also excessive shocks caused by the terrain abruptness. Although a marked interest is noted in the literature for evaluating human body response under the influence of shocks [52], only few investigators have addressed the study of suspension systems under shock excitations. Of the few published studies, Palanichamy et al. [53,54] presented an analytical study of the tractor suspension seats. The analytical vehicle-seat model comprising a linear single-degree-of-freedom seat suspension and a two-degree-of-freedom vehicle was analyzed to derive the optimal stiffness and damping design parameters of a suspension seat under both steady-state sinusoidal vibration and transient excitations. The transient excitation was idealized by a trapezoidal displacement input at the tire-ground interface with maximum amplitude of 50 mm.

For their analysis, Palanichamy et al. represented the human body as a seven-degree-of-freedom nonlinear system linked with the seat. Suspension seat design optimization was performed to minimize the amplitude of vibration transmitted to specific body parts, and the pitch vibration of the chassis, in the 0.5 to 11 Hz frequency range. While the peak amplitude response ratio occurred at a specific body part, namely the thorax, under steady-state sinusoidal vibration, the peak

response occurred at the driver-seat interface under transient vibration. A need to define the suspension seat design criteria depending upon the type of excitation is thus identified. The design criteria could require minimization of the vibration response amplitude at the driver-seat interface under transient or shock excitations, while at specific body parts under alternate excitations. The current state of knowledge on human response to shock and vibration clearly does not provide such a distinction between the shock and vibration component. The International Standard on whole-body vibration exposure [18] emphasizes reduction of the vibration at the point of entrance to the body, without specifying the distinctions as to the type of excitation.

Various performance indices and their influence on suspension design optimization have been proposed by Hrovat and Hubbard [55,56]. Although the performance indices are usually selected to minimize the rms relative displacement and sprung-mass acceleration, their study has shown that a performance criterion with certain weighting on the jerk, or rate of change of acceleration response attributed to transient excitations, yields different optimal suspension designs. The results of their study contradict the findings of Palanichamy et al. [53,54] that the same optimal stiffness and damping characteristics would apply under both sinusoidal and transient excitations, although the peak amplitude response may be very different under the two types of excitations.

In this chapter, the behaviour of the nonlinear suspension seat model defined in

Chapter 3 is analyzed under the influence of the shock excitations identified in Chapter 2 for off-road vehicles. Upon validation, the model is used to estimate the influence of various suspension seat design parameters under two response conditions: (a) suspension travel within the permissible stroke (no interactions with the bump stops); (b) suspension travel exceeding the permissible travel (interactions with the bump stops). While it is recognized that protection of the driver against the ill-effects of vibration and shock constitutes a priority, near optimal suspension seat design parameters are identified with respect to performance indices established on the basis of the current standard on whole-body vibration exposure and its proposed revision [12,18]. A brief review of the current state of knowledge on human response to transient or shock excitations is first presented as a prerequisite to defining the vibration exposure assessment methods, most likely to apply under shock excitations.

4.2 Literature Review on Human Response to Shocks

Most studies dealing with the subject of human response to shocks have concentrated primarily on subjectively assessing the discomfort experienced when exposed, and on attempting to derive the potential link of such exposure with low back pain, recognized as the most important health-related effect for seated drivers. In fact, one of the earliest models for describing human response to vibration considers shock as the main component for assessing the severity of vibration on the spine. The "Dynamic Response Index", or DRI [57], constitutes the basis of this model and represents the peak acceleration response of a single-degree-of-freedom

model normalized to the acceleration due to gravity, g. The DRI is thus intended to be a measure of the peak stress acting on the spine when the one-degree-of-freedom model parameters are selected to match those of the spine. This model was developed with an objective to account for back injuries among the aircraft pilots, related to seat ejections. The model may represent an extreme case involving much more severe vibration acceleration levels than could be expected for vehicles encountering road discontinuities or obstacles.

4.2.1 THEORY ON PATHOLOGICAL MECHANISMS LEADING TO BACK PAIN

Objective measures in support of the hypothesis that shocks may be more detrimental to health than "regular" vibration have been performed using electromyography (emg) measurements [58]. These were aimed at determining whether trunk muscles could react immediately to transient whole-body vibration, a condition that would help in stabilizing the spine by reducing the relative motion between vertebrae. Under transient excitations, muscle response was found to be too slow to adequately protect the spine, the measured time constant being in the order of 100 ms. Relaxation periods after exposure to transient vibration were also observed, contrasting with constant muscular activity measured under continuous alternating motions. These results thus suggest that the body would offer perhaps less protection under the influence of shocks than under constant vibration.

Development of an assessment method necessitates the knowledge of precise mechanisms leading to low back injuries under exposure to shock motions. A

number of hypotheses relating low back injuries to exposure to shock motions have been proposed. Sandover [59] postulated that exposure to shock loads can accelerate disc degeneration by mechanical loading of the end-plate and subchondral bone after repeated impacts. These changes may lead to higher stresses in the vertebrae and to low back pain. This could even have implications in terms of the impact forces experienced during walking [60]. In analogy to fatigue failure of inanimate materials, it was postulated that a simple relation between applied stress and number of cycles to failure may exist. On this basis, a dose value may be derived proportional to the number of peaks of the weighted signal and an exponential function of the level of acceleration. However, data on the spinal load response under exposure to shocks, and on the possible effects of this load are scarce. Future work on in vivo effects on the mechanical response to shocks of seated humans is clearly needed to identify the injury mechanisms [61].

4.2.2 SHOCK EXPOSURE ASSESSMENT METHODS

The subject of human response to transients or shock excitations has been controversial ever since the publication of the ISO 2631/1 standard [18]. This standard describes the relative importance of vibration impulsiveness in terms of the crest factor, defined as the ratio of peak frequency-weighted to root-mean-square (rms) acceleration. The rms-averaging assessment method, along with the vibration limits defined in the standard, are considered to be applicable for crest factor below a certain preset value, this value being 3 in the original version, and later extended to 6 in more recent versions. The current standard thus does not offer vibration

limits to assess the exposure to vibration with high crest factors, such as motions encountered in off-road vehicles, with reported crest factor values well in excess of 6 [29].

The view that exposure to occasional high amplitude impacts, such as those resulting from a vehicle passing over bumps, may be more detrimental than exposure to low level vibration [16] has prompted the search for more appropriate methods to assess the influence of shock motions. Revision of the ISO 2631/1 standard led to a Draft International Standard which includes an assessment method for evaluating exposure to whole-body vibration with crest factor larger than 9 [12]. The proposed method, based on root-mean-quad (rmq) acceleration, assesses the exposure to motions with high crest factor by providing greater weighting to the peak motions. Wikstrom et al. [62] employed up to 40 different assessment methods to analyze the shock response of seated individuals in an attempt to correlate the results with subjective ratings of discomfort. The study demonstrated that methods based upon the rms and rmq or associated dose values yield better correlation with the discomfort ratings than the other proposed assessment methods relying on peak acceleration, the impulse extended dose or the shock response spectrum analyses. Many similar studies conducted on the assessment of shock motions resulted in highly contradictory findings. A study conducted by Kjellberg et al. [63] concluded that the rms method tends to underestimate the influence of shocks, while the studies reported by Griffin and Whitham [64] supported the rmq method. A number of other studies have reported relatively insignificant differences between the rms

and rmq methods [65,66,67]. In view of the contradictory findings reported in the literature, the use of more complex methods, such as rmq, has been strongly criticized. Moreover, it has often been argued that the exposure limits proposed in the current ISO 2631/1 are perhaps not restrictive enough when shocks are involved and that the crest factor is perhaps a poor indicator of the proper method to be used. However, the data does not yet exist to identify a specific method considered to be the most appropriate. For this reason, it may seem appropriate at this stage to consider several of the proposed methods when assessing shock responses.

4.3 Suspension Seat Model Validation under Shock Excitation

The analytical model of the suspension seat validated for sinusoidal and random excitation classes in Chapter 3 is further validated for shock excitations. This validation is accomplished by comparing the driver mass acceleration response measured in the laboratory with that computed using the analytical model. The shock excitations arising from the tire interactions with an idealized half-sine shaped obstacle of width 200 mm and height of 75 mm were generated through analysis of an in-plane vehicle model. The shock excitations corresponding to 10 different vehicle speeds were synthesized in the laboratory as described in section 2.5.4, representing the motions at the seat attachment point.

4.3.1 MEASUREMENT OF DRIVER MASS RESPONSE UNDER SHOCK EXCITATIONS

The SIFRA suspension seat was fixed to the platform of the WBVVS and loaded

with the sandbags, as described in section 3.5.1. A triaxial seat accelerometer was placed at the interface of the seat and the lower sandbag to monitor z-axis motion ($\ddot{z}_2$), while a single axis accelerometer was fixed on the simulator platform underneath the seat to monitor the seat input acceleration ($\ddot{z}_0$). The seat was successively submitted to each of the synthesized shock motions defined in section 2.5.4, representing the motions at the seat attachment point caused by the vehicle passing over the same obstacle at different speeds, ranging from 1 to 10 km/h.

4.3.2 COMPUTATION OF DRIVER MASS RESPONSE UNDER SHOCK EXCITATIONS

The nonlinear differential equations of motion for the suspension seat model, (3.1) to (3.7), are solved using numerical integration for shock excitations in the specified speed range (1 - 10 km/h) to derive the acceleration response, $\ddot{z}_2$, of the driver mass. The model parameters, identified from the static and dynamic tests and summarized in Table 3.1, are used. The shock excitations derived from the tire-obstacle interactions at certain speeds could not be generated in the laboratory due to design constraints, specifically the flow rate capacity of the WBVVS. Thus, for the purpose of validating the model, the input displacement, z_0, to the seat model is computed upon integration of the measured acceleration excitation, $\ddot{z}_0$, of the simulator platform.

4.3.3 IDENTIFICATION OF PERFORMANCE INDICES

Although the current standard on whole-body vibration exposure does not specifically refer to shock motions apart from defining the crest factor, it has been established that acceleration at the driver-seat interface must be minimized to enhance driver protection under vibration exposure. Since the human driver is represented by a rigid mass in this part of the work, the instantaneous peak acceleration and the overall frequency-weighted rms acceleration at the driver mass should be kept as low as possible. Since the current standard supports a frequency weighting referred to as W_z for vertical vibration, while the proposed revision introduces a modified weighting, W_k, both the W_z- and W_k-frequency-weighted rms accelerations at the seat-driver mass interface, together with the instantaneous unweighted acceleration are selected as the performance indices. From the measured and computed acceleration time traces at the driver mass, the weighted rms accelerations are obtained from:

$$a_{w,rms} = \sqrt{\int_{f_1}^{f_2} |H(s)|^2 \, S_{\ddot{z}_2}(f) \, df} \qquad (4.1)$$

where $a_{w,rms}$ is the frequency-weighted rms acceleration, $S_{\ddot{z}_2}(f)$ is the acceleration PSD at the seat-driver mass interface, f_1 and f_2 are the lower and upper frequency limits of the weighting filters and H(s) represents the frequency response functions of the W_z and W_k weighting filters given by equations (3.22) to (3.25). The weighted accelerations can also be computed in the time domain using the procedure

described in section 3.6.2, although implying considerably more cumbersome computations.

Under the influence of shock excitations, or whenever the crest factor is greater than 9, the proposed revised standard introduces a new assessment method based on the fourth power of the acceleration, or root-mean-quad (rmq) acceleration. Although the revised standard does not require an evaluation of the rmq acceleration, it defines a Vibration Dose Value (VDV) related to a_{rmq} and exposure duration T, as described earlier in equation (1.6). For design purposes, the overall frequency-weighted rmq accelerations at the seat-driver mass interface, using W_z and W_k weightings, are also considered as additional performance indices when assessing shock responses. The computation of frequency weighted rmq acceleration response of the analytical model involves simultaneous solution of 5 and 6 coupled second-order differential equations for the filters and suspension seat system, as discussed earlier in Chapter 3. Determination of the rmq values of the measured vibration response also involves cumbersome analyses associated with the integration of the fourth power of the measured signals, and application of the weightings. Alternatively, the frequency-weighted rmq acceleration may be computed from the acceleration power spectral density response in the following manner:

$$a_{w,rmq} = \left[\int_{f_1}^{f_2} |H(s)|^2 \, S_{\ddot{z}_2}(f) \, df \right]^{1/4} \qquad (4.2)$$

where $a_{w,rmq}$ is the weighted rmq acceleration, $S_{\ddot{z}_2^2}(f)$ is the PSD of the square of the acceleration response, $\ddot{z}_2 \mid \ddot{z}_2 \mid$, of the driver mass. Special care must be taken when using this technique, to consider both positive and negative portions of the squared acceleration signal when evaluating the PSD function.

In view of the lack of a general concensus on the most accurate assessment method or the frequency weighting applicable to shock motions, additional performance indices relying on unweighted rms and rmq accelerations at the seat-driver mass interface are also considered. These performance indices are computed from equations (4.1) and (4.2) while setting the filter transfer function, H(s), equal to unity. Alternatively, the unweighted rms and rmq accelerations may be computed from their basic definitions, equations (3.21) and (1.5), using unity weighting factor.

In summary, the various assessment methods defined in the current and in the proposed revised standards, along with variations of these methods, are considered as the basis for defining the performance indices for design analyses and analytical model validation under shock excitations. These assessment methods involve the computation of the following response variables at the driver mass-seat interface:

- the instantaneous unweighted acceleration in the time domain;
- the W_z frequency-weighted rms acceleration in the 1.0 to 80 Hz frequency range;
- the W_k frequency-weighted rms acceleration in the 0.5 to 80 Hz frequency range;

- the W_z frequency-weighted rmq acceleration in the 1.0 to 80 Hz frequency range;
- the W_k frequency-weighted rmq acceleration in the 0.5 to 80 Hz frequency range;
- the overall unweighted rms acceleration in the 1.0 to 80 Hz frequency range;
- the overall unweighted rmq acceleration in the 0.5 to 80 Hz frequency range.

4.3.4 MODEL VALIDATION BASED ON ACCELERATION TIME RESPONSES

Figure 4.1 presents a comparison of time histories of the measured and computed unweighted driver mass acceleration response, for shock inputs resulting from the off-road vehicle passing over a half-sine bump, at speeds ranging from 1 to 10 km/h. These vibration signals include the responses from both wheel inputs, best seen at lower vehicle speeds by the two distinct decaying envelopes.

The results show a generally good agreement between the theoretical and experimental response. The measured peak acceleration values, however, are observed to be considerably larger than those computed from the model, specifically in the 2 to 6 km/h speed range. For the obstacle width considered (i.e. 200 mm), this particular speed range results in vehicle excitation frequencies in the neighbourhood of either the vehicle or the seat resonant frequency. Maximum seat excitation amplitude occurs at a speed of 4 km/h, resulting in an excitation frequency of 2.78 Hz, close to the vehicle's resonant frequency. Figure 4.2 shows the PSD of unweighted driver mass acceleration response at a speed of 4 km/h, indicating a large peak at 2.78 Hz. The primary excitation frequency corresponding to a speed

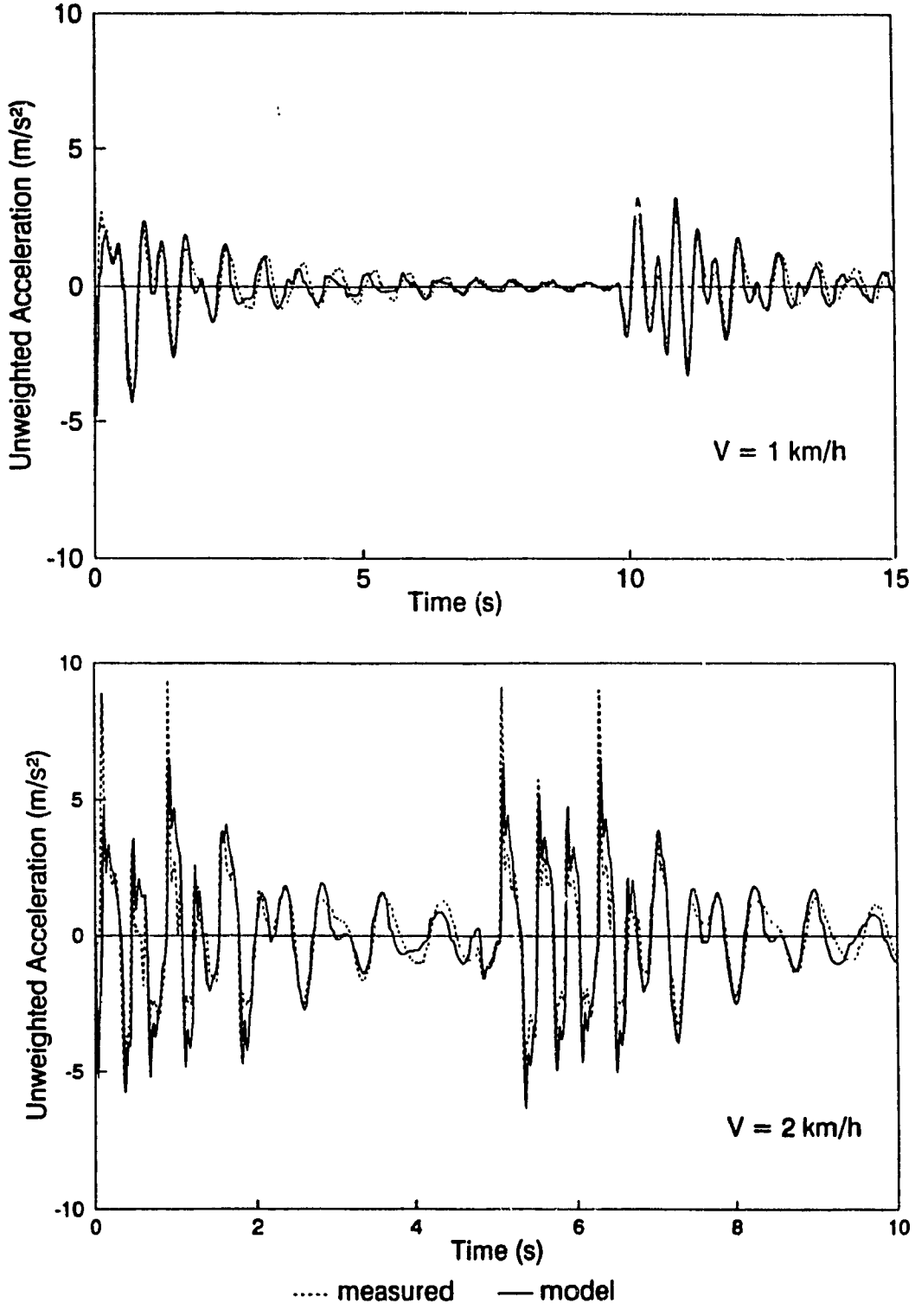

Figure 4.1 Measured and computed unweighted acceleration time traces of the driver mass under a 75 mm peak displacement shock input at the specified vehicle speeds.

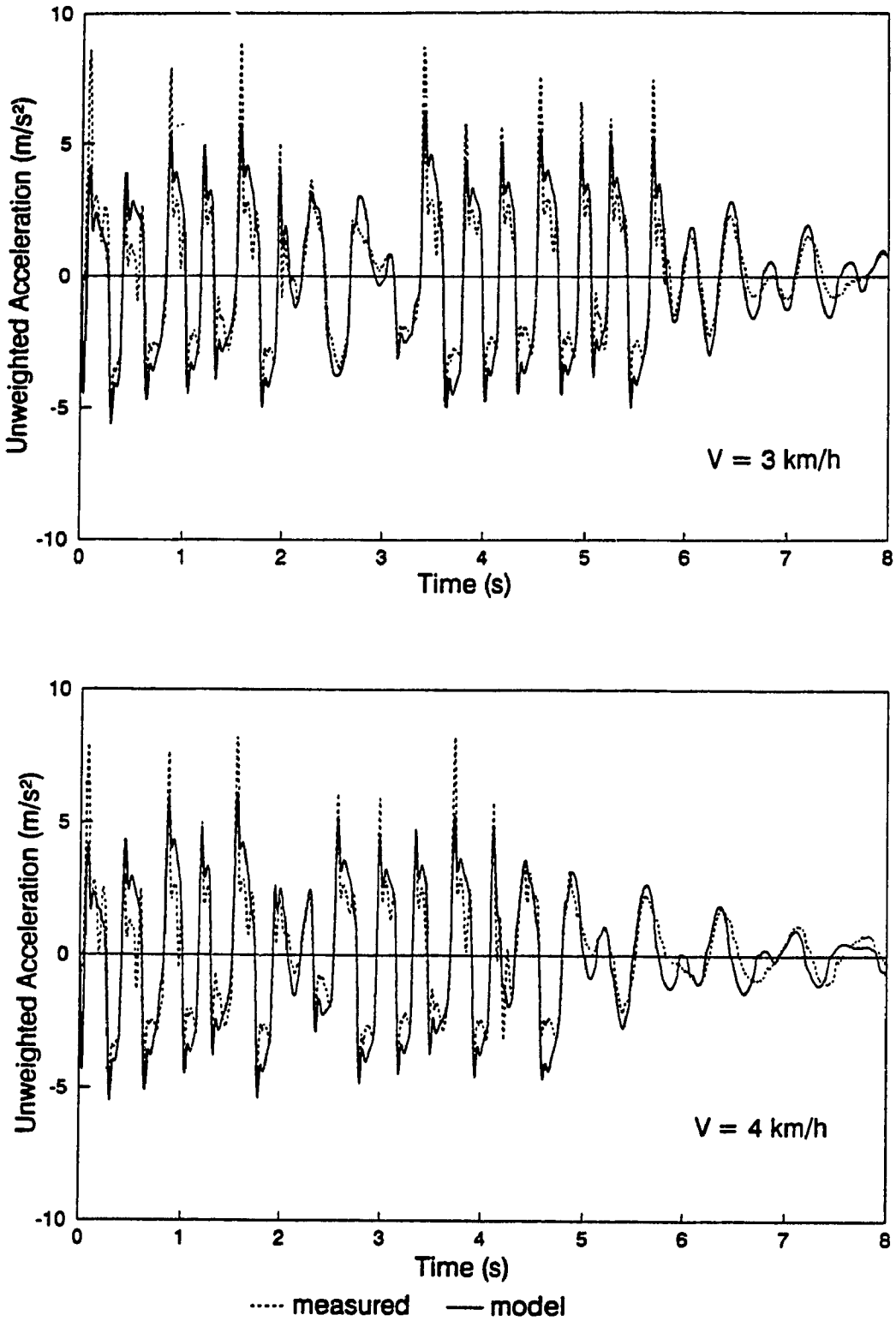

Figure 4.1(cont'd) Measured and computed unweighted acceleration time traces of the driver mass under a 75 mm peak displacement shock input at the specified vehicle speeds.

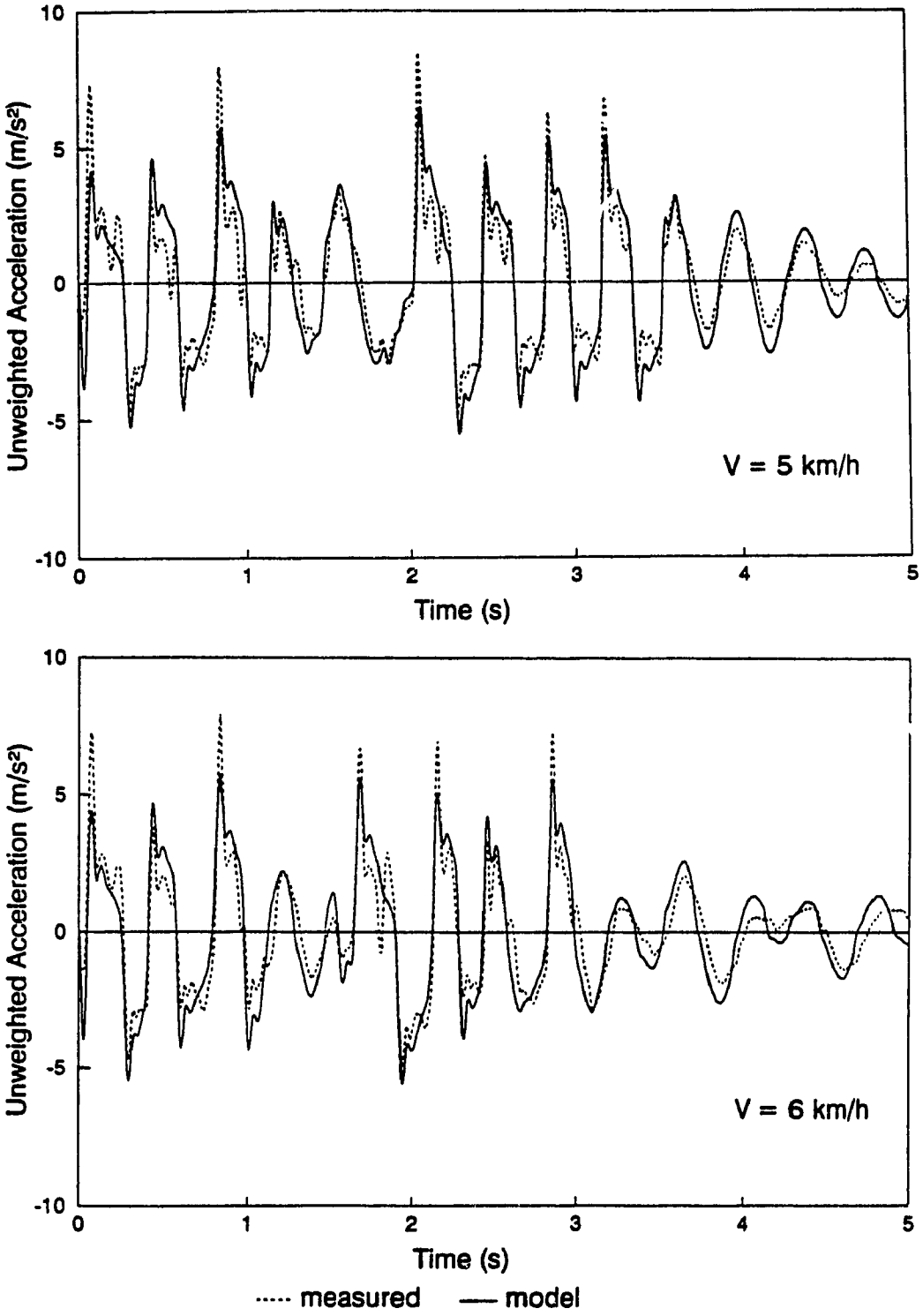

Figure 4.1(cont'd) Measured and computed unweighted acceleration time traces of the driver mass under a 75 mm peak displacement shock input at the specified vehicle speeds.

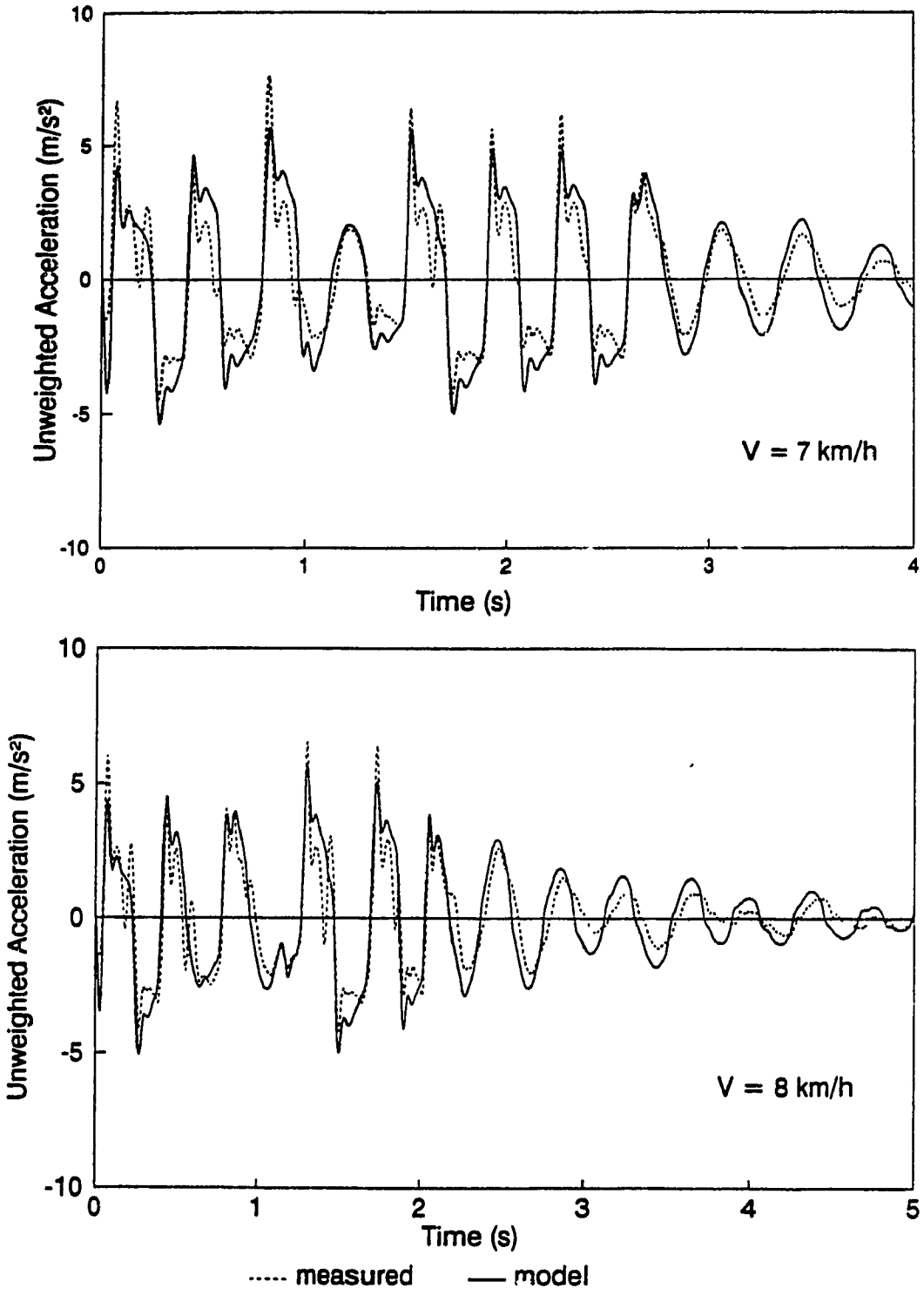

Figure 4.1(con'd) Measured and computed unweighted acceleration time traces of the driver mass under a 75 mm peak displacement shock input at the specified vehicle speeds.

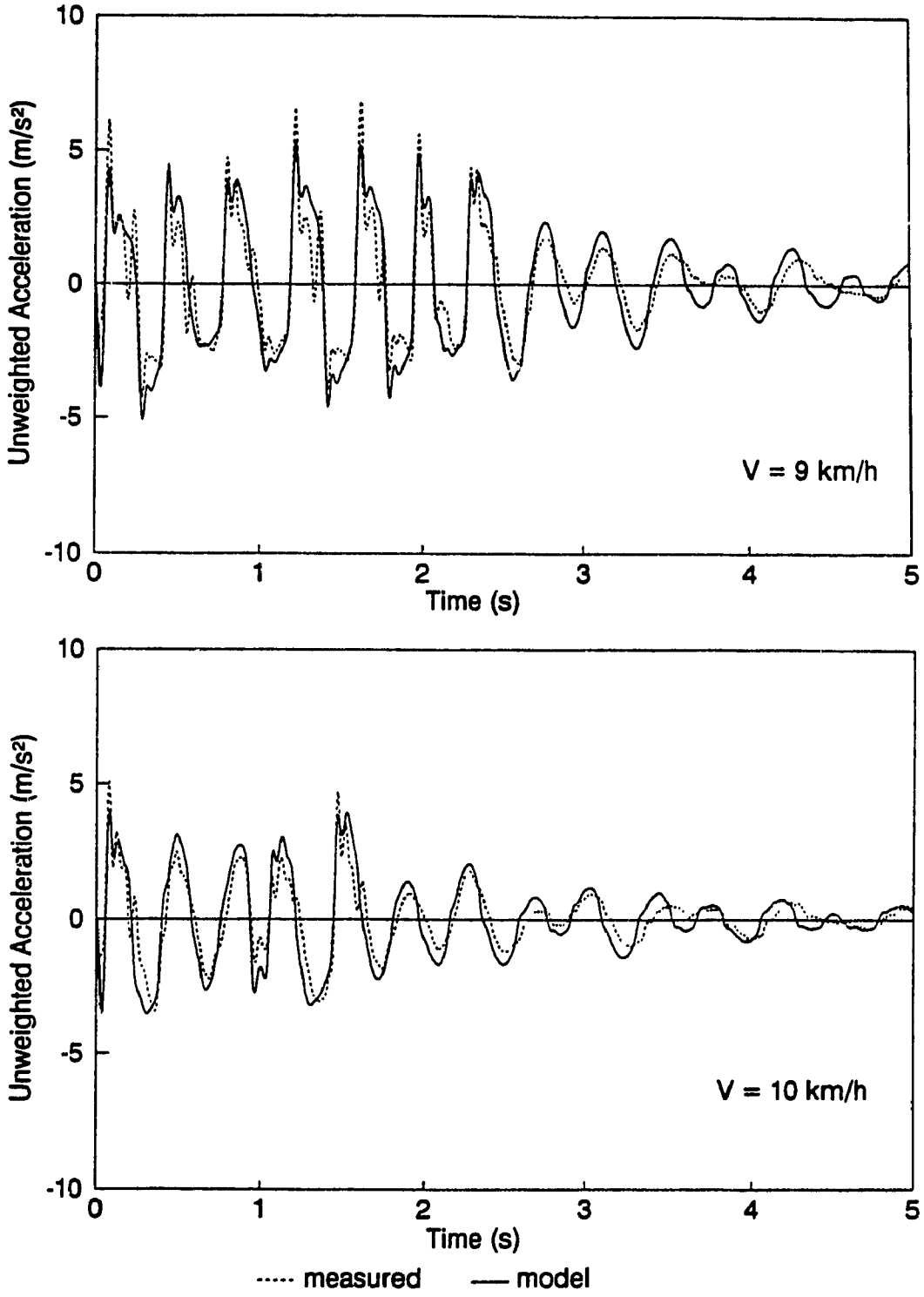

Figure 4.1(cont'd) Measured and computed unweighted acceleration time traces of the driver mass under a 75 mm peak displacement shock input at the specified vehicle speeds.

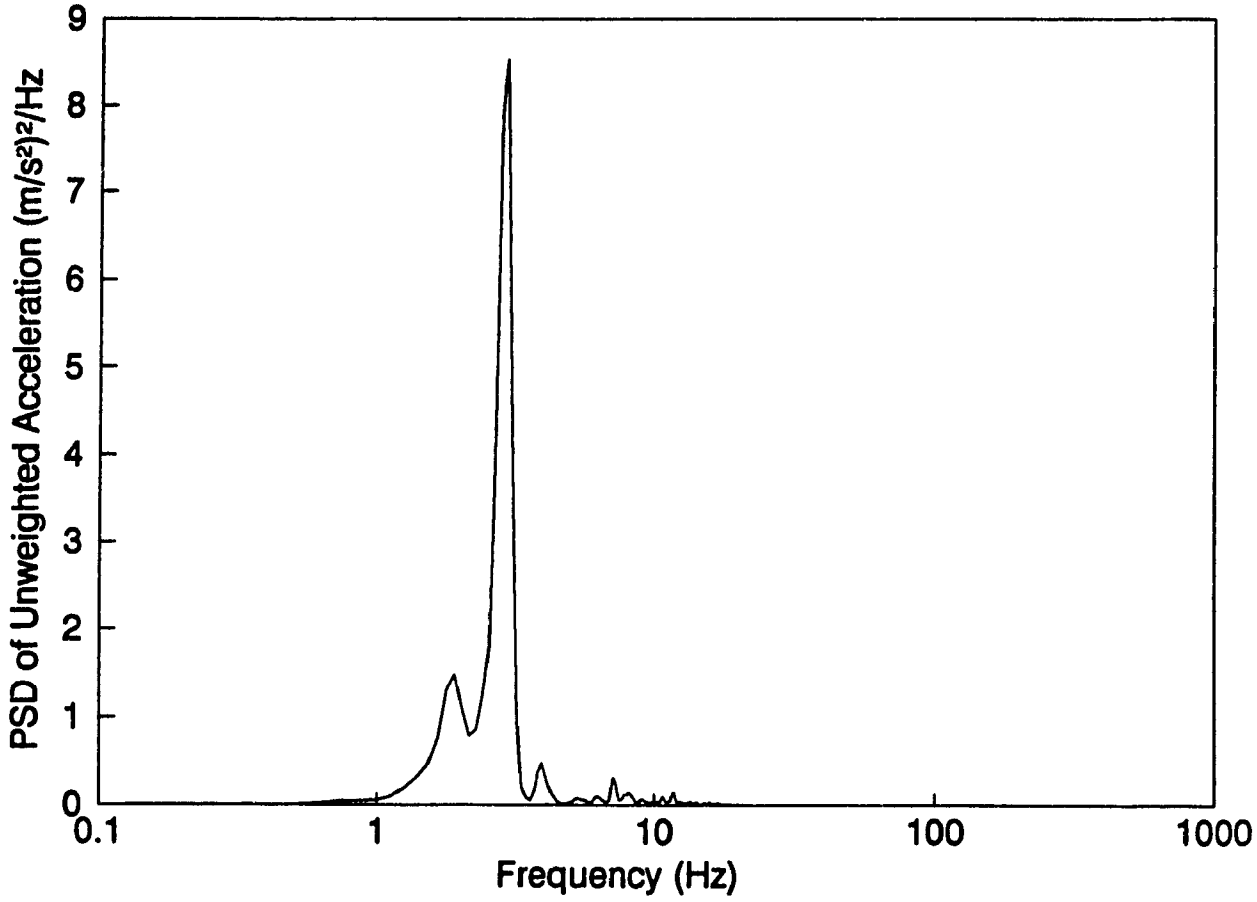

Figure 4.2 Power spectral density (PSD) of the computed unweighted driver mass acceleration response under a 75 mm peak displacement shock input at a speed of 4 km/h.

of 2 km/h (1.39 Hz) is observed to be close to the seat resonant frequency, leading to large response of the driver mass.

Within the speed range 2 to 6 km/h, the most significant discrepancies between the measured and computed acceleration response occur only for specific positive peaks. This observation, together with the asymmetric nature of measured acceleration response, suggest that the discrepancies may be related to lift-off of the mass (sandbag) under upward motion and its interactions with the seat accelerometer upon return. The separation of the load from the seat during the experiments may be further supported by the most significant amplitudes of motion occurring within the 2-6 km/h speed range. At higher speeds, the attenuation provided by the suspension seat is observed to be more significant, owing to the much higher excitation frequencies occurring beyond its resonance. Apart from the occasional positive peaks, the measured response is observed to be slightly lower than the computed response in the 7 - 10 km/h speed range.

4.3.5 MODEL VALIDATION BASED ON WEIGHTED RMS ACCELERATIONS

The overall W_z- and W_k-weighted rms acceleration responses of the driver mass are computed as a function of vehicle speed using the recommended weighting factors. The weighted rms accelerations were computed in the time and frequency domains using equations (3.1), (3.21) and (3.22) for the time domain and (4.1) for the frequency domain. A comparison of the W_k-weighted rms acceleration derived from the two methods at a speed of 4 km/h revealed that frequency domain yields a value

identical to that derived from the time domain. The W_k frequency-weighted overall rms accelerations were computed as 2.147 ms^{-2} and 2.146 ms^{-2} from time and frequency domain procedures, respectively. Considering the insignificant differences between the results, and the relative computational ease of the frequency domain approach, all the subsequent analyses were performed using the frequency domain method.

Figure 4.3 presents a comparison of the W_z- and W_k-weighted accelerations of the measured and the model response characteristics, together with the weighted acceleration of the excitation. The overall rms acceleration of the base excitation is computed from the measured response, which is observed to taper off at speeds above 3 km/h. At the speed of 10 km/h, the weighted base acceleration is observed to decrease, although the excitation amplitude is more considerable at larger speeds. This is attributed to the rms averaging performed over progressively shorter time durations for increasing vehicle speed.

The results show that the seat provides an attenuation of the overall frequency-weighted rms accelerations over the entire range of vehicle speeds investigated. The suspension seat exhibits highest attenuation (i.e. lowest S.E.A.T. value) at a speed of 5 km/h when the performance index based upon the W_k-weighted rms acceleration is used, and at 8 km/h, when the performance index based upon the W_z-weighted acceleration is used. The suspension seat exhibits least attenuation at a speed of 1 km/h, where low frequency vibration is predominant, irrespective of the

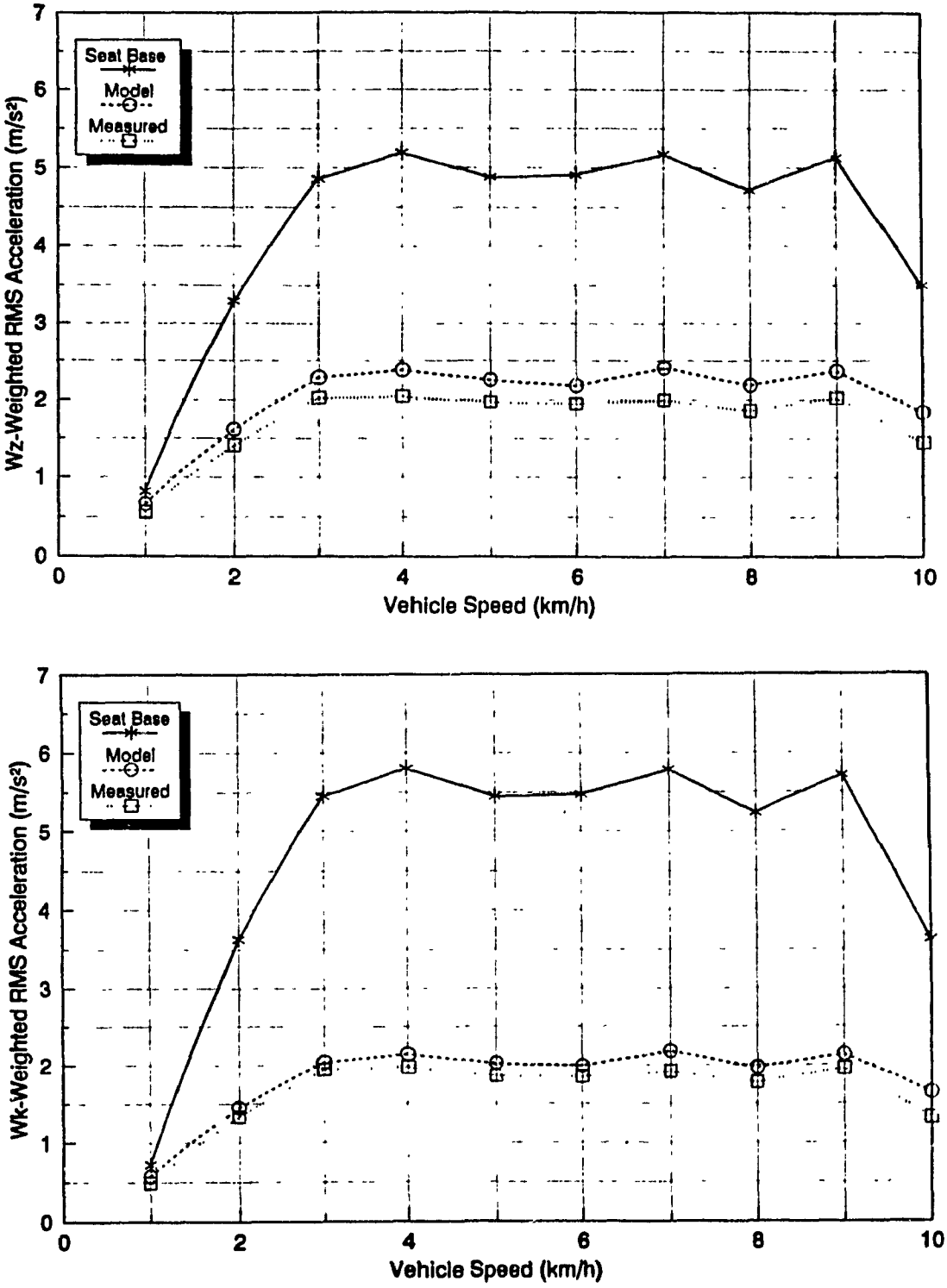

Figure 4.3 Comparison of measured and computed W_z- and W_k- weighted rms acceleration response. (Excitation: 75 mm half-sine displacement) and corresponding base excitation.

performance index used. The W_k-weighted rms acceleration at the base is generally larger than that obtained using the W_z weighting, which implies that the contribution of low frequency components in the 0.5 to 1.0 Hz frequency range is not negligible. This is further emphasized by the fact that, at frequencies ranging between 1 and 5 Hz, the weighting provided by W_z is more pronounced than that with W_k. In contrast, the W_z-weighted acceleration at the driver mass is larger than with W_k, indicating largest contribution from the 1 to 5 Hz frequency components.

Although the measured and model responses exhibit similar trends, the rms weighted acceleration response of the model is slightly larger than that of the measured response. In the worst case, the errors are observed to be nearly 14% and 20 % based upon the W_k-and W_z-weighted rms accelerations, respectively. The analytical model response correlates better with the measured response in the entire speed range when the W_k weighting is applied. Considering that the average operating speed of an off-road vehicle, such as a log skidder, is 5 km/h, the overestimation in exposure level predicted by the model will be in the order of 5 % based on W_k-weighted values, and 15% when using the W_z weighting.

Although the large amplitude peaks observed in the time domain response characteristics relate to the severity of the shock motions, the contribution of these peaks to the overall weighted rms acceleration appears to be insignificant. While the weighted rms acceleration model response is slightly larger than the measured response, the acceleration time response of the model revealed peak magnitudes

considerably lower than those of the measured response (Figure 4.1). This further suggests the negligible contributions of the high magnitude peaks when rms time average is performed.

4.3.6 MODEL VALIDATION BASED ON WEIGHTED RMQ ACCELERATIONS

Figure 4.4 presents a comparison of W_z- and W_k-weighted rmq accelerations of the measured and model response characteristics, together with the weighted rmq acceleration of the seat excitation as a function of the vehicle speed. These weighted rmq accelerations were computed from acceleration time signals, using the frequency domain technique, defined in equation (4.2). The frequency domain technique for computation of the weighted rmq acceleration requires considerably fewer operations than the time domain approach, which involves simultaneous solution of 10 and 12 first-order differential equations, respectively, for the W_z- and W_k-weighted values computed from the model. Computation of the weighted measured response in the time domain also requires solution of 6 and 8 differential equations, respectively, for the W_z and W_k weighting filters. The results derived from the two techniques are compared to demonstrate the validity of the simpler frequency domain method. The two methods provide weighted rmq acceleration values in very close agreement. For the computed acceleration time response of the driver mass at a vehicle speed of 4 km/h, the time domain and frequency domain methods result in W_k-weighted rmq acceleration values of 2.93 ms^{-2} and 2.83 ms^{-2}, respectively. In view of the small error of 3.4 % associated with

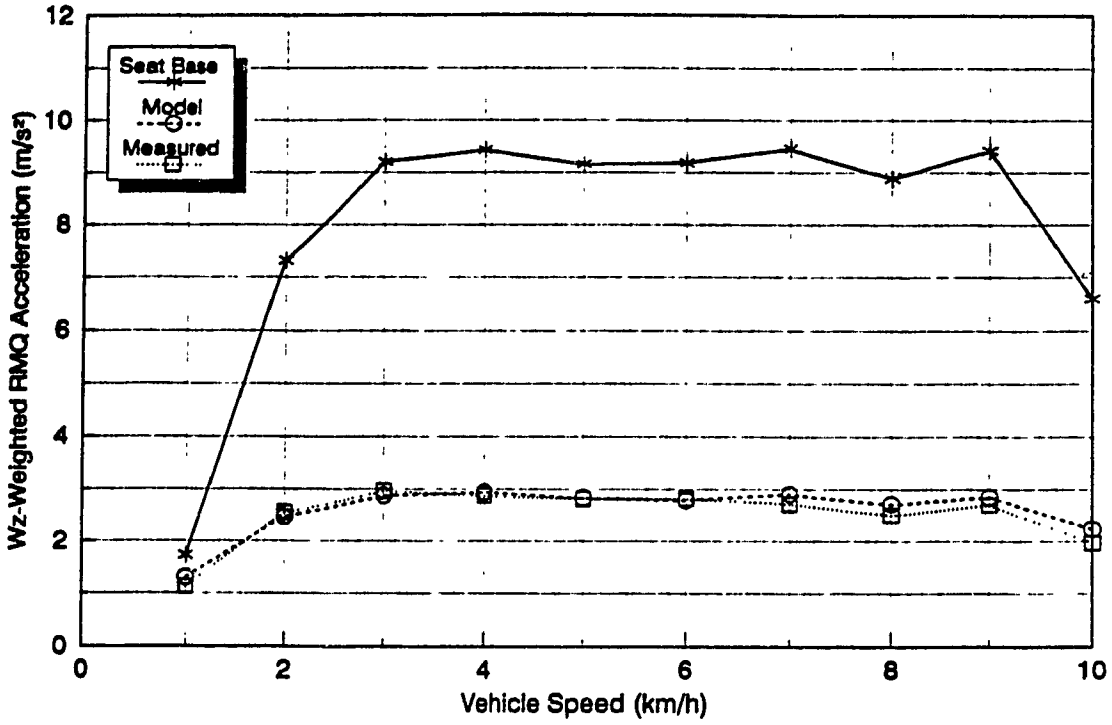

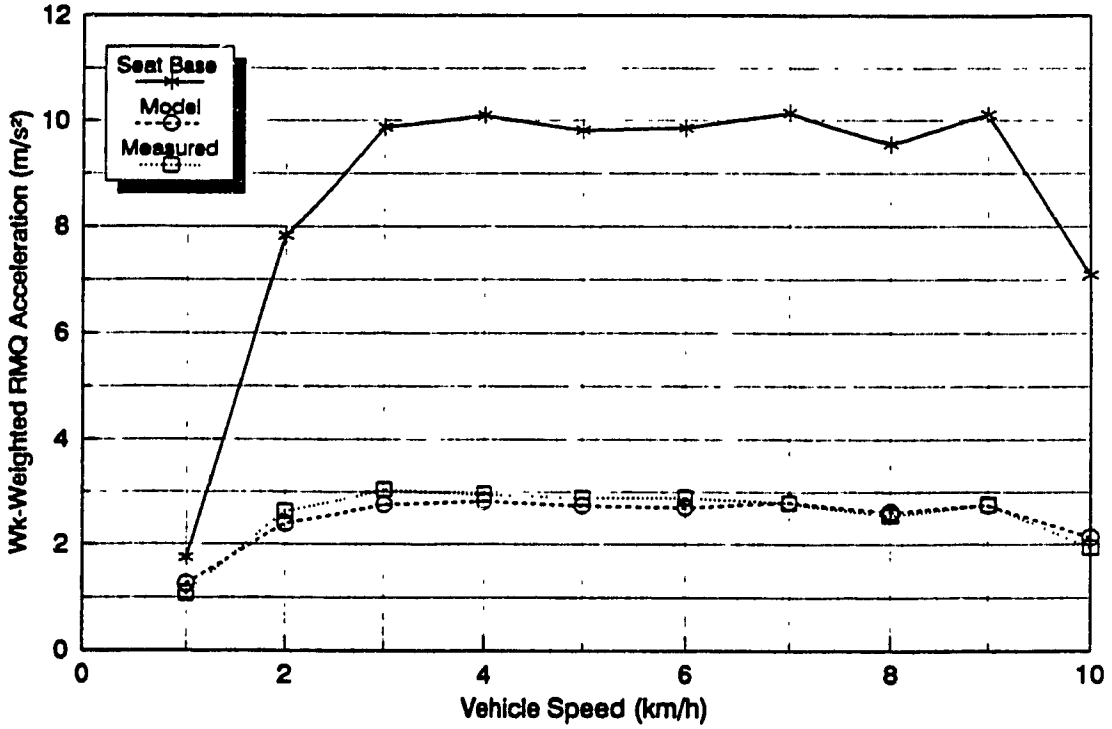

Figure 4.4 Comparison of measured and computed W_z- and W_k-weighted rmq acceleration response (Excitation: 75 mm half-sine displacement) and corresponding base excitation.

the frequency domain method, this procedure was used in all subsequent computations.

Figure 4.4 reveals a very close agreement between measured and computed weighted rmq acceleration response at the driver mass, while the largest difference is observed to be in the order of 6.7% for W_k weighting and 8% for W_z weighting. While the computed weighted rms acceleration response was observed to be larger than measured (Figure 4.3), the rmq acceleration of measured response is slightly greater than that of the model response in the 2 to 6 km/h speed range. The results show that the rmq method places greater emphasis on the large magnitude acceleration peaks, which predominantly occur in the 2 - 6 km/h speed range, as illustrated in Figure 4.1. Figure 4.4 further shows good vibration attenuation properties of the suspension seat, as illustrated earlier in Figure 4.3 in terms of the weighted rms acceleration. The maximum attenuation based upon the S.E.A.T. values, occurs at a speed of 9 km/h for both weighting filters. Similar to the rms weighted acceleration, the W_k-weighted rmq acceleration of the base excitation is slightly larger than the W_z-weighted rmq acceleration. However, unlike the rms accelerations, the rmq values at the driver mass are identical under both weightings.

A comparison of the magnitude of the frequency weighted rms and rmq values, presented in Figures 4.3 and 4.4, for both the base and seat acccelerations indicates that the magnitude of rmq accelerations is significantly larger than the corresponding rms accelerations. Depending on the speed, the magnitude of the

weighted rmq accelerations at the base, in some cases, is more than twice that of the weighted rms acceleration. Although the differences between the weighted rms and rmq acceleration of the driver mass are slightly less, the significantly larger values resulting from the rmq computation may have much importance in terms of dose assessment when shocks are involved.

4.3.7 MODEL VALIDATION BASED ON UNWEIGHTED RMS AND RMQ

Figure 4.5 illustrates a comparison of the measured and computed unweighted rms and rmq accelerations as a function of vehicle speed. The figure also illustrates the overall unweighted rms and rmq accelerations of the base excitations. The results show trends similar to those presented in Figures 4.3 and 4.4. While the unweighted rmq acceleration yields excellent correlation between the measured data and the model response, the unweighted rms acceleration reveals certain errors. The peak error in rms acceleration response is approximately 16%, which reduces to less than 5% for the unweighted rmq values. As with the magnitudes of weighted accelerations, the unweighted rmq accelerations are observed to be significantly larger than the rms magnitudes of accelerations, especially for the base excitation. The contributions of the larger instantaneous peaks recorded during measurements, although believed to be linked with an undesired experimental condition, appear to be less significant since both the measured and computed unweighted rmq accelerations are reasonably close.

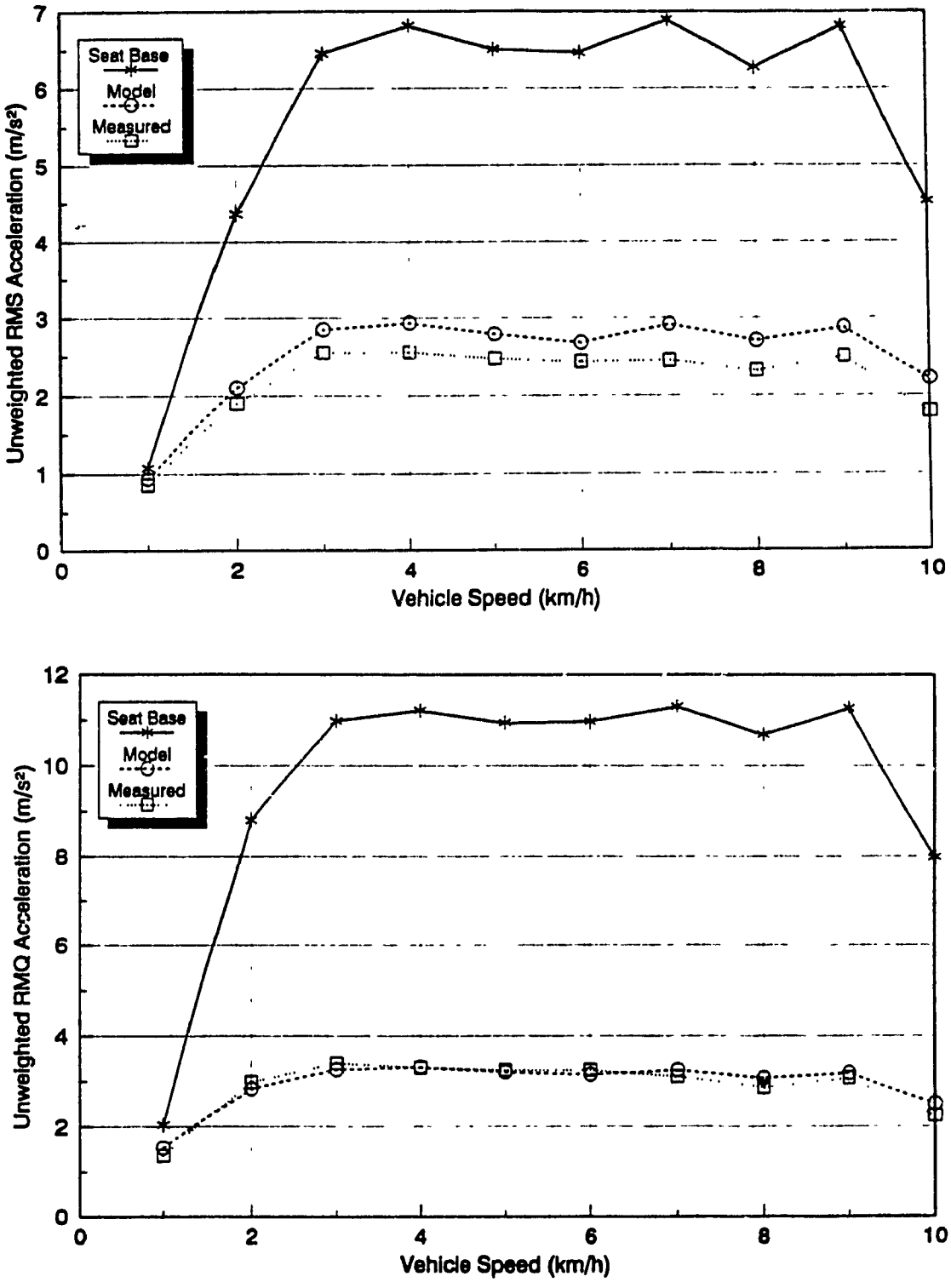

Figure 4.5 Comparison of measured and computed unweighted rms and rmq acceleration responses (Excitation: 75 mm half-sine displacement) and corresponding base excitations.

4.4 Analysis of the Combined Vehicle-Seat Model under Varying Shock Inputs

In the previous section, the two-degree-of-freedom nonlinear suspension seat model was validated under shock inputs characterized by a two-degree-of-freedom vehicle model subject to a half-sine displacement excitation with peak amplitude of 75 mm and width of 200 mm. The shock input characteristics were modified by varying the vehicle speed in the 1 to 10 km/h range. The excellent agreement with the measured acceleration response at the driver mass, particularly when the rmq procedure is selected as the performance index, demonstrates the validity of the suspension seat model for predicting the response under shock excitations. The shock isolation properties of the suspension system, however, may be strongly affected by the severity of shock excitations, primarily due to interactions with the motion-limiting stops. The performance characteristics of the suspension seat are thus investigated for different levels of shock excitations, obtained by varying the peak amplitude of the half-sine displacement excitation. The coupled suspension seat-vehicle model illustrated in Figure 4.6 is analyzed to assess the impact of varying shocks on the seat suspension performance. The analyses are performed for different vehicle speeds ranging from 1 to 10 km/h and half-sine displacement inputs with peak amplitudes of 50, 100 and 150 mm, while the obstacle width is maintained at 200 mm. The differential equations of motion of the combined four-degree-of-freedom vehicle-seat model are given by:

$$m\ddot{z} + F_{Tf}\left(z, z_{pf}, \theta, t\right) + F_{Tr}\left(z, z_{pr}, \theta, t\right) - F_S\left(x_1, \beta\right) - F_K\left(x_1\right) - F_F\left(\dot{x}_1\right) - F_D\left(\dot{x}_1, \alpha\right) = 0. \quad (4.3)$$

$$I\ddot{\theta}+\ell_f F_{Tf}\left(z,z_{pf},\theta,t\right)-\ell_r F_{Tr}\left(z,z_{pr},\theta,t\right)+\ell_S\left\{F_S\left(x_1,\beta\right)+F_K\left(x_1\right)+F_F\left(\dot{x}_1\right)+F_D\left(\dot{x}_1,\alpha\right)\right\}=0. \tag{4.4}$$

$$m_S\ddot{z}_1+F_S\left(x_1,\beta\right)+F_K\left(x_1\right)+F_F\left(\dot{x}_1\right)+F_D\left(\dot{x}_1,\alpha\right)-F_c\left(x_2,\dot{x}_2\right)=0. \tag{4.5}$$

$$m_0\ddot{z}_2+F_c\left(x_2,\dot{x}_2\right)=0. \tag{4.6}$$

where the relative displacements are given by:

$$x_2 = z_2 - z_1$$

$$x_1 = z_1 - z_0 = z_1 - z + \ell_S\theta \tag{4.7}$$

In the above equations, the front and rear tire forces are given by equation (2.7), while equations (3.2) to (3.7) provide the expressions for the forces developed by the suspension seat components. These equations are solved in the time domain, using numerical integration, for the shock inputs defined by equations (2.4) and (2.8).

Of the various performance indices identified in the preceeding sections for validating the model, only three rely specifically on methods advocated within the current standard and its proposed revision for assessing whole-body vibration exposure when shocks are involved. In the current standard, only the rms averaging

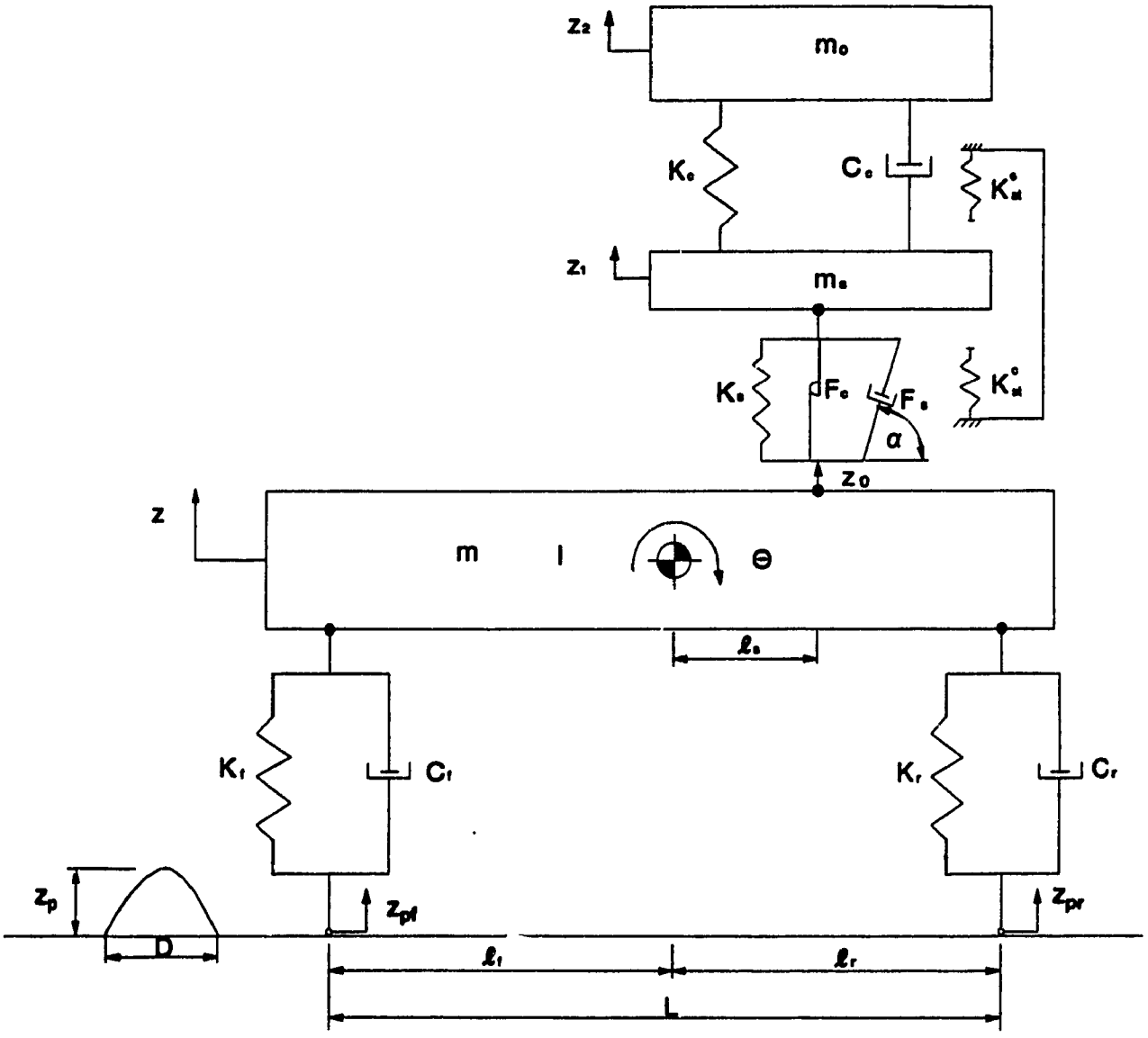

Figure 4.6 Four-degree-of-freedom combined vehicle-seat model for the assessment of driver mass shock response.

method is defined, using the W_z weighting, although no specific method is defined for shock motions for which the crest factor is greater than 6. In the proposed revised standard, the W_z weighting is replaced with the W_k weighting for assessing vertical vibration. The rmq averaging, however, is recommended in the revised standard in addition to the rms averaging for motions involving crest factors in excess of 9. Based upon the recommendations of the current standard and its proposed revision, the assessment of exposure to whole-body vibration comprising shock motions necessitates the determination of the following performance indices at the driver-seat interface:

- the W_z frequency-weighted rms acceleration in the 1.0 to 80 Hz frequency range (current standard);
- the W_k frequency-weighted rms acceleration in the 0.5 to 80 Hz frequency range (proposed revision);
- the W_k frequency-weighted rmq acceleration in the 0.5 to 80 Hz frequency range (proposed revision).

The influence of varying levels of shock inputs on the driver mass vibration exposure levels is estimated, using the three assessment methods identified above. The weighted accelerations are computed from the driver mass acceleration responses derived from the combined vehicle-seat model.

4.4.1 INFLUENCE OF SHOCK INPUT VARIATIONS ON WEIGHTED RMS ACCELERATIONS

Figure 4.7 illustrates the overall W_z-weighted rms acceleration response at the driver mass (seat) and at the seat attachment point (base) as a function of vehicle speed and magnitude of shock input arising from obstacle heights of 50, 100 and 150 mm. A comparison of the seat and base weighted acceleration levels for different shock excitations reveals that the degree of attenuation provided by the seat is directly related to the characteristics of the shock motions.

For an obstacle height of 50 mm, the seat provides vibration attenuation over the entire range of vehicle speeds, while the attenuation at low speeds is only minimal. In the 3 to 10 km/h speed range, however, the S.E.A.T. value for shock excitations caused by a 50 mm half-sine pulse is in the order of 0.7. When the magnitude of shock excitation is increased by increasing the peak displacement amplitude of the pulse to 100 mm, the seat attenuates vehicle vibration only at speeds exceeding 6 km/h. At lower speeds, the seat tends to amplify the base vibration and the maximum S.E.A.T. value approaches 2.7 at a speed of 3 km/h. A further increase in the peak displacement amplitude of the pulse to 150 mm results in the seat amplifying the base acceleration levels over almost the entire speed range, except at 10 km/h. Under these conditions, the peak S.E.A.T. value approaches 2.9 at a speed of 3 km/h.

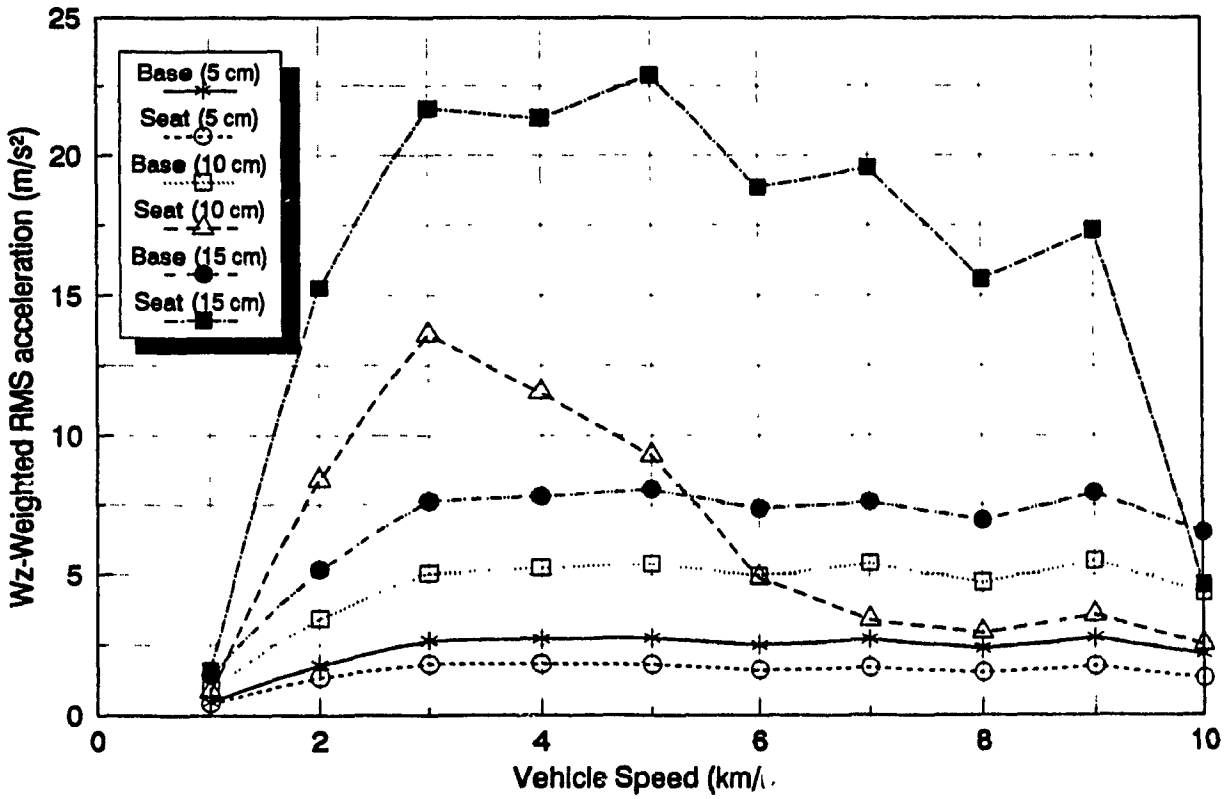

Figure 4.7 Influence of obstacle height and vehicle speed on W_z-weighted rms accelerations computed at the driver mass and at the seat attachment point using the combined vehicle-seat model.

The results clearly illustrate that the performance characteristics of suspension seats under shock excitations are strongly related to the shock input characteristics, determined from the vehicle speed and the obstacle height. The poor suspension performance under higher levels of shock excitations is attributed to the excessive relative displacement response of the suspension. For excitations arising from obstacle heights of 100 and 150mm, the relative displacement of the suspension was observed to exceed the permissible travel, implying an interaction with the highly stiff motion limiting bump stops. The shock excitations due to the 50 mm half-sine pulse yield suspension relative motion within the permissible travel, leading to noticeable attenuation.

The apparent effect of bump stop interactions on the exposure levels is further assessed by comparing the W_z-weighted rms acceleration at the driver mass for various obstacle heights at a speed of 3 km/h. The corresponding W_z-weighted rms acceleration at the driver mass is observed to vary from 1.72 ms^{-2} for a 50 mm obstacle to 21.6 ms^{-2} for a 150 mm obstacle, which illustrates a significant increase in apparent exposure level considering that the seat bottoming occurs frequently in off-road vehicle driving.

Figure 4.8 illustrates the W_k-weighted rms acceleration response for different vehicle speeds and peak pulse displacements. The trends are quite similar to those observed with the W_z-weighted values, with acceleration levels being slightly lower when the W_k weighting is applied.

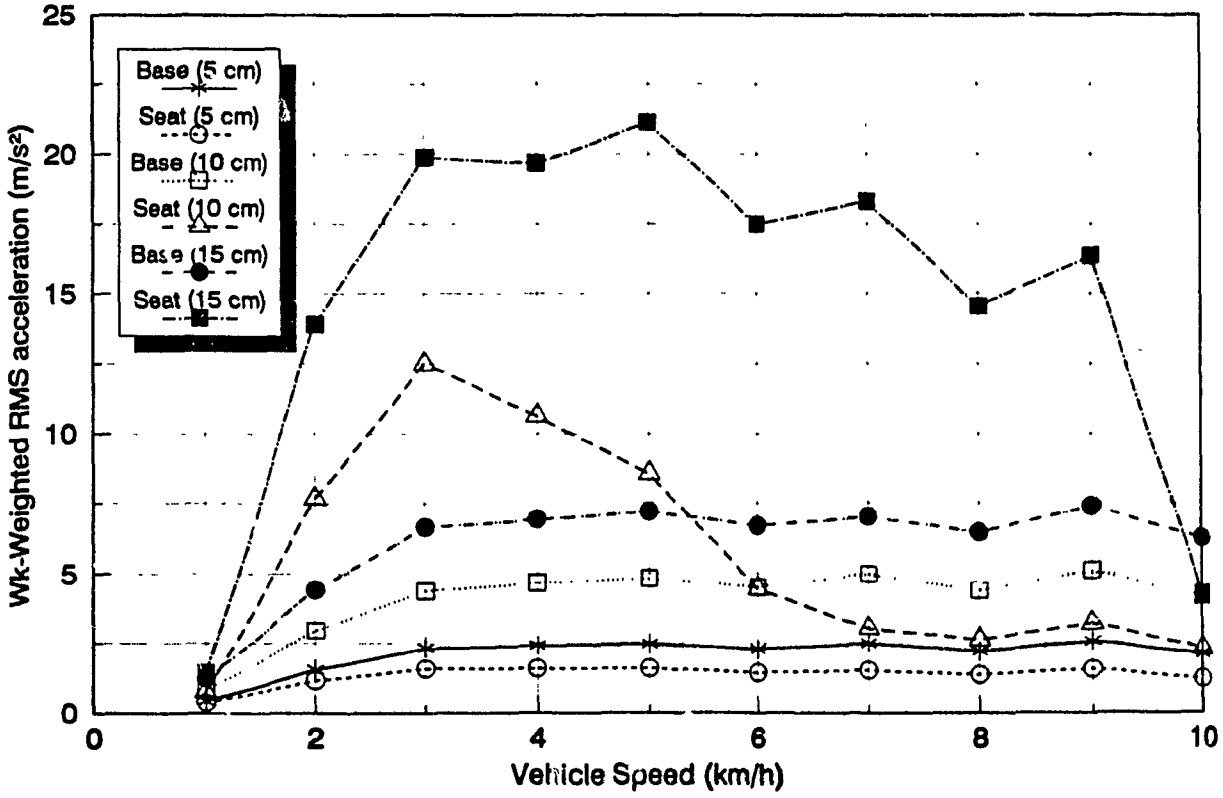

Figure 4.8 Influence of obstacle height and vehicle speed on W_k-weighted rms accelerations computed at the driver mass and at the seat attachment point from the combined vehicle-seat model.

4.4.2 INFLUENCE OF SHOCK INPUT VARIATIONS ON WEIGHTED RMQ ACCELERATIONS

Figure 4.9 presents the W_k-weighted rmq accelerations computed at the driver mass and at the seat base for various obstacle heights and vehicle speeds. Apart from the significantly larger acceleration values predicted using this technique, the pattern is observed to be quite similar to that established with weighted rms values. At a vehicle speed of 3 km/h, the W_k-weighted rmq acceleration at the driver mass is 2.8 ms^{-2} for a 50 mm obstacle, 23.3 ms^{-2} for a 100 mm obstacle, and 36.1 ms^{-2} for a 150 mm obstacle. The corresponding S.E.A.T. values computed on the basis of rmq accelerations are 0.71, 3.0 and 3.17 for the respective obstacle heights. The estimated performance of the seat is thus very slightly impeded when the performance index is based upon the weighted rmq acceleration as opposed to that based upon the rms method.

4.5 Suspension Seat Model Parametric Study under Shock Excitations

Two distinct suspension performance characteristics can be identified from the results presented in Figures 4.7 to 4.9, one involving an interaction with the elastic bump stops, the other in the absence of such interactions. A parametric study is thus carried out to identify the best possible design characteristics under both conditions. The parametric study is performed using the combined vehicle-seat model, shown in Figure 4.6, subject to two shock inputs: (i) half-sine pulse with peak amplitude displacement of 50 mm leading to suspension relative displacement within the permissible travel; and (ii) half-sine pulse with peak displacement amplitude of

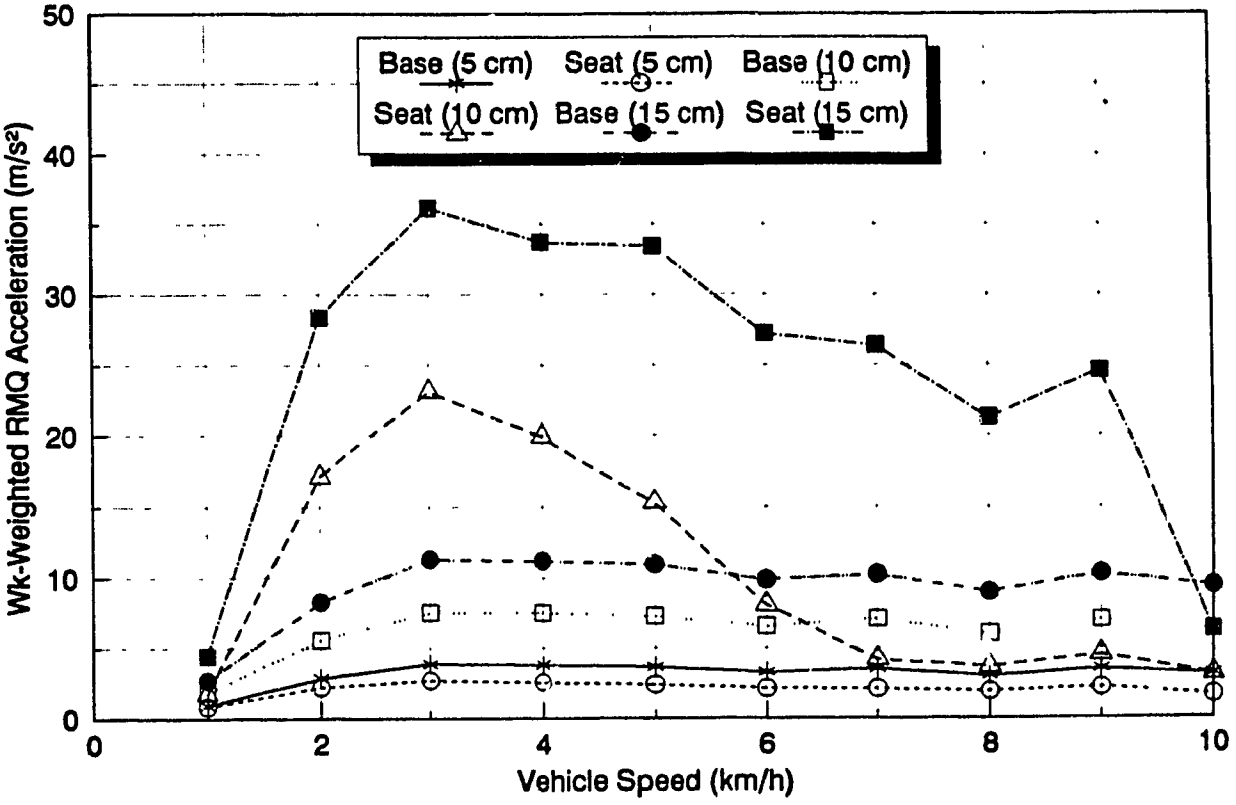

Figure 4.9 Influence of obstacle height and vehicle speed on W_k-weighted rmq accelerations computed at the driver mass and at the seat attachment point from the combined vehicle-seat model.

100 mm leading to interactions with the bump stops. A vehicle speed of 3 km/h is selected to perform the analysis since it was found to provide the largest driver mass acceleration response for a 100 mm obstacle, as shown in Figures 4.7 to 4.9.

The parametric analysis is performed in a manner analogous to that described in Chapter 3, namely by varying the suspension seat model parameters one at a time from 0.4 to 1.6 times the baseline values identified in Table 3.1. The performance indices selected are those identified in section 4.4, namely overall W_z- and W_k-weighted rms accelerations and W_k- weighted rmq acceleration at the driver mass.

4.5.1 RESPONSE TO SHOCK EXCITATIONS WITHOUT BUMP STOP INTERACTIONS

Figures 4.10, 4.11 and 4.12 summarize the results of the parametric sensitivity analysis based on the W_z-weighted rms, the W_k-weighted rms and the W_k-weighted rmq driver mass acceleration response, respectively. The results are derived for a shock input of 50 mm peak displacement, implying no interactions with the bump stops. A comparison of the figures reveals almost similar relative influence of the model parameters on all three performance indices selected. The parameters found to have the most influence on the seat acceleration exposure levels are, in order of importance, the low damping coefficient, C_L, corresponding to blow-off stage, the suspension stiffness, K_s, the suspension mass, m_s, and the high damping coefficient, C_H, corresponding to bleed flows. Variations in other parameters of lesser importance yield less than 5% variation in the acceleration response. These

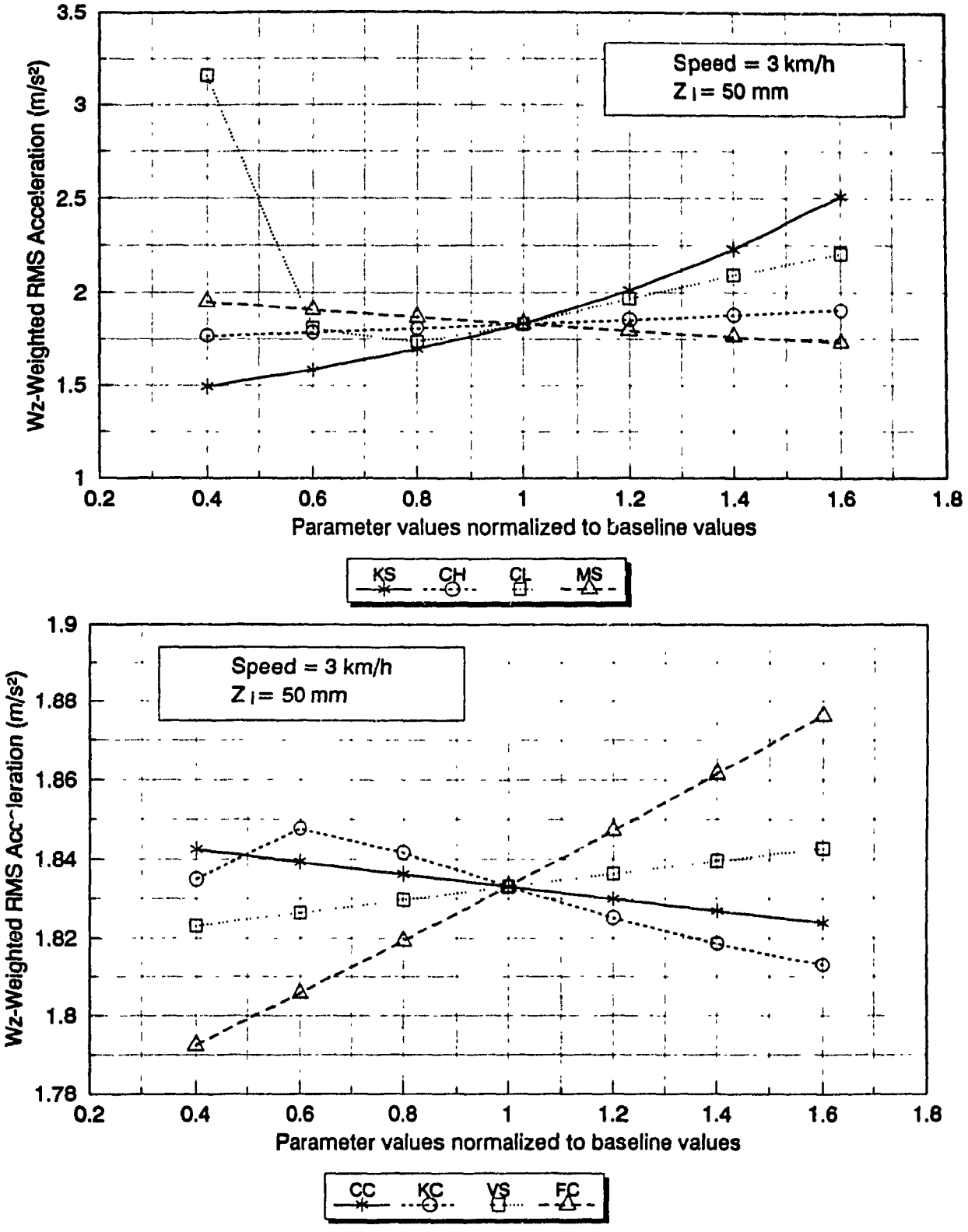

Figure 4.10 Influence of suspension seat model parameters on the W_z-weighted rms acceleration of the driver mass for a 50 mm peak displacement shock input at a vehicle speed of 3 km/h (obstacle width: 200 mm).

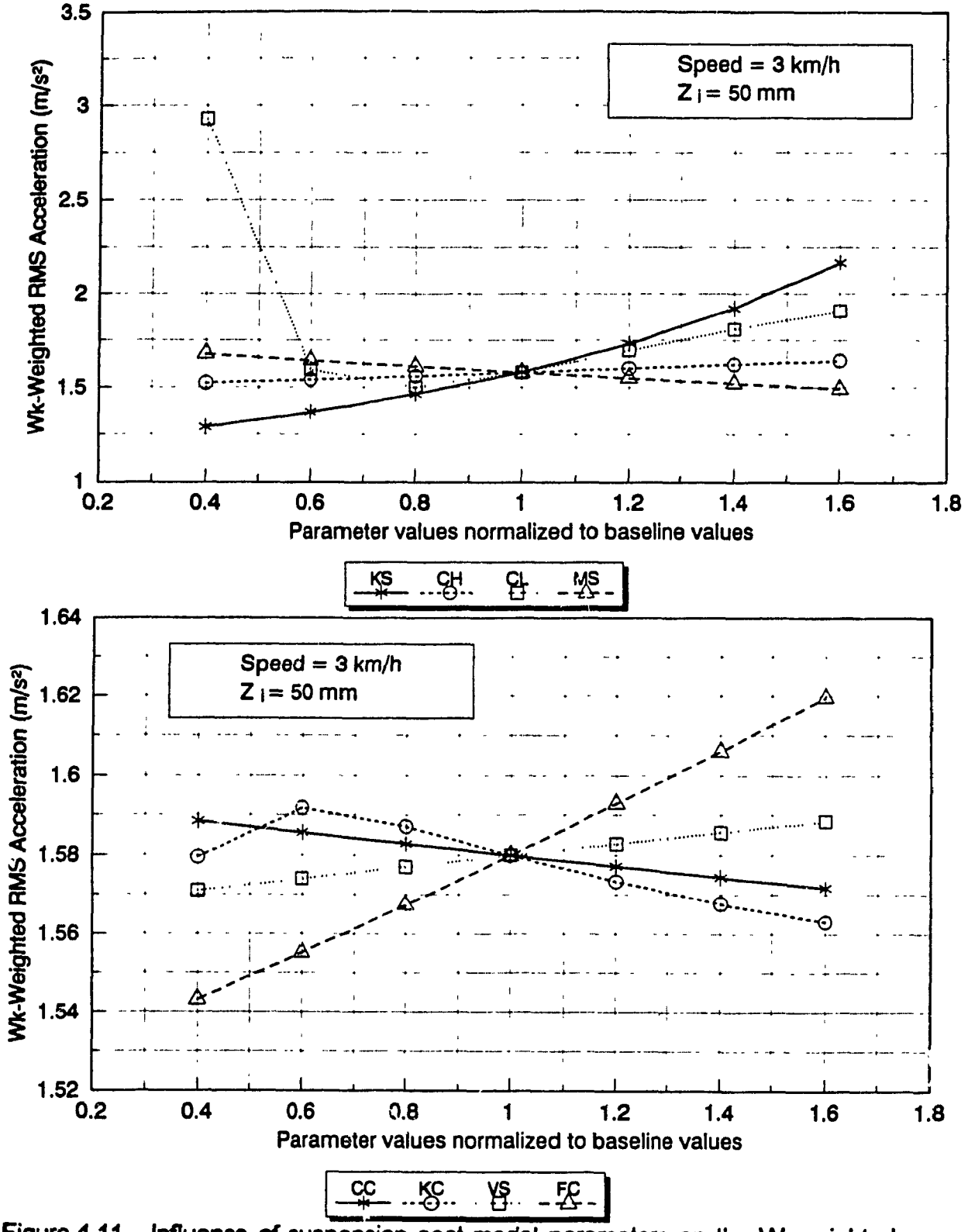

Figure 4.11 Influence of suspension seat model parameters on the W_k-weighted rms acceleration of the driver mass for a 50 mm peak displacement shock input at a vehicle speed of 3 km/h (obstacle width: 200 mm).

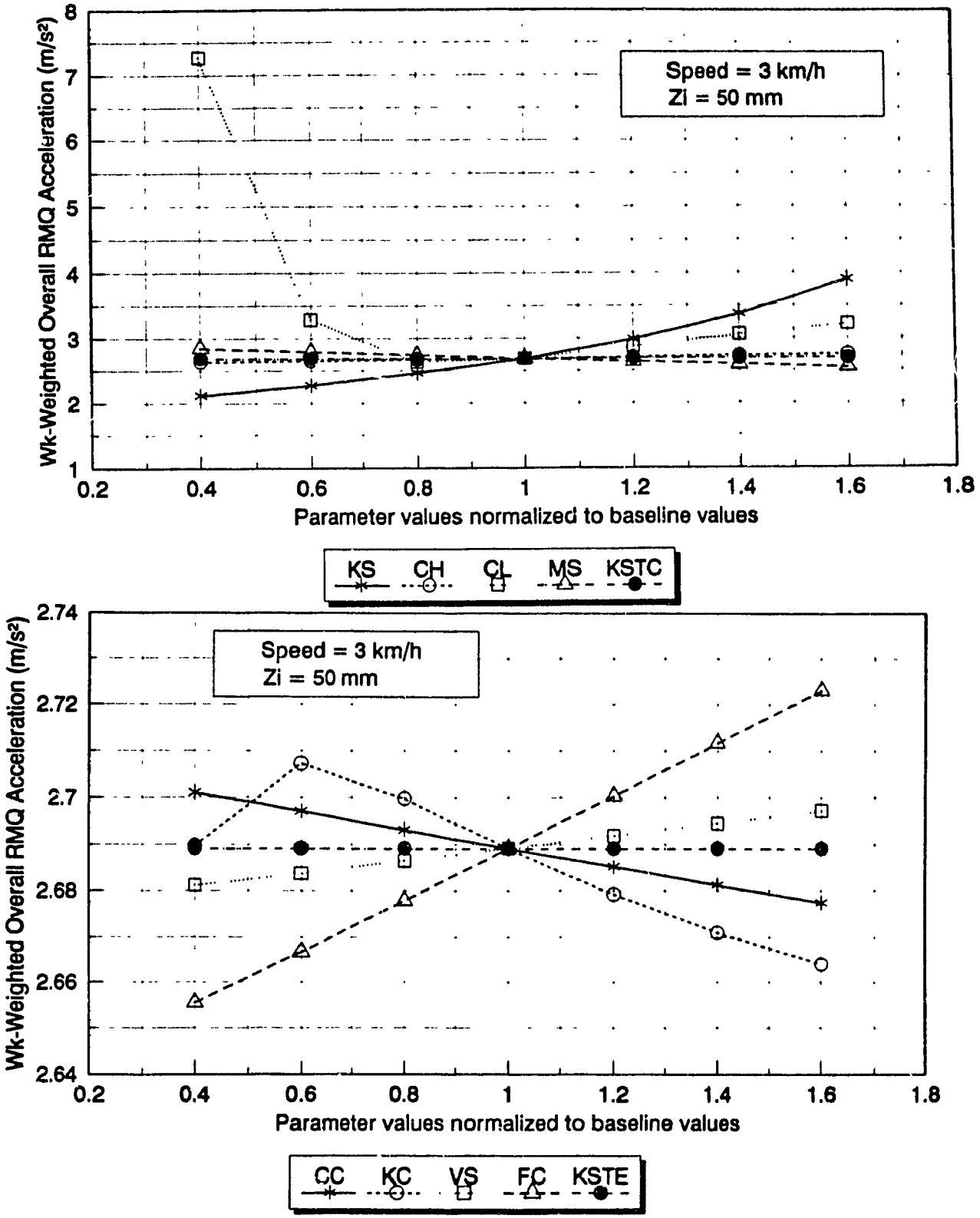

Figure 4.12 Influence of suspension seat model parameters on the W_k-weighted rmq acceleration of the driver mass for a 50 mm peak displacement shock input at a vehicle speed of 3 km/h (obstacle width: 200 mm).

parameters, in order of importance, include Coulomb damping force, F_c, cushion stiffness, K_c, cushion damping coefficient, C_c, and shock absorber transition velocity, V_s.

In order to provide the lowest vibration exposure for the drivers under such conditions, the results suggest the following suspension seat design guidelines involving the selection of:

- a shock absorber with lower damping coefficients corresponding to bleed flows (C_H) and blow-off flows (C_L, reduced to 80% of the nominal value), and lower transition velocity (V_s);
- a reduced suspension spring stiffness (K_s);
- an increased suspension mass (m_s);
- a reduced Coulomb damping force (F_c);
- a seat cushion with increased stiffness and damping coefficients (K_c and C_c).

The above design recommendations are quite similar to those established in section 3.6.3 for the ISO 2 random excitation class, except for the lower values of damping coefficient, C_L, which in that case, reduced the exposure levels. A further decrease of the C_L value, however, will lead to a significant increase in the exposure level, as illustrated in Figures 4.10 to 4.12. The C_L value equal to 80% of its baseline value yields the lowest exposure level.

Since the seat dominant excitation frequency produced by the vehicle passing over

the defined obstacle at a speed of 3 km/h is approximately 2.08 Hz, a decrease in the seat natural frequency caused by a reduction in the suspension spring rate yields improved vibration attenuation at the excitation frequency. An increase in the suspension mass also yields a slightly lower suspension seat resonant frequency, leading to better vibration attenuation at the excitation frequency. However, the corresponding decrease in the damping ratio due to increased mass impedes the effect at the seat resonant frequency, although the increase in suspension mass has much less influence on vibration attenuation than the reduction in suspension stiffness.

An increase in the shock absorber damping coefficients corresponding to bleed and blow-off stages (C_H and C_L) tends to suppress the response corresponding to the suspension seat resonant frequency, while impeding the suspension performance at higher excitation frequencies. Since the seat resonant frequency as computed from the model is nearly 1.3 Hz, a reduction in the high and low damping coefficients yields improved vibration attenuation at the excitation frequency, estimated at 2.08 Hz for a vehicle speed of 3 km/h. However, the low damping coefficient corresponding to blow-off stage affects the suspension performance more than the high damping coefficient. Furthermore, a reduction in the shock absorber transition velocity affects the suspension performance in a beneficial manner by providing the low blow-off damping over an extended range of operation.

An increase in the cushion stiffness tends to reduce the resonant acceleration

transmissibility, while leading to only slight improvement in the attenuation characteristics at higher frequencies. The effect of varying the cushion damping is observed to be insignificant within the range of values investigated. A reduction in Coulomb friction force due to shock absorber seal and linkages tends to provide better vibration isolation while increasing the resonant response.

The parameters found to affect the exposure levels in a highly significant manner under the ISO 2 random excitation class, also show considerable influence under the 50 mm shock input. Although the ISO 2 and shock excitations exhibit considerable differences in magnitude and frequency characteristics, the influence of suspension parameters on the exposure level follows a similar trend, provided the interactions with the bump stops is not present. The exposure levels resulting from a 50 mm single shock event, however, are significantly higher than under ISO 2 excitation. For a seat with baseline parameters, the results presented in Figures 4.10 to 4.12 for a single shock event indicate values of W_z- and W_k-weighted rms acceleration of 1.82 and 1.59 ms^{-2}, respectively, while the W_k-weighted rmq acceleration is 2.7 ms^{-2}. The weighted rms accelerations are thus 70 to 80% higher than computed under ISO 2 excitation and would result in the ISO 2631/1 " exposure limit" being reached after 1.5 h, while the " health guidance caution zone" defined in the revised standard would be exceeded after 1 hour. On the basis of the W_k-weighted rmq value, the " health guidance caution zone" would be exceeded after 30 minutes of exposure to such events.

From the results of the parametric study, a reduction of suspension stiffness to 40% of its initial value provides the greatest reduction in exposure levels (≅20%). These reductions in exposure levels due to a single shock event result in increases in tolerable daily exposure durations to 2 h for the "exposure limit" (W_z-weighted rms) and the "health guidance caution zone" (W_k-weighted rms), but to 1 h when based on W_k-weighted rmq. Although single shock events usually occur intermittently during a workday, the results presented above indicate the significant contribution such events can have on the daily exposure levels.

4.5.2 RESPONSE TO SHOCK EXCITATIONS INVOLVING BUMP STOP INTERACTION

Figures 4.13, 4.14 and 4.15 illustrate the influence of suspension parameters on the W_z-weighted rms, the W_k-weighted rms and the W_k-weighted rmq acceleration response, respectively, of the suspension seat subject to shock excitations due to a 100 mm peak displacement pulse. The pulse excitation considered at the vehicle tires resulted in excessive relative displacement response of the suspension seat and thus interactions with the bump stops. The low damping coefficient, C_L, exhibits the strongest influence on the vibration exposure levels at the driver mass under such excitations. In contrast with the behaviour observed for a 50 mm shock input, a large value of C_L results in the lowest exposure levels. Other suspension parameters that affect the exposure levels, in order of importance, include: the cushion stiffness, K_c, the extension bump stop stiffness, K_{st}^e, the suspension stiffness, K_s, and the compression bump stop stiffness, K_{st}^c. Variations in

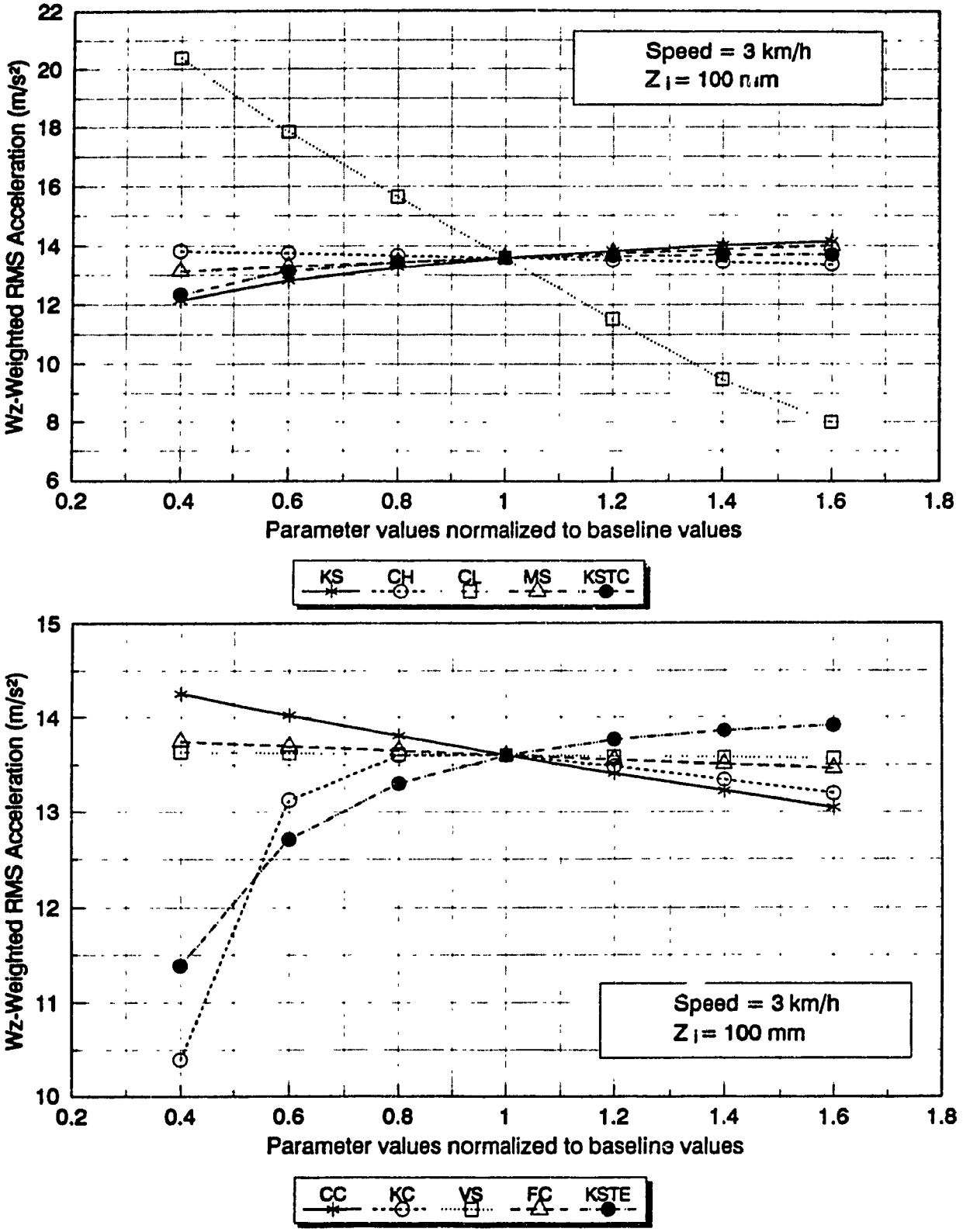

Figure 4.13 Influence of suspension seat model parameters on the W_z-weighted rms acceleration of the driver mass for a 100 mm peak displacement shock input at a vehicle speed of 3 km/h (obstacle width: 200 mm).

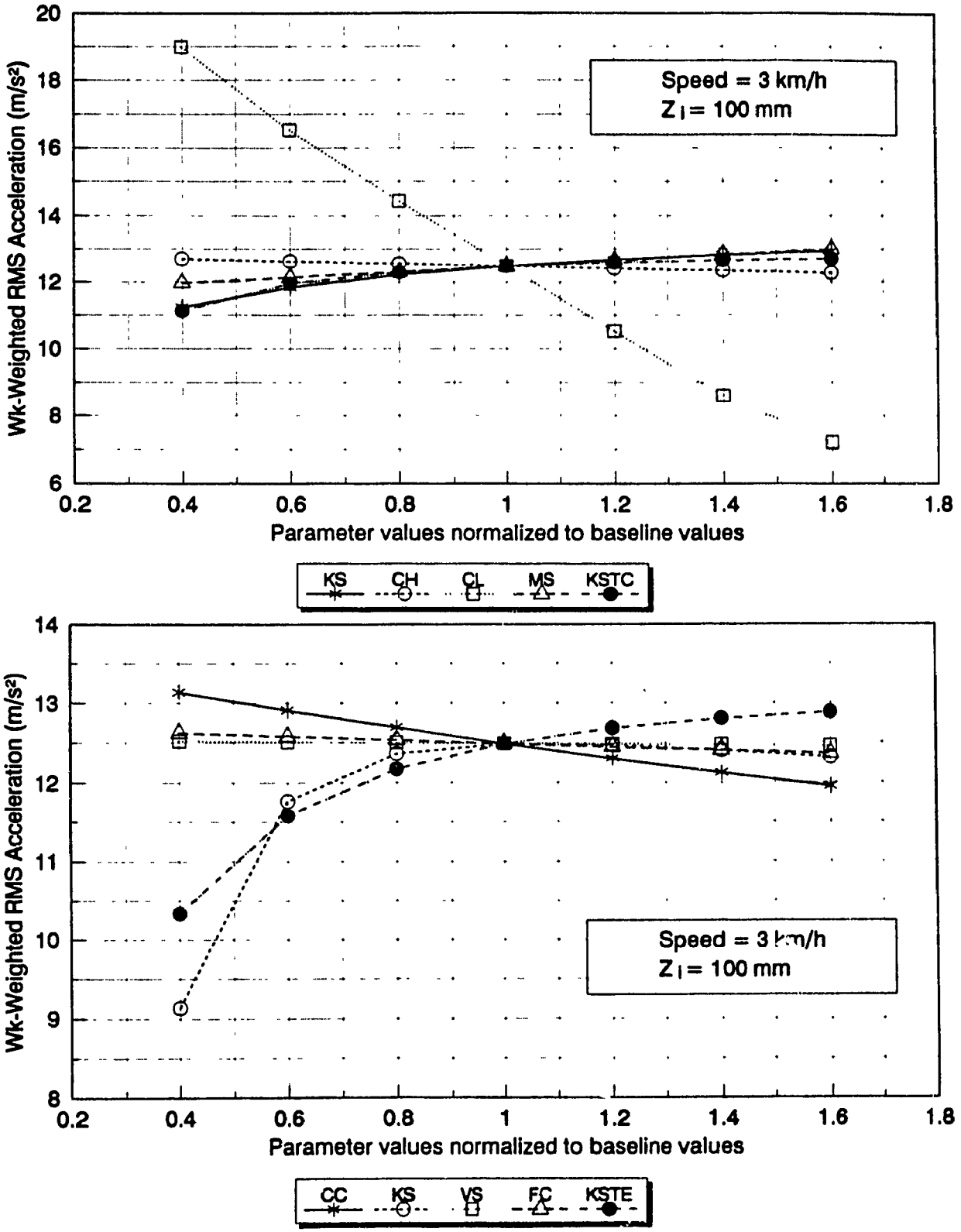

Figure 4.14 Influence of suspension seat model parameters on the W_k-weighted rms acceleration of the driver mass for a 100 mm peak displacement shock input at a vehicle speed of 3 km/h (obstacle width: 200 mm).

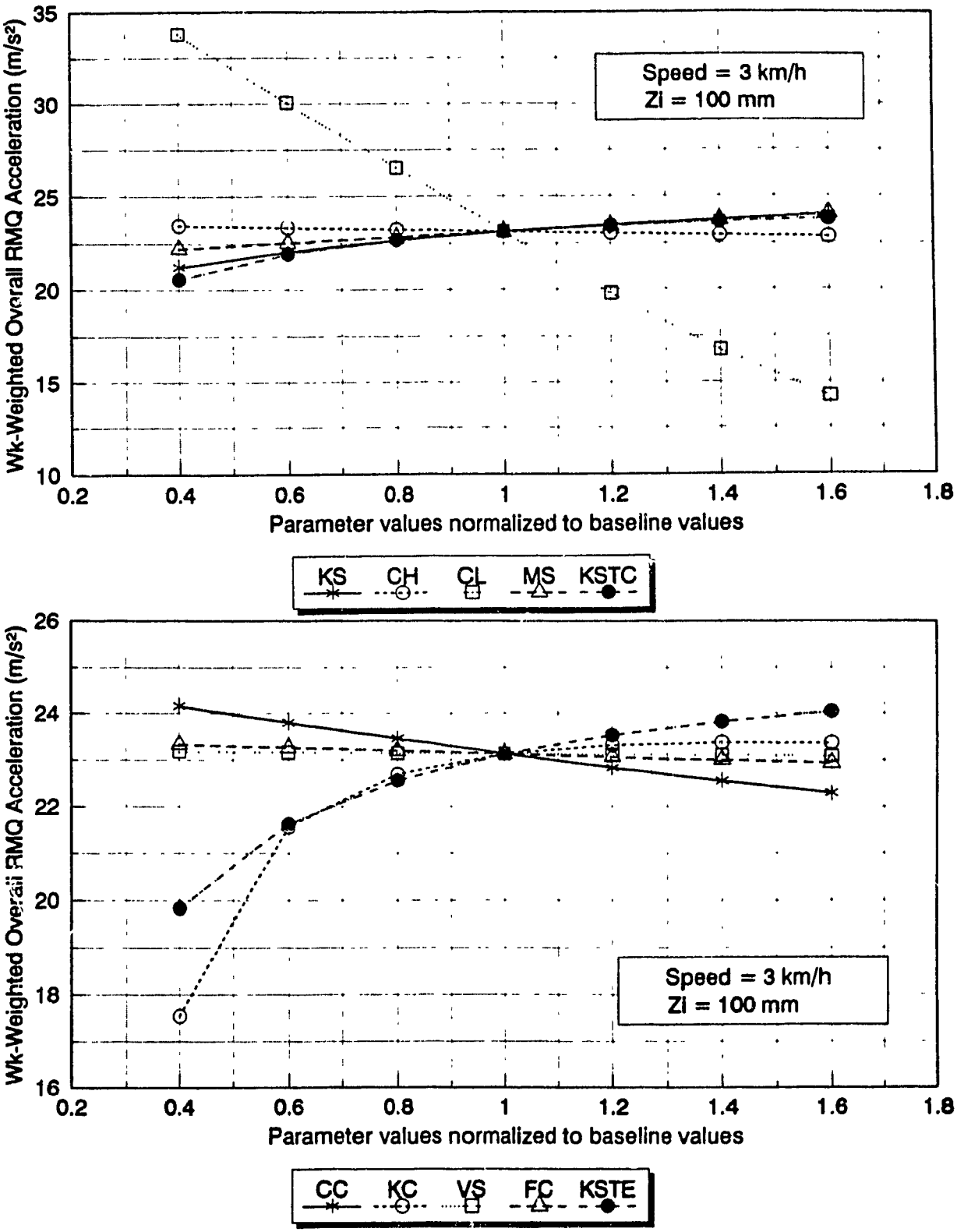

Figure 4.15 Influence of suspension seat model parameters on the W_k-weighted rmq acceleration of the driver mass for a 100 mm peak displacement shock input at a vehicle speed of 3 km/h (obstacle width: 200 mm).

suspension parameters, such as the cushion damping, C_c, the suspension mass, m_s, the high damping coefficient, C_H, and the Coulomb friction damping force, F_C, affect the exposure levels in a relatively less significant manner. Variations of these suspension parameters over the specified range result in less than 10% variations in the exposure levels, while the shock absorber transition velocity, V_s, shows no influence.

The design recommendations for suspension seats subject to shock motions and interactions with the bump stops can be derived from an examination of Figures 4.12 to 4.15. A suspension seat with the following design characteristics will yield considerable reduction in the vibration exposure levels:

- a shock absorber with higher damping coefficients corresponding to bleed and blow-off stages irrespective of the transition velocity;
- softer extension and compression bump stops;
- a softer suspension spring;
- lower suspension mass;
- a higher Coulomb damping force;
- cushion with reduced stiffness and increased damping coefficient.

Apart for the suspension spring stiffness and the cushion damping coefficient, the above guidelines are in direct opposition with the trends observed in situations not involving an interaction with the bump stops. The low damping coefficient is

observed to have by far the most influence on the exposure levels, involving variations of more than 200% when varied over the entire range of values. In contrast, variations in stiffness characteristics of the cushion and extension bump stop result in variations in the order of 20 to 30 %, while variations in the stiffness of suspension and compression bump stop show 10 to 20% variations in the exposure levels. Considering the exposure levels predicted by each method, the lowest exposure is achieved for a large value of C_L, while all the other parameters are set equal to their baseline values. Higher values of C_L can lead to a 40% reduction in the exposure level when compared to that of the baseline suspension. All the other parameters listed in the design recommendations lead to relatively less reductions in the exposure levels.

The interactions with the bump stops encountered under a 100 mm shock input not only yield considerably higher exposure levels but also alter the dominant excitation frequency. For a seat with a suspension stiffness equal to its baseline value, the interaction with the bump stops tends to increase the magnitude of excitation near the seat resonant frequency. Increased shock absorber and Coulomb damping forces, and lower cushion stiffness are thus highly desirable to effectively suppress the resonant response. A reduction in the suspension stiffness, however, yields an increase in the suspension relative displacement and thus more frequent interactions with the bump stops. The corresponding predominant excitation frequency thus tends to shift beyond the seat resonant frequency. The seat suspension with lower resonant frequency well below the predominant excitation

frequency then provides increased attenuation performance. Furthermore, a reduction in the suspension mass results in improved vibration attenuation performance due to relatively low inertia impacts against the motion limiting stops. A reduction in the stiffness of the bump stops tends to reduce the peak forces caused by the interactions and thus, the transmitted vibration.

The vibration exposure levels resulting from single events created by a 100 mm shock input are extremely severe, being close to 8 times those computed with a 50 mm shock input. For a suspension seat with baseline parameters, the W_z- and W_k-weighted rms accelerations are 13.6 and 12.5 ms^{-2}, respectively, while the W_k-weighted rmq acceleration is 23.2 ms^{-2}. The exposure to only a few single shock events of this nature within a workday would constitute a health hazard, irrespective of the assessment method used. Optimization of the seat suspension to include a high value of low damping coefficient would not be sufficient to reduce the health hazard significantly.

4.5.3 RECOMMENDED SUSPENSION SEAT PARAMETERS FOR OFF-ROAD VEHICLES

From the results of the parametric sensitivity analysis, it is apparent that the relative influence of the suspension seat design parameters under shock excitation is dependent upon whether or not the shock excitations create an interaction with the suspension travel limiting bump stops. Under conditions involving no such interactions, the suspension seat behaviour under shock excitation is similar to that

determined under continuous motions such as the ISO 2 random excitation class. The recommended suspension seat design parameters can thus be identified to satisfy the exposure requirements under vibration predominant around the resonant frequency of the vehicle, which frequently occurs well beyond the seat resonant frequency. For intense shock excitations, however, the effects of bump stop interaction tend to create an apparent excitation of the driver mass at a frequency dependent on the frequency of the interactions. For the suspension seat model considered in this study, with the baseline parameters identified in Table 3.1, the frequency of interactions occurs near the seat resonant frequency. The design recommendations thus need to be defined to suppress the resonant vibration. Since the design requirements for attenuating vibration near the resonant frequency contradict with those required to attenuate vibration at frequencies above, the suspension seat for off-road vehicle applications frequently subject to shock motions poses a complex design problem involving a compromise between the resonant and isolation performance. Since the suspension damping affects both the resonant and isolation performance in a significant manner, it is highly recommended to employ tunable shock absorbers in suspension seats used in off-road vehicles. The suspension damping can then be varied conveniently to meet the requirements dependent upon the terrain conditions. Furthermore, softer bump stops may be incorporated to reduce the magnitude of forces resulting from the interactions.

In driving situations involving predominantly bump stop interactions, the design guidelines defined in section 4.5.2 should be followed as best as possible, while a

compromise between the reduced exposure levels and increased relative displacement of the driver mass must be achieved. In cases involving relative displacements predominantly within the clearance, the design guidelines defined in section 4.5.1 appear appropriate.

4.6 Summary

The nonlinear suspension seat model is validated under shock excitations arising from vehicle interactions with an idealized half-sine pulse obstacle. The model parameters, identified earlier in Chapter 3, are used and the validation is performed for shock inputs arising from a 200 mm wide pulse with peak amplitude of 75 mm, encountered at speeds ranging from 1 to 10 km/h. A number of performance indices are defined to assess the driver mass exposure levels under shock excitations The validity of the analytical model is demonstrated by the excellent agreement between the measured and computed response characteristics, which are presented in terms of frequency-weighted and unweighted rms and rmq accelerations. Although best results are obtained while basing the validation on the rmq acceleration values, the peak difference noted with rms accelerations are below 20%. Two distinct shock response characteristics of the suspension system are identified dependent upon the levels of shock excitations: (i) presence of interactions with the travel limiting bump stops caused by excessive relative motions; and (ii) relative displacement response of the suspension within the permissible travel and thus, no interactions with the bump stops. In situations not involving bump stop interactions, the influence of the various suspension seat design parameters on the driver mass

exposure levels is found to be similar to that established under ISO 2 random excitation class. The vibration exposure levels resulting from single shock events are considerably larger than under continuous vibration and the health criteria associated with the various assessment methods are quite limitative on tolerable daily exposure duration, particularly when bump stop interactions occur. Bump stop interactions are found to introduce an apparent excitation frequency closer to the seat resonant frequency. Under such conditions, the design requirements are found to contradict with those established with the absence of bump stop interactions.

CHAPTER 5

WHOLE-BODY BIODYNAMICS: A SYNTHESIS OF THE PUBLISHED DATA

5.1 Introduction

Although vehicle and seat suspension systems are, invariably, analyzed assuming negligible interactions of the human body, the body is known to have some influence on their vibration response. In an early study, Coermann [68] demonstrated that the dynamic response of the human body deviates considerably from that of a rigid mass at frequencies above 2 Hz. Recognizing the potential contributions of the human body to the suspension seat performance, Suggs and colleagues [69] developed a mechanical simulator to represent the human body dynamics for testing seats under high magnitude vibration. The study concluded that by replacing the human body with a rigid mass of equivalent weight, an overestimation of the seat amplification at resonance occurred, while the attenuation at high frequencies was exaggerated. The findings of the study were further supported by Griffin [6], as shown in Figure 5.1. The suspension seat performance is thus affected not only by the suspension design characteristics but also by the dynamics of the seated driver.

Current standards defining laboratory seat testing procedures under vibration recommend the use of both rigid mass and human subjects for

loading the seats. International Standards ISO 5007 [31] for agricultural tractor seats and ISO 7096 [32] for earth-moving machinery seats propose the use of two test persons of masses 59 ± 1 kg and 98 ± 5 kg when performing measurements under specified random excitations for such vehicles. Rigid mass testing is limited to sinusoidal excitation to determine the seat resonant frequency and peak base-to-seat vibration transmissibility magnitude.

Recognizing the potential safety hazards posed by subjecting humans to vibration, and the difficulty in maintaining and controlling specific experimental conditions related to body mass and posture, alternate seat testing procedures not involving the use of test subjects have been proposed. Fairley and Griffin [70] proposed a method to determine the dynamic stiffness of seats using a loading indenter and a linear seat model which, when combined with the dynamic response of the human body, resulted in the seat transmissibility characteristics of the seat-person system. The method provided relatively good agreement with the measured results involving subjects, although the computed resonant transmissibility magnitude had a tendency to be larger than the measured value. The proposed methodology, however, necessitates the precise knowledge of the human body dynamic response, which is not always easy to obtain under the prescribed experimental conditions.

Alternatively, the need for performing hazardous experiments involving human subjects to determine the suspension seat performance can be eliminated through the development of appropriate analytical models of both the suspension seat and the human body. The influence of human body dynamics on the acceleration transmissibility of a nonlinear suspension seat has been presented by Rakheja et al. [27] using one- and two-degree-of-freedom driver models proposed in the literature. The result obtained for constant amplitude sinusoidal displacement excitation of 2.5 cm peak-to-peak (Figure 5.2) demonstrated that the vibration transmissibility of the seat is 30 to 40% lower in the 2 to 4 Hz frequency range when human body model is incorporated. At frequencies above 5.5 Hz, however, the human body dynamics yields vibration attenuation inferior to the rigid mass. These results illustrate a strong influence of human body dynamics on the ride performance of suspension seat systems for both highway and off-highway vehicles where ride vibration predominates at frequencies above 2 Hz.

A number of biodynamic models are proposed in the literature to estimate the magnitudes of forces transmitted to particular subsystems within the body (e.g. the spine), to establish potential damage mechanisms, and to assess the tolerance to vibration under exposure to intense vibration levels [71]. Very few studies, however, focus on the dynamic response of the human body under typical vehicular vibration [34]. Furthermore, the

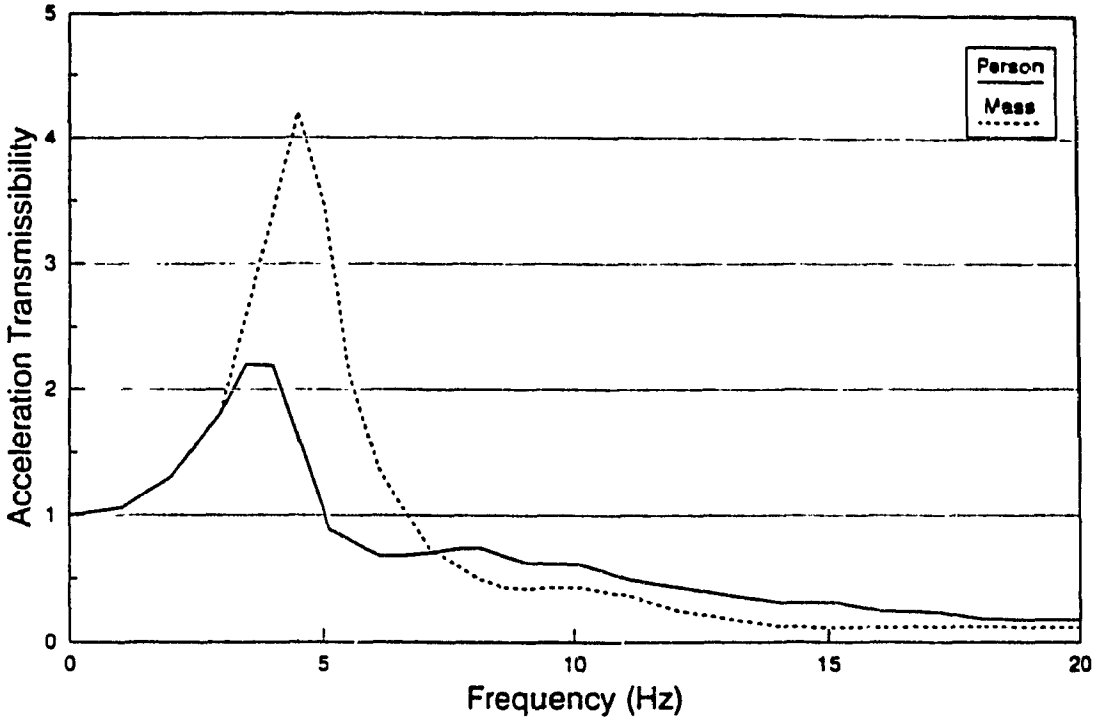

Figure 5.1 Reported vertical transmissibility characteristics of a foam and metal spring seat when loaded with a rigid mass and with a person of equivalent weight. (reproduced from Griffin, [6])

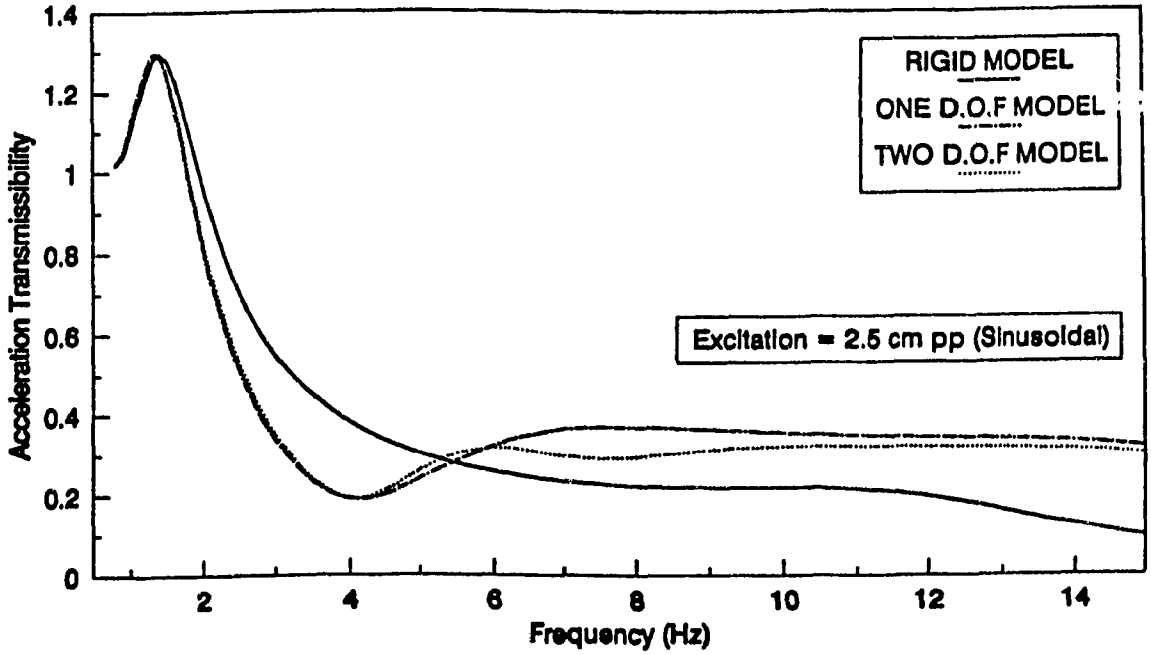

Figure 5.2 Comparison of a suspension seat computed vertical transmissibility when representing the driver as a rigid mass and while using one- and two-degree-of-freedom driver models.(Rakheja et al. [27])

majority of these models have been developed using the data measured under specific test conditions. Since the biodynamic response of the human body subject to vibration is strongly related to a wide range of intrinsic (e.g. person weight and posture) and extrinsic (e.g. vibration type, intensity, frequency) variables, the reliability of the proposed biodynamic models under varying conditions has not yet been demonstrated. The response characteristics of the proposed models are thus known to differ considerably, in view of varying intrinsic and extrinsic test variables.

In this chapter, the various biodynamic models of the human body subject to vibration are reviewed, specifically their response characteristics, experimental conditions, and the measured data. The biodynamic response characteristics reported in terms of both the driving-point mechanical impedance or apparent mass, and the seat-to-head vibration transmissibility are classified under different experimental conditions used in the studies. The test conditions are selected to represent the postural and excitation conditions encountered while operating off-road vehicles. The data reported in various published studies, grouped under similar test conditions, are synthesized to identify the influence of several variables, such as subject mass, seated posture, vibration intensity and frequency on the biodynamic response behaviour of the human body. The synthesized data is further used as a prerequisite to define target values of the biodynamic response functions which will be utilized to develop a human driver

model for estimating the suspension seat performance during off-road vehicle driving.

5.2 Review of Biodynamic Models

Human body comprising a complex combination of visco-elastic properties of muscles, bones, joints, etc., responds to whole-body vibration and shock motion in a highly complex manner. Many human body models have been proposed to assess the impact of whole-body vibration, the driver-suspension seat performance, the dynamic loads transmitted to the spinal structure, etc. These models range from simple single-DOF to complex nonlinear multi-DOF models. Majority of the models proposed in the literature are lumped-parameter models, where the parameters are identified from the measured biodynamic response data. The model parameters in the majority of the studies are identified from the mechanical impedance or vibration transmissiblity characteristics measured on live subjects. The driving-point mechanical impedance, defined as the complex ratio of the driving force to the velocity at the point of entry of vibration within the body, and the seat-to-head transmissibility, defined as the complex ratio of acceleration measured at the head to that at the seat, have been widely used in conjunction with curve-fitting algorithms to identify the model parameters. Such parameter identification techniques based upon curve-fitting of the measured characteristics of driving-point mechanical impedance or seat-to-head

transmissibility magnitude and phase pose two problems: (i) the model may be considered valid only in tne vicinity of the test conditions used in the study; (ii) the model parameters may not relate to any body segment characteristics. Multiple sets of model parameters may thus be derived such that the model response correlates reasonably well with the measured data.

Although the masses in a lumped-parameter model can be identified from anthropometric data, the restoring and dissipative properties of various body segments are difficult to establish. The stiffness and damping elements of the model thus need to be identified from the measured biodynamic response data using certain curve-fitting algorithms. Several models, however, define masses which cannot be associated with a specific segment of the body. Furthermore, many of the proposed models have been devised based on ejection seat data and represent the human response to high level impacts. Many concerns have thus been raised concerning the validity of these models for vibration exposure encountered in off-road vehicles. Other models, reported in the literature, have been derived from test data acquired with subjects sitting on seats without backrest and subjected to sinusoidal vibration of varying intensity. It may thus be questioned whether these models could be applied in situations representative of those encountered by off-road vehicle drivers.

In the following sections, various biodynamic models reported in the literature

are briefly reviewed in view of the response characteristics, parameter identification techniques and their validity for off-road vehicle driving applications. While majority of the model parameters are identified by matching either the measured driving-point mechanical impedance characteristics or the seat-to-head vibration transmissibility, only few studies have utilized both sets of data. The uniqueness of many of these models may thus be questioned in view of the large scatter of data published on impedance and transmissibility characteristics of the human body.

5.2.1 SINGLE-DEGREE-OF-FREEDOM MODELS

In the simplest single-DOF models, the mass of the subject supported by the seat is lumped at a single point and linked to the base through a parallel spring and damper combination. The stiffness k and damping ratio ζ usually represent the characteristics of the spinal column. Such models are generally known to adequately characterize the human response up to the main body resonance, beyond which the model response may differ significantly from the measured response.

Perhaps the most widely used single-DOF model is based on the "dynamic response index" or DRI principle which relates to the relative severity of vibration, more particularly the shocks, since it finds its basis on seat ejection data. The DRI constitutes the peak stress or acceleration acting on the spine,

defined as:

$$DRI = \frac{k\delta_{max}}{mg} = \frac{\omega_n^2 \delta_{max}}{g} \qquad (5.1)$$

where δ_{max} is the peak relative displacement or spring deflection caused by the shock motion. The model, illustrated in Figure 5.3a [33], thus relates to body deflection under a shock motion. The mass m of the model represents the mass due to upper torso and the head [33]. While the spring rate k is meant to represent the restoring properties of the spine, the viscous damping coefficient c of the spine and the adjacent tissues is selected to match the mechanical impedance data reported by Coermann [68]. The natural frequency and the damping ratio of the proposed model are 8.42 Hz and 0.2245, respectively.

Payne [71] proposed an improved DRI model to fill the gap between single events or shocks and continuous vibration. The proposed model comprised of four parallel and uncoupled single-DOF models, was realized upon combining the DRI model, also known as the "spinal" or "shock response" model, with three additional single-degree-of-freedom (SDOF) models: "visceral"; "body vibration"; and "low frequency", as shown in Figure 5.3b. While the visceral model represents the visceral mode, the body vibration model is not associated with any particular physiological system and its parameter values were selected to agree with tolerance boundaries or limits such as those defined in the ISO

2631 standard [18]. The low frequency model is introduced to account for the low frequency motion sickness effects. The natural frequencies of the "low frequency", "visceral" and "body vibration" models are 0.25 Hz, 3.99 Hz and 8.42 Hz, respectively, and the corresponding damping ratios are 1.0, 0.4 and 1.0. The damping ratio of the low frequency model was selected as 1.0 based upon the motion sickness incidence and tracking error data available at the time. For each of these four models, a "Vibration Ride Ratio" (VRR) is defined, representing their respective rms acceleration outputs normalized to 1 g for some defined input. A "Vibration Ride Quality Index" (VRQI) is then defined as the maximum VRR value of the four systems, which is used to judge the degree of severity of the exposure. For example, a VRQI value of 0.5 is considered severe, limiting the exposures to 1 h or less. A VRQI of 0.1 is considered tolerable for long term exposure.

Coermann [68] proposed a SDOF model of the human body, as shown in Figure 5.3c, where the model parameters were identified to fit the driving-point mechanical impedance data measured with subjects sitting without their feet and back supported. The model parameters were identified for two different postures (erect and relaxed) using the data acquired under sinusoidal excitations only. The model response correlated well with the measured response, in both the magnitude and phase, up to the primary body resonant frequency, beyond which significant differences were observed. In that

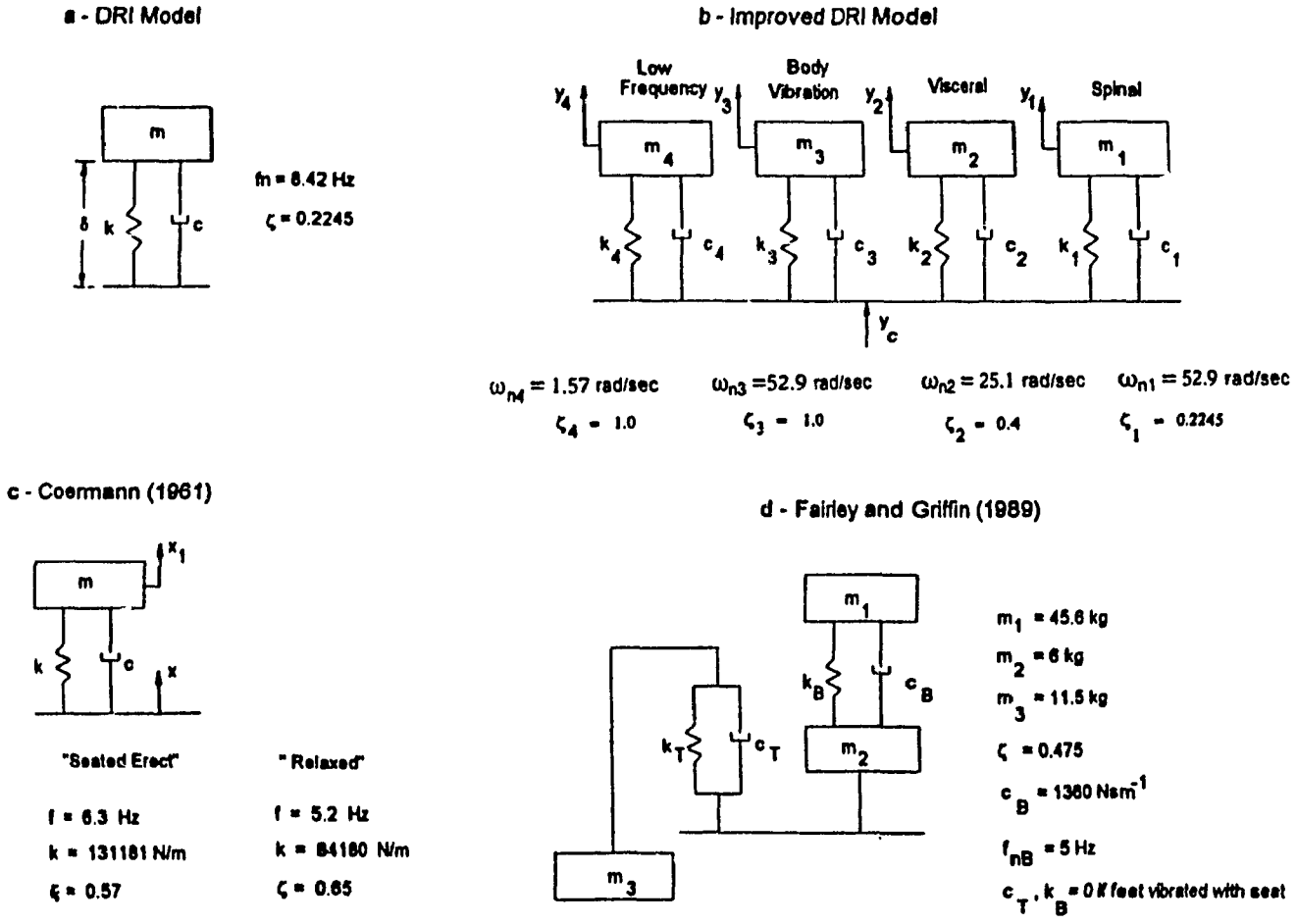

Figure 5.3 Single-degree-of-freedom biodynamic models defined in the literature, and associated parameter values: a) DRI model [33], b) Payne's improved DRI [71], c) Coermann [68], and d) Fairley and Griffin [73].

study, the seat-to-head transmissibility was also measured and compared with the model responses, which revealed important differences in transmissibility magnitude over the entire frequency range (1 to 20 Hz). While the model response revealed a resonant peak at 6.3 Hz, the measured data showed four peaks in the same frequency range: near 3 Hz, related to abdominal mass resonance; between 5 and 6 Hz; between 10 and 11 Hz; and near 15 Hz. The phase response of the vibration transmissibility, however, was not reported in the study.

The work performed by Coermann [68] was instrumental in establishing the dependence of the biodynamic response on the posture. The study proposed modifications of the model to match measured impedance characteristics for three body postures: sitting erect, sitting relaxed and standing. Modification of the model parameters was further required to match the mean impedance response of 8 subjects near the resonance. Thus, the method of matching peak impedance magnitude at resonance only, led to as many sets of parameters as there was available data. The danger of basing a model on the mean measured response of a group of individuals as opposed to data pertaining to a single subject has been addressed by Griffin [72].

Fairley and Griffin [73] proposed a SDOF model based on the measured mean apparent mass of 60 subjects, including male, female and children, sitting erect

without back support. The feet of the subjects were vibrated under 1.0 ms^{-2} random vibration. The apparent mass represents the ratio of the driving force to the resultant acceleration at the driving point, and is related to the driving-point mechanical impedance. As shown in Figure 5.3d, the seated body is represented by two masses: m_1 being the mass of the upper body moving relative to the platform, and m_2 being the mass of the body and of the legs supported on the platform but not moving relative to the platform. The mass of the legs m_3 was included in the model only when the feet were supported on a stationary footrest. The mass m_3 was linked to the stiffness and damping properties of the thighs (k_T and c_T) as shown in the figure. While the mean mass values were selected as reported in Figure 5.3d and the natural frequency of the upper body was set at 5.0 Hz, the damping coefficient, c_B, of the upper body was computed by minimizing the sum of the squared errors in apparent mass magnitude at each frequency. The normalized apparent mass of this model was reported to be within plus and minus one standard deviation of the normalized apparent masses of the 60 subjects. This model however did not consider seat-to-head transmissibility data, nor did it include the effect of back support or the posture.

5.2.2 TWO-DEGREE-OF-FREEDOM MODELS

Suggs [34] proposed a two-DOF biodynamic model of the human body to characterize the response over a frequency range comprising the first two

resonant frequencies of the body. On the basis of this model, a "ride quality" dumrny was constructed to perform vibration testing of vehicle seats [74]. The model, shown in Figure 5.4a, was derived from the measured mechanical impedance characteristics of 11 male subjects, showing a primary and a secondary resonance of the seated subjects near 4.5 Hz and 8 Hz, respectively [69]. The tests were performed with subjects seated upright, with feet supported, hands in lap, exposed to sinusoidal vibration of 2.54 mm peak-to-peak amplitude in the 1.75 to 10 Hz frequency range. The proposed model comprises two lumped masses, m_1 (pelvis and abdomen), and m_2 (head and chest), suspended from a common rigid frame of mass m_0, representing the spinal column [34].

The model parameters were determined using a trial-and-error method until convergence with the measured mean mechanical impedance magnitude was obtained. The mass of the unsprung component ,m_0, was adjusted to 5.7 kg to yield a total mass of 60.7 kg supported by the seat, corresponding to a 77.3 kg subject. On the basis of these parameter values and the measured magnitude of mechanical impedance , a mechanical simulator was constructed to perform vibration testing of seats [74]. While the seat-to-head vibration transmissibility was not considered in deriving the model, the base-to-seat transmissibility characteristics of seats loaded with the mechanical simulator were reported to be in agreement with those measured with a person, provided

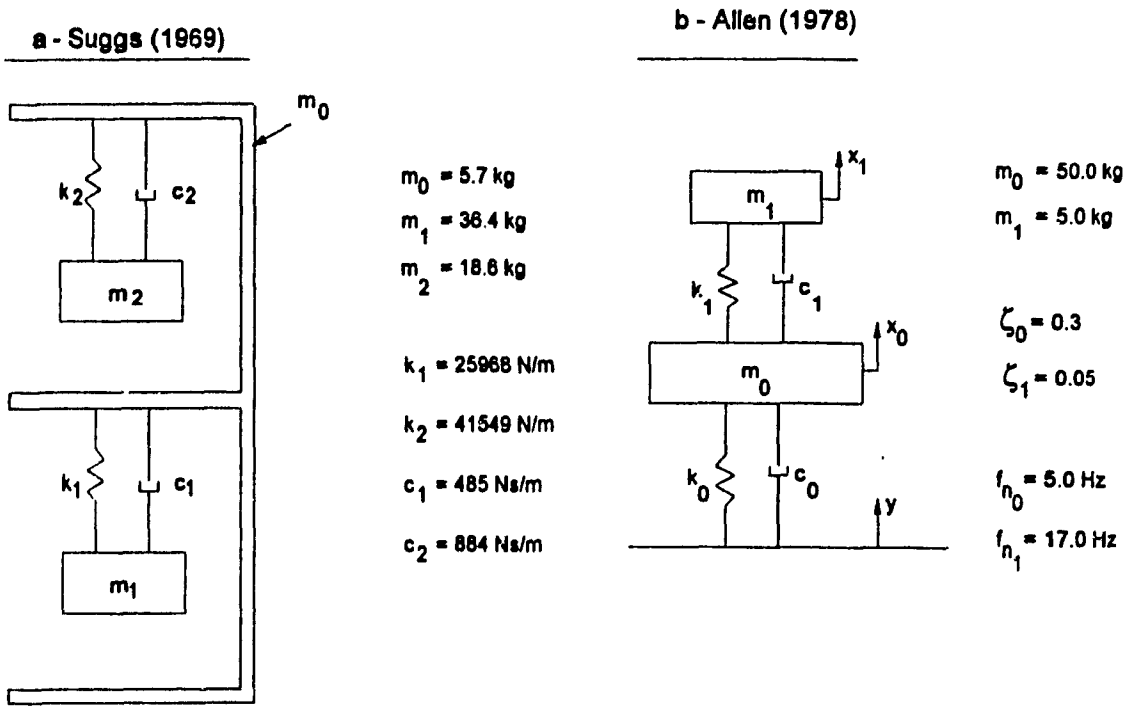

Figure 5.4 Two-degree-of-freedom biodynamic models defined in the literature, and associated parameter values: a) Suggs [34], and b) Allen [75].

the weight and experimental conditions matched those defined in the model.

Allen [75] derived a two-DOF biodynamic model of the human body using known characteristics of the human body or subsystems. The model, shown in Figure 5.4b, consists of a "primary system" ($m_0 = 50$ kg, $f_{n0} = 5.0$ Hz, and $\zeta_0 = 0.3$) to characterize the upper body response, and a "secondary system" ($m_1 = m_0/10$, $f_{n1} = 17$ Hz, $\zeta_1 = 0.05$) representing the head. The model response to sinusoidal excitations was used to derive vibration tolerance curves illustrating the sensitivity of subsystems to vibration within specific frequency ranges. The validation of the proposed model, however, has not been reported.

5.2.3 MULTI-DEGREE-OF-FREEDOM MODELS

A variety of multi-degree-of-freedom models have been proposed in the literature, ranging in complexity from a few lumped masses to several inter-linked subsystems, depending upon the intended application of the model. Demic [76] investigated the response of the human body subject to shock excitations produced by falling heights of 50 and 75 mm, by measuring the transfer functions of three main subsystems of the body, namely the waist/seat, the back/waist and the head/back. The measured data revealed respective resonances in the 8 - 9 Hz, 3 - 5 Hz and 23 - 24 Hz frequency bands. Although the measured resonant frequencies compared well with the published data obtained under harmonic and random excitations, larger

variations were observed with the dynamic amplification at resonance. A nonlinear three-DOF model, shown in Figure 5.5a, was thus proposed to account for nonlinear body response to high intensity shock excitations. The model incorporates nonlinear restoring and dissipative forces, using linear and cubic dependencies on displacement and velocity, respectively. The model parameters were identified by matching the model responses with the measured transfer functions only.

Payne [77] proposed a four-DOF model shown in Figure 5.5b as an extension of the "spinal model" described in section 5.2.1. The proposed model comprises mass m_1 representing the buttocks and pelvis with their characteristic stiffness k_1 and damping coefficient c_1 linked to mass m_3, representing the spine and upper thorax. The masses m_2 and m_4 representing the viscera, and head and neck, respectively, are attached to mass m_3. While the viscera mass m_2 was not linked with the buttocks and pelvis, considerations of a coupling between m_2 and m_1 was argued. This model thus presents an addition of three subsystems, represented by masses m_1, m_2 and m_4, to the "spinal model" based upon the DRI concept. The strong influence of m_1 on the mechanical impedance being closest to the driving-point, justified its inclusion in the model. The masses m_2 and m_4 were incorporated to account for the "visceral mode" between 3 and 3.5 Hz, and the head resonance near 30 Hz. The model parameters were estimated by first fixing the masses to provide

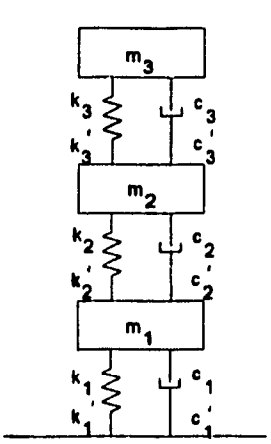

a - 3 DOF Non - Linear Model - Demic (1987)

$m_1 = 42.0$ kg

$m_2 = 23.0$ kg

$m_3 = 5.0$ kg

$k_1 = 80000$ N/m	$k_1' = 10000$ N/m^3
$c_1 = 10$ Ns/m	$c_1' = 2$ Ns^3/m^3
$k_2 = 25000$ N/m	$k_2' = 5000$ N/m^3
$c_2 = 20$ Ns/m	$c_2' = 2$ Ns^3/m^3
$k_3 = 70000$ N/m	$k_3' = 10000$ N/m^3
$c_3 = 40$ Ns/m	$c_3' = 10$ Ns^3/m^3

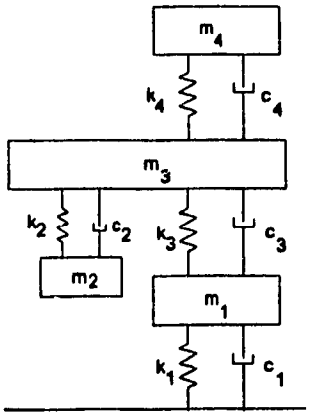

b - 4 DOF Model - Payne (1971)

$m_1 = 29.0$ kg	$k_1 =$ variable	$\omega_{n1} = 47.6$ rad/sec	$\zeta_1 = 0.25$
$m_2 = 6.8$ kg	$k_2 = 2838$ N/m	$\omega_{n2} = 20.4$ rad/sec	$\zeta_2 = 0.60$
$m_3 = 21.8$ kg	$k_3 =$ variable	$\omega_{n3} = 65.0$ rad/sec	$\zeta_3 = 0.10$
$m_4 = 5.45$ kg	$k_4 = 204820$ N/m	$\omega_{n4} = 192.3$ rad/sec	$\zeta_4 = 0.15$

Figure 5.5 Multi-degree-of-freedom biodynamic models defined in the literature, and associated model parameter values: a) Demic [76], and b) Payne [77].

the seated mass of 63.2 kg, representing a 72.7 kg man. Based on biomechanical properties and observed biodynamic behaviour of the subsystems, either constant or a probable range of values of stiffness and damping coefficients were identified. A final set of model parameters was selected based upon the mechanical impedance measured by Coermann [68]. The stiffness coefficients k_1 and k_3 were proposed as variables to account for variations in the muscle tension in the buttocks and the spine with the nature and magnitude of excitation.

Mertens and colleagues [78,79] developed a comprehensive biodynamic model involving the comparison of both the impedance and vibration transmissibility magnitude and phase characteristics with the experimental results. Since the study was intended for ejection seat studies applications, the experiments were performed with subjects exposed to static acceleration levels ranging from 1 to 4 g, superimposed over 0.4 g rms acceleration amplitude in the 2 to 20 Hz frequency range. Measured driving-point mechanical impedance and seat-to-head transmissibility characteristics indicated an increase in the whole-body resonance with increasing static acceleration. The resonant frequencies were observed near 5 Hz, 11 Hz, 12 Hz and 13 Hz, respectively, under 1 g, 2 g, 3 g and 4 g accelerations. Using the measured data, and biomechanical data of the human body, a linear multi-DOF model was proposed, as shown in Figure 5.5c. The model comprises five lumped masses due to the legs (m_1), the

c - Mertens (1978)

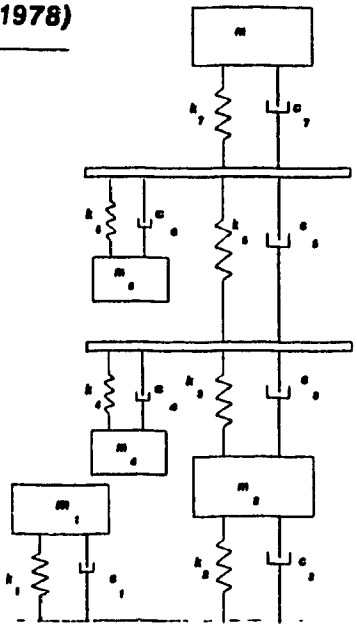

m_1 = 15.0 kg
m_2 = 10.0 kg
m_4 = 15.0 kg
m_6 = 22.0 kg
m_7 = 7.0 kg

k_1 = 47966 N/m
k_2 = 250000 N/m
k_3 = 200000 N/m
k_4 = 17913 N/m
k_5 = 160000 N/m
k_6 = 42559 N/m
k_7 = 89537 N/m

c_1 = 678 Ns/m
c_2 = 4000 Ns/m
c_3 = 1000 Ns/m
c_4 = 622 Ns/m
c_5 = 2000 Ns/m
c_6 = 948 Ns/m
c_7 = 633 Ns/m

Figure 5.5c Multi-degree-of-freedom biodynamic model defined by Mertens et al. [78,79], and associated parameter values.

buttocks (m_2), the abdominal system (m_4), the chest system (m_6), and the head (m_7). The values for these masses were extracted from anthropometric measurements of the human body with a mass of 69 kg. Since the legs were believed to contribute considerably to the driving-point impedance and less significantly to the vibration transmissibility, the leg model was decoupled from the rest of the body. The masses m_4 and m_6 are coupled to the spinal column, with the lumbar spine represented by the constants k_3 and c_3, the thoracic spine represented by k_5 and c_5, and the cervical spine by k_7 and c_7. This model thus supports the suggestions by Smith [80] that the spine, the upper torso or chest, and the head appear to be coupled. The range of these stiffness constants was identified from the published studies as: $100 \leq k_3 \leq 300$ N/mm; and $150 \leq k_5 \leq 200$ N/mm. Other stiffness values were estimated from the reported damped resonant frequencies of the body parts, namely 8.25 Hz for the legs, 4.4 Hz for the abdomen, 6.06 Hz for the chest and 16.5 Hz for the head. The damping ratios of the human body were estimated to vary between 0.2 and 0.6. Final model parameters were selected as those which provided the closest agreement with the measured biodynamic response functions. Under normal gravity, close agreement with the experimentally measured driving-point mechanical impedance and seat-to-head transmissibility magnitude and phase is reported for the model parameters chosen.

Amirouche and Ider [81] used nine body segments to represent the human

d - Amirouche (1988)

Name	Mass (kg)
Lower torso	11.76
Center torso	2.69
Upper torso	17.36
Neck	0.88
Head	4.42
Upper arm	2.22
Lower arm	2.15
Upper leg	9.68
Lower leg	4.42

Segment	Stiffness Coefficient (N/m)	Damping Coefficient (Ns/m)
Lower torso	50000	1100
Middle torso	105000	1800
Upper torso	105000	1800
Neck	120000	1500
Head	120000	1500

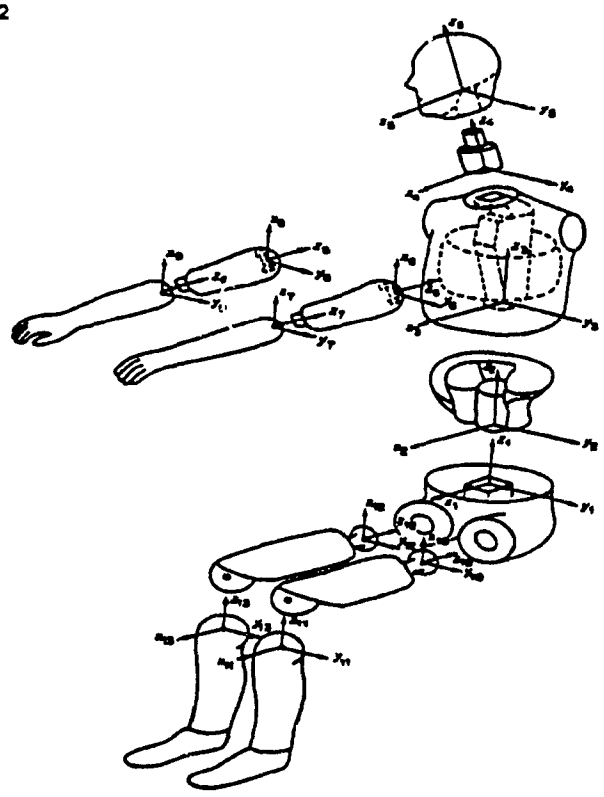

Figure 5.5d Multi-degree-of-freedom biodynamic model defined by Amirouche and Ider [81], and associated parameter values.

body, namely the head, the neck, the upper torso, the upper arm, the lower arm, the middle torso, the lower torso, the upper leg and the lower leg as shown in Figure 5.5d. Corresponding mass values were chosen to match those of a 50th percentile sized dummy. Stiffness and damping coefficients were determined by curve-fitting the results of the simulation to match the experimental seat-to-lumbar vertebrae transmissibility characteristics determined by Panjabi et al.[82] under low level sinusoidal vibration in the 2 to 15 Hz frequency range. Stiffness and damping coefficients of the legs and of the arms were found to have little effect on the vibration of the main body. Comparing the predicted seat-to-head transmissibility magnitude response with those published in the literature, closest agreement was obtained with that reported by Coermann [68] for subjects maintaining a relaxed posture. However, this was found to be only true up to the first resonant peak, beyond which significant differences were observed. Driving-point mechanical impedance was not considered in deriving this model.

Patil and Palanichamy [83] have combined a two-degree-of-freedom tractor model with a seven degree-of-freedom nonlinear human occupant model to simulate its response when subjected to sinusoidal vibration of 0.05 m amplitude, in an effort to optimize the seat suspension parameters. The design optimization was based on minimizing the transmissibility ratios and relative displacements of the body parts. Human body model validation was

accomplished by comparing the predicted pelvis-to-head transmissibility with the data reported in the literature, mostly in earlier studies. The model, presented in Figure 5.5e, was based on that proposed by Muskian and Nash [84], except that damping and elasticity of the buttocks were added. The masses in the model include those due to head, back, torso, thorax, diaphragm, abdomen and pelvis. The restoring and dissipative characteristics of the torso, thorax, diaphragm and abdomen were represented by nonlinear springs and dampers. Parameter values of the human body were based on the measured characteristics of the subsystems as reported in [84]. The results of the simulation were reported to provide good agreement with the expected head-to-pelvis vibration transmissibility ratio, providing a resonant peak at 3 Hz. The driving-point mechanical impedance, however, was not considered in deriving this model.

ISO Committee Draft CD 5982 [85] proposes a multi-DOF biodynamic model to characterize both the standardized driving-point mechanical impedance and seat-to-head transmissibility of the human body exposed to vibration. Although the proposed four-DOF model, shown in Figure 5.5f, represents both seated and standing human subjects, the model parameters differ depending on the posture. For the seated human body, the masses m_1, m_2, m_3 and m_4 are selected as 8.24 kg, 8.05 kg, 44.85 kg and 13.86 kg, respectively, which are not associated with any specific subsystems of the human body. The model

e - Patil et al. (1988)

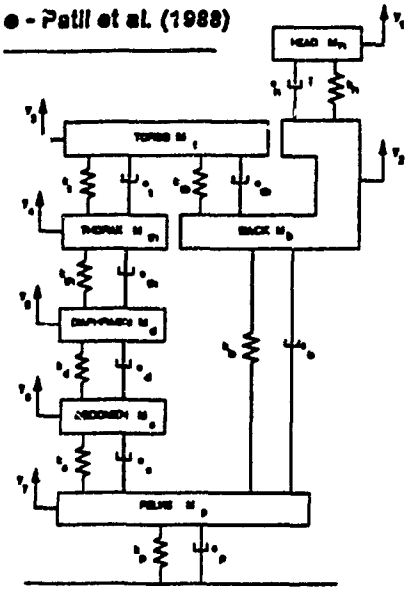

Parameter values of occupant model

Mass M (kg)	Damping constant C (kN/m/s)	Spring constant K (kN/m)
M_h = 5.45	C_h = 3.50	K_h = 62.0
M_b = 6.62	C_b = 3.00	K_b = 62.0
M_t = 32.782	C_t * = 3.50	K_t † = 0.677
	C_{th} * = 3.00	K_{th} † = 62.0
M_{th} = 1.362	C_{th} * = 0.292	K_{th} † = 0.677
M_d = 0.455	C_d * = 0.292	K_d † = 0.677
M_a = 5.021	C_a * = 0.292	K_a † = 0.677
M_p = 27.23	C_{th} * = 0.371	K_p = 25.5

* The units of damping constants, giving rise to linear and nonlinear forces, are kN/m/s and kN(m/s)^3, respectively.

† The units of spring constants, giving rise to linear and nonlinear forces, are kN/m and kN/m3 respectively.

f - ISO CD 5982 (1993)

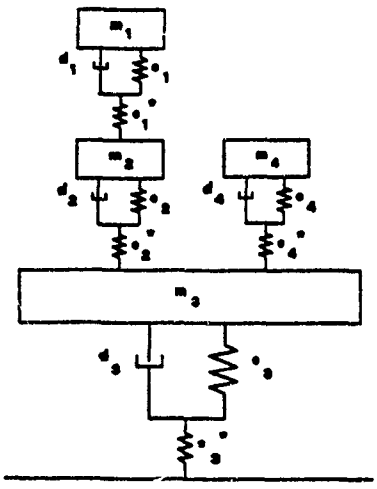

	Unit	Model I Sitting Body Position
m_1	kg	6.34
m_2	kg	8.05
m_3	kg	44.86
m_4	kg	13.86
c_1	N/m	22.00 x10^6
c_2	N/m	20.13 x10^6
c_3	N/m	66.56 x10^3
c_4	N/m	98.47 x10^3
c_1^*	N/m	90.00 x10^7
c_2^*	N/m	66.00 x10^6
c_3^*	N/m	62.34 x10^4
c_4^*	N/m	66.30 x10^3
d_1	Ns/m	748.1
d_2	Ns/m	678.6
d_3	Ns/m	2864.6
d_4	Ns/m	901.6

Figure 5.5 Multi-degree-of-freedom biodynamic models defined in the literature, and associated parameter values: e) Patil and Palanichamy [83], and f) ISO CD 5982 [85].

parameters were adjusted to match the driving-point mechanical impedance and seat-to-head transmissibility magnitude and phase characteristics established as the mean value of data reported for subjects of different weight, with vaguely defined postures, under sinusoidal vibration in the 1 to 2 ms^{-2} amplitude range. For the seated human body, the proposed model yields relatively good agreement with the standardized mechanical impedance magnitude, though large discrepancies occur with the impedance phase. Considerable differences in the transmissibility magnitude near the resonant frequency and at frequencies beyond 25 Hz, are also observed. The model response reveals large errors in the transmissibility phase over most of the frequency range considered.

5.2.4 SUMMARY OF BIODYNAMIC MODELS

The various biodynamic models of the human body reviewed in this section may be grouped into four distinct classes, according to the methodology used for estimating the model parameters. The first group of models concerns those involving parameter identification based upon measured or reported natural frequencies or transmissibility characteristics of specific segments. Such models were often proposed to characterize the response behaviour of specific body segments under shock or high intensity vibration, but were rarely validated in terms of the whole-body response. The second group of models includes those involving parameter identification based upon magnitude and phase characteristics of the measured or reported whole-body driving-point

mechanical impedance or apparent mass. The majority of the data used in deriving these models was obtained under sinusoidal excitations, and the seat-to-head transmissibility was either not reported or resulted in a poor fit. The third class of models comprises those derived to satisfy the vibration transmissibility characteristics of certain specific segments of the body, while simultaneously matching the driving-point mechanical impedance or apparent mass response characteristics. Although a good agreement is observed with the vibration transmissibility of the body segments, the seat-to-head transmissibility response, in general, deviates considerably from the measured data. The final group of models involves the determination of model parameters based upon matching the magnitude and phase characteristics of both driving-point mechanical impedance or apparent mass and seat-to-head transmissibility. Although this approach enhances the uniqueness of the models, the complexities associated with curve-fitting the four different sets of data increase considerably. Only two of the models reported in the reviewed literature fall within the last category: Mertens [78], and ISO CD 5982 [85]. Both models, however, rely on the measured data obtained under sinusoidal vibration only.

Since the components of the proposed ISO model do not relate to any specific body segments, the corresponding response characteristics cannot be used to enhance an understanding of the human body behaviour under vibration.

Alternatively, the model proposed by Mertens can be considered to be unique, since it correlates with both the whole-body biodynamic response functions, while incorporating the biomechanical data for specific body segments. The model, however, was defined to satisfy biodynamic response functions measured under relatively high levels of sinusoidal excitation with subjects sitting with feet not supported. The validity of the model for applications to vehicle driver may thus be questioned. Furthermore, off-road vehicle driving usually involves different postures (leaning against a backrest, sitting erect or sitting with a slouched posture), hands in contact with a steering wheel, and feet supported either on the floor or on pedals, while the vibration excitation is random in nature. From the review, it is apparent that none of the models reported in the literature were derived under the conditions encountered in off-road vehicle driving.

The development of a biodynamic model of a seated human body under typical off-road driving conditions is extremely vital to study the driver-suspension seat performance. The biodynamic response characteristics reported in the literature are thus reviewed to enhance an understanding of the human body response to whole-body vibration, to establish the relative influence of varying operating conditions encountered in off-road vehicle driving, and to identify the essential properties of a suitable driver model, such as number of DOF, range of model parameters, linear or nonlinear restoring and dissipative properties, etc.

5.3 Synthesis of the Published Data on Whole-Body Driving-Point Mechanical Impedance

The driving-point mechanical impedance of a system is defined as the complex ratio of force to velocity measured at the driving point, expressed as [86]:

$$Z(j\omega)=\frac{F(j\omega)}{\dot{z}(j\omega)}=|Z(j\omega)|e^{j\phi_z(\omega)} \qquad (5.2)$$

where Z(jω) and F(jω) represent the complex mechanical impedance and the force driving the system at the angular frequency ω. $\dot{z}(j\omega)$ is the resulting vertical velocity of the system due to the applied force, |Z(jω)| is the magnitude of the complex impedance and $\phi_Z(\omega)$ is the phase angle between the applied force and the resultant velocity. Under random vibration, the mechanical impedance may be derived from:

$$Z(j\omega)=\frac{G_{FV}(j\omega)}{G_{VV}(j\omega)} \qquad (5.3)$$

where $G_{FV}(j\omega)$ represents the cross-spectral density of the input and output, while $G_{VV}(j\omega)$ represents the auto-spectral density of the response.

Alternatively, the apparent mass M(jω) is defined as the ratio of the complex

driving force to the resultant acceleration, $\ddot{z}(j\omega)$, of the system. Under harmonic motion, the apparent mass may be related to the driving-point mechanical impedance in the following manner:

$$M(j\omega)=\frac{F(j\omega)}{\ddot{z}(j\omega)}=\frac{Z(j\omega)}{j\omega}=|M(j\omega)|e^{j\phi(\omega)} \qquad (5.4)$$

where $|M(j\omega)|$ represents the apparent mass magnitude, and $\phi(\omega)$ here corresponds to the phase between the applied force and the resultant acceleration.

The mechanical impedance or apparent mass response provides valuable insight into the behaviour of a vibrating system, since it can be conveniently related to the characteristic curves of simple elements such as masses, springs and dampers. Figure 5.6 illustrates the magnitude and phase impedance characteristics of pure mechanical elements. The mechanical impedance of more complex systems may be interpreted by identifying analogous behaviour of the system with that of the simpler elements or a combination of them. As an example, Figure 5.7 illustrates the mechanical impedance characteristics of a SDOF system formed by assembling the elements for which the mechanical impedance was shown in Figure 5.6. A comparison of Figures 5.6 and 5.7 clearly illustrates that the system behaves like a pure mass at low frequencies

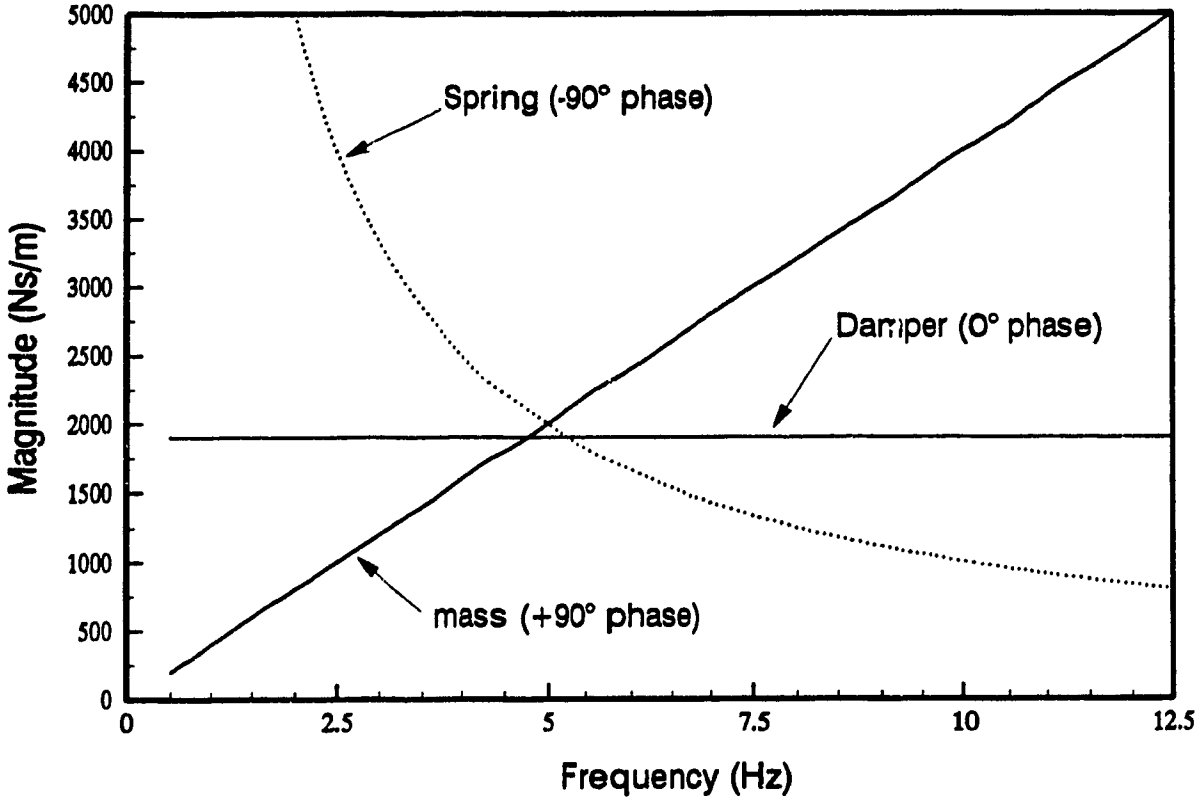

Figure 5.6 Mechanical impedance magnitude of individual elements of a system for which the mass is 63.6 kg, the damping ratio is 0.475 and the natural frequency is 5 Hz.

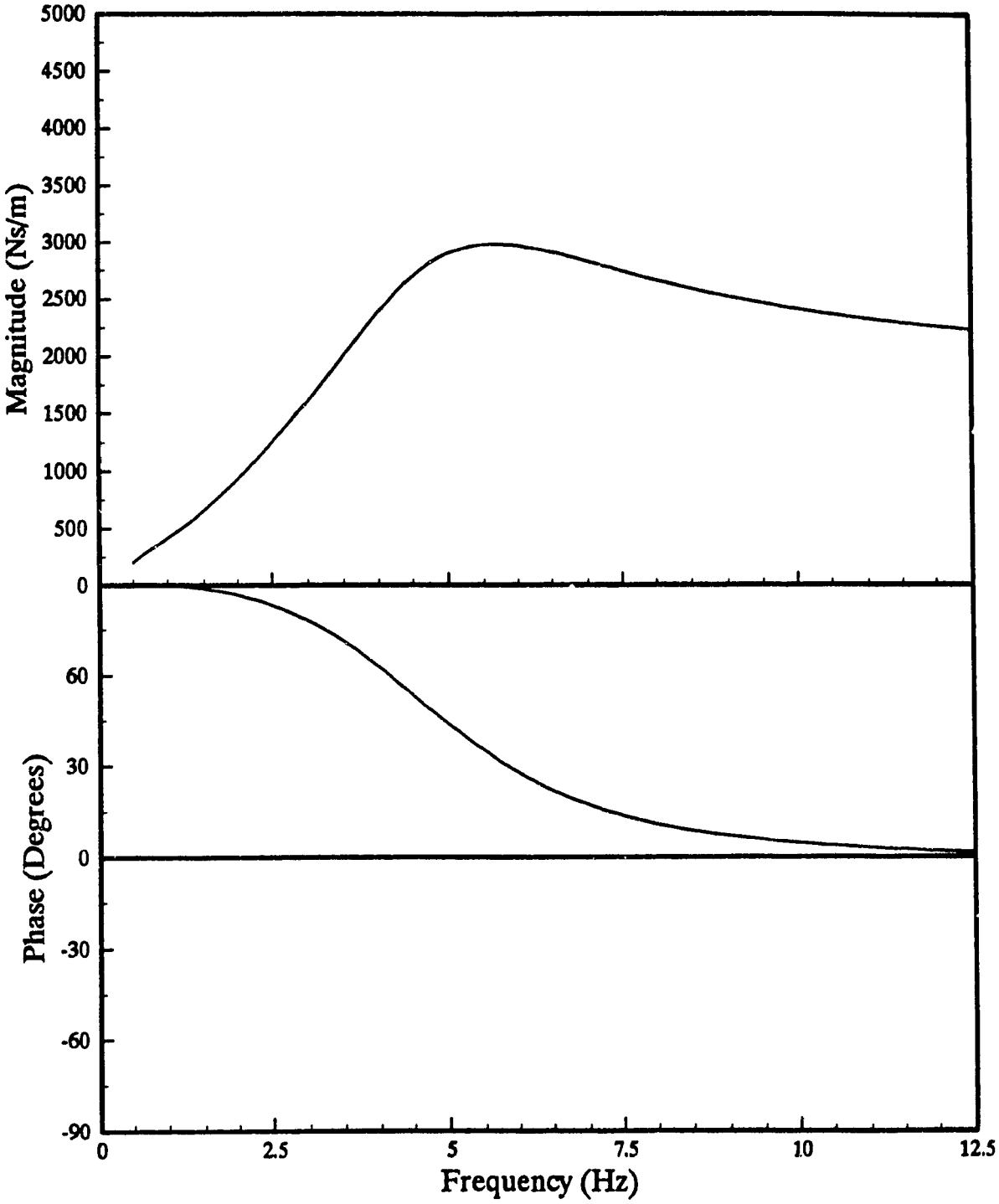

Figure 5.7 Mechanical impedance magnitude and phase of a system formed by assembling individual elements, providing a mass of 63.6 kg, a damping ratio of 0.475 and a natural frequency of 5 Hz.

(below 1.5 Hz). In the vicinity of the resonant frequency, the mechanical impedance approaches its peak value and the system is controlled more by the damper (flat behaviour). Finally, at excitation frequencies above the resonant frequency, there exists a region where the system exhibits spring-like behaviour (impedance magnitude decreasing with increasing frequency). This example illustrates that by using the properties of pure elements, a mechanical model of the system may be established from the mechanical impedance or apparent mass response.

The driving-point mechanical impedance of systems, however, is influenced by many factors, such as nonlinear behaviour of a subsystem, nature and type of excitation. The mechanical impedance of a seated human subject is known to be related to the position of the feet and arms, the seated posture, the backrest support, the weight and build of the subjects, the type of seating arrangement, etc. The relative influence of one or more of these variables on the expected mechanical impedance or apparent mass characteristics determines the validity and reliability of a single universal model in predicting the response behaviour with reasonable accuracy.

5.3.1 IDENTIFICATION OF PUBLISHED DATA SETS AND TEST CONDITIONS

The driving-point mechanical impedance of the human body has been extensively investigated to enhance an understanding of the biodynamic

response of subjects exposed to vibration, and to permit development of human body models. Although the response characteristics of the human subjects have, invariably, been measured under carefully controlled conditions, considerable differences are known to exist among the data reported by various investigators. These differences may be attributable, in part, to the different methods and test conditions employed, and to the potential dependence upon: (a) the nature and type of vibration excitation; (b) the posture; (c) anthropometric parameters of the subjects; (d) the inherent nonlinear dynamic properties of the biological tissues. The differences among the various reported data sets have raised serious concerns on the validity of the reported results and the measurement techniques. A need to derive generally acceptable values of impedance magnitude and phase has thus been identified.

Table 5.1 summarizes the various test conditions employed in different investigations, specifically, the population of subjects, type, magnitude and frequency of excitation, postural constraints and the reported biodynamic response characteristics. In many of the earlier experiments, such as those conducted by Coermann [68], Vogt [87], Suggs [69] and Miwa [88], the number of subjects was usually relatively small, and only sinusoidal excitation was used, not generally representative of the type of excitation and levels of vibration usually encountered in practice. In many of these studies, the feet of the subjects were either not supported or supported but not vibrated, a

TABLE 5.1

Characterization of the Published Data on Whole-Body Mechanical Impedance

Authors	Population			Excitation			Posture	Reported function
	Number	Sex	Weight	Type	Level	Freq. Range (Hz)		
Coermann (1962) [68]	8	M	155-219 lbs	Sinusoidal	0.1 g 0.3 g 0.5 g	1-20	Sitting erect and relaxed. Feet unsupported, no backrest	Impedance magnitude and phase
Vogt, Coermann, Fust (1968) [87]	10	M	176 lbs (mean)	Sinusoidal	0.5 g 2.0 g and 3.0 g	2-15	Sitting slightly erect, feet not vibrated	Impedance magnitude and phase
Suggs, Abrams, Stikeleather (1969) [69]	11	M	128-198 lb, mean : 162 lb	Sinusoidal	0.10 in p-p	1.75-10	Upright, hands in lap, feet supported, no backrest	Mean mechanical impedance magnitude and phase
Miwa (1975) [88]	5	M	50-76 kg	Sinusoidal	0.1 g	3-200	Kneeling, sitting erect and relaxed, and standing, feet unsupported	Impedance magnitude and phase

TABLE 5.1 (CONTINUED)

Characterization of the Published Data on Whole-Body Mechanical Impedance

Authors	Population			Excitation			Posture	Reported function
	Number	Sex	Weight	Type	Level	Freq. Range (Hz)		
ISO CD 5982 (N 226) (1993) [85]	39	?	51-93.8 kg	Sinusoidal	1-2 ms^{-2}	0.5-31.5	Vaguely defined, 10 persons had feet supported by footrest moving with seat, various restraint systems (e.g. seat belts)	Mean mechanical impedance magnitude and phase
Fairley & Griffin (1984) [89]	10	M	65-75 kg mean : 68 kg	Random (40s)	1.5 ms^{-2} rms	2.5-30	Upright, no backrest, feet supported on stationary footrest & hanging free	Mean apparent mass, modulus & phase
Hinz & Seidel (1987) [90]	4	M	56-83 kg	Sinusoidal	1.5 and 3.0 ms^{-2} rms	2-12	"Moderately" Erect sitting	Mean apparent mass & phase at each level
Griffin (1990) [6]	24 24 12	M F Children	(Normalized)	Random	1.0 ms^{-2} rms	0.25-20	Upright, no backrest, footrest vibrating, hands in lap	Apparent mass and phase (also normalized to mass)

TABLE 5.1 (CONTINUED)

Characterization of the Published Data on Whole-Body Mechanical Impedance

Authors	Population			Excitation			Posture	Reported function
	Number	Sex	Weight	Type	Level	Freq. Range (Hz)		
Fairley & Griffin (1989) [73]	8		57-85 kg	Random	1.0 ms^{-2}		4 postures : normal comfortable upright, erect upright, tense upright, back supported, feet supported on footrest moving with platform	Apparent mass & phase
	8		57-85 kg	Random	0.25, 0.50, 1.0, 2.0 ms^{-2} rms			
Sandover (1982) [91]	1		77 kg	Random	1.0, 2.0, 2.3 ms^{-2} rms		Erect with various conditions of feet and arms	Apparent mass and phase
	6		52.7 87.2 kg	Random				

TABLE 5.1 (CONTINUED)

Characterization of the Published Data on Whole-Body Mechanical Impedance

Authors	Population			Excitation			Posture	Reported function
	Number	Sex	Weight	Type	Level	Freq. Range (Hz)		
Fairley & Griffin (1986) [70]	8	M	57-85 kg	Random	1.0 ms^{-2} rms	0.5-20	Upright, lower legs vertical, hands in lap, no backrest, footrest moving with platform	Modulus of apparent mass and phase
	1	M		Random	0.25, 0.50, 1.0, 2.0 ms^{-2} rms	0.5-20	Same, hard and soft seats	Modulus of apparent mass
Fairley & Griffin (1983) [92]	1			Random (Gaussian)	1.0 ms^{-2} rms	0.25-20	No backrest, hard and soft seat, feet supported and not supported	Modulus of apparent mass and phase
Mertens (1978) [78]	6 3	M F	57-90 kg	Sinusoidal	0.4 g rms + 1 - 4g static acceleration	2-20	Sitting upright, feet not supported	Mech. impedance + phase under 1-4 g acceleration

condition not common in most driving situations [68,87]. Many studies have neglected the influence of sitting posture on the impedance characteristics, raising doubt on the applicability of the reported data to vehicle driving situations [69,87]. Other studies have drawn contradictory conclusions on the influence of sitting posture. Coermann [68] demonstrated a definite postural effect, indicating a lower primary resonant frequency and lower impedance magnitude for a relaxed sitting condition as opposed to the erect sitting. The study by Miwa [88], however, showed insignificant influence of the two postures on the mechanical impedance characteristics.

In view of the significant discrepancies among the reported data, it may be postulated that variations in experimental conditions, subject population, and amplitude of excitation are partly responsible for some of the differences. The work by Vogt [87] is perhaps a good example of the significance of varying test conditions, which showed a significant increase in primary resonance of the seated body as the acceleration excitation level changed from 1 g to 3 g. However, at significantly lower excitation levels, Miwa [88] reported a slight decrease in the primary resonant frequency with an increase in the excitation level from 0.1 to 0.3 g acceleration, when measuring impedance of kneeling subjects. A synthesis of the published data to compute generally acceptable target values thus necessitates appropriate consideration of the test conditions, and subsequent selection of data reported for similar test conditions.

5.3.2 STANDARDIZED MECHANICAL IMPEDANCE

The ISO Committee has recently circulated a draft document (ISO CD 5982) [85] on the d iving-point mechanical impedance and seat-to-head transmissibility characteristics of the standing and sitting human body. The reported curves, however, do not distinguish the data obtained under different test conditions, such as excitation amplitudes, postures and feet and back supports. To derive these curves, the data reported in various studies was grouped to obtain average impedance and phase characteristics, and the associated envelopes of potential target values, while neglecting the variations in test conditions. For the sitting human body, the standardized mechanical impedance characteristics were derived using the data reported for a total population of 39 subjects in the 51 to 93.8 kg mass range, using sinusoidal excitations with amplitude varying from 1 to 2 ms^{-2}, in the 0.5 to 31.5 Hz frequency range. The data was extracted from studies in which the posture was often vaguely defined as "upright body position", involving both "feet supported" and "not supported" conditions for seated individuals.

Figure 5.8 illustrates the mean and envelopes of mechanical impedance data for the seated subjects exposed to vertical vibration in the 0 to 12 Hz frequency range as proposed in the ISO CD 5982 document. The curves show that the body behaves similar to a pure mass at exitation frequencies below 2 Hz. Maximum mechanical impedance magnitude occurs in the vicinity of 5 Hz,

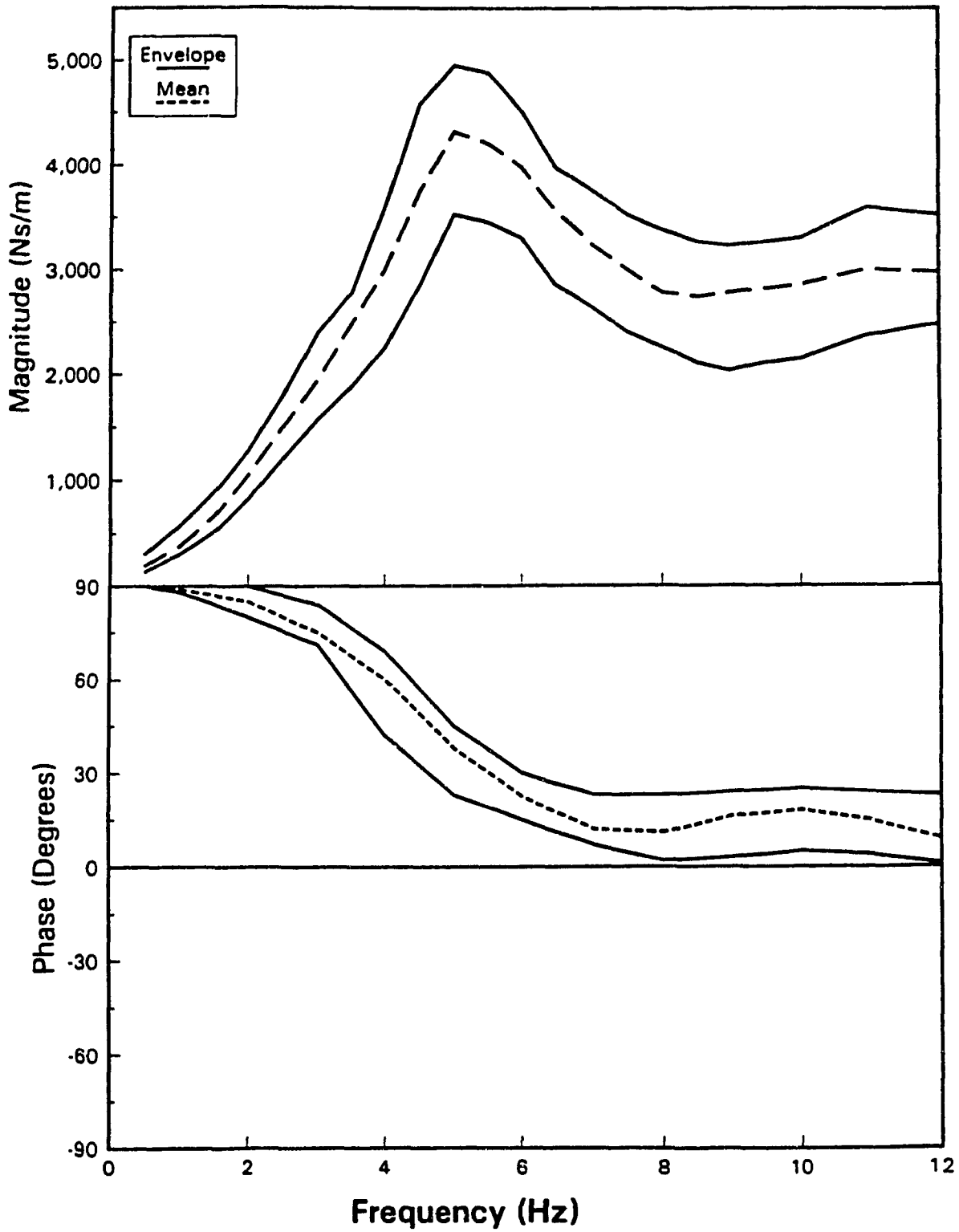

Figure 5.8 Mean standardized whole-body mechanical impedance characteristics of sitting individuals within the 51 to 93.8 kg mass range, as proposed in the ISO CD 5982 [85] (1 - 2 ms^{-2} sinusoidal excitations, posture vaguely defined).

which corresponds to whole body resonance. The impedance characteristics in the 5 - 8 Hz frequency range relate to those of a spring. A second body resonance is expected to occur in the 10 to 15 Hz frequency range, beyond which the body tends to behave as a spring-damper combination. The general application of the proposed mean standardized values to situations involving sitting human subjects raises many serious concerns in view of extensive variations in the experimental conditions used in deriving the proposed impedance characteristics.

5.3.3 SYNTHESIS OF SELECTED DATA SETS

In view of the extensive variations in the test conditions employed in various studies summarized in Table 5.1 and the significant discrepancies in the published data, the data sets reported under similar test conditions are selected for further analysis and synthesis. An attempt is made to select and group the data sets reported under test conditions which conform to those encountered in vehicle driving operation.

Since the vehicle driving necessarily involves feet supported either on the floor or on the pedals, the mechanical impedance data sets measured with feet not supported are discarded. The synthesis is thus limited to data reported in references [69, 85, 90, 73, 91, 70 and 92], as identified in Table 5.1. Of these, the data reported in [69, 85 and 90] was obtained under sinusoidal

excitations only, while the data reported in the remaining studies involved random excitations of varying magnitudes. Table 5.2 presents the 71 data sets extracted from these studies, of which only four sets were measured using sinusoidal excitations. Majority of the data obtained under random excitations was extracted from studies by Sandover [91], and by Fairley and Griffin [73], who reported data under various amplitudes of excitations and postures. Only two data sets were obtained while the subjects leaned against a backrest, and one data set only was reported for a slouched sitting posture. Majority of the data applies to the sitting erect posture without back support, while the hands are in lap. Only seven data sets apply to the "hands in a driving position" condition, all of which were extracted from Sandover's study [91].

All the data sets listed in Table 5.2 for a sitting posture without backrest support are synthesized to compute the mean values of the impedance magnitude and phase together with the envelopes. The range of impedance values, illustrated in Figure 5.9, demonstrates the large variations in the mechanical impedance characteristics reported for different excitations, mass of subjects and other experimental conditions. The results illustrate that the impedance magnitude may vary from almost 1250 Ns/m to approximately 4400 Ns/m in the vicinity of 7 Hz. The corresponding variation in the impedance phase, although not as significant as in the case of magnitude, is observed to be from 10° to 48°. The large range of magnitude and phase values clearly

TABLE 5.2

Characterization of Mechanical Impedance Data Sets According to the Prescribed Test Conditions

Data Set #	Ref.	Excitation Type	# of subjects	Mass (kg)	Hand Position	Backrest Support	Response Function
1	[69]	Sine,0.1 in	11	73.6	in lap	None	Z,ϕ
2	[85]	Sine, 1-2"	39	51-93.8	NR*	NR*	Z,ϕ
3	[90]	Sine, 1.5"	4	56-83	NR*	NR*	M,ϕ
4	[90]	Sine, 3.0"	4	56-83	NR*	NR*	M,ϕ
5	[70]	Random,1.0"	8	57-85	in lap	None	M,ϕ
6	[70]	Random,.25"	1	NR*	in lap	None	M
7	[70]	Random,0.5"	1	NR*	in lap	None	M
8	[70]	Random,1.0"	1	NR*	in lap	None	M
9	[70]	Random,1.5"	1	NR*	in lap	None	M
10	[92]	Random,1.0"	1	NR*	NR*	None	M,ϕ
11-18	[73]	Random,.25"	8	57-85	in lap	None	M
19-26	[73]	Random,0.5"	8	57-85	in lap	None	M
27-34	[73]	Random,1.0"	8	57-85	in lap	None	M
35-42	[73]	Random,1.5"	8	57-85	in lap	None	M
43	[91]	Random,2.3"	1	77	in lap	None	M,ϕ
44	[91]	Random,2.3"	1	77	driving	None	M,ϕ
45	[91]	Random,1.0"	1	60.7	in lap	None	M,ϕ
46	[91]	Random,1.0"	1	87.2	in lap	None	M,ϕ
47	[91]	Random,1.0"	1	81.7	in lap	None	M,ϕ
48	[91]	Random,1.0"	1	52.7	in lap	None	M,ϕ
49	[91]	Random,1.0"	1	75.3	in lap	None	M,ϕ
50	[91]	Random,1.0"	1	70	in lap	None	M,ϕ
51	[91]	Random,2.0"	1	60.7	in lap	None	M,ϕ
52	[91]	Random,1.0"	1	60.7	driving	None	M,ϕ
53	[91]	Random,2.0"	1	87.2	in lap	None	M,ϕ
54	[91]	Random,1.0"	1	87.2	driving	None	M,ϕ
55	[91]	Random,2.0"	1	81.7	in lap	None	M,ϕ
56	[91]	Random,1.0"	1	81.7	driving	None	M,ϕ
57	[91]	Random,2.0"	1	52.7	in lap	None	M,ϕ
58	[91]	Random,1.0"	1	52.7	driving	None	M,ϕ
59	[91]	Random,2.0"	1	75.3	in lap	None	M,ϕ

TABLE 5.2 (CONTINUED)

Characterization of Mechanical Impedance Data Sets According to the Prescribed Test Conditions

Data Set #	Ref.	Excitation Type	# of subjects	Mass (kg)	Hand Position	Backrest Support	Response Function
60	[91]	Random,1.0**	1	75.3	driving	None	M,ϕ
61	[91]	Random,2.0**	1	70	in lap	None	M,ϕ
62	[91]	Random,1.0**	1	70	driving	None	M,ϕ
63	[91]	Random,1.0**	6	52.7-87.2	in lap	None	M,ϕ
64	[73]	Random,1.0**	8	57-85	in lap	None	M
65	[73]	Random,1.0**	8	57-85	in lap	None	M
66	[73]	Random,1.0**	8	57-85	in lap	None	M
67	[73]	Random,1.0**	1	75	in lap	None	M
68	[73]	Random,1.0**	8	57-85	in lap	Yes	M
69	[73]	Random,1.0**	1	75	in lap	Slouched	M
70	[91]	Random,2.3**	1	77	in lap	Yes	M,ϕ
71	[91]	Random,2.3**	1	77	in lap	None	M,ϕ

* Not Reported
** rms acceleration in ms^{-2}.

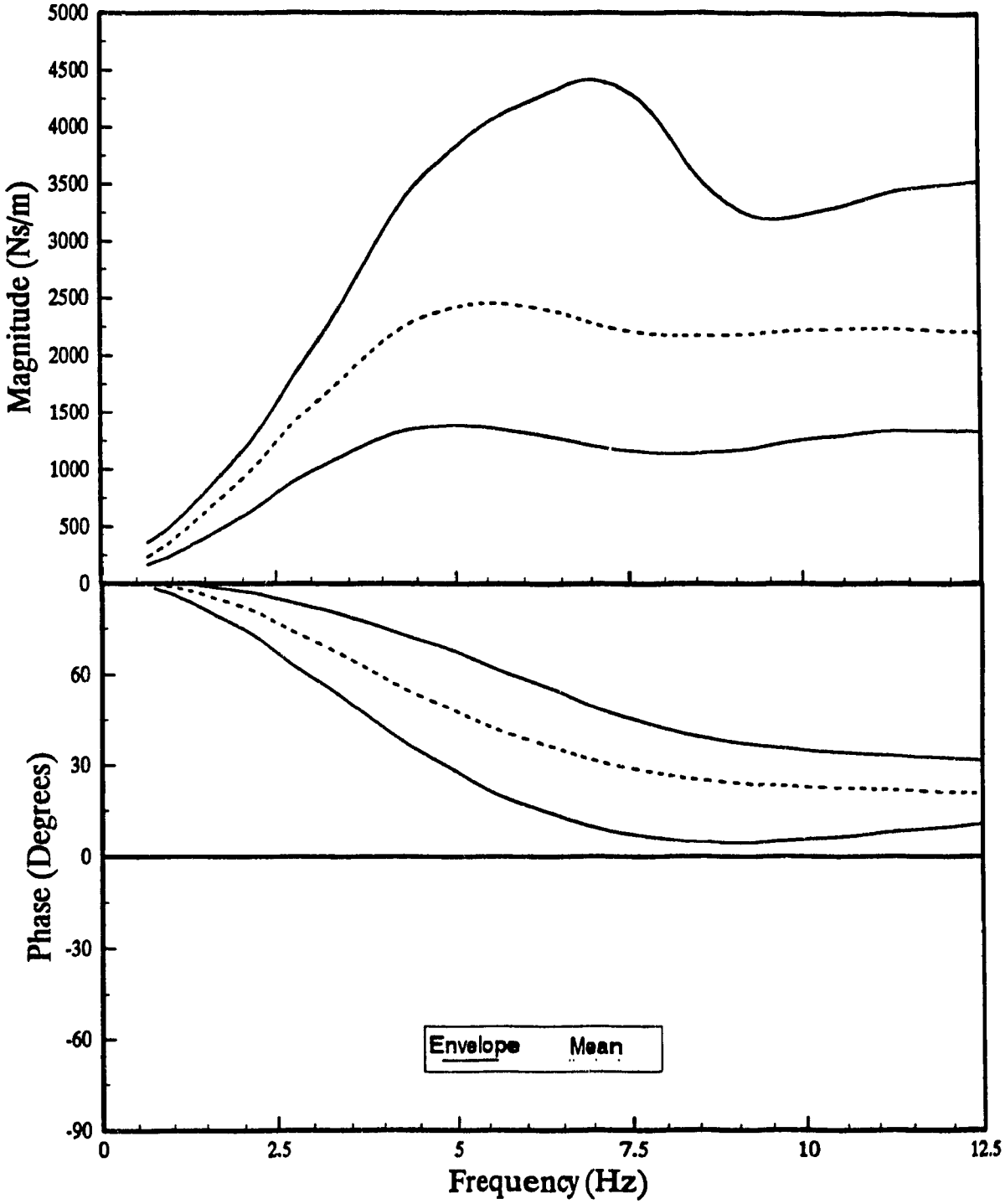

Figure 5.9 Mean whole-body mechanical impedance computed by synthesizing the data sets identified for subjects sitting, without back support.

demonstrates the extent of the variations that may be expected when the test conditions are not given appropriate consideration. A comparison of this synthesized data with the ISO proposed standardized curve, presented in Figure 5.8, reveals that the magnitude of the mean synthesized mechanical impedance is significantly lower than that proposed in the draft standard in the entire frequency range. While the mean values of the synthesized and standardized curves exhibit a peak at a similar frequency, the magnitude of the mean synthesized curve is well below the magnitude of the lower limit curve proposed in the draft standard. The mean impedance phase response from the synthesized data is observed to be slightly larger than the mean values indicated in the proposed standardized curve. The significant differences observed between the synthesized data and the proposed standardized curves raise a serious doubt on the relevance of defining a single universal curve characterizing the mechanical impedance of sitting subjects.

The measured impedance magnitude and phase data reported in various studies are further compared to illustrate the extent of variations between data sets, as shown in Figure 5.10. The results further reveal that the ISO proposed mean standardized impedance magnitude exceeds those of almost the entire data sets. The figure illustrates five data sets (# 1,2,3,5 and 63 listed in Table 5.2) extracted from the references [69, 85, 90, 70, and 91]. These studies have reported both the mechanical impedance (or apparent mass) and phase for

subjects sitting erect under excitation levels below 2 ms^{-2}. The significant discrepancies among the reported data may be attributed to variations in excitation (sinusoidal 0.1 in constant displacement amplitude, sinusoidal 1.5 and 1 - 2 ms^{-2} rms acceleration, random 1 ms^{-2} rms acceleration), subject mass (51 - 93.8 kg), hand position, back support and posture. Upon neglecting the data proposed by ISO, which is clearly outlier, the remaining data sets are analyzed to yield mean values and envelopes of the magnitude and phase as shown in Figure 5.11. A comparison of this synthesized data with the synthesized curves presented in Figure 5.9 reveals that the magnitude of variations is considerably reduced by omitting the standardized data.

Upon recognizing the significant variations among the reported data sets and the associated test conditions, a further attempt is made to group the data sets under similar excitation levels and posture. Table 5.3 illustrates the grouping of the identified data sets under three specific postures and four different vibration excitations. The different sitting postures include: erect with non-supported back (ENS), erect with back supported (EBS), and slouched (SLO). The three postural classifications are further combined with two hand positions: hands in lap and hands in a driving position while holding a steering wheel. The data sets are then grouped for different excitations: 1, 2 and >2 ms^{-2} random inputs; and sinusoidal vibration with rms acceleration in the 1-3 ms^{-2} range. This grouping of the data sets is then used to determine the apparent influence of

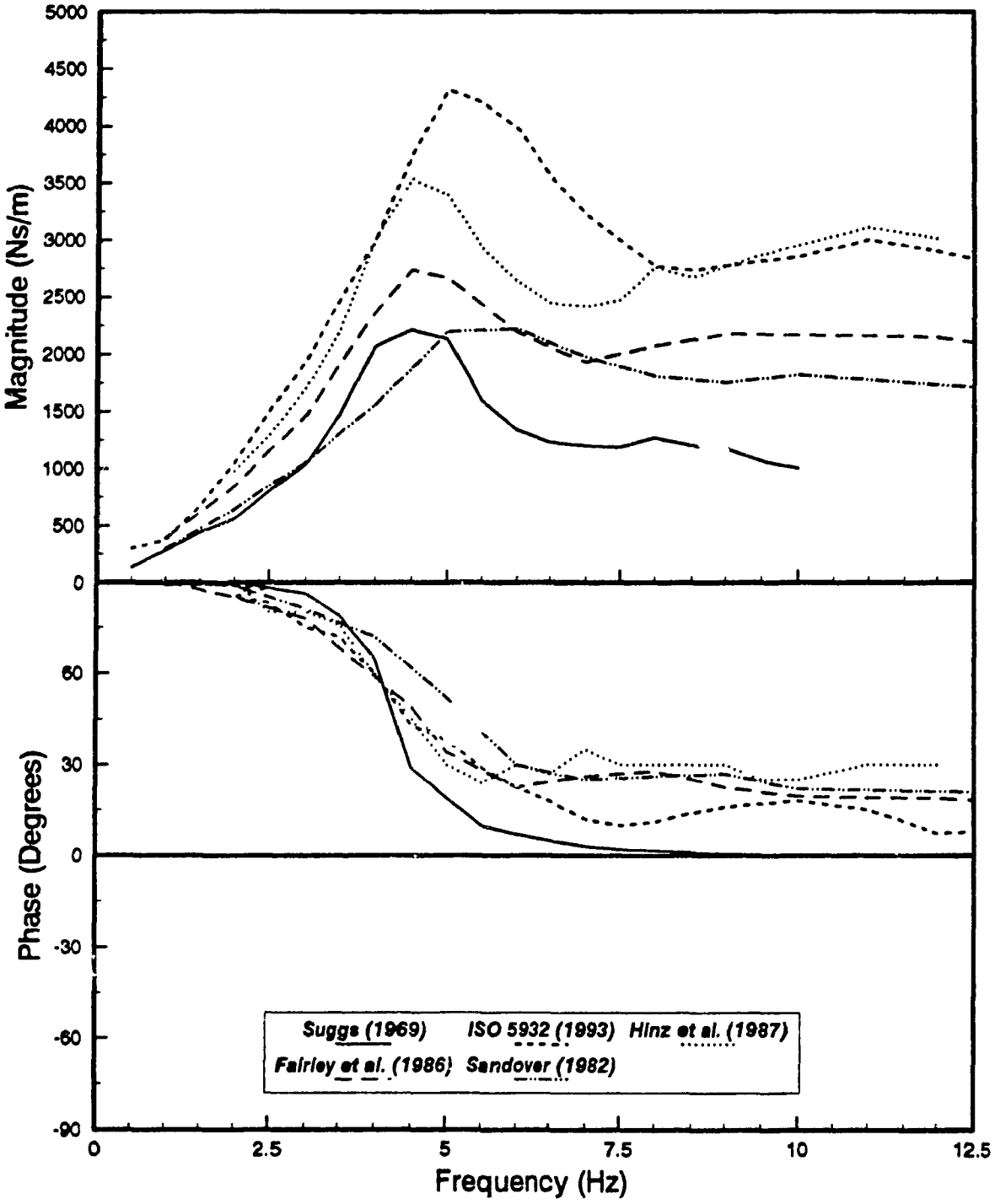

Figure 5.10 Whole-body mechanical impedance data reported in the literature for sitting individuals exposed to vibration amplitudes lower than 2 ms^{-2} (data sets 1,2,3,5 and 63).

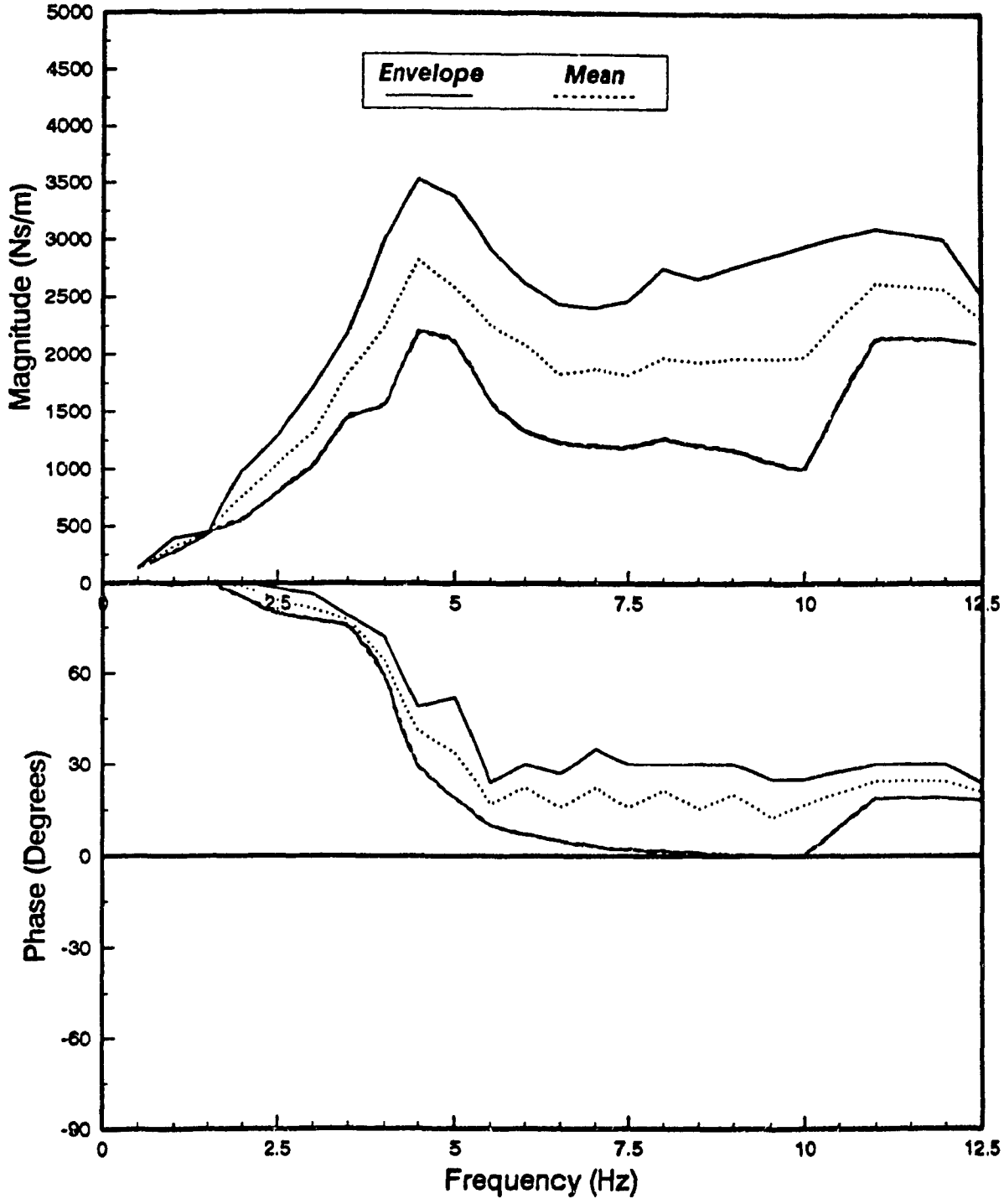

Figure 5.11 Mean whole-body mechanical impedance obtained from the synthesis of data sets (1,3,5,63) reported for sitting individuals exposed to vibration amplitudes lower than 2 ms^{-2} (excluding data from ISO CD 5982).

posture, hand position, excitation type, and excitation amplitude on the driving-point mechanical impedance magnitude and phase. The data groups presented in Table 5.3 clearly illustrate that the majority of the reported data sets were acquired for the ENS posture with the hands in lap. A synthesis is performed on each data group and the synthesized data is smoothened. The data reported in terms of apparent mass was converted into mechanical impedance using equation (5.4).

TABLE 5.3

Data Sets Associated with Each Posture and Excitation Type

POSTURE	EXCITATION RMS ACCELERATION			
	Sine 1 - 3 ms^{-2}	Random 1 ms^{-2}	Random 2 ms^{-2}	Random >2 ms^{-2}
ENS, hands in lap	1 - 4	5,8,10, 27-34,45-50,63-67	51,53,55, 57,59,61	43,71
ENS, driving position	-	52,54,56, 58,60,62	-	44
EBS, hands in lap	-	68	-	70
SLO, hands in lap	-	69	-	-

5.3.4 APPARENT INFLUENCE OF TYPE OF EXCITATION

The data groups identified for sinusoidal and random excitations are analyzed to establish the influence of the type of excitation on the mechanical driving-point impedance characteristics irrespective of the hand position, the posture and the back support. The amplitude of excitation is

observed to vary in the 1 to 3 ms^{-2} range for all the data sets considered. Under sinusoidal excitation, 3 of the 4 data sets identified in Table 5.3 are considered, omitting the data provided in ISO CD 5982. An analysis of the experimental test conditions employed in these studies reveals that averaging of these data sets represents the mechanical impedance characteristics of 15 subjects in the 56 to 83 kg mass range, with a mean mass of 73 kg. A total of 44 data sets, considered for random excitation, represent the average mechanical impedance of 16 subjects in the 53 to 87 kg range, with a mean mass of 72 kg. The mean values of all the data sets considered are illlustrated in Figure 5.12 in terms of both impedance magnitude and phase.

The mean values of impedance magnitude corresponding to sinusoidal and random excitations appear to be in reasonable agreement in two frequency ranges: (i) at low frequencies, below 2.5 Hz, and (ii) between 6 and 9 Hz. In the resonant frequency region, and at frequencies exceeding 9 Hz, the synthesized data under sinusoidal excitation results in impedance magnitude considerably larger than that attained for random excitations. It should be noted that the range of amplitude for both excitations is quite similar. Moreover, under sinusoidal excitation, the body resonant frequency is observed to occur at a slightly lower frequency. The resonant frequency is observed to lie between 4.5 and 5 Hz for average subject mass ranging from 72 to 73 kg

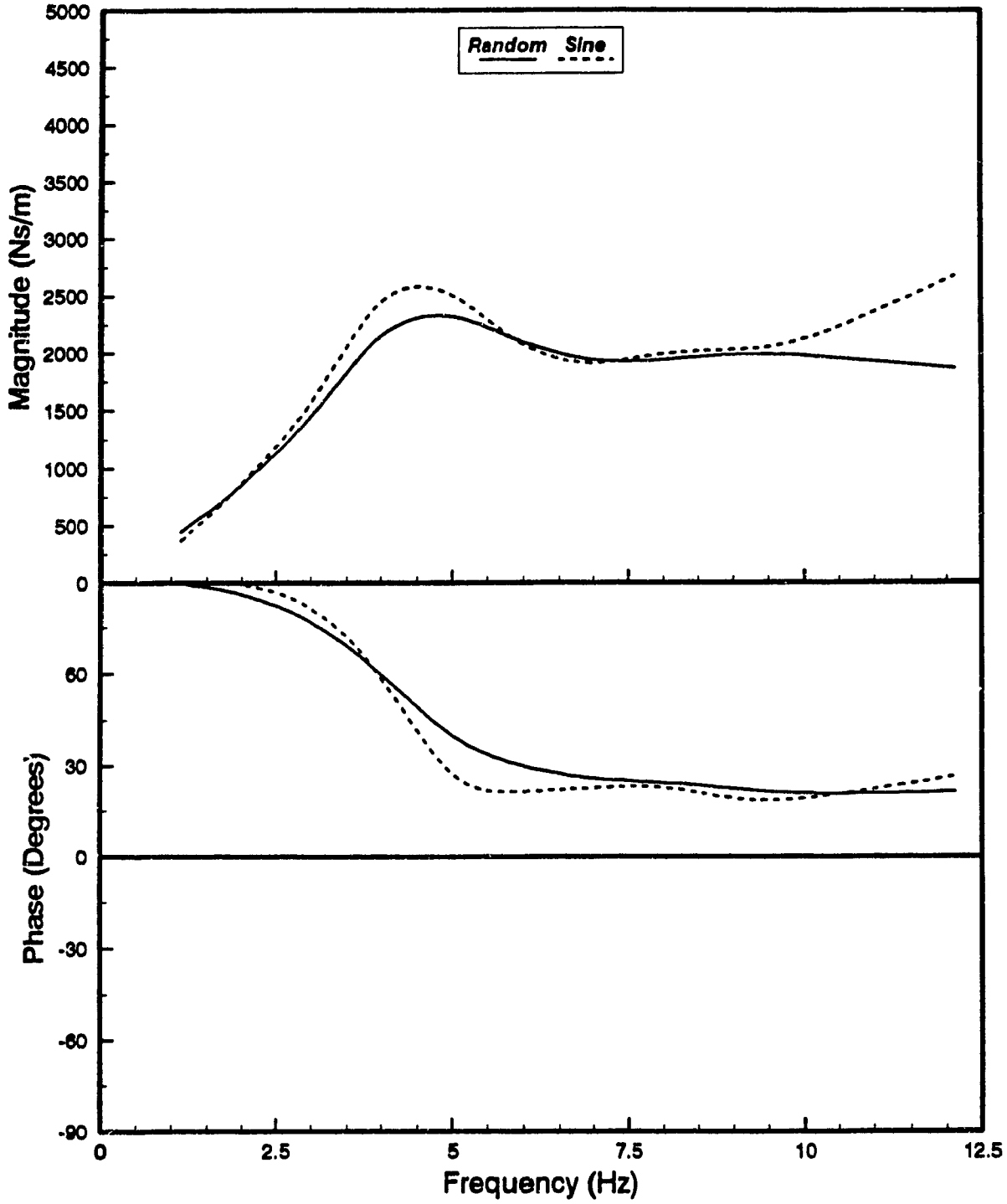

Figure 5.12 Apparent influence of the excitation type on whole-body mechanical impedance from synthesized data (excitation amplitude 1 - 3 ms^{-2}, mean subject mass: 72 kg for sinusoidal, 73 kg for random).

under the two excitations. The average impedance phase response under the excitations is quite similar, except in the vicinity of the resonant frequency region. The observed phase response under random excitations is observed to be larger than that established under sinusoidal excitation near the resonant frequency. The peak phase difference is approximately 10°, which occurs near the resonant frequency.

The results of the synthesized data reveal that sine and random excitations may lead to slightly different impedance characteristics, particularly in the resonant frequency region. This data synthesis, however, could not account for possible variations arising from data sets obtained using different experimental procedures.

5.3.5 APPARENT INFLUENCE OF EXCITATION AMPLITUDE

A study of the different data groups identified for different levels of random excitations alone permits the evaluation of the influence of the excitation amplitude on the mechanical impedance characteristics. The data sets for the ENS posture with hands in lap condition, as identified in Table 5.3, are analyzed to study the influence of three levels of random excitations: 1, 2 and >2 ms^{-2} rms acceleration. A total of 22 data sets are available for random excitation level of 1 ms^{-2} rms acceleration, which represent the impedance characteristics of 15 subjects in the 52.7 to 87.2 kg mass range,

with a mean mass of 72 kg. The synthesis of data sets corresponding to 2.0 ms^{-2} random excitation includes 6 data sets reported for 6 subjects within the mass range of 52.7 to 87.2 kg, with a mean mass of 71 kg. Finally, only two data sets are available for excitation levels greater than 2.0 ms^{-2}, reported for only one subject of 77 kg mass. The data groups for three levels of random excitations are synthesized to yield the mean impedance magnitude and phase, as shown in Figure 5.13.

The results of the study show that the amplitude of excitation affects the resonant frequency and impedance magnitude. The resonant frequency of the seated body tends to decrease with an increase in the magnitude of random excitation. This observation is further supported by measurements performed by Griffin [73], for excitation amplitudes varying between 0.25 and 2.0 ms^{-2}. While the magnitude of impedance remains unchanged at frequencies below 4 Hz, when the excitation amplitude is increased from 1.0 to 2.0 ms^{-2}, the magnitude at frequencies above 4 Hz decreases with increasing excitation level. This pattern, however, is not apparent for excitation levels greater than 2 ms^{-2}, which may be attributed to the lack of data sets (only 2) for such excitation levels. Furthermore, the acquisition of these data sets for only one subject raises concerns on their validity. The impedance phase response for an excitation level of 1 ms^{-2} is quite similar to that for 2.0 ms^{-2} excitation. The mean phase response corresponding to

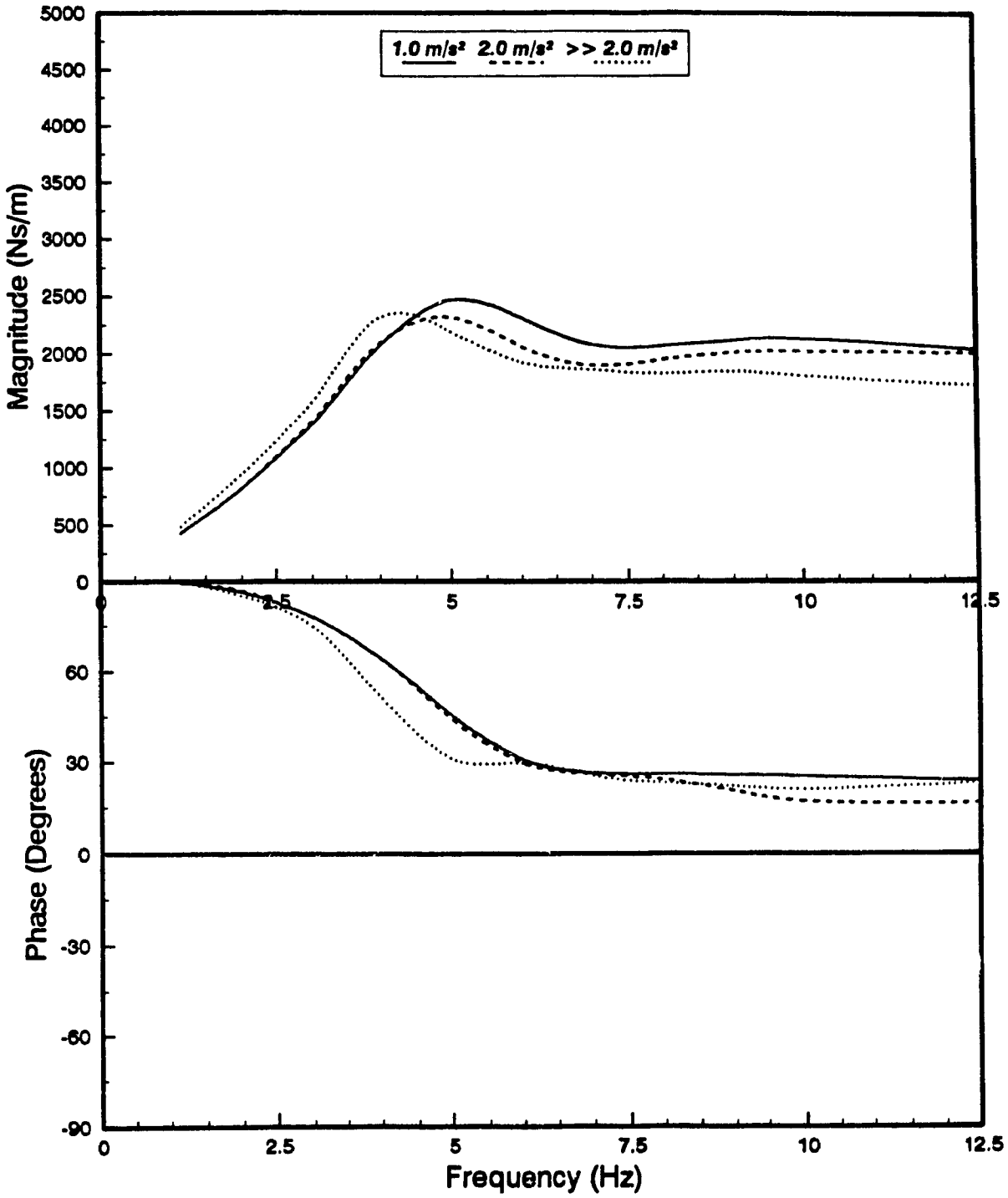

Figure 5.13 Apparent influence of excitation amplitude on whole-body mechanical impedance from synthesized data (random excitation, ENS posture, hands in lap, mean subject mass: 72, 71 and 77 kg for increasing amplitude).

excitation levels above 2.0 ms^{-2} differs from that under 1.0 and 2.0 ms^{-2}, in the 3 - 6 Hz frequency range. This difference may again be attributed to the above described test conditions used for >2.0 ms^{-2} excitation.

The linear or nonlinear nature of the biodynamic response of the seated human body exposed to vibration has been strongly debated by the researchers in view of the highly contradictory results published in different studies. Variations in the impedance magnitude and resonant frequency with excitation amplitude implies somewhat nonlinear behaviour of the human body. Griffin [73] concluded that softening of the system and thus, reduction in the resonant frequency occurs with an increase in the excitation amplitude. The findings of Griffin's study contradicted the results of the study performed by Mertens [78], which showed an increase in the resonant frequency as the magnitude of steady-state acceleration in a centrifuge was increased from 1 to 4 g. Sandover [91] reported no clear differences in the impedance characteristics with changes in stimulus levels and postulated that relatively small differences may be attributed to postural changes necessary to adapt to changing vibration levels. The study thus supported the hypothesis that the biodynamic response of the human body to vibration is perhaps linear, specifically for short exposure periods. The biodynamic response behaviour, however, may be considered nearly linear within a limited range of moderate vibration levels.

5.3.6 APPARENT INFLUENCE OF THE SITTING POSTURE

Various data groups identified in Table 5.3 are analyzed to establish the influence of sitting posture on the biodynamic response of the human body. A study of the data groups reported for different sitting postures, defined as ENS, EBS and SLO is undertaken to establish their apparent influence on the mechanical impedance characteristics. The synthesis, however, is possible only for random excitation at a level of 1 ms^{-2} and for "hands in lap" condition. Under such conditions, the synthesized data for the ENS posture is the same as shown in Figure 5.13 corresponding to 1 ms^{-2} random excitation and a mean subject mass of 72 kg. For the EBS posture, only one data set is available, representing the average mechanical impedance of 8 subjects in the 57 to 85 kg range , with a mean mass of 72 kg. Only one data set is available for the SLO posture, obtained for one subject of mass 75 kg. Furthermore, the phase data is not available for SLO and EBS postures. The synthesized curves appear in Figure 5.14 for both impedance magnitude and phase.

From the results, it is apparent that the seated posture affects the mechanical impedance magnitude in a definite manner. It should be noted, however, that the synthesis of data for SLO and EBS postures is based upon a single data set and that the mean subject mass considered for the study of SLO posture is larger than that considered for EBS and ENS postures.

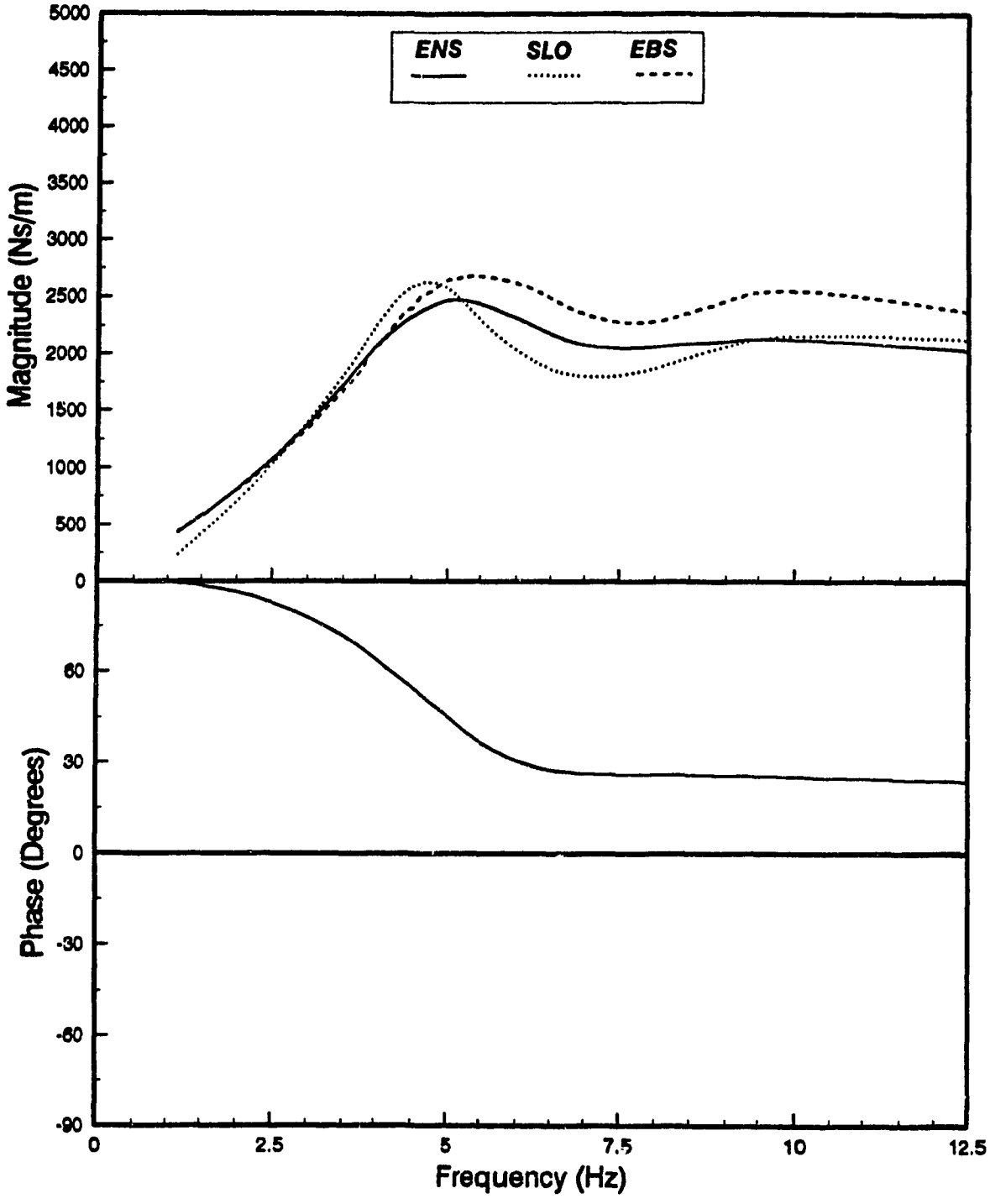

Figure 5.14 Apparent influence of posture on whole-body mechanical impedance from synthesized data (1 ms^{-2} random excitation, hands in lap, mean subject mass: 72 kg for ENS and EBS, 75 kg for SLO).

The results of the synthesis show that the addition of a back support to an erect sitting posture tends to increase the impedance magnitude at frequencies beyond 4 Hz. The slouched posture yields a decrease in the body resonant frequency, as shown in Figure 5.14. In view of the lack of reported data, specifically for the EBS and SLO postures, it is quite difficult to attribute the differences in impedance magnitude to postural positions alone. Many individual factors may also contribute to the changes in impedance, including differences in mass and muscle tension among the subjects. From the synthesized literature, it can only be concluded that posture constitutes a factor that most probably affects the mechanical impedance response of the seated human body.

5.3.7 APPARENT INFLUENCE OF THE HANDS POSITION

While majority of the published data on whole-body mechanical impedance was obtained with subjects seated with their hands in lap, Sandover [91] reported impedance characteristics of the subjects with their hands in a driving position (while holding a steering wheel). From Table 5.3, it is apparent that data sets identified under "ENS, hands in lap" and "ENS, hands in a driving position" may be analyzed to study the influence of hands position on the biodynamic response characteristics, under 1 ms^{-2} random excitation. The synthesized data for the "hands in lap" position is identical to that presented previously for the ENS posture under 1 ms^{-2} random

excitation, for subjects with mean mass of 72 kg (Figure 5.13). The mean impedance characteristics for the ENS posture with "hands in a driving position" are obtained by averaging 6 data sets, representing the measurements performed on 6 subjects with mass ranging from 52.7 to 87.2 kg (mean mass of 71 kg). The mean impedance characteristics are compared for the two hand positions, as shown in Figure 5.15.

Hands placed in the lap tend to increase the impedance magnitude at low frequencies (below 5 Hz), which may be attributed to increased mass supported by the seat. At frequencies above the primary body resonance, however, the hand position does not affect the impedance magnitude. Primary body resonant frequency of the seated body tends to increase slightly when the hands are placed in a driving position. The position of the hands, however, does not affect the impedance phase in a significant manner.

5.3.8 SYNTHESIZED VERSUS STANDARDIZED IMPEDANCE

Majority of the identified data sets and the synthesized impedance curves, presented in Figures 5.11 to 5.15, invariably show a mean impedance magnitude considerably lower than that proposed in the ISO CD document. The mean impedance magnitude obtained from the synthesis is observed to be even below the lower bound envelope proposed by the standardized

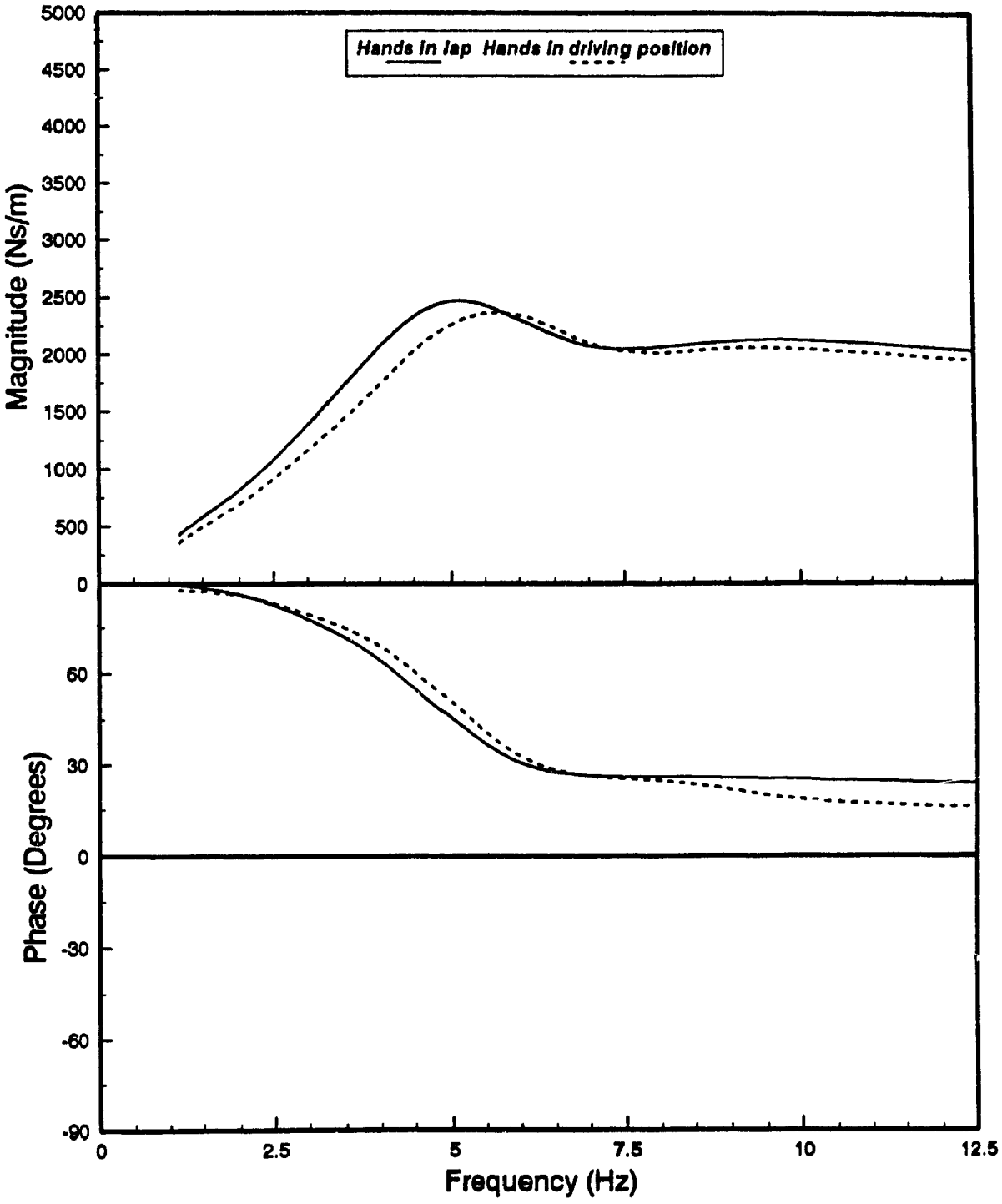

Figure 5.15 Apparent influence of hand position on whole-body mechanical impedance from synthesized data (1 ms^{-2} random excitation, ENS posture, mean subject mass: 72 kg and 71 kg).

impedance data. Although the standardized data was reported to have been obtained under sinusoidal excitation only, the mean mechanical impedance magnitude is 40 to 50% higher than that derived from the synthesis of the published data (Figure 5.12) measured under sinusoidal excitation within a similar range of amplitudes. While the synthesized data reveals the primary resonant frequency in the 4.5 to 5 Hz frequency range, the proposed standardized data exhibits the resonance closer to 5.0 Hz. The lower bound of the impedance magnitude proposed by ISO appears to closely agree with the mean values of synthesized impedance data up to 4 Hz, beyond which important differences are observed.

5.4 Synthesis of Published Data on Vertical Seat-to-Head Transmissibility

Seat-to-head transmissibility constitutes a transfer function representing the ratio of head to seat motion, which may be used to characterize the biodynamic response of the seated body. In contrast with driving-point mechanical impedance, which represents force and motion properties at the point of entry into the body, the transmissibility represents the transmission of motion through the body. Since acceleration response can be measured conveniently, the seat-to-head transmissibility is computed as the ratio of head acceleration $\ddot{z}_h(j\omega)$ to the acceleration at the seat $\ddot{z}_s(j\omega)$:

$$T(j\omega)=\frac{\ddot{z}_h(j\omega)}{\ddot{z}_s(j\omega)}=|T(j\omega)|e^{j\phi_T(\omega)} \qquad (5.5)$$

where $|T(j\omega)|$ denotes the transmissibility magnitude at angular frequency ω, while $\phi_T(\omega)$ represents the phase between head and seat acceleration.

For a seated person, the seat constitutes the point of entry of vibration into the body. Vibration transmissibility to the head has been most often reported in the literature, while the acceleration measurements at different body segments have been reported in only a few studies. Magnusson et al. [93] reported the measurements performed into the spinous process of the third vertebrae by inserting a pin-accelerometer, while the subjects were under local anaesthesia. While the measurement of head vibration can be conveniently performed using bite-bar or helmet-mounted accelerometers, the measurement at different body segments poses many complex problems. The "bite-bar" technique has been found to provide more reproducible results than with the helmet. The measurement of head vibration further provides considerable insight into the vibration discomfort and vision problems, which are well identified effects of vibration exposure. The intrinsic and extrinsic variables, such as body dimensions, posture, excitation type and intensity, and head position, however, are known to influence the seat-to-head transmissibility in a more significant manner than the driving-point mechanical impedance.

5.4.1 SELECTION OF PUBLISHED TRANSMISSIBILITY DATA

The biodynamic response characteristics of the seated human body is most

frequently reported in terms of driving-point mechanical impedance. Only few studies have reported the seat-to-head vibration transmissibility of the seated subjects. The lack of reported data on vibration transmissibility may be attributed to the difficulties associated with the measurements. Earlier work by Griffin [7], showed considerable variations in the transmissibility characteristics of subjects under reportedly identical test conditions, namely different levels of vertical sinusoidal vibration ranging from 0.2 to 4.0 ms^{-2} at each of 12 frequencies between 7 and 75 Hz. The measurements were performed with subjects sitting erect with their hands in lap and feet supported but not exposed to vibration. An attempt was later made to relate these variations to the differences in height, weight, age and body size of the subjects [72]. This only resulted in positive correlations showing a tendency towards lower seat-to-head transmissibility in heavier subjects, and differences in transmissibility of the men, women, and children. Later experiments conducted by Paddan and Griffin [94] with a group of 12 male subjects with mass ranging from 58 to 81 kg (mean mass of 70.8 kg) again revealed large differences in vibration transmissibility of different subjects. While the study established some significant correlations between the transmissibility measures and the subject characteristics (age, weight, height, body size), the study did not entirely account for the excessive intersubject variability.

The influence of posture on seat-to-head transmissibility has been investigated

by Griffin [31], who presented the transmissibility characteristics of a single subject exposed to vibration in the 1 to 50 Hz frequency range, under 8 different postures, ranging from slouched to erect. Depending upon the excitation frequency and the seated posture, the variations in measured transmissibility characteristics were observed in the order of 600 percent. The seat-to-head vibration transmissibility of subjects with their back supported has been reported in only one study [94]. The study concluded that leaning against a backrest increases the magnitude of head-transmitted vibration considerably, which was partly attributed to the backrest providing an additional transmission path for the vibration. The increase in seat-to-head transmissibility caused by the back support was further related to the resulting stiffening of the muscles and changes in the forces within the body.

Seat-to-head vibration transmissibility characteristics measured under different amplitudes of random and sinusoidal excitations reported only very little changes in transmissibility magnitude for sine sweep excitations ranging from 0.4 to 2.8 ms^{-2}. The differences in transmissibility magnitude measured under random and sine sweep motions were observed to be relatively small for excitation amplitudes of 1 ms^{-2} rms. The largest deviations in response under the two types of excitations occurred in the 16 - 40 Hz frequency range.

5.4.2 STANDARDIZED SEAT-TO-HEAD TRANSMISSIBILITY

The ISO Committee Draft document, CD 5982 [85], has proposed standardized seat-to-head transmissibility characteristics for the human body, specifying both magnitude and phase in the 0 to 31.5 Hz frequency range. Figure 5.16 illustrates the proposed transmissibility characteristics, which are reported to be applicable for both standing and sitting individuals in an upright body position, although the posture is only vaguely defined. The proposed standardized transmissibility curve is based on measured data of 50 subjects with average body mass of 75 kg, exposed to sinusoidal vibration of amplitude ranging from 2 to 4 ms^{-2}. The proposed transmissibility data is reported to be derived from averaging of different data sets established for both "feet supported" and "not supported" conditions.

The proposed standardized curve reveals the body resonance near 5 Hz, with resonant acceleration transmissibility approaching 1.4. The response characteristics of the human body model, proposed in the CD and presented in section 5.2.3, however deviate considerably from the proposed standardized transmissibility magnitude in the vicinity of the resonant frequency and at frequencies beyond 25 Hz. Poor agreement with the proposed phase data is also evident over most of the frequency range considered.

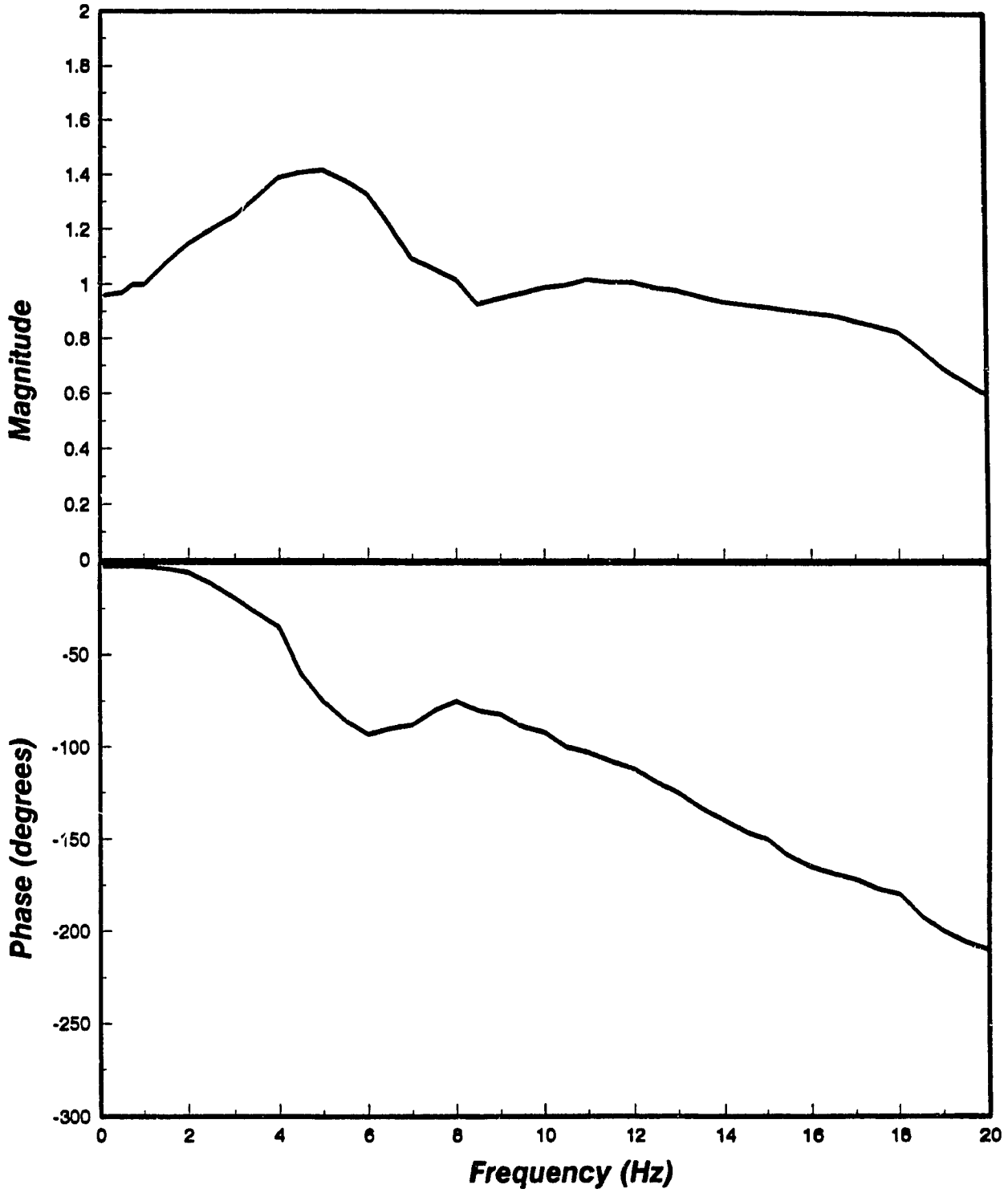

Figure 5.16 Standardized seat-to-head transmissibility characteristics of the human body as proposed in ISO CD 5982 (2 - 4 ms^{-2} sinusoidal excitation, mean body mass of 75 kg, vaguely defined posture).

5.4.3 SYNTHESIS OF DATA SETS

Six data sets, including that proposed in ISO CD 5982, are compiled from the literature for vertical seat-to-head transmissibility of seated subjects [68,78, 85,90,94]. Selection of the data sets was performed on the basis that both magnitude and phase had to be provided. The test conditions associated with each data set are summarized in Table 5.4. While most of the reported data sets refer to seated posture with no back support, one data set was reported for back supported condition. Furthermore, only one data set was reported under random excitations [94].

TABLE 5.4

Identification of Published Data Sets on Seat-to-Head Transmissibility

Data Set #	Ref.	Excitation	# of subjects	Mass (kg)	Backrest Support	Response Function
1	68	Sinusoidal	1	84	None	T
2	78	Sine, 4.0*	9	57-90	None	T,ϕ
3	90	Sine, 1.5*	4	56-83	None	T,ϕ
4	94	Random,1.75*	12	70.8	None	T,ϕ
5	94	Random,1.75*	12	70.8	Yes	T,ϕ
6	85	Sine, 2-4*	50	75	Probably None	T,ϕ

* rms acceleration in ms^{-2}.

The five data sets associated with the "back not supported" (ENS) position are reproduced in Figure 5.17, showing considerable variations in magnitude and phase among them. The transmissibility magnitude reported by Hinz

and Seidel [90] is clearly observed to deviate significantly from the other reported data, and thus may be considered as an outlier. Omitting this data set, and performing averaging and smoothing of the remaining four data sets results in the mean and associated envelope curves for the ENS posture, as shown in Figure 5.18. The mean transmissibility curve reveals a resonant frequency of the body occurring at 5 Hz with peak transmissibility magnitude of 1.45. Figure 5.19 presents the only data set available for the "back supported" (EBS) posture. In this case, the body resonance is observed to occur at 7 Hz, with peak transmissibility magnitude of 1.77.

5.4.4 SYNTHESIZED VERSUS STANDARDIZED TRANSMISSIBILITY DATA

Comparison of the synthesized seat-to-head transmissibility curves shown in Figure 5.18 for the ENS posture with those proposed by ISO (Figure 5.16) reveals a relatively good agreement. Although the ISO data was included in the synthesis of the ENS curves, other individual data sets for transmissibility magnitude, excluding that of Hinz and Seidel, were found to follow the pattern established by the ISO curve. The transmissibility phase data reported by various investigators, however, reveals large discrepancies, particularly at frequencies beyond 10 Hz. In contrast, the transmissibility data for the EBS posture shows marked differences with the ISO data, suggesting that the latter was perhaps derived for subjects without back support.

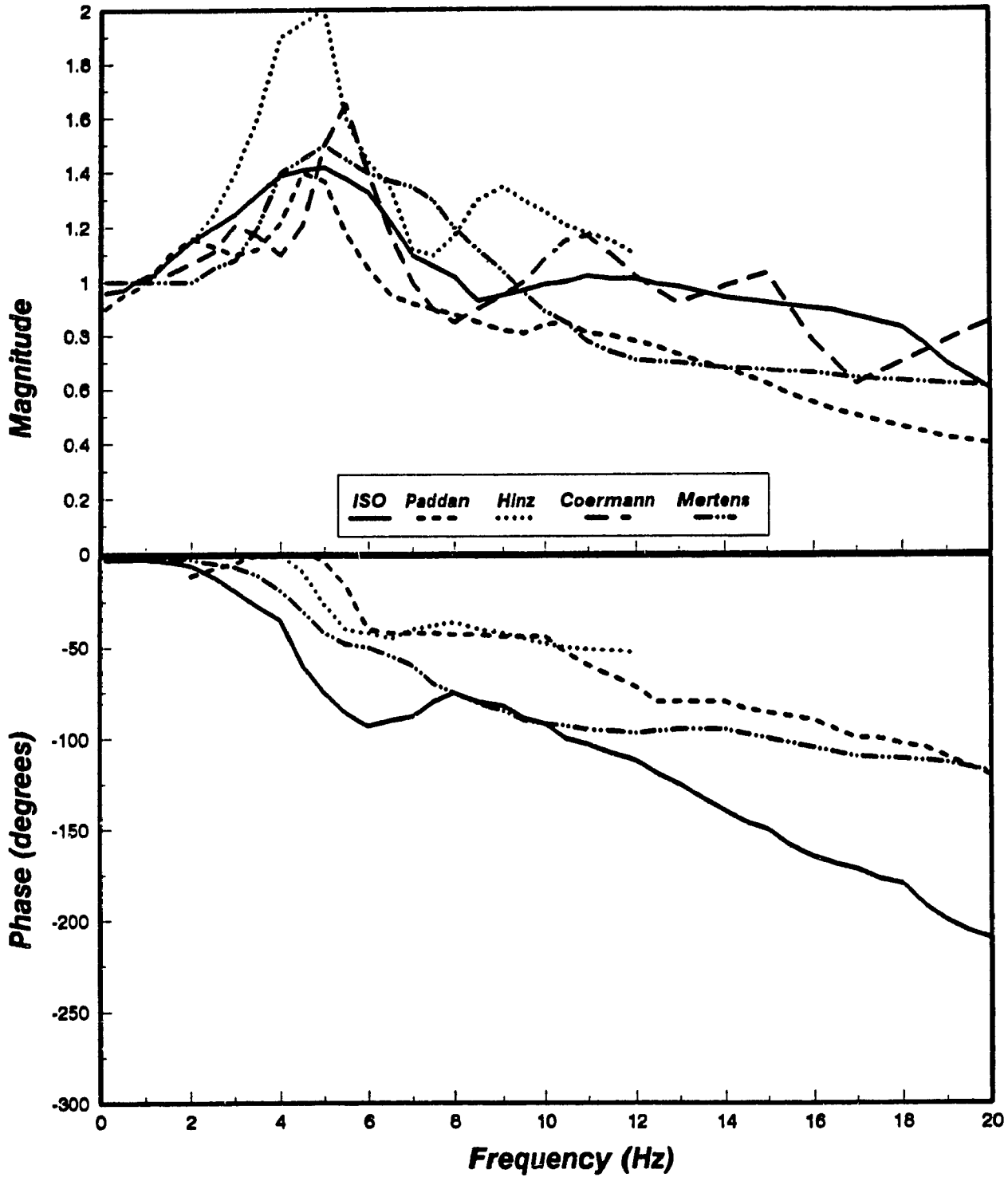

Figure 5.17 Seat-to-head transmissibility characteristics of the human body as determined from various data sets for sitting subjects maintaining an ENS posture ([85], [94], [90], [68], [78]).

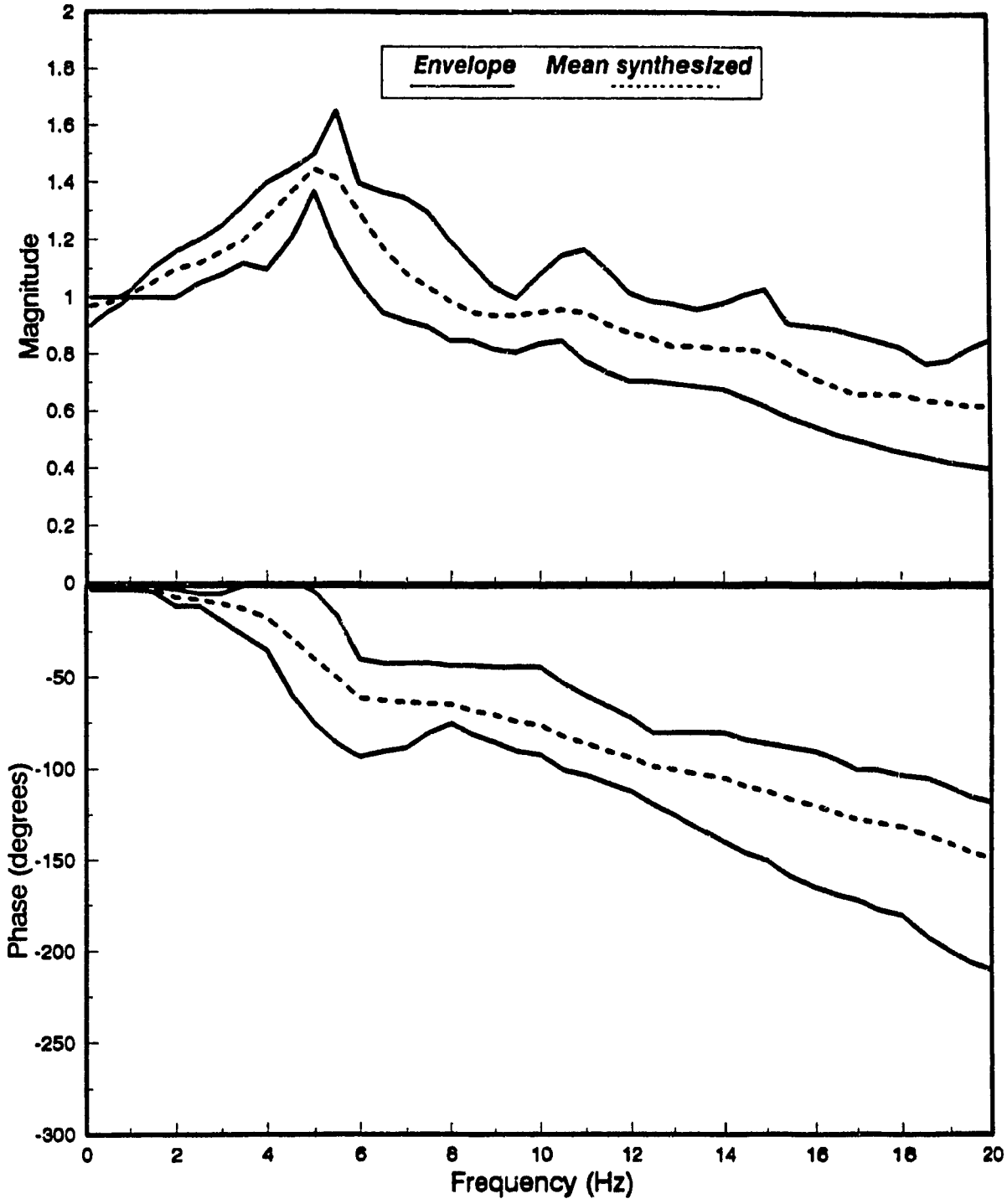

Figure 5.18 Synthesized seat-to-head transmissibility for sitting subjects maintaining an ENS posture (excluding Hinz data, [90]).

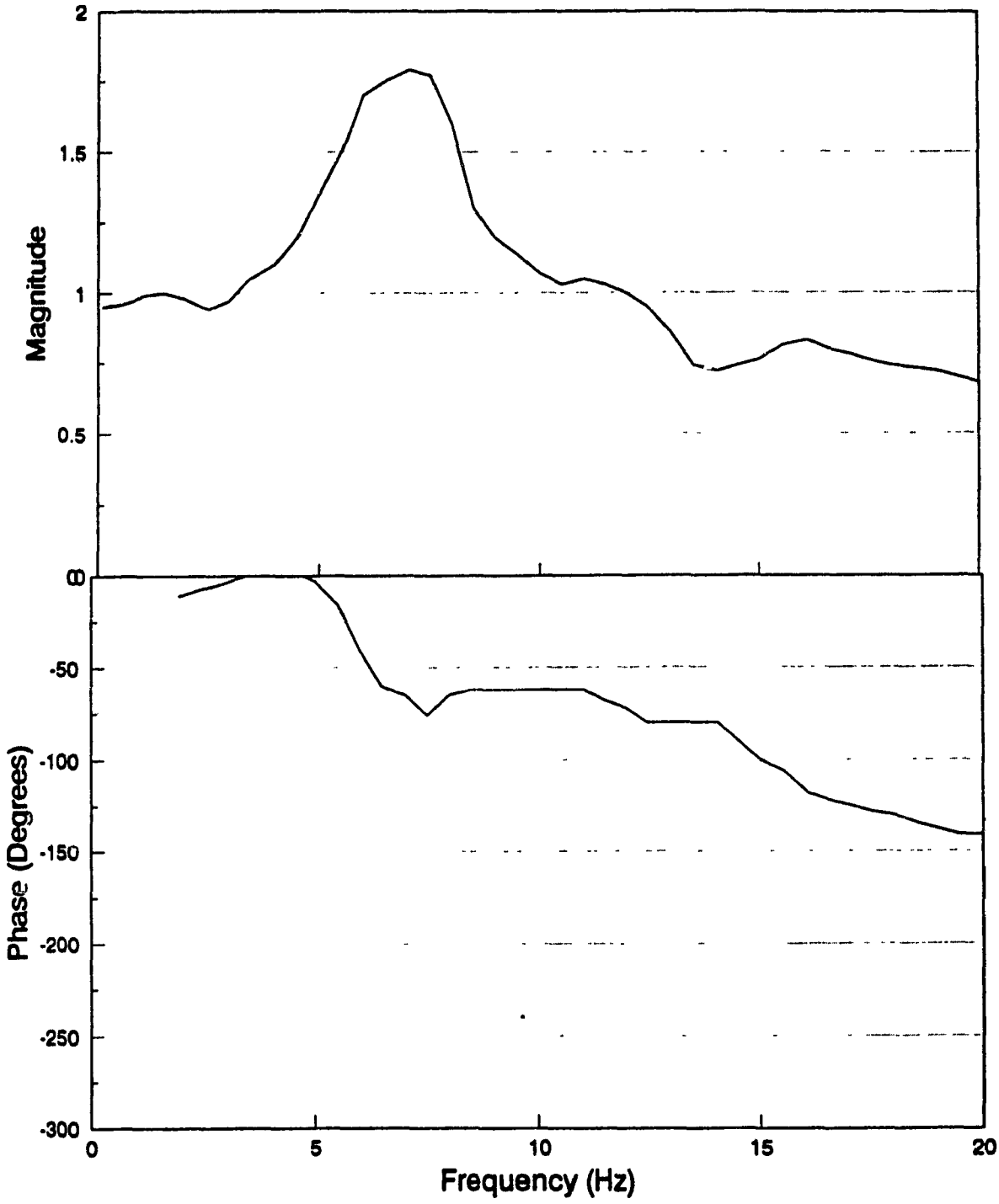

Figure 5.19 Seat-to-head transmissibility reported for sitting subjects maintaining an EBS posture (mean mass: 70.8 kg, 1.75 ms^{-2} random excitation), [94].

5.5 Summary

As a prerequisite to defining a human driver model, several biodynamic models proposed in the literature are reviewed and grouped according to the methodology used for estimating the model parameters. Since none of these models were derived under the conditions encountered in off-road vehicle driving, a data synthesis of published biodynamic response functions, grouped according to specific test conditions, is performed in an attempt to derive target values of driving-point mechanical impedance and seat-to head transmissibility characteristics applicable to off-road vehicle drivers. The synthesized driving-point mechanical impedance data shows a strong influence of seated posture, hand position and excitation type and amplitude on the magnitude and phase characteristics. Data on seat-to-head transmissibility magnitude and phase is also synthesized for seated subjects with and without backrest support. On that basis it is shown that a single universal model such as that proposed by ISO may not be appropriate to characterize off-road vehicle drivers. This is best seen by the large discrepancies observed between the synthesized driving-point mechanical impedance data and that proposed in the standard.

CHAPTER 6

BIODYNAMIC MODEL DEVELOPMENT FOR OFF-ROAD VEHICLE DRIVERS

6.1 Introduction

Off-road vehicle drivers are subjected to low frequency random vibration predominant at frequencies below 5 Hz. When driving, the feet are generally supported either on a vibrating cab floor or pedals, and the hands are in contact with either a steering wheel or handles. For a seated driver, the weight distribution on the seat may vary with the sitting posture adopted, such as erect or slouched positions, with or without backrest support. The adoption of a specific posture may be dictated by the constraints imposed by the seating configuration with respect to vehicular controls, or even by the degree of discomfort experienced by the driver in a given position.

In the preceeding chapter, the apparent influence of several experimental conditions used in characterizing the driving-point mechanical impedance of sitting subjects under the influence of vibration was estimated from a synthesis of published data. A strong dependence of mechanical impedance magnitude and phase was observed on the vibration excitation type and levels, and the subjects posture and hand positions, particularly in the vicinity of the whole-body resonant frequency. Important differences were also observed with the ISO proposed standardized mechanical impedance characteristics [85], derived

mostly under sinusoidal excitations, for subjects with vaguely defined postures. Many biodynamic models proposed in the literature have been based, to some extent, on the requirement of matching the model response with measured whole-body mechanical impedance or apparent mass characteristics within a specific frequency range. In view of the wide range of experimental conditions used in estimating such functions, and on their apparent influence on the mechanical impedance magnitude and phase, the application of these models to situations involving different sets of conditions could hardly be justified.

While the two most widely measured biodynamic response functions are the driving-point mechanical impedance or apparent mass, and the seat-to-head transmissibility, majority of the models have been developed on the basis of matching their response with either one of them. This technique usually provides good correlation with one, but yields large discrepancies with the other. In order to enhance the uniqueness of the model, both biodynamic response functions should ideally be satisfied, within reasonable limits.

In this chapter, a biodynamic model of the seated driver is formulated with appropriate consideration of the conditions representing off-road vehicle driving. The model parameters are estimated such that both driving-point mechanical impedance and seat-to-head transmissibility magnitude and phase are reasonably satisfied. Based on the synthesized data presented in the

preceeding chapter, target values of seat-to-head transmissibility characteristics are established. Since none of the synthesized mechanical impedance or apparent mass data is considered to be representative of off-road vehicle operation, the target values of driving-point mechanical impedance are established from extensive laboratory measurements performed on seven male subjects, under specific excitations and postural constraints, most representative of the conditions encountered by the off-road vehicle drivers. In order to account for reported deviations between rigid mass and human body behaviour at frequencies above 2 Hz, the human driver model developed in this chapter will eventually be combined with the suspension seat model to estimate the seat performance under different types of excitations.

6.2 Measurement of Whole-Body Mechanical Impedance

The single-axis WBVVS, described in Chapter 2, is used to measure the driving-point mechanical impedance characteristics representative of off-road vehicle drivers. A rigid seat was constructed, as illustrated in Figure 6.1, and instrumented to measure the driving force and the resulting velocity at the driving point. The seat pan (406 mm wide and 254 mm deep) and the backrest (406 mm wide and 508 mm high) were made of 6.35 mm thick aluminium plate, and the seat was supported on four legs, 39x39 mm in cross-section and 424 mm high. The backrest was attached to the seat pan through brackets and pivots to achieve variable inclinations of the back support.

The rigid seat was mounted on a force platform fixed to the WBVVS using four Sensotec Model 41 load cells installed at the four corners of a 406 mm square steel plate, 25 mm thick. The output of each of the load cells was connected to a summing junction built within the Sensotec amplifier to achieve a direct measure of the total force. Calibration was accomplished by zeroing the static weight of the force platform and rigid seat, such that the weight of the sitting subject alone could be recorded. A uniaxial accelerometer was fixed directly underneath the seat pan to measure the acceleration transmitted at the seat or driving point. A block diagram of the experimental set-up is shown in Figure 6.2. The measured force and acceleration signals were analyzed to derive the driving-point mechanical impedance in the 0 - 10 Hz frequency range. The impedance magnitude and phase response characteristics were directly obtained from the B&K 2035 dual-channel FFT analyzer.

6.2.1 MASS CANCELLATION

The dynamic force measured by the force platform comprises the components due to the biodynamic response of the seated body, and the inertia forces of the rigid seat and the force platform. In order to isolate the force component due to the biodynamic response of the human body, an inertia cancellation is performed to eliminate the contributions of the seat alone. The seat inertia force cancellation is achieved by subtracting the real and imaginary components of impedance characteristics of the seat alone measured under each type of

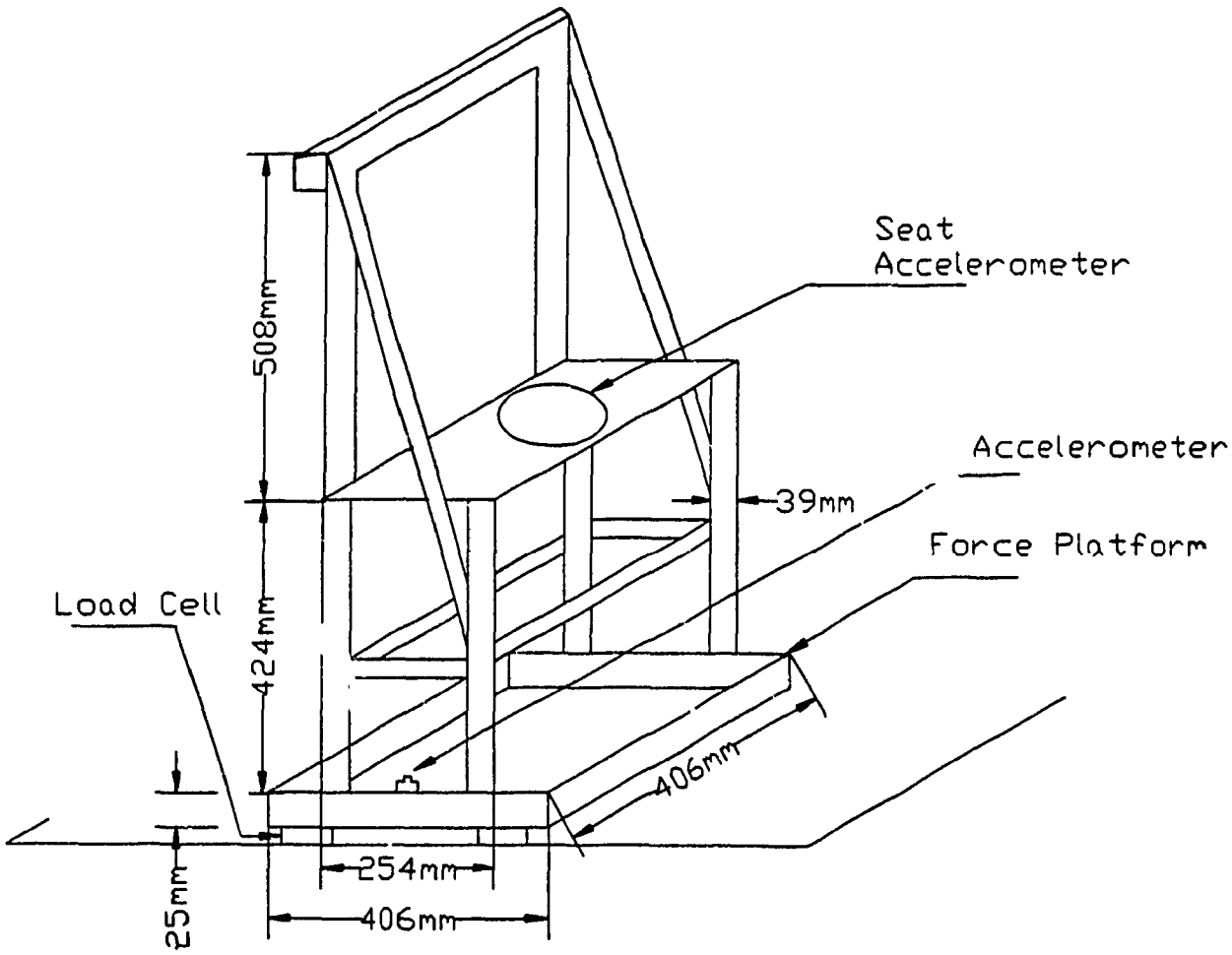

Figure 6.1 **Schematic of the rigid seat used for performing whole-body driving-point mechanical impedance measurements.**

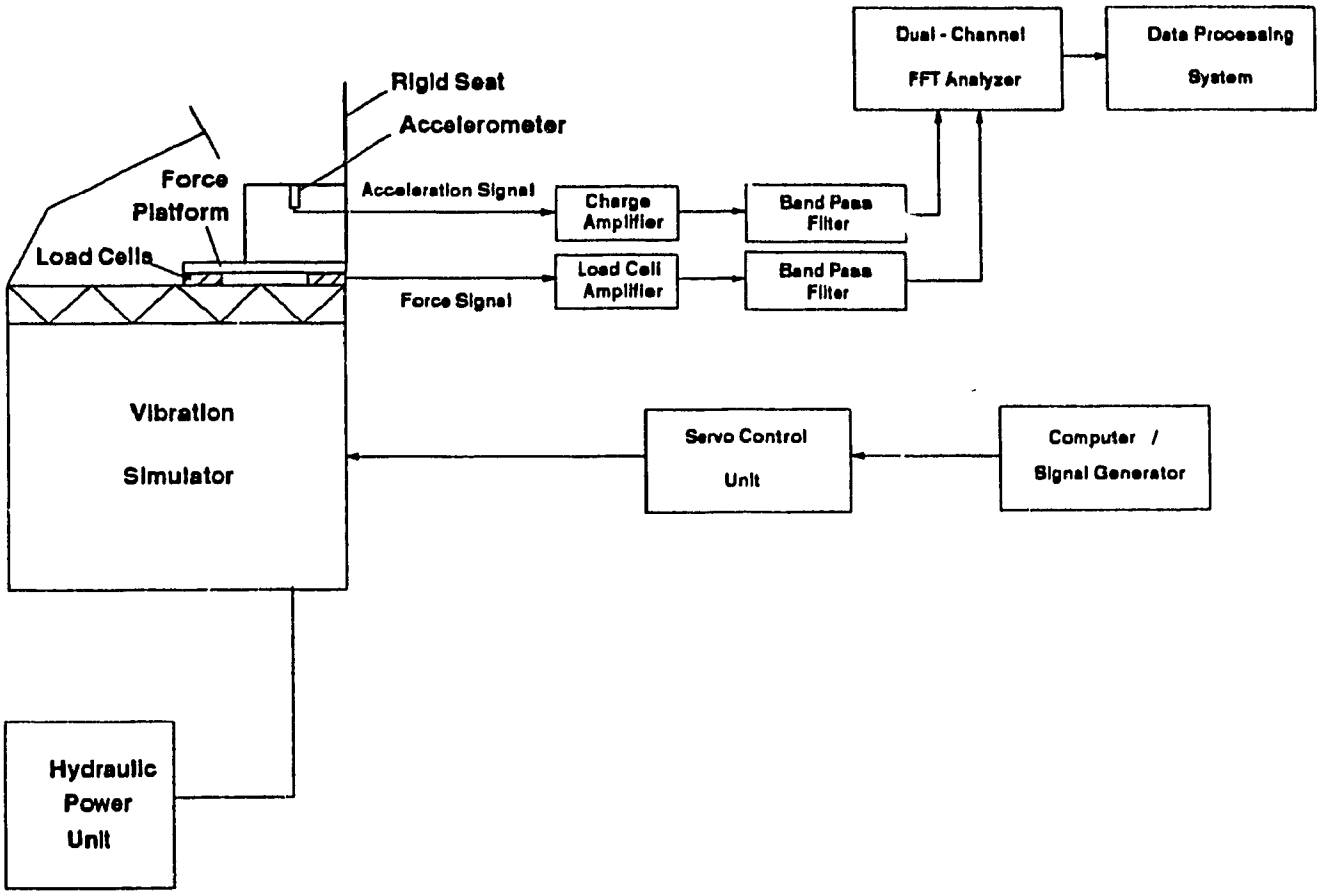

Figure 6.2 Block diagram of the driving-point mechanical impedance measurement set-up.

excitation, from the real and imaginary components of the impedance of the seat-human system. This correction is performed at each frequency within the range of interest. Mechanical impedance magnitude and phase characteristics of the subjects alone are then computed using the real and imaginary parts of the response function.

6.2.2 VIBRATION EXCITATION CLASSES

In order to derive generally acceptable values of driving-point mechanical impedance magnitude and phase of subjects seated in typical off-road vehicle environments, the measurements are performed under different random excitation classes representing a wide range of off-road vehicles. The four random excitation classes, identified in Chapter 2, namely ISO 1, ISO 2, Class I and Class II defined in ISO standards 5007 [31], and 7096 [32], are used. In view of the dependency of mechanical impedance on the type and level of excitation, as observed from the results of the synthesis, the measurements are also performed for sinusoidal and broad-band random excitations in the 0.625 to 10 Hz frequency range at levels of W_z frequency-weighted rms accelerations of 1.0, 1.5 and 2.0 ms^{-2}. Sinusoidal sweep excitations are defined in a manner analogous to that described in Chapter 2, and the required acceleration levels are achieved by adjusting the control gain of the WBVVS servo-controller. Broad-band random excitations are produced using a white noise generator and the required acceleration levels are obtained by adjusting the control gain.

In summary, the driving-point mechanical impedance measurements are performed for the ten different vibration excitations listed below:

- 3 levels of sinusoidal vibration swept in the 0.625 - 10 Hz frequency range (overall W_z frequency-weighted rms accelerations: 1.0, 1.5 and 2.0 ms^{-2});
- 3 levels of broad-band random excitations in the 0.625 - 10 Hz frequency range (overall W_z frequency-weighted accelerations: 1.0, 1.5 and 2.0 ms^{-2});
- 4 random classes of off-road vehicle vibration: ISO 1, ISO 2, Class I, and Class II defined in ISO standards 5007 and 7096.

6.2.3 TEST SUBJECT POPULATION

Seven male subjects took part in the experiments aimed at evaluating the impedance characteristics of off-road vehicle drivers while maintaining specific predefined postures. Table 6.1 presents the age, stature and masses (standing erect, and sitting on a rigid seat) of the subjects. These subjects were within the age group 30 to 40 years old with mean mass of 72.3 kg while standing. The standard deviation of the mass is quite significant (8.8 kg) owing to the much smaller mass of subject S in relation with the others. Overall, 73.6% of the weight was found to be supported by the seat for the subjects considered, while maintaining an erect sitting posture without back support, and with the feet resting on the platform. The hands were kept in a driving position while holding a steering wheel. In order to limit the subjects mass range, the results

obtained with subject S were later disregarded, increasing the mean mass of subjects to 75.4 kg and reducing the corresponding standard deviation to 3.9 kg.

TABLE 6.1

Characteristics of the Test Subject Population

SUBJECT	AGE (years)	HEIGHT (m)	MASS (kg) STANDING	MASS (kg) SITTING
A	31	1.70	77.8	57.0
P	36	1.78	69.6	51.0
B	30	1.83	80.9	57.7
J	33	1.73	73.2	55.6
R	32	1.70	74.8	57.4
D	32	1.80	75.9	54.1
S	40	1.68	54.0	39.6

All the subjects who participated in the experiments had no previous record of low back pain. They were thoroughly informed on the contents of the experiments prior to the testing and were requested to sign a consent form, a copy of which is included in Appendix A. The duration of vibration exposure for any given test did not exceed 2.5 minutes under random excitations and 6 minutes under sinusoidal excitations. Although these tests were repeated several times to include variations in posture and vibration excitation types, attempts were made to limit the exposure duration to two hours in any given

day for a particular subject. Prior to testing, each subject was familiarized with the operation of the safety features incorporated in the simulator. They were also encouraged to stop the testing whenever they would consider it appropriate to do so.

6.2.4 POSTURAL CONSTRAINTS

Measurements of driving-point mechanical impedance are performed for each test subject while sitting on the rigid seat described previously, with their feet resting flat on the WBVVS platform. Subjects are instructed to place the hands on the steering wheel and to maintain a predefined sitting posture without leaning against the steering wheel. Three sitting postures are defined as:

- sitting erect with only the lower back in contact with the backrest; also referred to as the "erect back not supported" (ENS) posture;
- sitting erect with most of the back in contact with the backrest; also referred to as the "erect back supported" (EBS) posture;
- sitting in a slouched (SLO) posture, the upper body having a more pronounced inclination towards the front than with the ENS posture, while the lower back is in contact with the backrest.

For each subject, the experiments are repeated for each of the three postures identified above, under all ten vibration excitations identified in section 6.2.2. In addition, a few experiments are conducted for a seat backrest inclination

angle of 14° to the vertical. When not otherwise specified, the backrest is set at right angle to the seat surface.

6.3 Analysis of Measured Whole-Body Mechanical Impedance Data

6.3.1 INTER-SUBJECT VARIABILITY

Figure 6.3 presents a comparison of measured mechanical impedance magnitude and phase characteristics of the seven male subjects sitting erect without back support (ENS), with feet resting on the platform and hands in contact with the steering wheel. The measurements were performed under swept sinusoidal excitation of 1 ms^{-2} W_z-weighted rms acceleration. These results indicate significant variations in impedance magnitude and phase among the subjects. Impedance magnitude is distinctly lower for subject S over most of the frequency range investigated due to considerably lower mass of the subject. This data set is clearly distinct from that of the other subjects, and the largest variations among the data sets occur in the neighbourhood of the main body resonant frequency. The deviations among the impedance magnitude and phase of different subjects may be related to the differences in subjects mass, considering that subject S had a significantly lower mass than the other six subjects. Furthermore, subjects A and R, being the heaviest subjects among the sample, exhibit impedance magnitude and phase characteristics distinctly different from that of the other subjects, particularly in the resonant frequency region. The resonant frequency for these two subjects is observed to occur

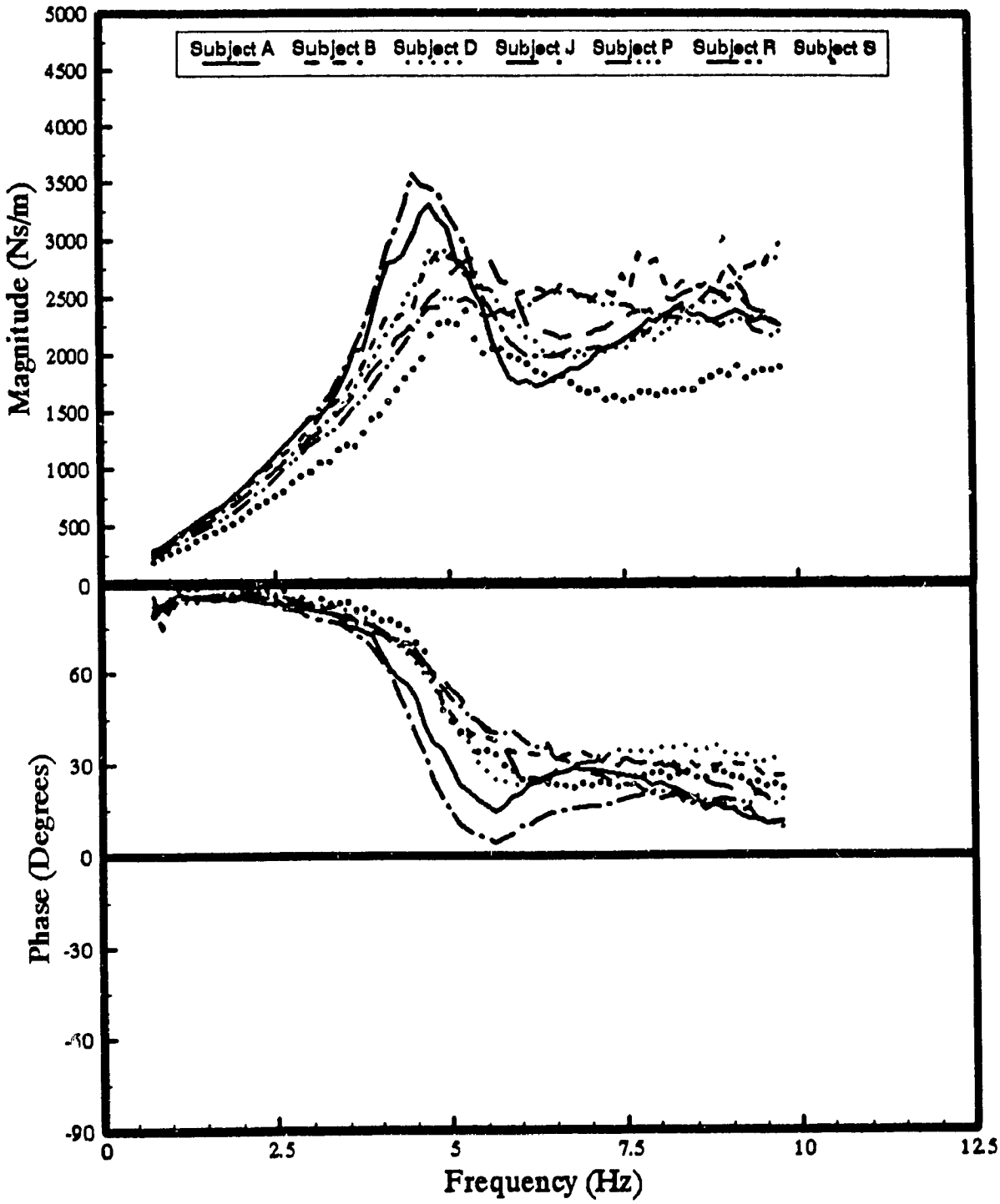

Figure 6.3 Individual driving-point mechanical impedance characteristics of 7 male subjects, maintaining an ENS posture, under 1 ms^{-2} sine sweep excitation.

more towards 4.5 Hz, in contrast with 5.0 Hz for the majority of the other subjects.

The impedance magnitude and phase characteristics of individual subjects are analyzed to derive the average and the lower and upper bounds of the response. Figure 6.4 illustrates the average impedance magnitude and phase curves along with the associated lower and upper bounds. The resonant frequency based on the combined data sets is observed near 5.0 Hz, and the magnitude of deviation between the lower and upper bounds is quite significant, specifically near and above the resonant frequency. The magnitude of this deviation, however, reduces considerably when the data set corresponding to subject S is excluded, as shown in Figure 6.5. The exclusion of this data set, however, affects the impedance phase envelope in an insignificant manner. The data obtained with subject S is thus excluded for all further analyses, and the following results represent the subjects with mean mass of 74.5 kg.

The mean values of impedance magnitude and phase presented in Figures 6.4 and 6.5 reveal that impedance magnitude increases with increasing frequency up to the main body resonant frequency, in the neighbourhood of 5 Hz. At frequencies above the main resonance, the impedance magnitude tends to decrease, followed by a slight increase at frequencies beyond 7.5 Hz, indicating

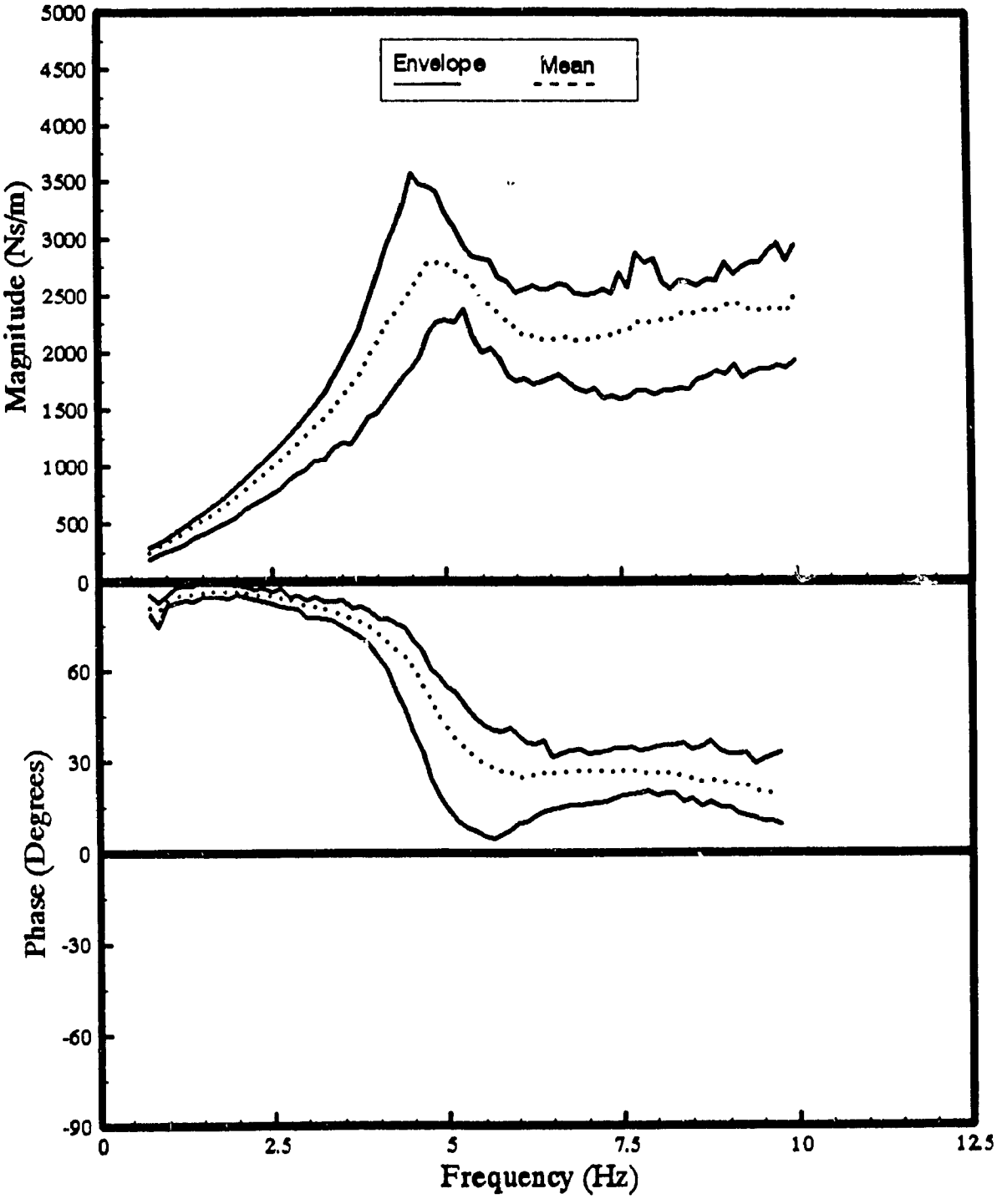

Figure 6.4 Mean and associated envelopes of driving-point mechanical impedance characteristics for 7 male subjects of mean mass 72.3 ± 8.8 kg, maintaining an ENS posture, under 1 ms^{-2} sine sweep excitation.

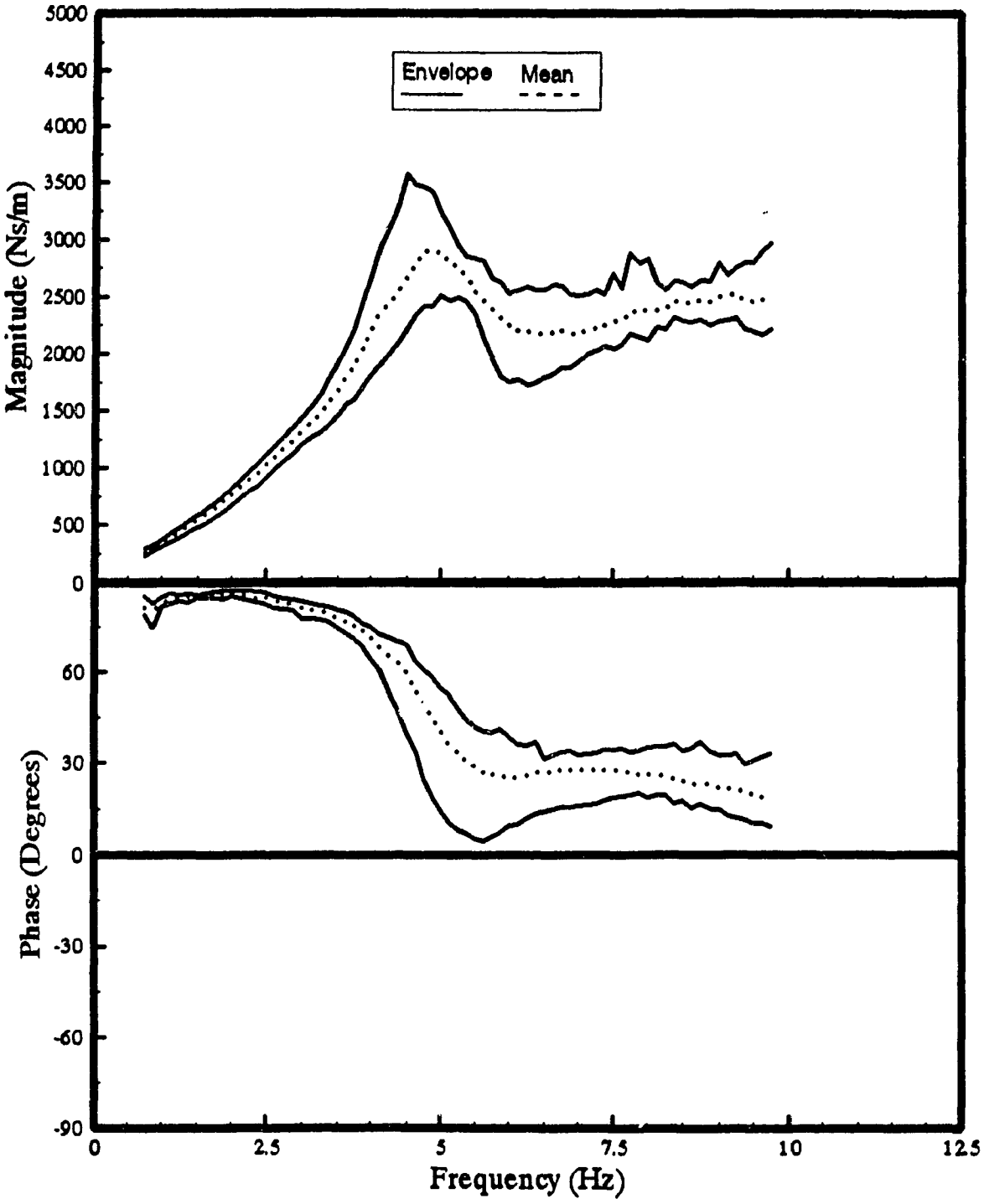

Figure 6.5 Mean and associated envelopes of driving-point mechanical impedance characteristics for 6 male subjects of mean mass 75.4 ± 3.9 kg, maintaining an ENS posture, under 1 ms^{-2} sine sweep excitation

a possible second body resonance at higher frequency. The impedance phase response decreases from 90° at low frequencies to nearly 40° at the resonant frequency, beyond which it tends to stabilize.

6.3.2 INFLUENCE OF VIBRATION EXCITATION AMPLITUDE

Measured impedance characteristics acquired under different amplitudes of swept sinusoidal and broad-band random excitations are analyzed to investigate the influence of excitation amplitude on the biodynamic response. The amplitude of excitation is expressed in terms of overall W_z frequency-weighted rms accelerations (1.0, 1.5 and 2.0 ms^{-2}). The impedance characteristics of six subjects (mean mass = 75.4 kg) are analyzed and presented in terms of average magnitude and phase response. Figures 6.6, 6.7 and 6.8 present the average response characteristics under three different amplitudes of sinusoidal excitations for ENS, EBS and SLO postures, respectively. Figures 6.9, 6.10 and 6.11 present the mean response characteristics under random excitations for ENS, EBS and SLO postures, respectively. Although the results do not show a significant influence of excitation amplitude on the mechanical impedance characteristics, the resonant frequency tends to decrease slightly for certain postures, when the amplitude of excitation is increased. The impedance phase values also decrease slightly with an increase in the excitation amplitude under certain posture and excitation. Although the observation of lower natural frequency with increased level of excitation is supported by the findings

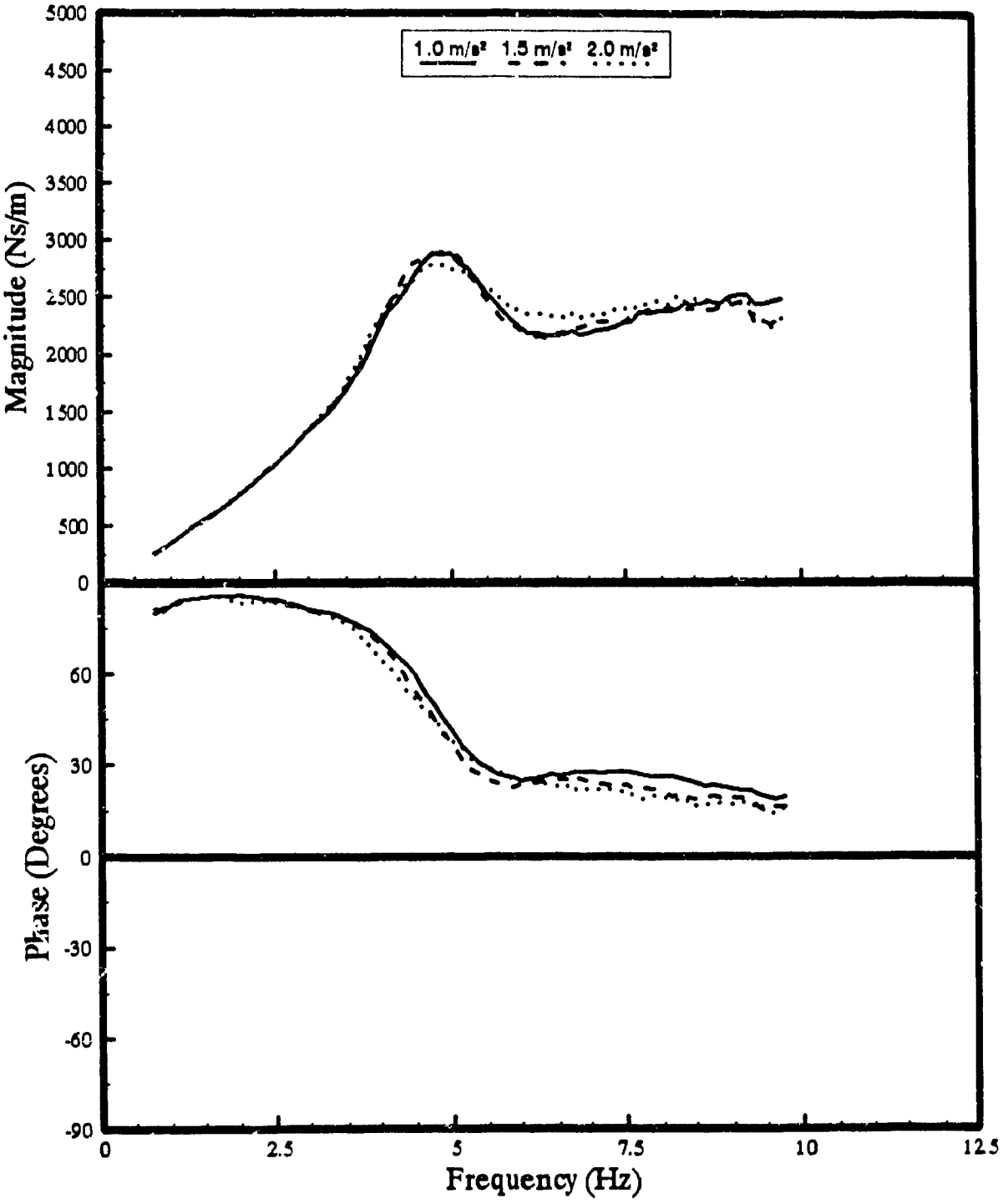

Figure 6.6 Mean driving-point mechanical impedance characteristics measured under different levels of sine sweep excitations, for subjects with mean mass of 75.4 kg, maintaining an ENS posture.

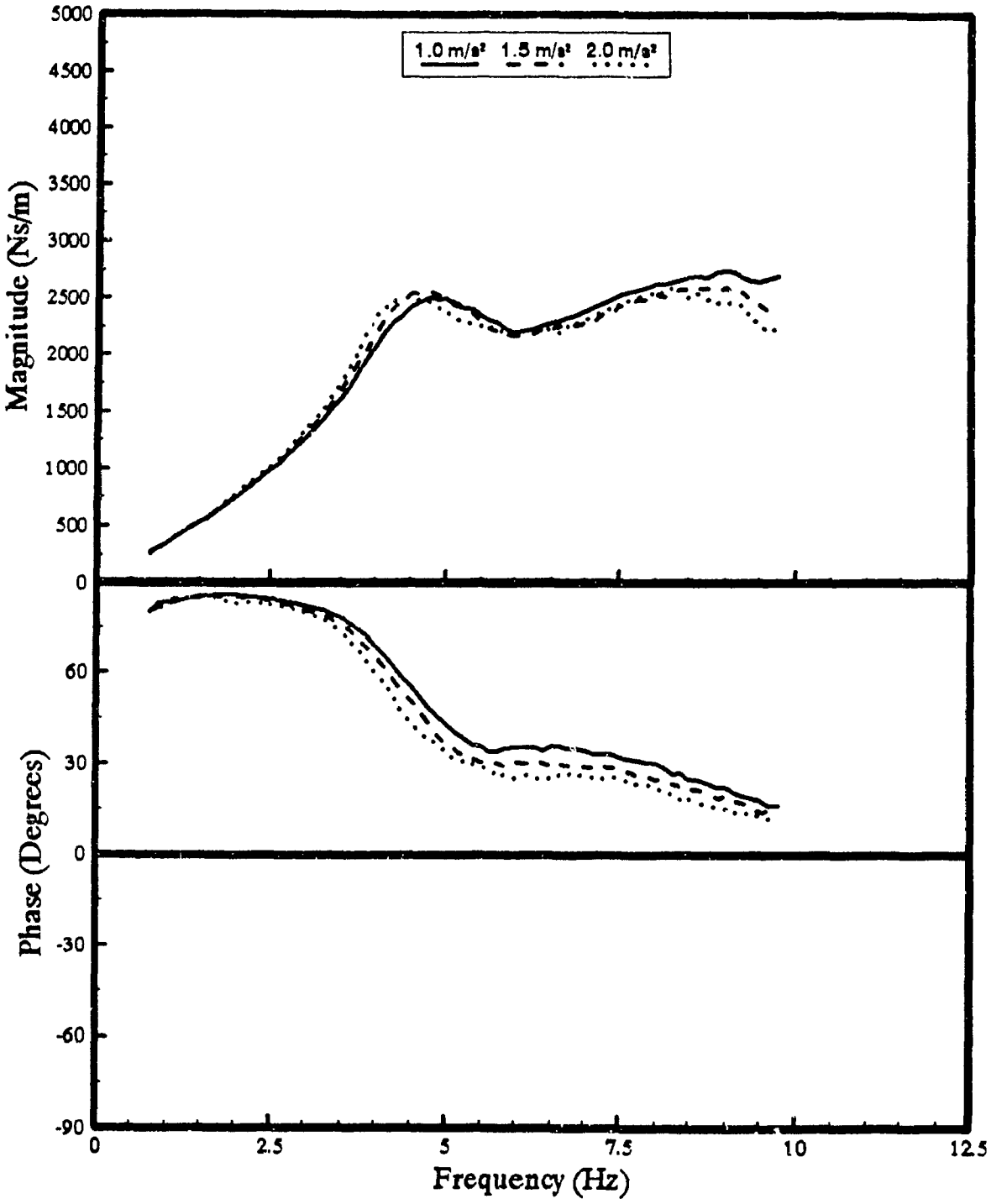

Figure 6.7 Mean driving-point mechanical impedance characteristics measured under different levels of sine sweep excitations, for subjects with mean mass of 75.4 kg, maintaining an EBS posture.

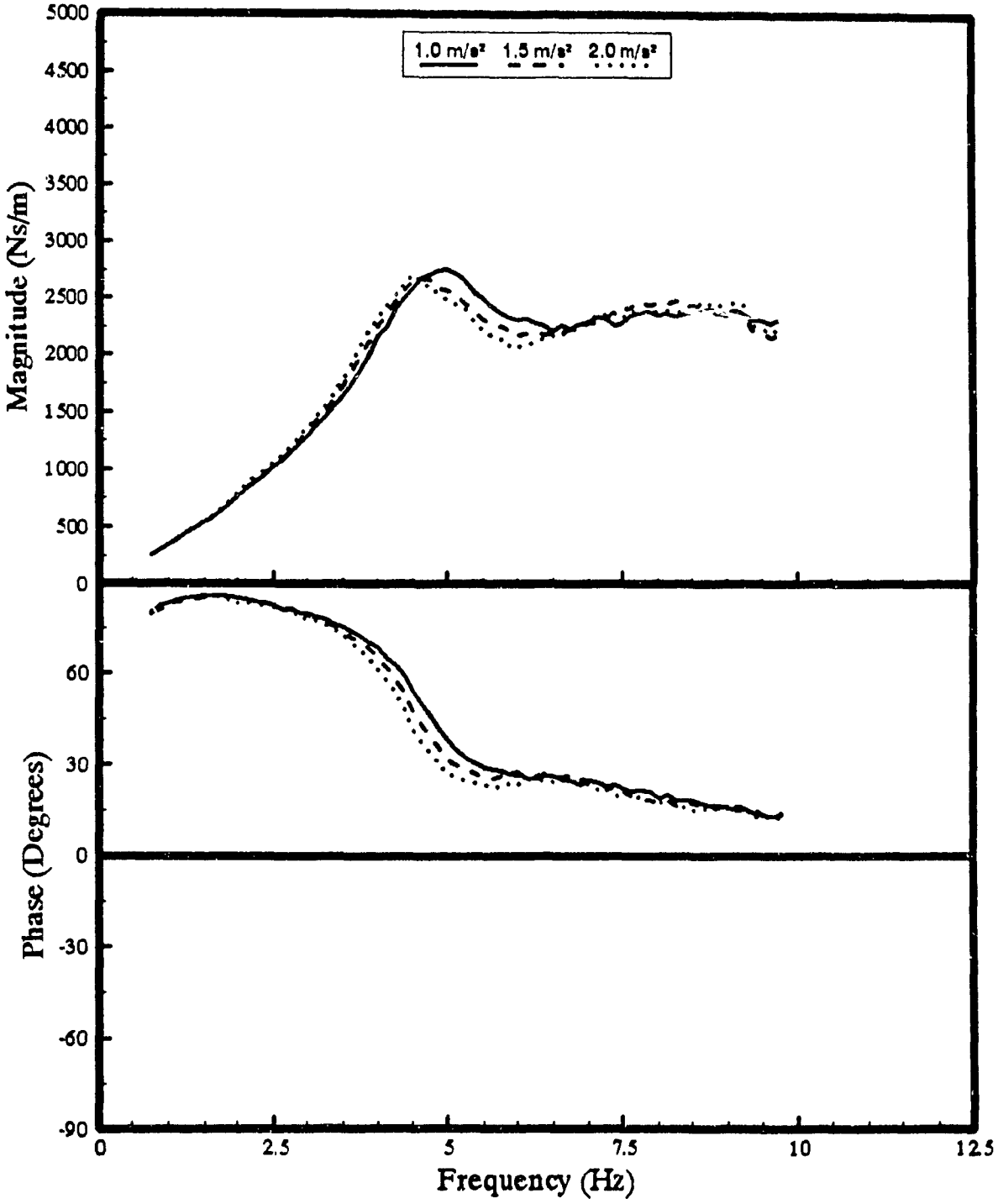

Figure 6.8 Mean driving-point mechanical impedance characteristics measured under different levels of sine sweep excitations, for subjects with mean mass of 75.4 kg, maintaining a SLO posture.

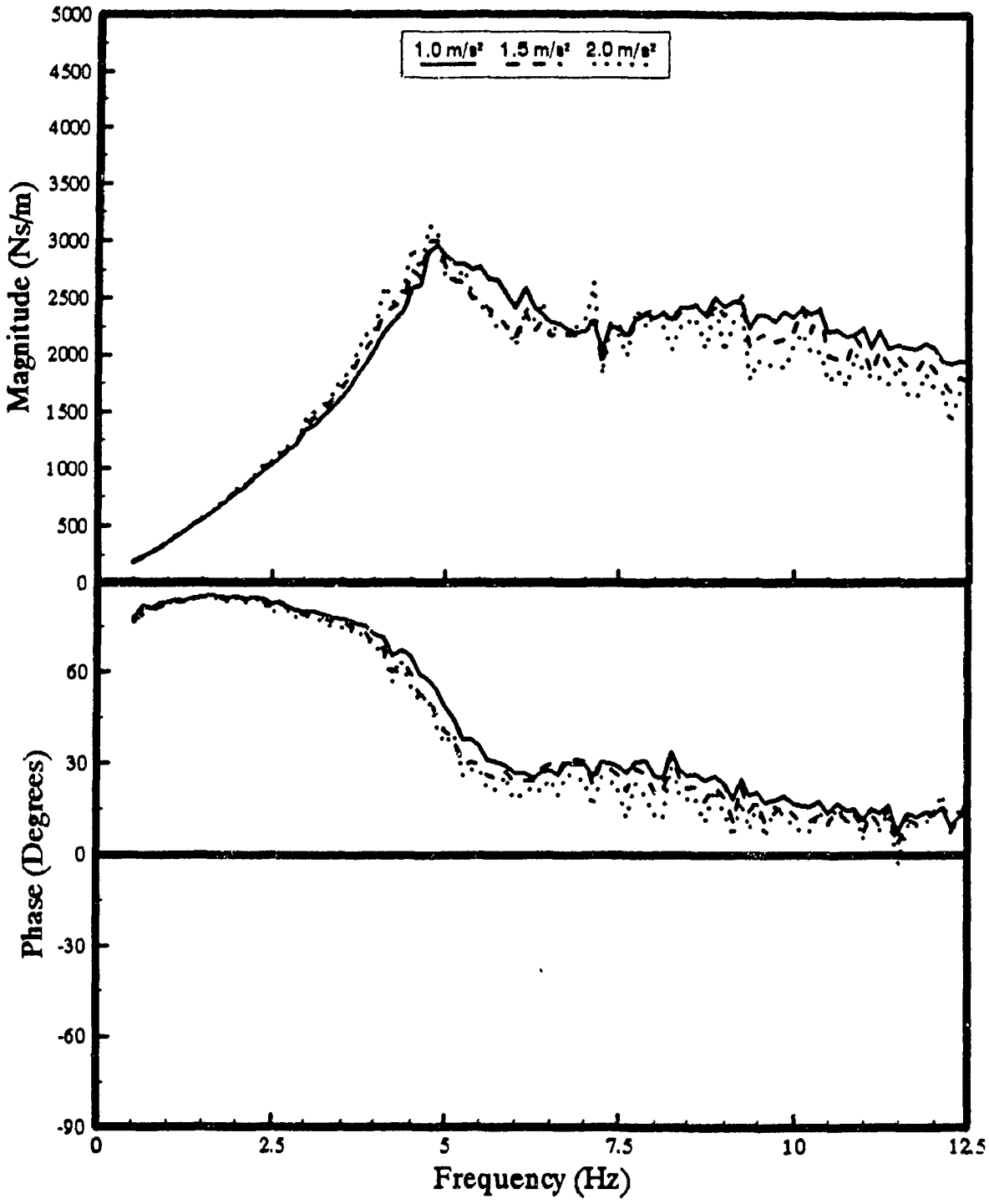

Figure 6.9 Mean driving-point mechanical impedance characteristics measured under different levels of broad-band random excitations, for subjects with mean mass of 75.4 kg, maintaining an ENS posture.

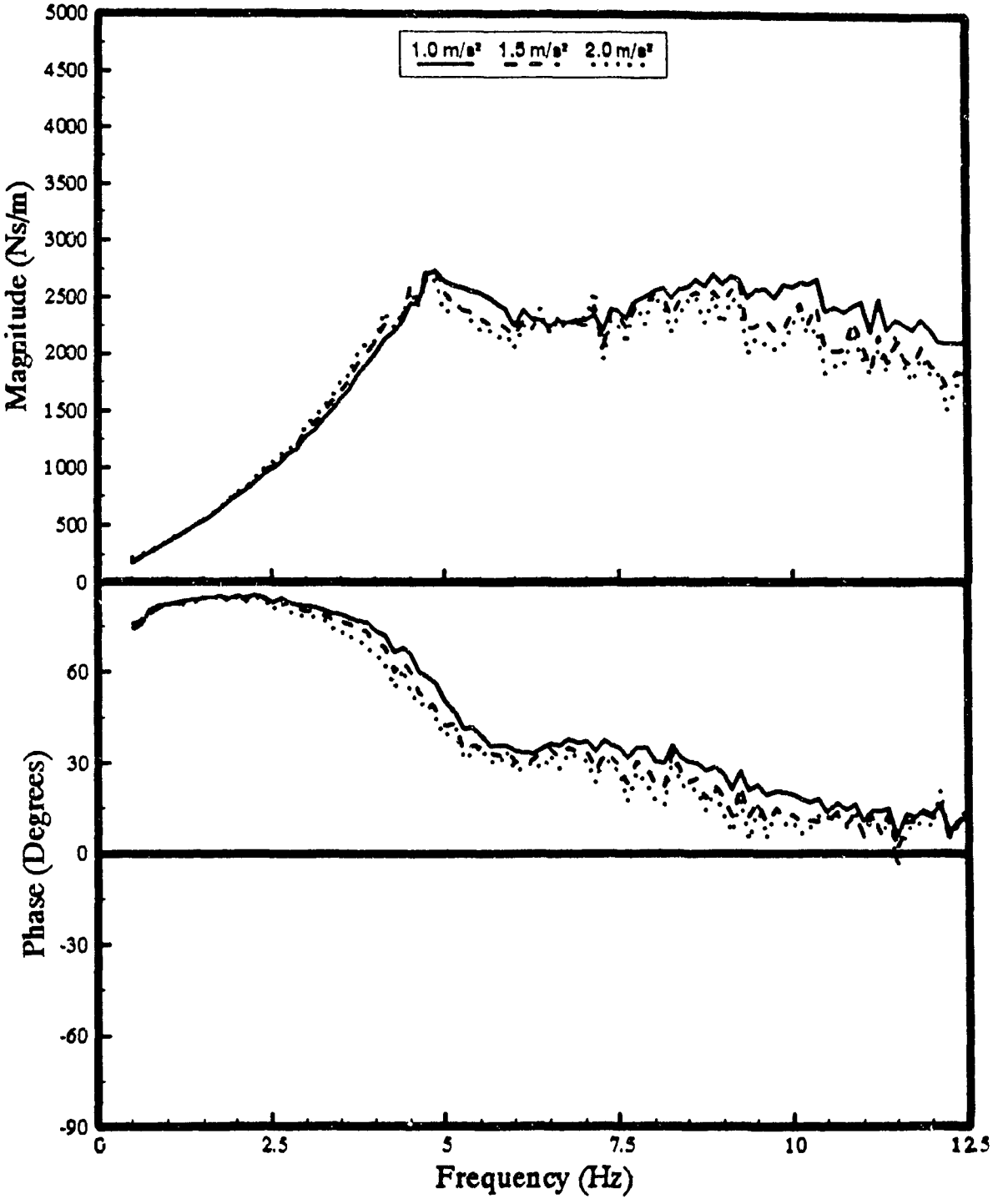

Figure 6.10 Mean driving-point mechanical impedance characteristics measured under different levels of broad-band random excitations, for subjects with mean mass of 75.4 kg, maintaining an EBS posture.

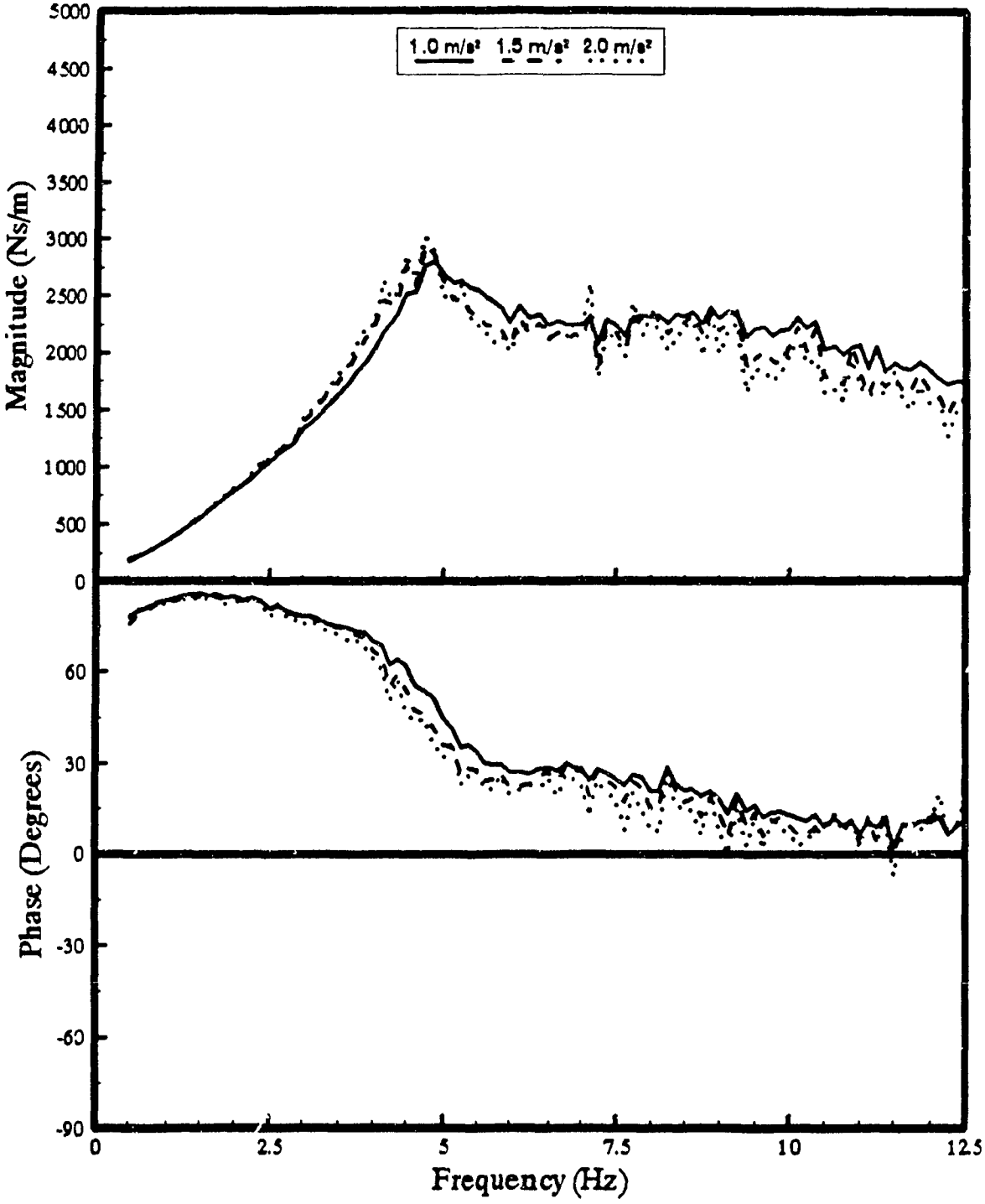

Figure 6.11 Mean driving-point mechanical impedance characteristics measured under different levels of broad-band random excitations, for subjects with mean mass of 75.4 kg, maintaining a SLO posture.

reported by Griffin [73], the trends observed in measured data reveal that a reduction in the fundamental frequency cannot be attributed to amplitude alone. While the reduction in fundamental frequency with increasing amplitude is observed for EBS and SLO postures only under sinusoidal excitations, the pattern is quite apparent for broad-band random excitations. Furthermore, the magnitude of changes observed may well be within the range of errors associated with the measurements, the averaging and smoothing of the data. An examination of the impedance curves obtained from the synthesis of the published data, presented in Figure 5.13, reveals a more pronounced effect of excitation amplitude on the fundamental natural frequency. However, from the results of the present study, it is concluded that the impedance response is relatively insensitive to the excitation amplitude for the subjects and the types and excitation amplitudes considered.

6.3.3 INFLUENCE OF THE SITTING POSTURE

Upon recognizing the insignificant influence of vibration excitation amplitude on the measured whole-body mechanical impedance within the frequency and amplitude ranges considered, averaging of the curves presented in Figures 6.6 to 6.11 is performed for each posture and excitation type. The resulting curves are shown in Figures 6.12 and 6.13 for sinusoidal sweep and broad-band random excitations, respectively. Mechanical impedance magnitude and phase are presented for three different postures: "erect back not supported" (ENS),

"erect back supported" (EBS) and "slouched" (SLO).

The resulting impedance magnitude and phase curves show a similar dependence upon posture, irrespective of the type of excitation. The impedance magnitude is influenced by the seated posture, specifically in the vicinity of the resonant frequency. Under sinusoidal excitations, the EBS and SLO postures yield a resonant frequency slightly lower than that observed for the ENS posture. Under random excitations, however, the effect of posture on the fundamental frequency is not noticeable. The influence of sitting posture on the impedance phase response is also observed to be insignificant. The results show that sitting erect without back support yields the highest mechanical impedance magnitude at resonance, while sitting erect with back support leads to the lowest. The impedance magnitude corresponding to the slouched posture is somewhere in between those for the ENS and EBS postures at the resonant frequency. At frequencies above 7 Hz, the EBS posture, however, yields impedance magnitude larger than that measured for the ENS and SLO postures. The influence of posture on the impedance magnitude is not noticeable at frequencies below 4 Hz. This is further emphasized in Figures 6.14 and 6.15, which present the mean mechanical impedance characteristics measured under the random excitation classes: ISO 1 and ISO 2 for the former, Class I and Class II for the latter figure. Since the vibration environment of off-road vehicles grouped under these four classes predominates at frequencies

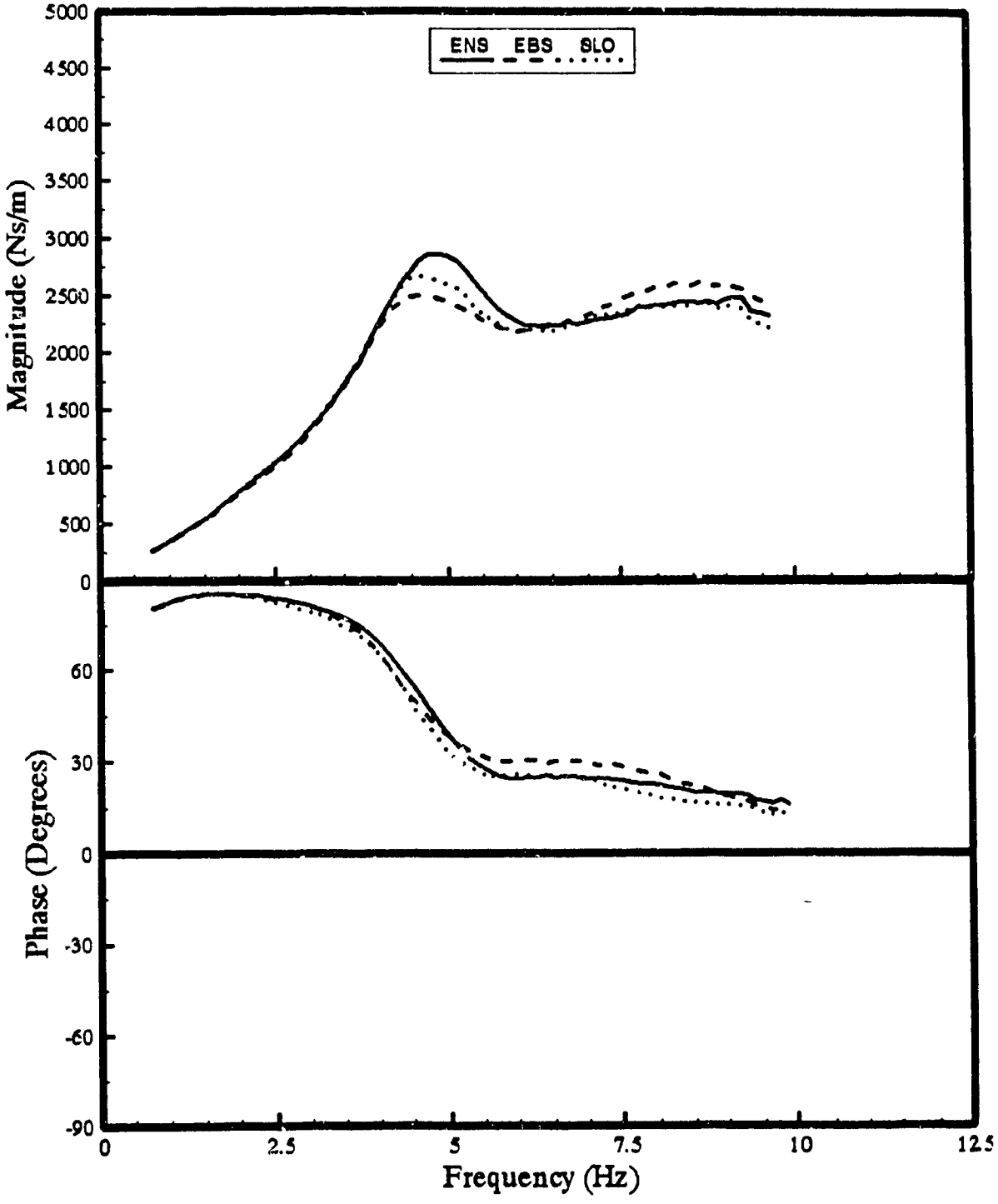

Figure 6.12 Mean driving-point mechanical impedance characteristics measured under sine sweep excitations within the range 1.0 to 2.0 ms^{-2}, for subjects with mean mass of 75.4 kg, maintaining various postures.

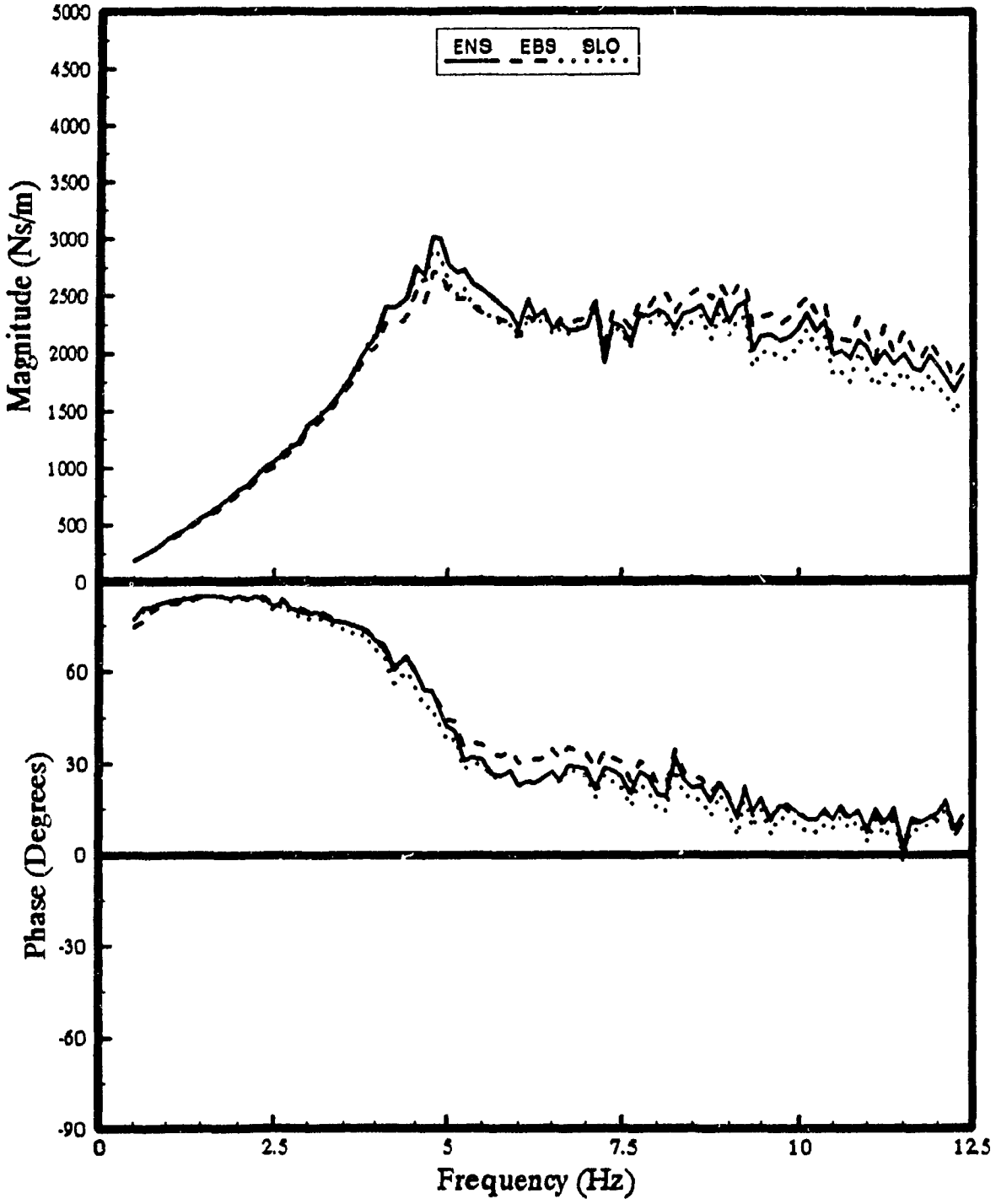

Figure 6.13 Mean driving-point mechanical impedance characteristics measured under broad-band random excitations within the range 1.0 to 2.0 ms^{-2}, for subjects with mean mass of 75.4 kg, maintaining various postures.

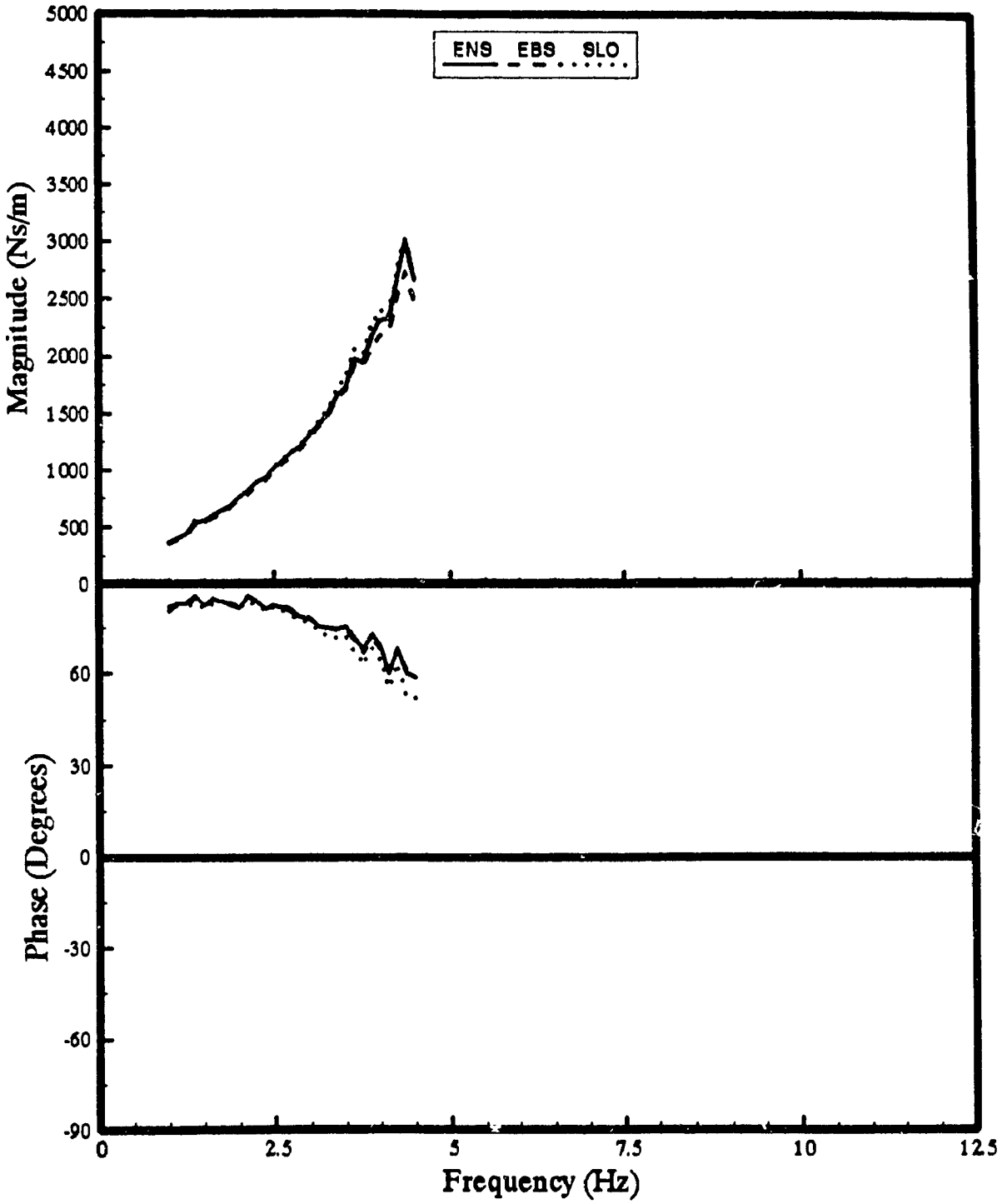

Figure 6.14 Mean driving-point mechanical impedance characteristics measured under ISO 1 and ISO 2 excitation classes, for subjects with mean mass of 75.4 kg, maintaining various postures.

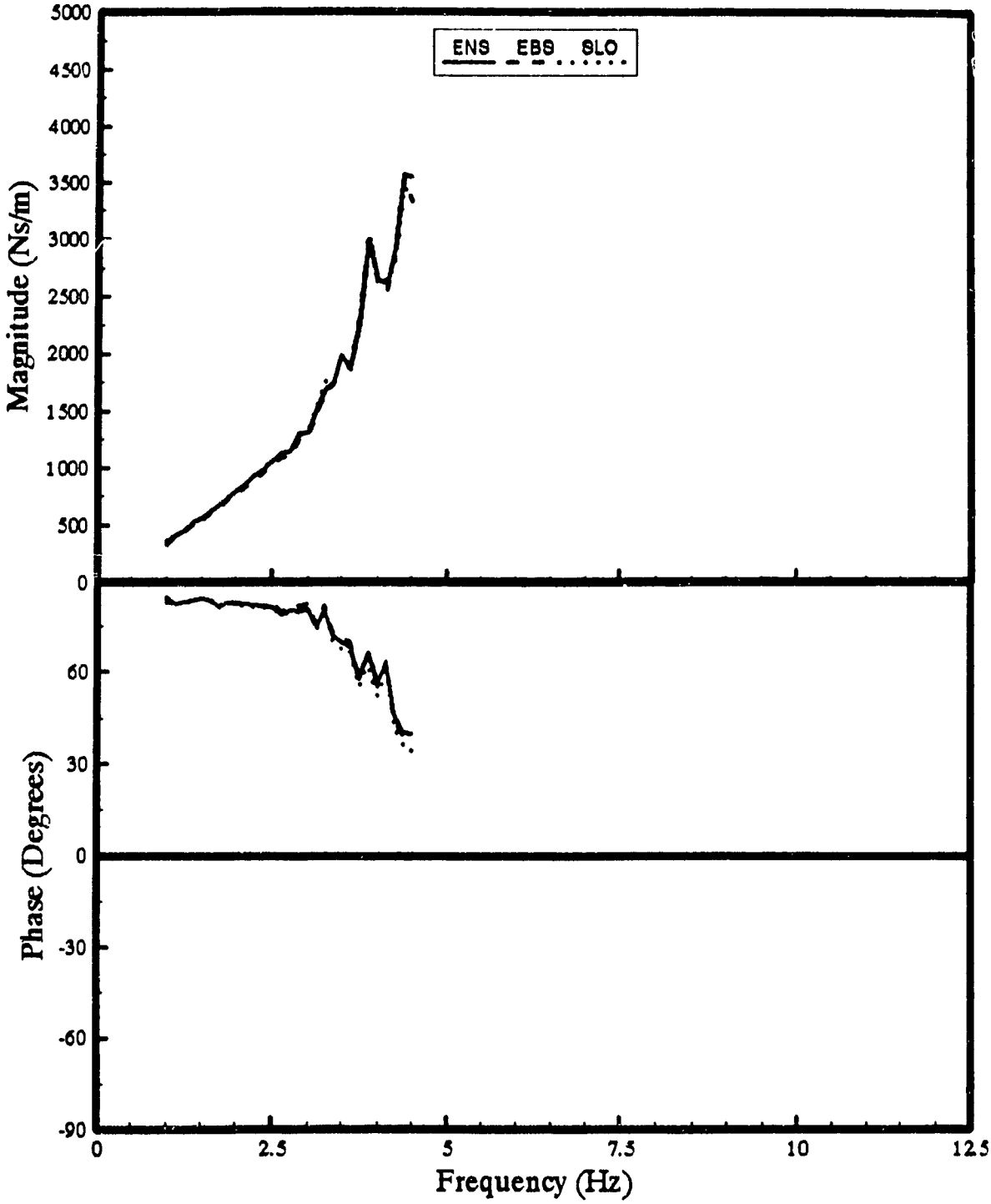

Figure 6.15 Mean driving-point mechanical impedance characteristics measured under Class I and Class II random excitations, for subjects with mean mass of 75.4 kg, maintaining various postures.

below 4 Hz, the impedance characteristics are shown only up to 4 Hz. The results follow a pattern similar to that observed for sinusoidal and broad-band random excitations, revealing insignificant influence of posture at frequencies below 4 Hz.

The measured impedance characteristics for different postures are further compared to the data derived from the synthesis of published data shown in Figure 5.14. While the synthesized data reveals the highest mechanical impedance magnitude at resonance for the EBS posture and the lowest for the ENS posture, the measured data shows just the opposite. At excitation frequencies below 4 Hz and above 7 Hz, however, the measured and synthesized data exhibit similar trends, although considerable differences are observed in the impedance magnitude. These differences are attributable to the limited number of reported data sets available for the synthesis, especially for the EBS and the SLO postures, and the variations in the test conditions employed in the reported studies. Both the synthesized and the measured data, however, suggest that the sitting posture affects the whole-body mechanical impedance magnitude in a definite manner.

Interestingly, the trends observed in impedance magnitude near the resonant frequency in relation with posture appear to be consistent with the observation made of the variations of the static weight supported by the seat under

different postures. The vertical static load measured by the force platform was observed to be highest for the ENS posture, and lowest for the EBS posture. The component of vertical load supported by the seat was observed to be strongly related to the posture for most subjects. It may thus be postulated that the effect of posture on the impedance magnitude in the resonant frequency region may be partly attributed to variations in the vertical mass component associated with the three postures. The hypothesis is further supported by the results presented in Figure 6.3, where the resonant mechanical impedance magnitude of heavier subjects was observed to be larger than that of light weight subjects. Since the variations in vertical load in the force platform were observed to be less than 10% for different postures, the differences in mechanical impedance cannot be attributed to changes in mass alone.

6.3.4 INFLUENCE OF TYPE OF VIBRATION EXCITATION

Extracting the results from Figures 6.12 to 6.15 obtained under various types of vibration excitations, and regrouping according to posture result in the mechanical impedance curves plotted in Figures 6.16 to 6.18 for the ENS, EBS and SLO postures, respectively. For each posture, the impedance characteristics obtained under different types of vibration excitation show excellent agreement. Figures 6.16 to 6.18 present the comparison of mechanical impedance characteristics measured under sine and broad-band

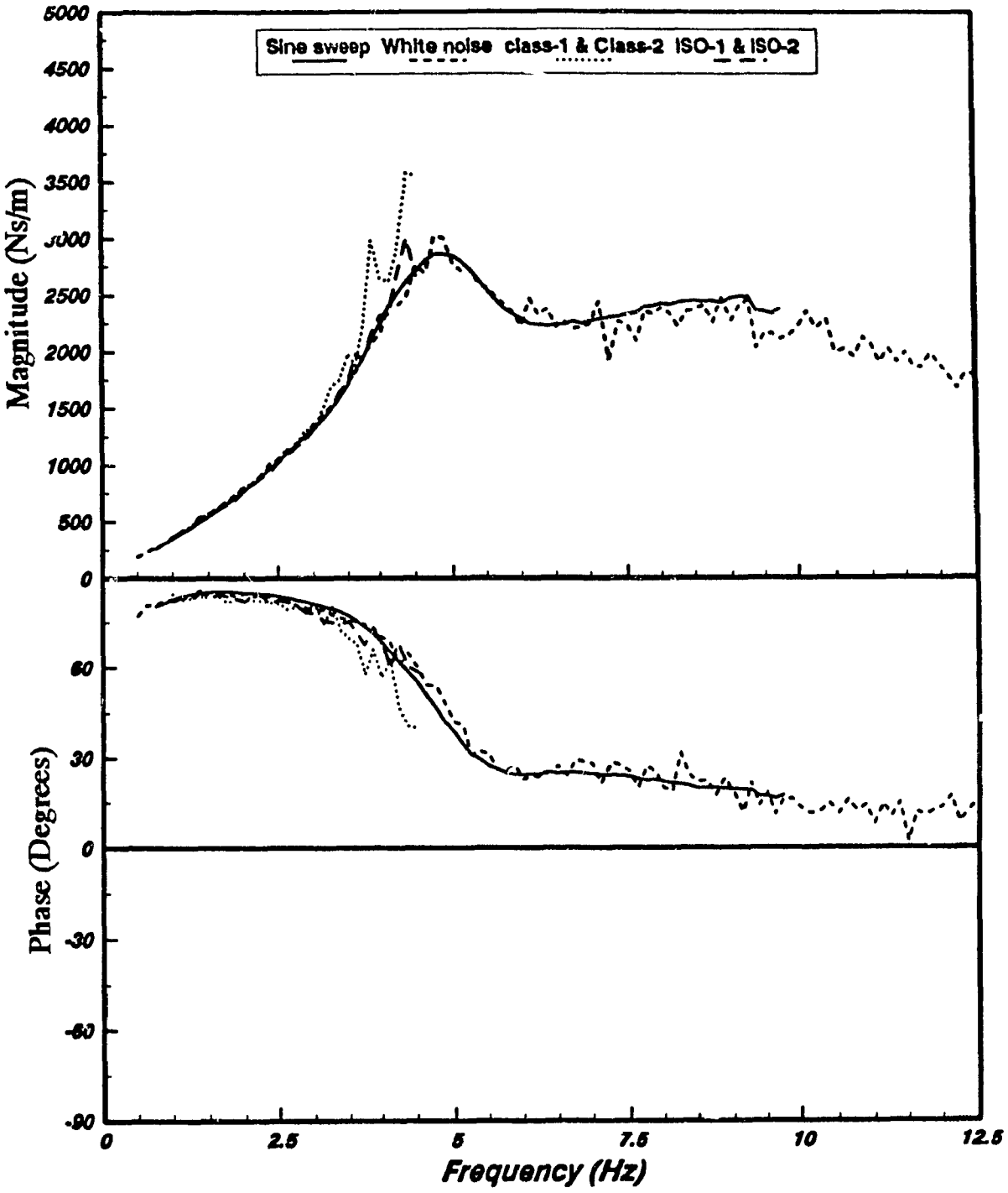

Figure 6.16 Mean driving-point mechanical impedance characteristics measured under various excitation types, for subjects with mean mass of 75.4 kg, maintaining an ENS posture.

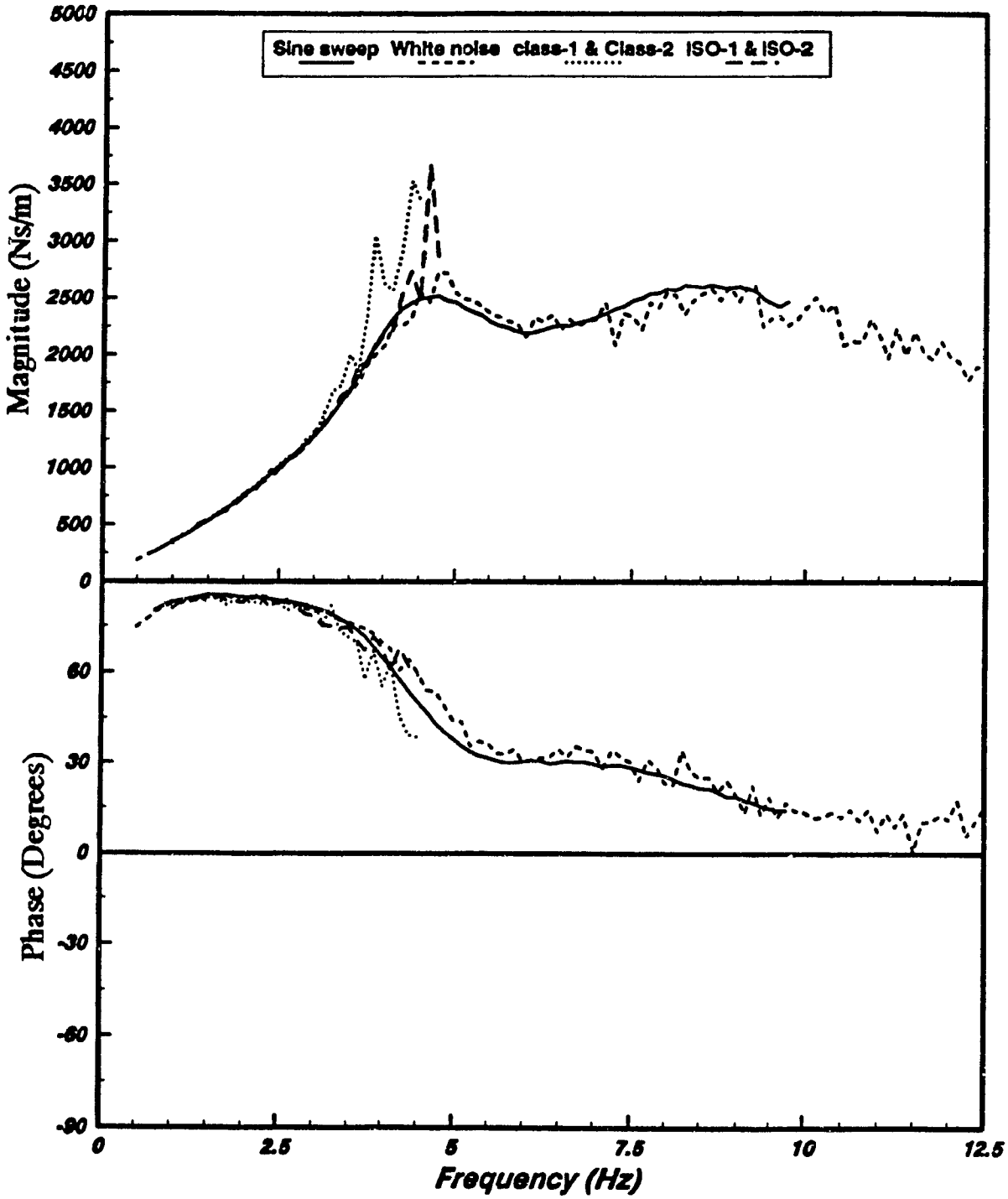

Figure 6.17 Mean driving-point mechanical impedance characteristics measured under various excitation types, for subjects with mean mass of 75.4 kg, maintaining an EBS posture.

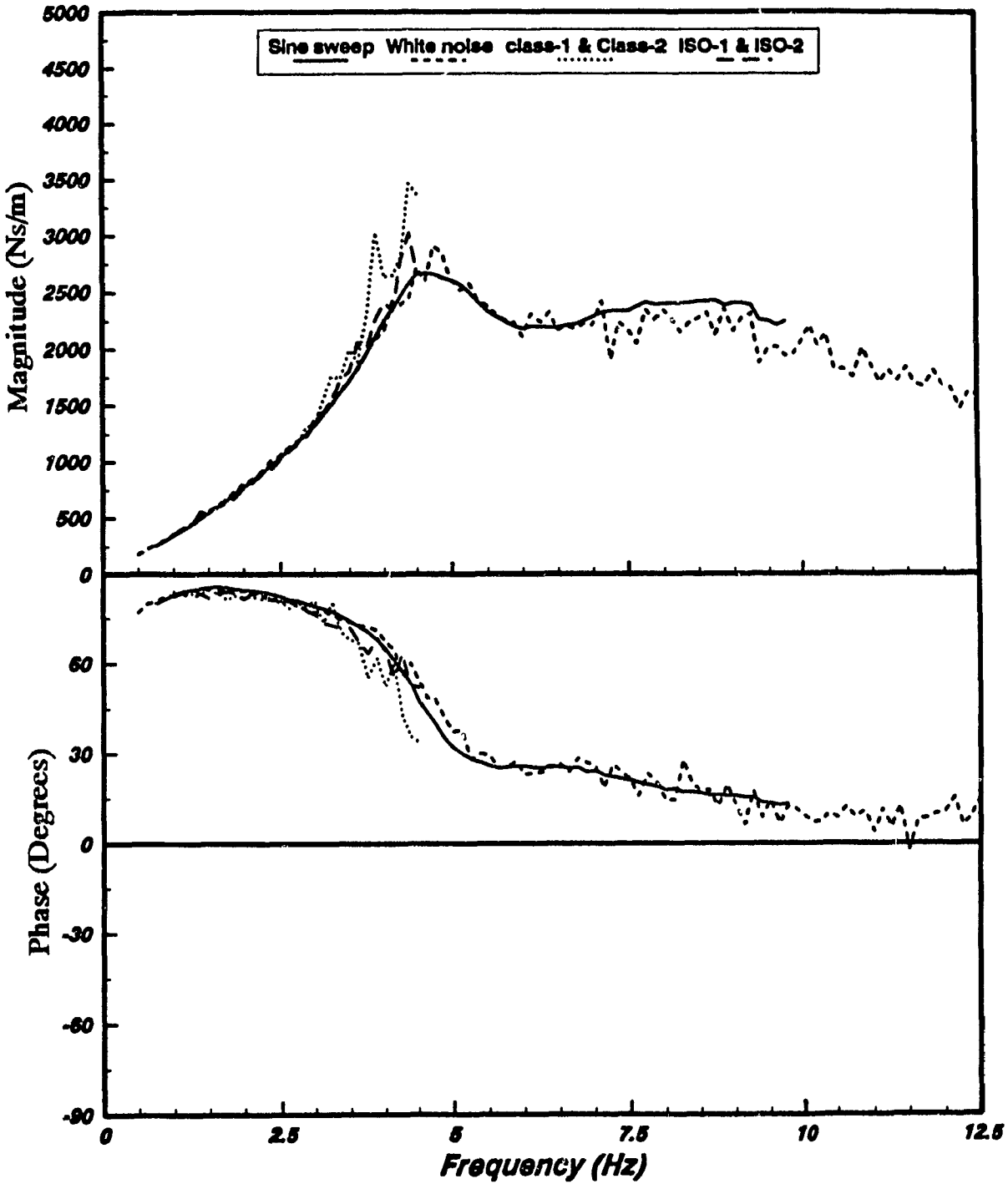

Figure 6.18 Mean driving-point mechanical impedance characteristics measured under various excitation types, for subjects with mean mass of 75.4 kg, maintaining a SI.O posture.

random excitations in the 1.0 to 2.0 ms^{-2} amplitude range, and the four random excitation classes defined for off-road vehicles. The differences noted at frequencies above 3 Hz for the off-road vehicle vibration classes is most probably due to the experimental errors associated with measurements performed under very low level vibration energy present at frequencies above 3 Hz for these excitations.

The results presented in these figures suggest that the selected excitation types, within the amplitude and frequency ranges investigated in this study, do not affect the mechanical impedance characteristics of the sitting subjects. The excellent agreement found using off-road vehicle excitation classes further suggests that the mechanical impedance characteristics determined under sinusoidal or broad-band random vibration may be conveniently used for development of a human driver model, to ensure its validity over a wider frequency range. Although the synthesized data, presented in Figure 5.12, showed some differences in impedance characteristics under sine and random excitations within a similar range of excitation amplitudes, these deviations may be attributed to the synthesis of different data sets obtained under varying test conditions.

6.3.5 INFLUENCE OF BACKREST ANGLE

Mean mechanical impedance characteristics measured under sine and broad-

band random excitations, respectively, are shown in Figures 6.19 and 6.20 for backrest angles of 0 and 14 degrees. The mean impedance magnitude and phase response refer to the EBS posture only. The results clearly illustrate that leaning against an inclined backrest tends to suppress and smooth out the resonant peak observed for vertical backrest support. This smoothing effect may be related to increased dissipation property of the body supported by an inclined backrest. This behaviour is observed for both sine and random inputs, on both mechanical impedance magnitude and phase. The behaviour of the body leaning against an inclined backrest thus appears to be more like that of a pure damper at higher frequencies, while being that of a pure mass at low frequencies. When the backrest is vertical, the behaviour appears to be similar to that of a mass, spring and damper combination. The results further reveal that the impedance magnitude at higher frequencies increases when the backrest is inclined, irrespective of the type of excitation.

6.3.6 MEASURED VERSUS STANDARDIZED MECHANICAL IMPEDANCE

The results of the measurements performed using subjects (mean mass of 75.4 kg) sitting on a rigid seat with feet supported on a vibrating platform and hands in contact with a steering wheel have shown that posture and backrest angle are probably the two most important variables that affect the whole-body mechanical impedance characteristics. These results, however, are applicable under the types and amplitudes of vibration excitations considered. In view of

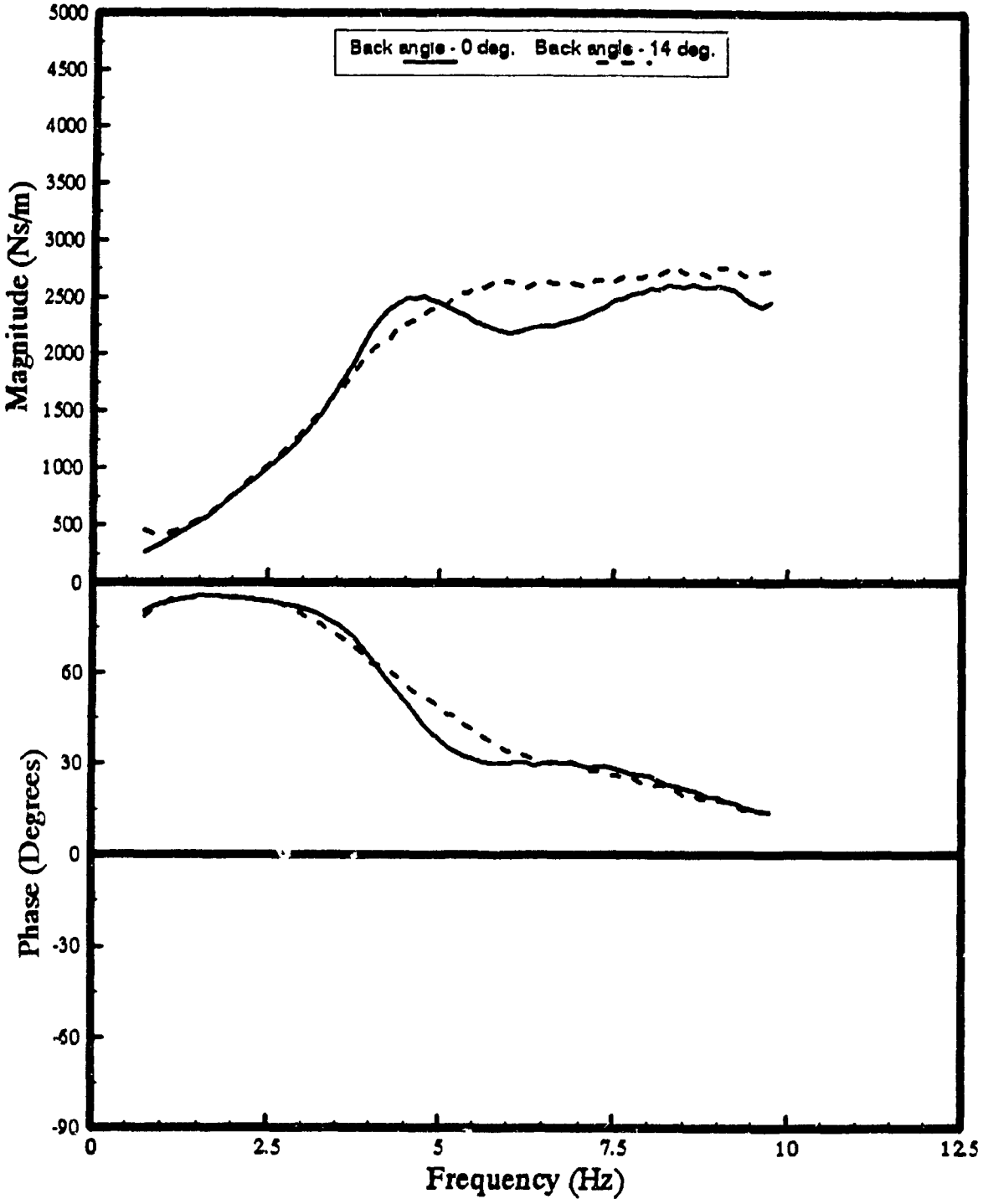

Figure 6.19 Mean driving-point mechanical impedance characteristics measured under sine sweep excitations between 1.0 and 2.0 ms^{-2} for subjects with mean mass of 75.4 kg, maintaining an EBS posture, on a seat with 0° and 14° backrest angles.

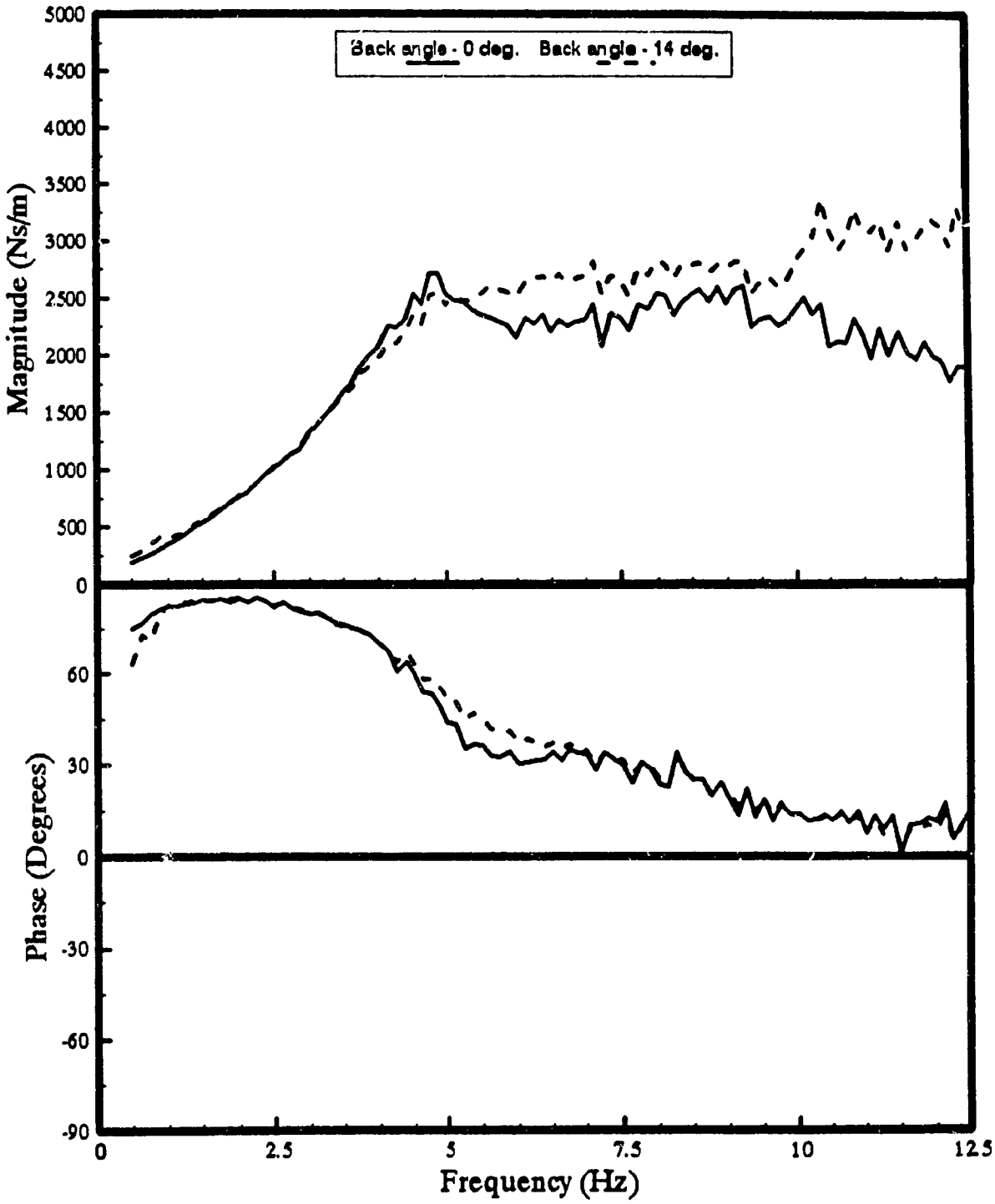

Figure 6.20 Mean driving-point mechanical impedance characteristics measured under broad-band random excitations between 1.0 and 2.0 ms^{-2} for subjects with mean mass of 75.4 kg, maintaining an EBS posture, on a seat with 0° and 14° backrest angles.

the insignificant differences observed for sine and random excitations at levels ranging from 1.0 to 2.0 ms^{-2} weighted accelerations, Figure 6.12 probably summarizes best the mechanical impedance characteristics of a vehicle driver seated on a seat with vertical backrest, while assuming different postures.

The measured biodynamic response of the seated driver under vehicular vibration are compared to the proposed standardized mechanical impedance characteristics defined for subjects within a similar mass range, and the excitation type and levels as shown in Figure 6.21. The figure clearly illustrates significant differences between the measured and proposed standardized data in both the impedance magnitude and phase. While the measured phase data falls within the envelope of the proposed data over most of the frequency range, the measured magnitude is observed within the proposed envelope only at frequencies above 7.5 Hz. At excitation frequencies below 7.5 Hz, the measured impedance magnitude is considerably lower than the proposed mean data and the difference between the two data is as large as 50%. While the measured magnitude data is observed to be below the lower bound of mechanical impedance proposed by ISO, the measured phase data is within the proposed envelope, except in the 6 to 8 Hz frequency range. The differences in the measured and ISO proposed impedance characteristics are observed for all the sitting postures, which is not clearly defined in the ISO document.

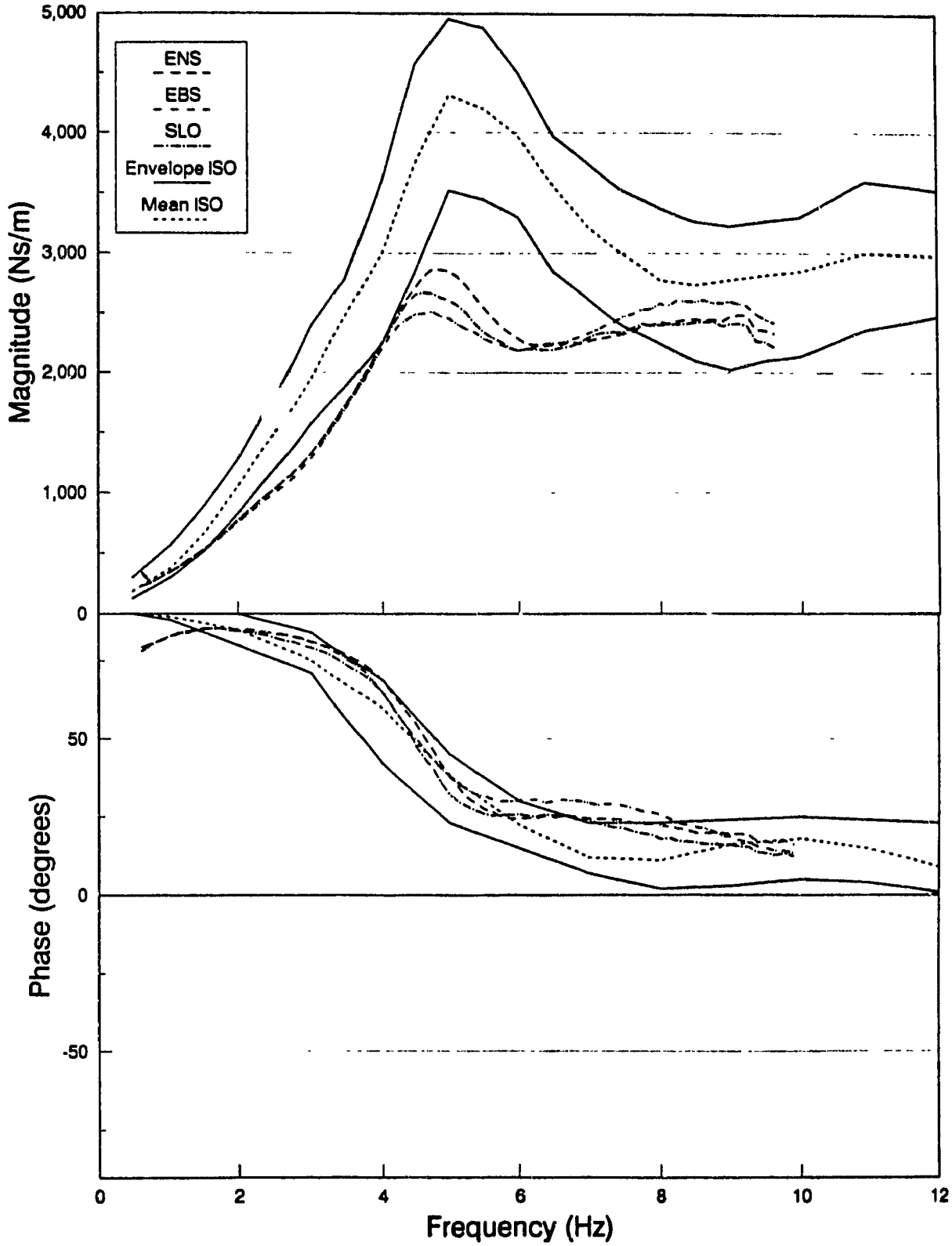

Figure 6.21 Comparison of standardized and measured mean driving-point mechanical impedance characteristics for subjects with mean mass of 75.4 kg, maintaining various postures, under sine sweep excitations from 1.0 to 2.0 ms^{-2}.

6.4 Biodynamic Response Characteristics of Off-Road Vehicle Drivers

The biodynamic response characteristics of off-road vehicle drivers are expressed in terms of most probable values of driving-point mechanical impedance and seat-to-head transmissibility magnitude and phase, in the 0.75 to 10 Hz frequency range. The most probable or target values of driving-point mechanical impedance are derived from both the measured and synthesized data, while seat-to-head transmissibility target values are established from the synthesized data only.

6.4.1 TARGET VALUES OF DRIVING-POINT MECHANICAL IMPEDANCE

Figures 6.22 to 6.24 present the measured mean driving-point mechanical impedance characteristics for subjects maintaining ENS, EBS and SLO postures respectively, showing the corresponding envelopes of measured values. Upper and lower bounds were established from the variations observed at different amplitudes of sine sweep excitation ranging from 1.0 to 2.0 ms^{-2} frequency-weighted accelerations. These curves are considered to be the most probable or target values of impedance response characteristics of off-road vehicle drivers in view of the insignificant variations observed under different random and sinusoidal excitations within the specified range of amplitudes. The proposed most probable values of impedance represent the biodynamic response characteristics of subjects with mean mass of 75.4 kg, seated on a rigid seat with vertical backrest, while their feet are supported on a vibration

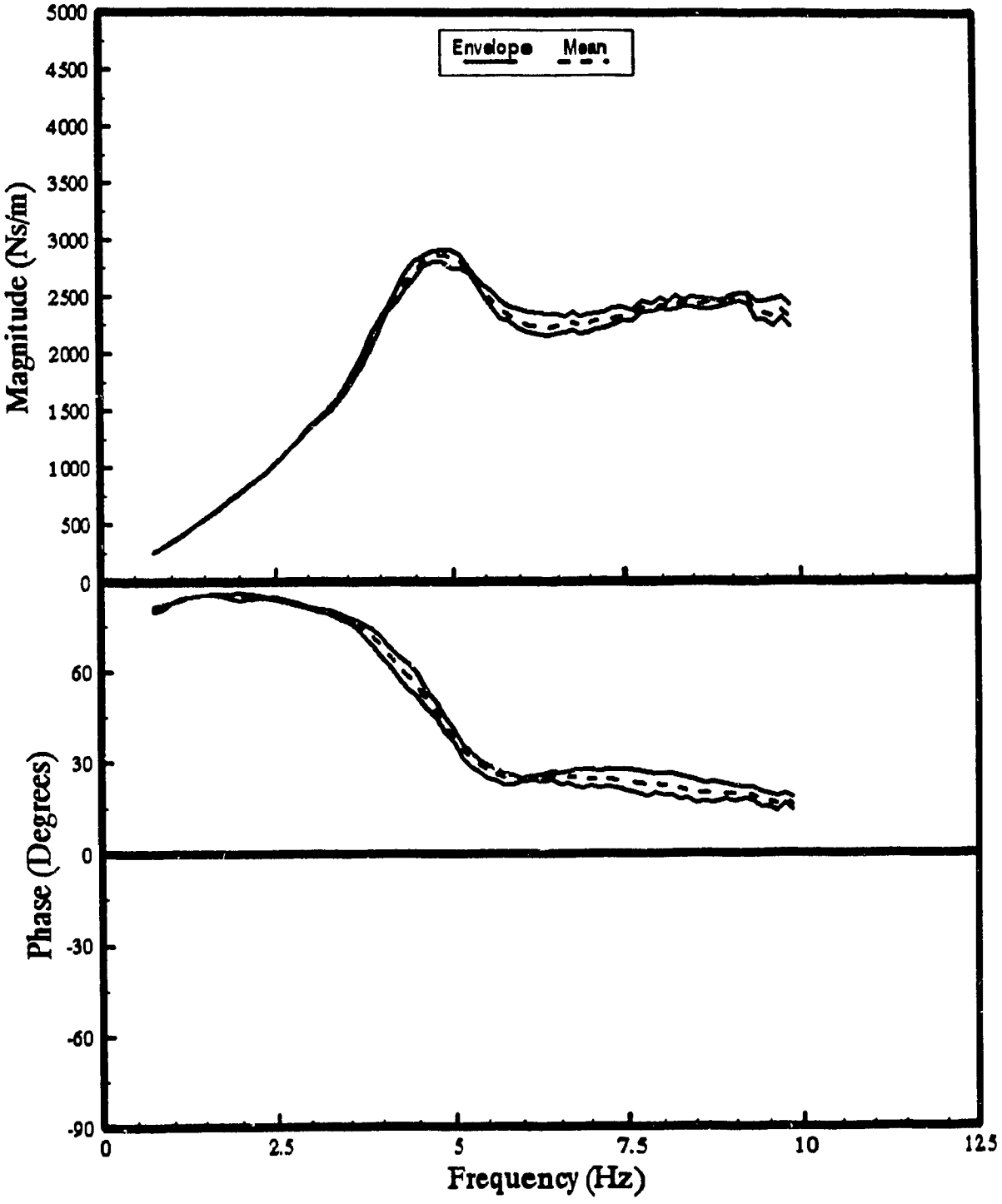

Figure 6.22 Mean and associated envelopes of driving-point mechanical impedance characteristics for off-road vehicle drivers of mean mass 75.4 kg, maintaining an ENS posture under excitation levels from 1.0 to 2.0 ms^{-2}.

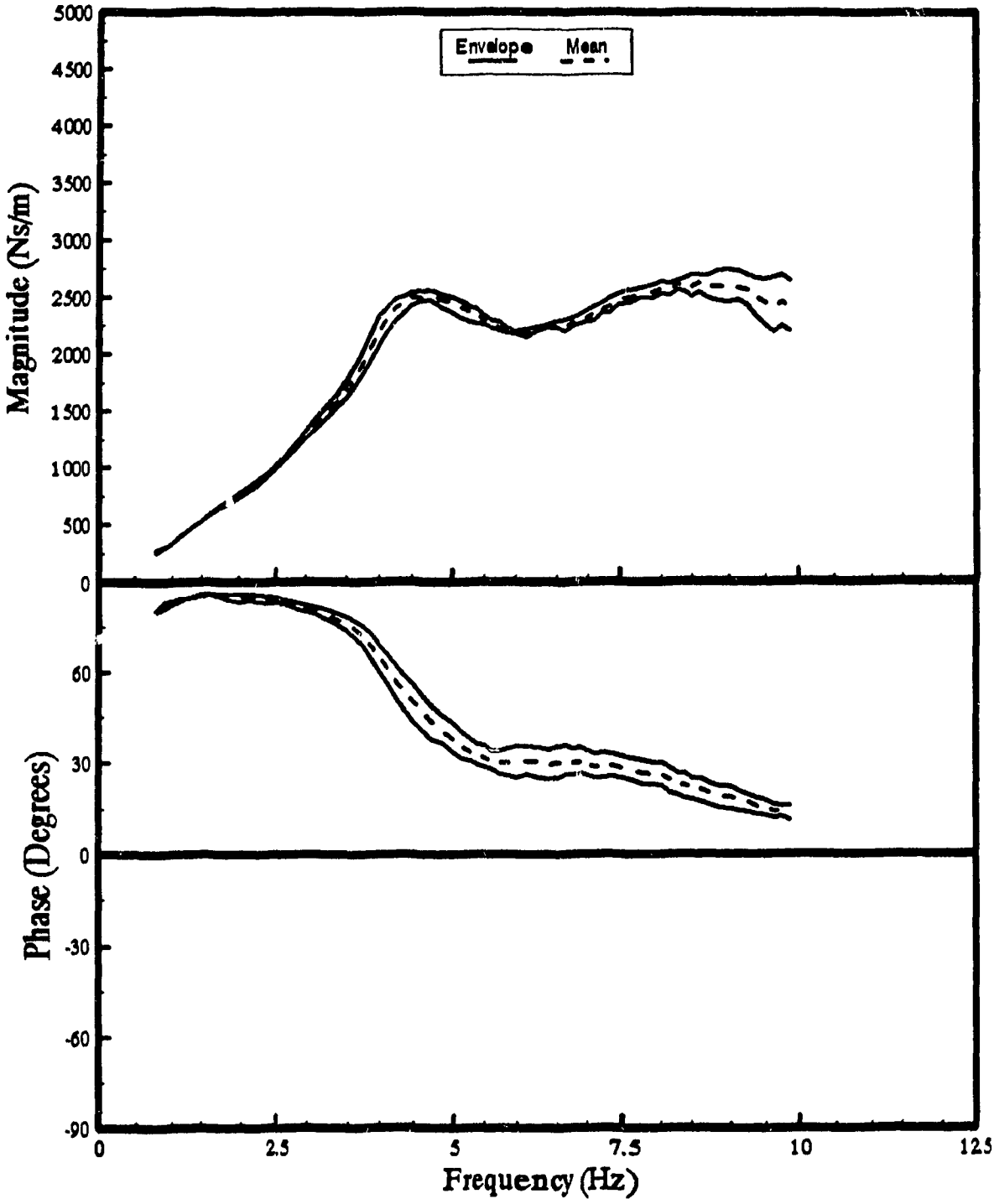

Figure 6.23 Mean and associated envelopes of driving-point mechanical impedance characteristics for off-road vehicle drivers of mean mass 75.4 kg, maintaining an EBS posture under excitation levels from 1.0 to 2.0 ms^{-2}.

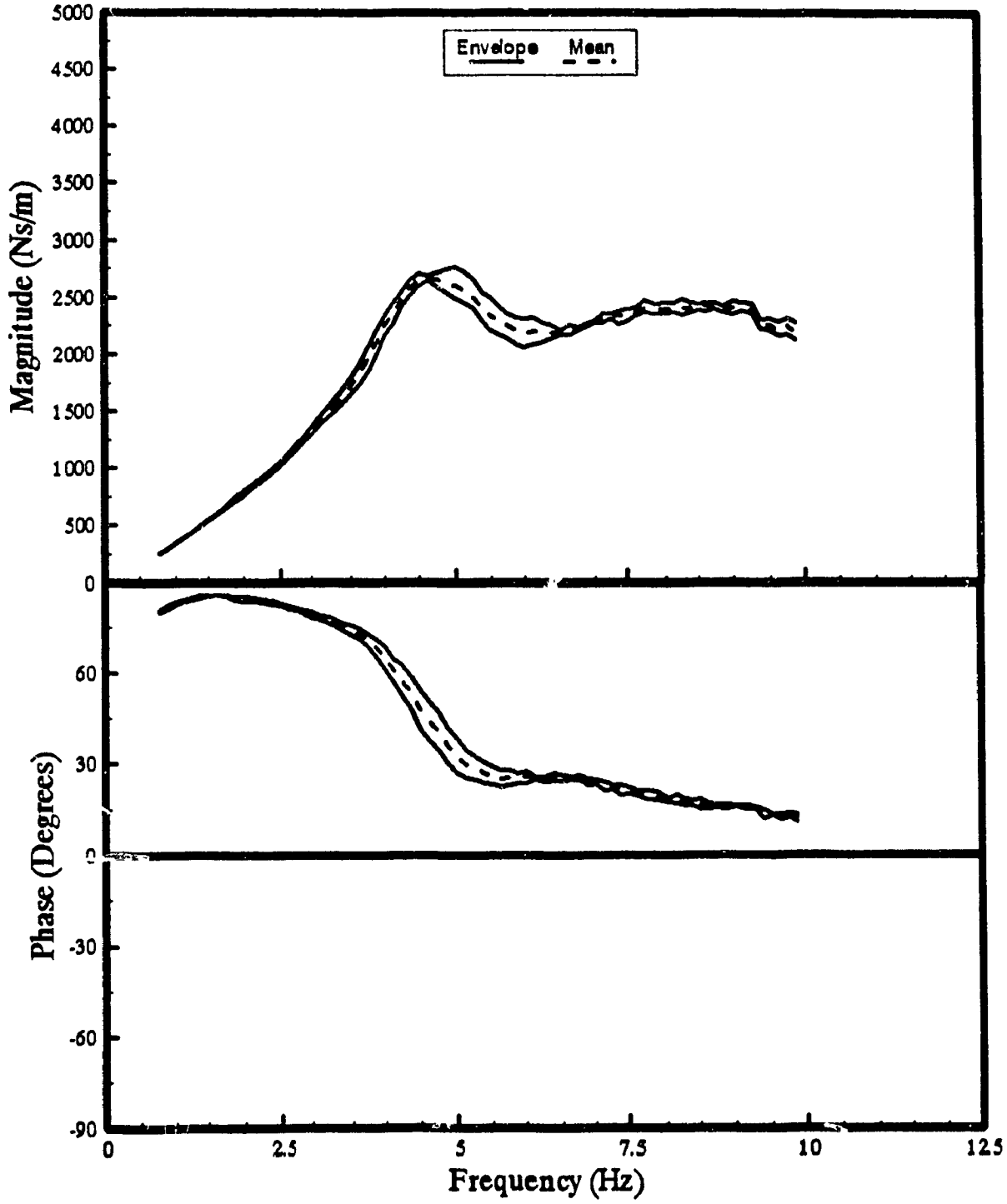

Figure 6.24 Mean and associated envelopes of driving-point mechanical impedance characteristics for off-road vehicle drivers of mean mass 75.4 kg, maintaining a SLO posture under excitation levels from 1.0 to 2.0 ms^{-2}.

platform and their hands are in contact with a steering wheel.

Figure 6.25 illustrates a comparison of the measured mean mechanical impedance characteristics for the ENS posture with those derived from the synthesis of four published data sets (Figure 5.11, excluding the proposed standardized curve) obtained for subjects maintaining a similar posture under excitation levels ranging from 1 to 2 ms^{-2}. A close agreement between the mean measured magnitude and mean values of the synthesized data is clearly demonstrated at frequencies below 5 Hz. The measured mean impedance magnitude and phase curves lie within the envelopes established by the synthesis of reported data sets, over most of the frequency range considered during the measurements. The apparent lack of published data for the EBS and SLO postures prevents such comparison with the measured data.

While the measured data correlates reasonably well with the synthesized data for the ENS posture under well-defined experimental conditions, the measured and synthesized data differ considerably from the proposed standardized mechanical impedance characteristics. These deviations suggest that the ISO proposed data is perhaps inappropriate under conditions encountered while driving a vehicle. In view of the dependency of mechanical impedance on the subject posture, mass and backrest angle, the definition of a single generalized response curve may lead to considerable errors. From the

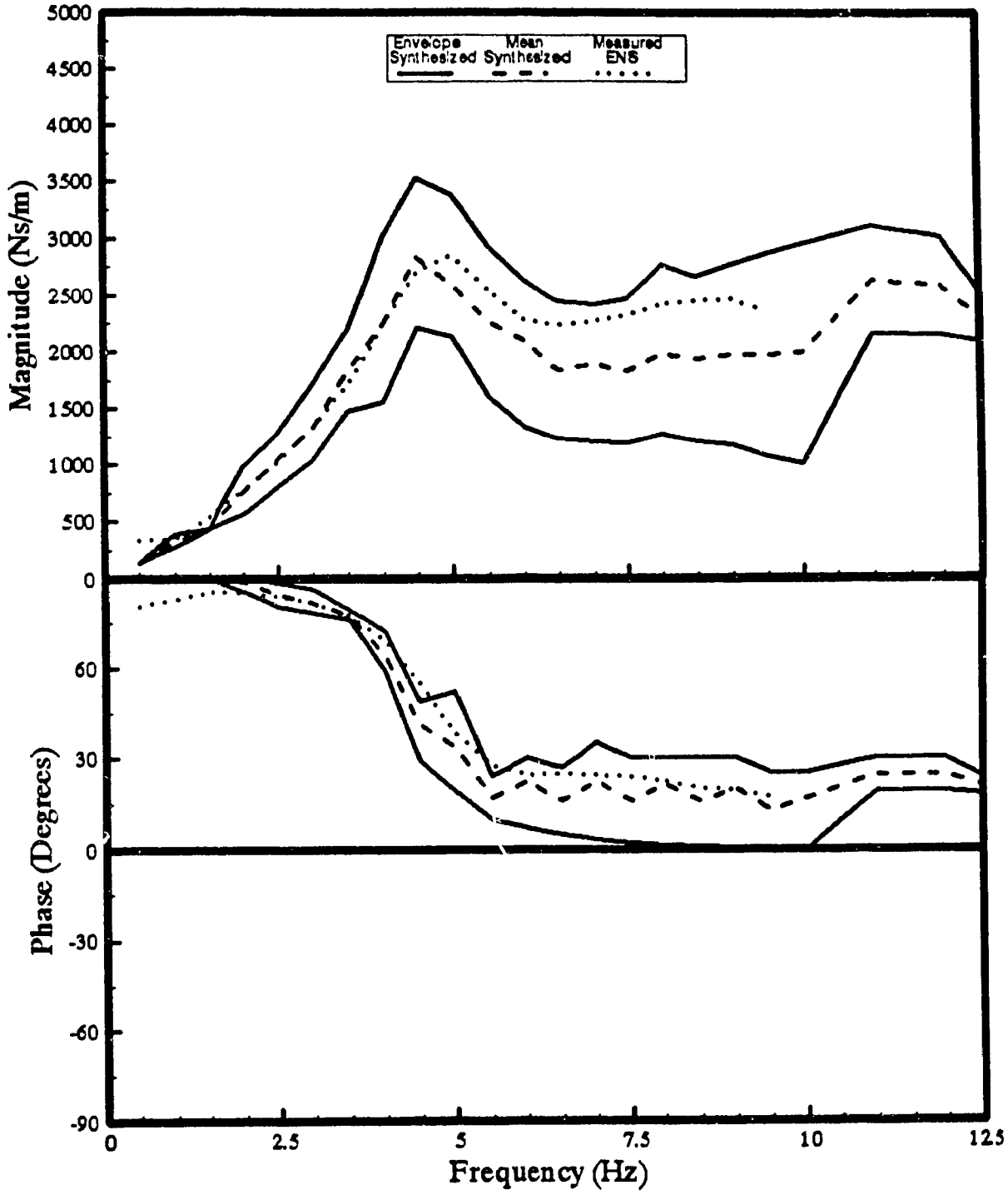

Figure 6.25 Comparison of mean and associated envelopes of synthesized driving-point mechanical impedance characteristics with the mean measured data for subjects with mean mass of 75.4 kg, maintaining an ENS posture, under a similar range of excitations.

synthesized and measured impedance data, it is apparent that mechanical impedance magnitude and phase characteristics can be defined within relatively close bounds for a specific set of experimental conditions. Application of these results to other situations involving significant differences in postures, subject masses, and excitation levels and frequencies may result in large errors, as observed from the significant differences between measured impedance characteristics and the proposed standardized curve.

It may thus seem appropriate to consider the data presented in Figures 6.22 to 6.24 as the most probable or target driving-point mechanical impedance characteristics for three different postures. These target values are considered suitable for development of a human driver model applicable in off-road vehicle vibration environments. Tables 6.2 to 6.4 provide a listing of these values within the 0.75 to 9.875 Hz frequency range for subjects maintaining ENS, EBS and SLO postures, respectively, on a seat with 0° backrest angle. The upper and lower limits on these values are also specified at each frequency, expressing the variations of the biodynamic response about the mean values. These variations, in general, are observed to be largest near the resonance and at higher frequencies, but are usually within 10% of the mean values. On the basis of these curves, whole-body resonance is predicted as 4.875 Hz for the ENS posture, and as 4.75 Hz for both the EBS and SLO postures. At resonance, the change in posture from ENS to EBS leads to variations in

TABLE 6.2

Vertical Driving-Point Mechanical Impedance Characteristics of a Vehicle Driver Maintaining an ENS Posture

	Magnitude (Ns/m)			Phase (degrees)		
Frequency (Hz)	Upper Limit	Lower Limit	Mean Value	Upper Limit	Lower Limit	Mean Value
0.75	263	260	261	81	80	80
1.0	352	348	350	83	83	83
1.5	547	541	544	85	85	85
2.0	778	768	772	86	84	85
2.5	1036	1029	1032	84	83	84
3.0	1339	1317	1328	81	81	81
3.5	1732	1684	1707	78	76	77
4.0	2293	2203	2247	71	65	69
4.5	2808	2652	2716	59	52	55
4.75	2898	2805	2864	50	45	46
4.875	2907	2804	2867	45	40	42
5.0	2910	2753	2852	41	37	38
5.125	2864	2747	2804	36	32	34
5.25	2763	2715	2732	33	28	31
5.5	2603	2505	2552	29	25	28
5.75	2473	2313	2393	26	23	25
6.0	2393	2227	2291	25	24	24
6.5	2350	2177	2239	27	23	25
7.0	2349	2191	2268	27.5	22	25
7.5	2417	2286	2330	28	21	24
8.0	2487	2393	2427	26	19	22
8.5	2498	2408	2450	24	16	20
9.0	2508	2440	2474	22	17	20
9.5	2459	2300	2356	19	15	17
9.875	2428	2244	2317	18	14	16

TABLE 6.3

Vertical Driving-Point Mechanical Impedance Characteristics for a Vehicle Driver Maintaining an EBS Posture

	Magnitude (Ns/m)			Phase (degrees)		
Frequency (Hz)	Upper Limit	Lower Limit	Mean Value	Upper Limit	Lower Limit	Mean Value
0.75	278	259	266	80	80	80
1.0	349	345	346	83	82	83
1.5	535	533	534	85	85	85
2.0	776	741	756	86	83	84
2.5	1018	985	1003	84	83	84
3.0	1326	1254	1290	82	80	81
3.5	1760	1614	1689	78	74	76
4.0	2339	2081	2205	69	60	65
4.5	2545	2428	2494	56	44	50
4.75	2563	2478	2516	48	38	43
4.875	2529	2415	2478	46	36	40
5.0	2502	2379	2461	43	34	38
5.125	2466	2320	2409	40	32	36
5.25	2419	2290	2375	38	31	34
5.5	2340	2258	2291	36	29	32
5.75	2286	2207	2237	34	26	30
6.0	2204	2175	2189	35	25	30
6.5	2290	2231	2255	36	25	30
7.0	2391	2286	2331	34	26	30
7.5	2535	2439	2477	32	25	28
8.0	2636	2539	2584	30	23	26
8.5	2689	2506	2595	25	18	22
9.0	2742	2456	2603	22	15	19
9.5	2656	2265	2455	18	13	15
9.875	2646	2202	2409	16	11	14

TABLE 6.4

Vertical Driving-Point Mechanical Impedance Characteristics for a Vehicle Driver Maintaining a Slouched (SLO) Posture

	Magnitude (Ns/m)			Phase (degrees)		
Frequency (Hz)	Upper Limit	Lower Limit	Mean Value	Upper Limit	Lower Limit	Mean Value
0.75	260	258	259	80	80	80
1.0	351	347	348	83	82	83
1.5	552	538	544	86	85	85
2.0	801	760	777	85	83	84
2.5	1061	1022	1037	83	82	82
3.0	1362	1292	1329	80	78	79
3.5	1791	1649	1724	76	72	74
4.0	2335	2172	2255	69	61	65
4.5	2718	2599	2661	54	42	48
4.75	2721	2602	2668	47	34	40
4.875	2753	2551	2634	42	30	36
5.0	2766	2496	2612	38	27	32
5.125	2728	2459	2568	35	26	30
5.25	2664	2408	2508	32	25	28
5.5	2504	2214	2343	29	24	26
5.75	2368	2147	2259	28	23	26
6.0	2314	2068	2188	28	24	26
6.5	2214	2175	2197	26	24	26
7.0	2300	2283	2293	25	23	24
7.5	2406	2290	2344	22	20	21
8.0	2457	2360	2403	19	18	18
8.5	2446	2390	2426	18	15	17
9.0	2467	2358	2412	16	15	16
9.5	2316	2217	2260	14	13	13
9.875	2280	2128	2187	13	11	12

impedance magnitude of more than 10 %. Alternately, for subjects leaning against a 14° inclined backrest, the values plotted in Figure 6.19 may be considered as appropriate target values.

6.4.2 TARGET VALUES OF SEAT-TO-HEAD TRANSMISSIBILITY

While seat-to-head transmissibility characteristics were not measured in this study, the synthesized curves presented in Figure 5.18 for subjects maintaining an ENS posture are considered as applicable target values. The values corresponding to the mean synthesized curve in the 0.75 to 10 Hz frequency range are listed in Table 6.5. Upper and lower limits, representing the variations about the mean values resulting from combining the various data sets obtained under varying experimental conditions, are also presented in the Table. While the upper and lower bounds are observed to vary within 10% about the mean values over most of the frequency range, variations as large as 30% are observed near 7.5 Hz. The proposed target values exhibit the whole-body resonance at 5 Hz, which is quite close to 4.875 Hz established from the target mechanical impedance data for the ENS posture. Moreover, the proposed target values reveal a relatively good agreement with the ISO proposed seat-to-head transmissibility data [85], thus providing further support for the selection of the target values for the ENS posture. For the EBS posture, only one data set has been identified in the literature by Paddan & Griffin [94]. The reported data set is thus tentatively considered appropriate for defining the target values for

TABLE 6.5

Vertical Seat-to-Head Transmissibility Characteristics of a Vehicle Driver Maintaining an ENS Posture

	Magnitude			Phase (degrees)		
Frequency (Hz)	Upper Limit	Lower Limit	Mean Value	Upper Limit	Lower Limit	Mean Value
0.75	1.00	0.97	0.99	0	-2	-0.7
1.0	1.02	1.00	1.01	0	-2	-0.7
1.5	1.10	1.00	1.05	0	-3	-1.3
2.0	1.16	1.00	1.10	-2	-11	-6.0
2.5	1.20	1.05	1.12	-4	-11	-7.3
3.0	1.25	1.08	1.16	-4	-19	-9.7
3.5	1.32	1.12	1.20	0	-27	-12.3
4.0	1.40	1.10	1.28	2	-35	-17.3
4.5	1.45	1.21	1.37	3	-60	-29
5.0	1.50	1.37	1.45	-3	-75	-40
5.5	1.65	1.18	1.42	-16	-86	-50
6.0	1.40	1.05	1.30	-40	-93	-61
6.5	1.37	0.95	1.18	-42	-90	-62
7.0	1.35	0.92	1.09	-42	-88	-63
7.5	1.30	0.90	1.04	-42	-80	-64
8.0	1.20	0.85	0.99	-43	-75	-64
8.5	1.12	0.85	0.95	-43	-81	-68
9.0	1.04	0.82	0.94	-44	-85	-70
9.5	1.00	0.81	0.94	-44	-90	-74
10.0	1.08	0.84	0.95	-44	-92	-76

TABLE 6.6

Vertical Seat-to-Head Transmissibility Characteristics for a Vehicle Driver Maintaining an EBS Posture (Paddan & Griffin, [94])

Frequency (Hz)	Magnitude	Phase (degrees)
0.75	0.97	
1.0	0.99	
1.5	1.00	
2.0	0.98	-11
2.5	0.94	-7
3.0	0.97	-4
3.5	1.05	0
4.0	1.10	2
4.5	1.20	3
5.0	1.35	-3
5.5	1.50	-16
6.0	1.70	-40
6.5	1.75	-60
7.0	1.79	-65
7.5	1.77	-76
8.0	1.60	-65
8.5	1.30	-62
9.0	1.20	-62
9.5	1.14	-62
10.0	1.07	-62

subjects maintaining the EBS posture. The data set, presented in Table 6.6, however, suggests a whole-body resonant frequency in the neighbourhood of 7 Hz, which is considerably higher than the 4.75 Hz predicted from the driving-point mechanical impedance data for a similar posture.

6.5 Human Driver Model Development and Parameter Estimation

In this section, a four-degree-of-freedom linear human driver model is proposed for a seated subject maintaining an ENS posture. Off-road vehicle drivers frequently assume an ENS posture, due to excessive vehicle vibration and the desire to maintain adequate grip on the controls. The baseline model is thus established for the ENS posture alone and the model parameters are identified such that the model response correlates with both the target driving-point mechanical impedance and seat-to-head transmissibility magnitude and phase. While some of the model parameters are identified from the anthropometric and biomechanical data, a nonlinear programming based optimization technique is employed in conjunction with the target values to identify the remaining model parameters.

6.5.1 PROPOSED HUMAN DRIVER MODEL

The proposed human driver model, shown in Figure 6.26, comprises four masses, coupled by linear elastic and damping elements. The four masses represent the following four body segments: the head and neck (m_1); the chest

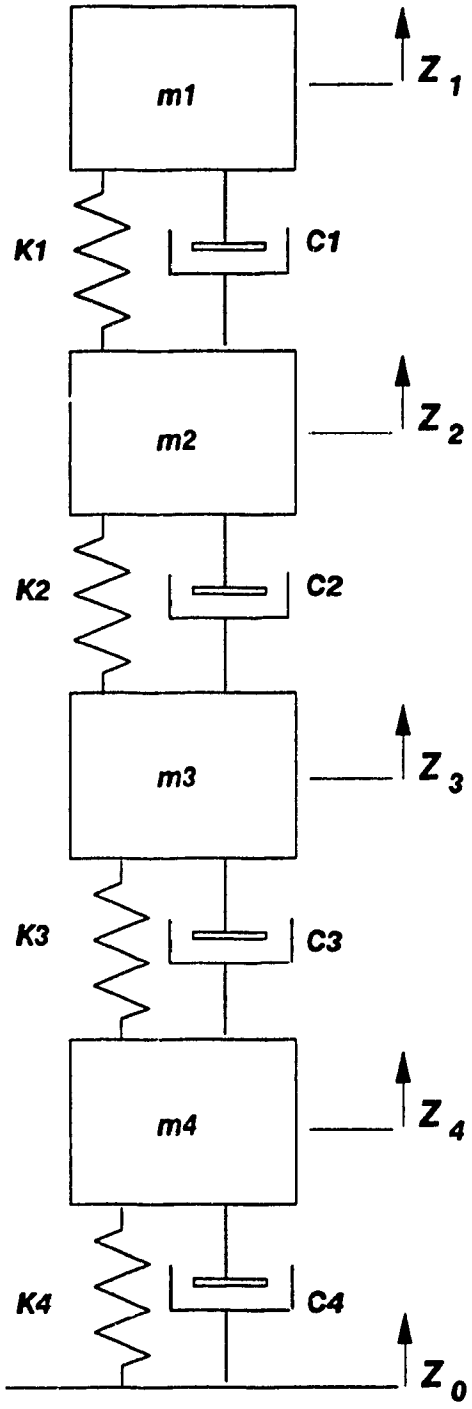

Figure 6.26 Proposed four-degree-of-freedom linear human driver model.

and upper torso (m_2); the lower torso (m_3); and the thighs and pelvis in contact with the seat (m_4). The mass due to lower legs and the feet is not included in this representation, assuming their negligible contributions to the biodynamic response of the seated body. This assumption is further justified in view of the evidence reported by Fairley [95], which concluded that the contribution of the legs to the vertical suspension seat transmissibility is relatively insignificant when both the footrest and the seat are vibrated. The hand and arm mass supported on the steering wheel is not incorporated in the model assuming its negligible contributions to the whole-body biodynamic response. The inertial properties of the four main body segments included in the model are identified from anthropometric data [96].

Although a single-DOF model may be attempted to satisfy the target impedance and transmissibility characteristics which exhibit only one resonance in the frequency range of interest, a higher order model is desirable to predict the biodynamic response around the secondary resonances. Smith [80] identified four resonance regions of the body in the frequency range below 20 Hz, depending upon the excitation: 5 to 7 Hz; 7 to 9 Hz; 10 to 14 Hz; and 16 to 19 Hz. While the first resonance region has often been associated with the resonance of the chest and upper torso, it has been suggested that the second and third resonance regions relate to the resonant motions of the thighs and pelvis in contact with the seat. The cervical spine or head and neck response

has been associated with the fourth region. Although the current analysis is limited to frequencies below 10 Hz, a four-DOF model is proposed such that the associated masses, stiffness and damping coefficients may be related to the biomechanical configuration of the whole body. The stiffness and damping properties of the buttocks and thighs are represented by K_4 and C_4, those of the lumbar spine by K_3 and C_3, those of the thoracic spine by K_2 and C_2, while those of the cervical spine by K_1 and C_1.

The dynamic characteristics of the human driver model shown in Figure 6.26 may be expressed by the following coupled differential equations:

$$m_i\ddot{z}_i + F_{Ki} + F_{Di} = F_{0i} \qquad i=1,2,\ldots,n \tag{6.1}$$

where m_i are the masses, $\ddot{z}_i$ are the accelerations and n is the number of degree-of-freedom. F_{Ki}, F_{Di} and F_{0i} are the restoring, dissipative and excitation forces, respectively, acting on mass i. Assuming linear stiffness and damping coefficients, these forces are expressed as:

$$F_{Ki} = \begin{cases} K_i(z_i - z_{i+1}) & i=1 \\ K_i(z_i - z_{i+1}) - K_{i-1}(z_{i-1} - z_i) & i=2,\ldots,n-1 \\ K_i z_i - K_{i-1}(z_{i-1} - z_i) & i=n \end{cases} \tag{6.2}$$

$$F_{Di}=\begin{cases} C_i(\dot{z}_i-\dot{z}_{i+1}) & i=1 \\ C_i(\dot{z}_i-\dot{z}_{i+1})-C_{i-}(\dot{z}_{i-1}-\dot{z}_i) & i=2,\ldots,n-1 \\ C_i\dot{z}_i-C_{i-1}(\dot{z}_{i-1}-\dot{z}_i) & i=n \end{cases} \quad (6.3)$$

$$F_{0i}=\begin{cases} 0 & i\neq n \\ K_i z_0+C_i\dot{z}_0 & i=n \end{cases} \quad (6.4)$$

where K_i and C_i are linear stiffness and damping coefficients, z_i and $\dot{z}_i$ represent vertical displacements and velocities, respectively. The above equations may be expressed in the following matrix form:

$$[M]\{\ddot{q}\}+[C]\{\dot{q}\}+[K]\{q\}=\{p\} \quad (6.5)$$

where [M], [C] and [K] are (nxn) mass, damping and stiffness matrices, respectively. {q} is a (nx1) vector of displacement response quantities, {p} is an (nx1) excitation force vector, and "·"and"··" designate the first and second derivatives with respect to time. Fourier transform of the above equation results in:

$$\{Q(j\omega)\} = [[K] - \omega^2[M] + j\omega[C]]^{-1}\{P(j\omega)\} \quad (6.6)$$

where {Q(jω)} and {P(jω)} are the complex Fourier transform vectors of {q} and

{p}, respectively, and ω is the angular frequency. The vector {Q(jω)} contains the complex displacement amplitude responses of the n masses as a function of frequency, $\{X_1(j\omega), X_2(j\omega), X_3(j\omega), X_4(j\omega)\}$, and {P(jω)} contains the complex excitation forces as a function of frequency, $\{0, 0, 0, (K_4+j\omega C_4)X_0(\omega)\}$, where $X_0(\omega)$ is the amplitude of displacement excitation. The driving-point mechanical impedance of the human driver model, defined as the ratio of the driving force to the driving point excitation velocity, is derived from:

$$Z(j\omega)=\frac{(K_4+j\omega C_4)[X_0(\omega)-X_4(j\omega)]}{j\omega X_0(\omega)} \qquad (6.7)$$

Equation (6.7) yields the driving-point mechanical impedance magnitude, $|Z(j\omega)|$, and phase, $\phi_Z(\omega)$, of the driver model subject to seat vibration. The complex seat-to-head transmissibility function is derived from:

$$T(j\omega)=\frac{X_1(j\omega)}{X_0(\omega)} \qquad (6.8)$$

6.5.2 ESTIMATION OF MODEL PARAMETERS

Many biodynamic models have been derived using trial-and-error curve-fitting techniques, such that the error between the computed and measured biodynamic response function is minimum. Majority of the biodynamic models

proposed in the literature are based upon the magnitude of measured mechanical impedance or apparent mass, while the impedance phase and seat-to-head transmissibility characteristics are ignored. Suggs [34] and Coermann [68] derived models using this approach, while concentrating on a specific frequency range. Such curve-fitting methods may lead to a proper fit over a specific frequency range, but rarely provide good results when extended over a broad frequency range. Alternatively, nonlinear programming based optimization techniques may be effectively employed to determine the model parameters, involving the use of a constrained optimization algorithm in conjunction with well-defined biodynamic response functions. A constrained objective function may be defined to minimize the error between the computed and the target values of specific biodynamic response functions over a specific frequency range.

In this study, an optimization software based on sequential search, NCONF [97], is employed to determine the human driver model parameters. Upon imposing some limit constraints on the model parameters, an objective function is formulated comprising the sum of squared errors between the computed and the target values for magnitude and phase of both the driving-point mechanical impedance and seat-to-head transmissibility functions. The model thus derived can provide reasonable correlation with both the impedance and transmissibility characteristics. Moreover, such a model development methodology contributes

to the attainment of uniqueness of the proposed model.

Starting with an assumed set of model parameters, the differential equations of motion are solved for unit displacement excitation to derive the driving-point mechanical impedance magnitude and phase using equation (6.7) and seat-to-head transmissibility magnitude and phase using equation (6.8). At each sequence of search, the sum of squared errors defined by an objective function over the entire frequency range is examined, and the procedure is re-initiated with modified parameter values when the error exceeds that from the previous search. The search is terminated when the computed error approaches the minimum value. In all cases, optimization is performed with several different starting values to verify the uniqueness of the set of model parameters.

6.5.3 MODEL CONSTRAINTS

On the basis of anthropometric data [96], the proportion of total body weight estimated for different body segments is 8.4% for the head and neck, 36.6% for the chest and upper torso, 13.4% for the lower torso, and 20% for the thighs and upper legs. For a seated driver with mean body mass of 75.4 kg, maintaining an ENS posture, 73.6% of the weight was found to be supported by the seat. For the total body mass of 55.5 kg supported by the seat, limit constraints are defined to ensure that the model masses conform with the anthropometric data. The limit constraints are expressed as ±10% variations

about the mean segment masses, while the total body mass is expressed as equality constraint:

$$5.31 \text{ kg} \leq m_1 \leq 6.49 \text{ kg};$$

$$23.31 \text{ kg} \leq m_2 \leq 28.49 \text{ kg};$$

$$8.55 \text{ kg} \leq m_3 \leq 10.45 \text{ kg};$$

$$12.78 \text{ kg} \leq m_4 \leq 15.62 \text{ kg; and}$$

$$\sum_{i=1}^{4} m_i = 55.5 \text{ kg}.$$

Development of a human body model involves complexities associated with identification of its restoring and dissipative properties. The biomechanical properties of the spine, chest and upper body are relatively unknown. Through studies performed on cadavers, Kazarian [98] identified a range of stiffness values for the lumbar spine (100 to 300 kN/m) and for the thoracic spine (150 to 200 kN/m). Mertens [78] proposed a human body model employing damping coefficients in the 500 to 4000 Ns/m range. Although the reported data represents relatively broad variations, the identified ranges can serve as effective limit constraints for the optimization problem while the damping coefficients are limited in the range proposed by Mertens. The following limit constraints on stiffness and damping coefficients are formulated using the published data:

Cervical spine:	$K_1 > 0$ kN/m;
Thoracic spine:	$150 \le K_2 \le 200$ kN/m;
Lumbar spine:	$100 \le K_3 \le 300$ kN/m;
Buttocks and thighs:	$K_4 > 0$ kN/m;
Damping coefficients:	$500 \le C_i \le 4000$ Ns/m.

6.5.4 OBJECTIVE FUNCTION

Two objective functions, $U_Z(\chi)$, and $U_T(\chi)$, related to the squared magnitude and phase errors associated with mechanical impedance and seat-to-head transmissibility functions, respectively, are formulated as:

$$U_Z(\chi)=\alpha_1\sum_{k=1}^{N}\left\{\lambda_k\left[|Z(j\omega_k)|-|Z_i(j\omega_k)|\right]\right\}^2+\alpha_2\sum_{k=1}^{N}\left\{\phi_Z(\omega_k)-\phi_{Zi}(\omega_k)\right\}^2 \qquad (6.9)$$

$$U_T(\chi)=\alpha_3\sum_{k=1}^{N}\left\{\psi_k\left[|T(j\omega_k)|-|T_i(j\omega_k)|\right]\right\}^2+\alpha_4\sum_{k=1}^{N}\left\{\phi_T(\omega_k)-\phi_{Ti}(\omega_k)\right\}^2 \qquad (6.10)$$

In the above equations, α_1, α_2, α_3, and α_4 are defined as weighting factors on the sum of squared impedance magnitude, impedance phase, transmissibility magnitude and transmissibility phase errors, respectively. k denotes a specific discrete frequency, and N is the total number of discrete frequencies considered within the 0.75 to 10 Hz frequency range. λ_k and ψ_k, are the frequency

weighting factors for the squared impedance and transmissibility magnitude errors, respectively. $|Z_t(j\omega_k)|$, $\phi_{Zt}(\omega_k)$, $|T_t(j\omega_k)|$, and $\phi_{Tt}(\omega_k)$ are the target values of impedance magnitude, impedance phase, transmissibility magnitude and transmissibility phase, respectively, identified in Tables 6.2 and 6.5. The computed impedance magnitude, impedance phase, transmissibility magnitude and transmissibility phase at frequency ω_k are expressed by $|Z(j\omega_k)|$, $\phi_Z(\omega_k)$, $|T(j\omega_k)|$, and $\phi_T(\omega_k)$, respectively. U_Z and U_T are the objective functions and χ is a vector of model parameter values, given by:

$$\chi = \{m_i, K_i, C_i\}^T \qquad i = 1,2, \quad ,n \qquad (6.11)$$

where "T" designates the transpose. The final constrained objective function is written as:

$$U(\chi) = \textit{Minimize}\ [U_Z(\chi) + U_T(\chi)] \qquad (6.12)$$

The weighting factors α_1, α_2, α_3, α_4 are selected to place relatively greater emphasis on the magnitude errors. α_1 and α_3 are thus selected considerably larger than α_2 and α_4. Since the peak impedance magnitude of nearly 2500 Ns/m is considerably larger than the peak transmissibility magnitude (1.45), the weighting factors α_1 and α_3 are appropriately selected to yield almost equal weighting of impedance and transmissibility magnitudes. The frequency

weighting factors, λ_k and ψ_k, are selected to emphasize the magnitude errors in the vicinity of the resonant frequency of the whole body. Each optimization search consists of computing the sum of squared errors at 24 distinct frequencies, and the search is terminated when both impedance and transmissibility magnitude errors are observed as minimum.

6.5.5 HUMAN DRIVER MODEL PARAMETERS

The solution of the constrained optimization problem, equation (6.12), resulted in the identification of the following model parameters:

m_1 = 5.31 kg	K_1 = 310 kN/m	C_1 = 400 Ns/m
m_2 = 28.49 kg	K_2 = 183 kN/m	C_2 = 4750 Ns/m
m_3 = 8.62 kg	K_3 = 162.8 kN/m	C_3 = 4585 Ns/m
m_4 = 12.78 kg	K_4 = 90 kN/m	C_4 = 2064 Ns/m

Figures 6.27 and 6.28 present a comparison of the impedance and transmissibility magnitude and phase response characteristics, respectively, with the target data. The difficulty in satisfying both the mechanical impedance and seat-to-head transmissibility functions may be appreciated by considering that a closer agreement is found with mechanical impedance, while larger discrepancies occur with seat-to-head transmissibility. From the driving-point mechanical impedance function, the resonant frequency of the model is

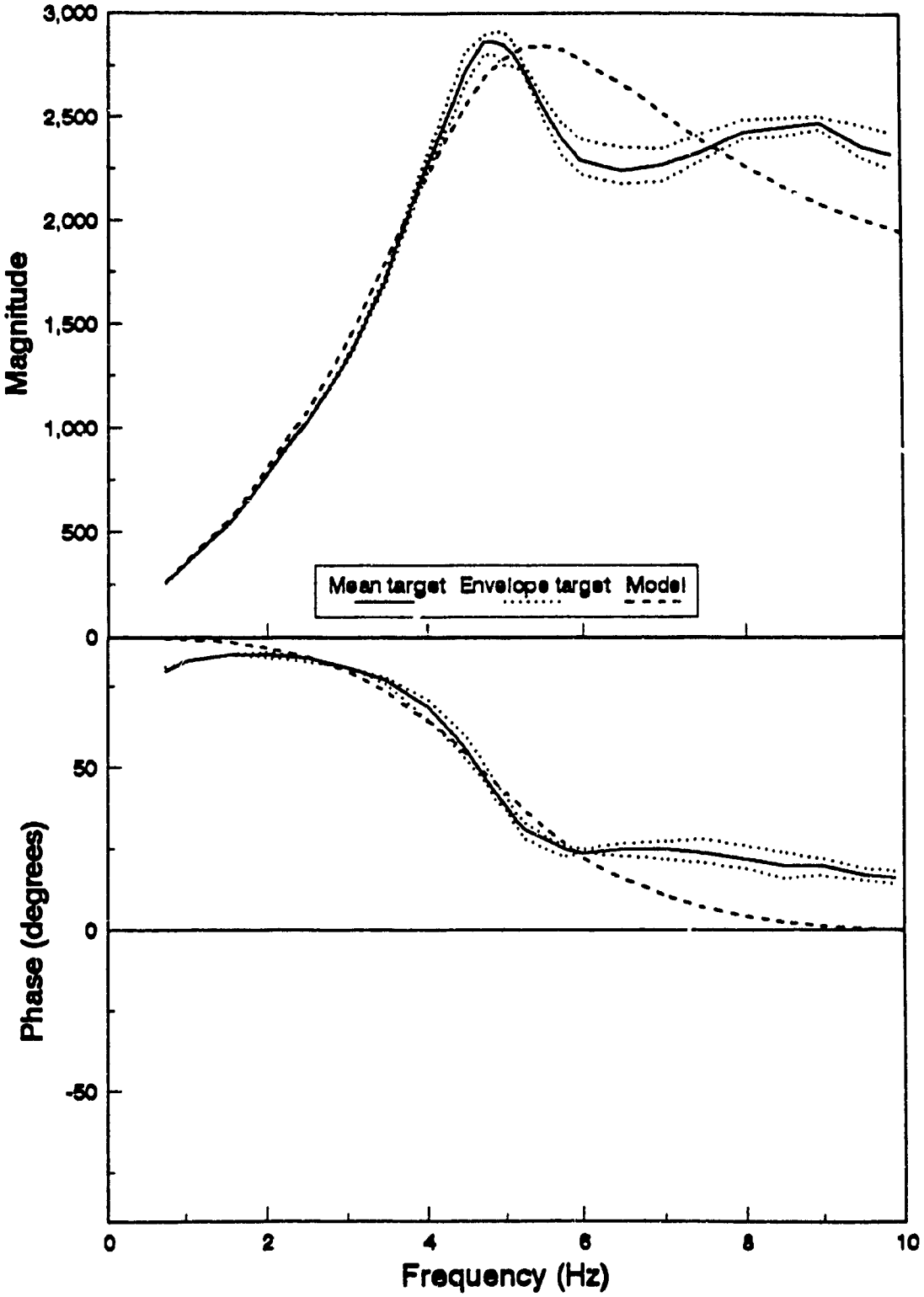

Figure 6.27 Comparison of target and computed driving-point mechanical impedance characteristics for an off-road vehicle driver maintaining an ENS posture.

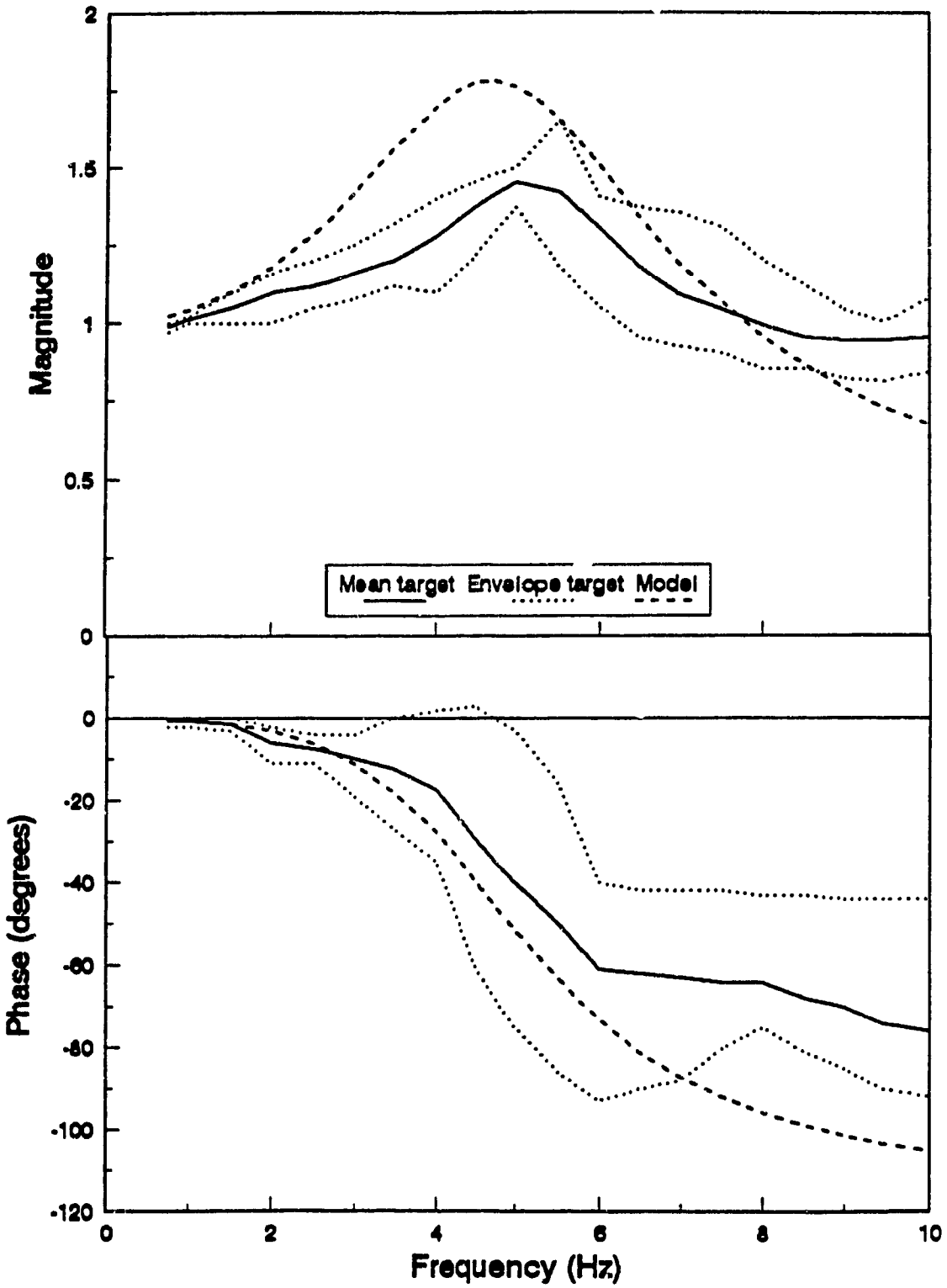

Figure 6.28 Comparison of target and computed seat-to-head transmissibility characteristics for an off-road vehicle driver maintaining an ENS posture.

observed to be 5.5 Hz, compared to 4.875 Hz derived from the target values. The peak model response (2833 Ns/m), however, is quite close to the corresponding target value (2867 Ns/m), an error of approximately 1.2%. The impedance magnitude errors, however, tend to increase at higher excitation frequency, the peak magnitude error approaching 20%. Thus appart from a slight upward shift in the resonant frequency, the model is found to predict impedance magnitude values generally within 20% of those defined as target values at any specific frequency within the 0.75 and 10 Hz frequency range. Driving-point mechanical impedance phase response of the model correlates well with the target data at frequencies up to 6 Hz, while the phase error increases at higher frequencies.

The seat-to-head transmissibility characteristics, presented in Figure 6.28, reveal relatively large errors between the model response and the target values. While the model response exhibits a resonant peak of 1.77 at 4.8 Hz, the corresponding target value is 1.45 at 5.0 Hz. Although the resonant frequencies correlate reasonably well, the model tends to overestimate the transmissibility magnitude by as much as 30 % at frequencies below 7 Hz. A relatively good agreement is observed for the phase response at frequencies below 6 Hz.

The model parameter values identified in this section represent a compromise

towards achieving acceptable mechanical impedance and seat-to-head transmissibility characteristics. While it was observed that significantly lower stiffness values of K_1, K_2, and K_3 provided closer agreement with the mechanical impedance target values, significantly larger values resulted in closer agreement with the seat-to-head transmissibility. The reverse trend was observed for the stiffness K_4. Moreover, a lower damping coefficient C_4 resulted in best correlation with the mechanical impedance, with large error in transmissibility magnitude. The variations in damping coefficients, C_1, C_2 and C_3, resulted in almost insignificant changes in impedance and transmissibility responses. The predicted values for the main body resonant frequency extracted from the two biodynamic response functions are within the range expected for the human body, usually reported around 5 Hz. For off-road vehicle drivers subjected to vibration predominantly below 5 Hz, the model is considered to provide satisfactory predictions for assessing whole-body dynamics under the influence of vibration.

6.6 Summary

A four-degree-of-freedom linear human driver model is proposed and its parameters are estimated using the target values of both driving-point mechanical impedance and seat-to-head transmissibility magnitude and phase at frequencies below 10 Hz. Target values of driving-point mechanical impedance characteristics are identified from laboratory measurements performed with

seated subjects maintaining various postures under different types of random and sinusoidal excitations within the 1.0 to 2.0 ms^{-2} amplitude range. The target values of seat-to-head transmissibility characteristics are established from the synthesis of published data reported under similar test conditions. While the derived model provides closer agreement with the mechanical impedance target values, the main body resonant frequency predicted from both biodynamic response functions is found to correspond, within close bounds, to that expected for the human body.

CHAPTER 7

VALIDATION AND RESPONSE ANALYSIS OF THE COMBINED SUSPENSION SEAT-HUMAN DRIVER MODEL

7.1 Introduction

The nonlinear suspension seat model developed in Chapters 3 and 4 is combined with the linear human driver model derived in the preceeding chapter in an attempt to account for the influence of whole-body dynamics on suspension seat vibration attenuation performance. The incentive for this study relies on indications from the literature that significant variations in suspension seat performance often arise when the seat is loaded with a rigid mass and with a person [6]. The development of an appropriate suspension seat-human driver model thus provides a convenient analytical tool for estimating the driver's response and the suspension seat performance under various types of vibration excitations, while eliminating the need for seat testing with human subjects. While the suspension seat model was conveniently validated on the basis of rigid mass loading for various types of excitations in Chapters 3 and 4, this chapter is concerned with the validation of the combined suspension seat-human driver model under deterministic, random and shock excitations. The influence of human driver dynamics on the vibration attenuation performance of a suspension seat under representative off-road vehicle excitations is demonstrated by

comparing the measured response characteristics of the seat-human system with those obtained using a rigid mass load. Upon validation, the combined seat-driver model is further used to estimate the influence of the suspension seat design parameters on the driver's whole-body vibration exposure levels under realistic off-road vehicle environment.

7.2 Influence of Body Dynamics on Suspension Seat Response

The influence of body dynamics on the suspension seat response is evaluated by comparing the vibration response characteristics of the seat loaded with a rigid mass (reported in Chapters 3 and 4) with those of the seat-human system. The measurements are performed with the SIFRA suspension seat using the WBVVS driven by the synthesized sinusoidal and random excitation signals defined in section 2.5. The tests are performed with a seated subject maintaining an ENS posture, with feet resting flat on the WBVVS platform and hands in contact with a steering wheel. The test data was acquired with subject J, identified in Table 6.1, with mass supported by the seat equal to 55.6 kg (73.2 kg while standing), which is slightly lower than the mass of 63.6 kg used as the rigid load.

Figure 7.1 illustrates a comparison of the vertical seat acceleration transmissibility characteristics measured under sinusoidal sweep excitation with a rigid mass and with a human subject. The peak resonant

transmissibility of the seat-human system is close to that measured with a rigid load, since the human body is known to behave similar to a rigid mass at very low frequencies. The difference in mass between the rigid and the human subject load, however, can acount for the difference in resonant frequency and resonant transmissibility magnitude observed in Figure 7.1. The acceleration transmissibility response of the seat-human system, however, differs considerably from that of the rigid mass at higher excitation frequencies. These discrepancies are attributed to the resonances of the human body at higher frequencies. A rigid seat load provides an overestimation of the seat attenuation performance by as much as 25% in the 1.3 to 4.0 Hz frequency range, when compared to that of the seat with a human subject. Since off-road wheeled vehicle vibration is predominant in this frequency range, the performance characteristics of such a seat loaded with a rigid mass would be grossly exagerated. This is further illustrated in Figure 7.2 through comparison of the measured rms acceleration response spectra of the seat with rigid mass and human subject loads under ISO 2 random excitation, which predominates at 2.65 Hz. At the predominant excitation frequency, the rms acceleration response at the seat with subject J is observed to be 0.64 ms^{-2} and 0.46 ms^{-2} when the seat is loaded with a rigid mass, thus close to 30% lower than the true acceleration response measured with a human subject.

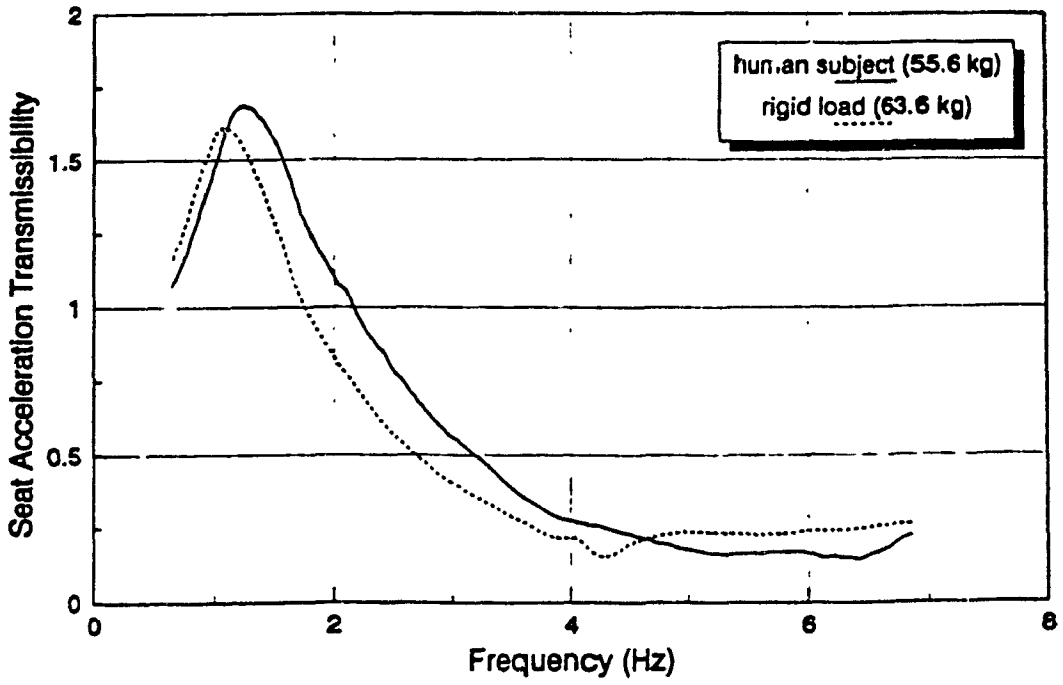

Figure 7.1 Comparison of seat vertical acceleration transmissibility measured with a rigid mass load (63.6 kg) and a with a human subject (55.6 kg on the seat) under sinusoidal sweep excitation.

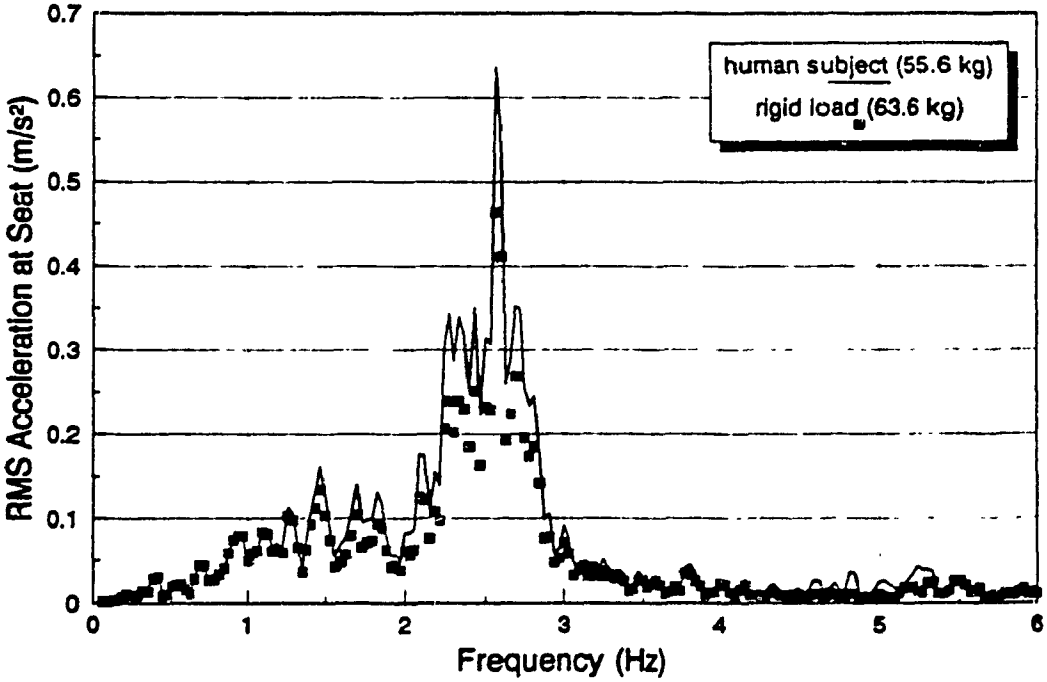

Figure 7.2 Comparison of seat vertical rms acceleration response measured with a rigid load (63.6 kg) and with a human subject (55.6 kg) under ISO 2 random excitation class.

The results presented in Figures 7.1 and 7.2 clearly indicate that for applications in wheeled off-road vehicles, the attenuation performance of the seat can be overestimated by as much as 30% when contributions due to human body dynamics are neglected. This difference is relatively small in comparison with the results reported by Griffin [6] for a foam and metal spring seat (Figure 5.1), for which differences of more than 100% on acceleration transmissibility magnitude were observed at specific frequencies between rigid and person seat loads. The influence of whole-body dynamics on the seat attenuation performance is highly dependent on the characteristics of the seat itself. For a relatively stiff seat such as that used by Griffin, with resonant frequency close to 4 Hz, the lightly damped and highly rigid seat-load interface results in significant amplification of the vibration at resonance when the load is rigid. The elasticity and dissipative properties provided by the human buttocks and thighs contribute considerably to reduce the magnitude of the resonant peak and the resonant frequency, while impeding the attenuation performance at higher frequencies. Since the human body behaves similar to a rigid mass under excitation frequencies below 2 Hz, the contributions of the human body dynamics near resonance are almost insignificant when a low natural frequency suspension seat is considered. At higher excitation frequencies, particularly in the isolation range, the combined restoring and dissipative properties of the seat and human body contribute considerably to the overall

vibration attenuation performance. The study of the driver-suspension seat system, thus necessitates appropriate consideration of the coupled dynamics associated with the suspension seat and the human body, along with the characteristics of the vibration excitation.

7.3 Development of a Combined Suspension Seat-Human Driver Model

A combined suspension seat-human driver model, shown in Figure 7.3, is developed upon combining the nonlinear suspension seat model presented in Chapters 3 and 4 with the linear human driver model presented in Chapter 6. The equations of motion of the resulting five-degree-of-freedom model are derived as:

$$m_S\ddot{z}_1 + F_S(x_1,\beta) + F_K(x_1) + F_F(\dot{x}_1) + F_D(\dot{x}_1,\alpha) - K_4^*x_2 - C_4^*\dot{x}_2 = 0 \quad (7.1)$$

$$m_4\ddot{z}_2 + K_4^*x_2 + C_4^*\dot{x}_2 - K_3x_3 - C_3\dot{x}_3 = 0 \quad (7.2)$$

$$m_3\ddot{z}_3 + K_3x_3 + C_3\dot{x}_3 - K_2x_4 - C_2\dot{x}_4 = 0 \quad (7.3)$$

$$m_2\ddot{z}_4 + K_2x_4 + C_2\dot{x}_4 - K_1x_5 - C_1\dot{x}_5 = 0 \quad (7.4)$$

$$m_1\ddot{z}_5 + K_1x_5 + C_1\dot{x}_5 = 0 \quad (7.5)$$

where the seat suspension forces $F_K(x_1)$ due to suspension spring, $F_F(\dot{x}_1)$ due to Coulomb friction, $F_S(x_1,\beta)$ due to bump stops, and $F_D(\dot{x}_1,\alpha)$ due to shock absorber damping are given by equations (3.3) to (3.7). The relative displacements associated with each mass are expressed as: $x_1=(z_1-z_0)$, $x_2=(z_2-z_1)$, $x_3=(z_3-z_2)$, $x_4=(z_4-z_3)$, and $x_5=(z_5-z_4)$. The model parameters

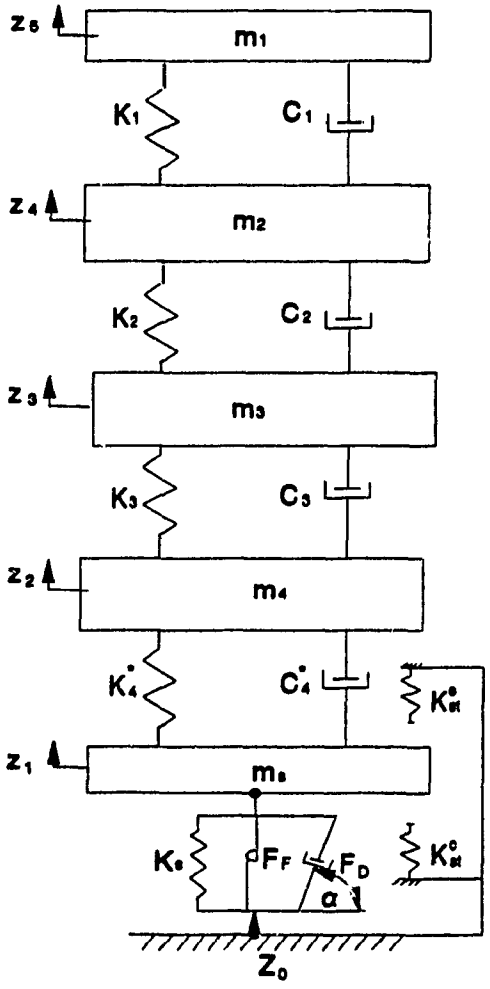

Figure 7.3 Combined suspension seat-human driver model.

are derived from those listed in Table 3.1 for the suspension seat, and in section 6.5.5 for the seated human body. The driver-seat interface is represented by the constants K_4^*, and C_4^*, representing the equivalent restoring and dissipative properties derived for a series combination of cushion and driver buttocks and thighs stiffness and damping coefficients, expressed as:

$$K_4^* = \frac{K_4 K_c}{K_4 + K_c} \quad ; \quad C_4^* = \frac{C_4 C_c}{C_4 + C_c} \tag{7.6}$$

In the above equations, the motion z_2 of mass m_4, representing the buttocks and thighs, serves as an indicator of the vibration exposure of the driver under an excitation represented by z_0. Simultaneous solution of the nonlinear differential equations (7.1) to (7.5) is thus required to determine the acceleration response $\ddot{z}_2$ of mass m_4.

7.4 Validation of the Combined Suspension Seat-Human Driver Model

In order to demonstrate the validity of the analytical model, the computed vibration response characteristics of the combined suspension seat-human driver model are compared with those derived from laboratory tests performed using the WBVVS for a seat loaded with a human subject. The nonlinear differential equations of motion (7.1) to (7.5) are solved for

harmonic, random and shock excitations using the technique defined in sections 3.4.1 and 3.4.2.

7.4.1 MODEL VALIDATION UNDER SINE SWEEP EXCITATION

Figure 7.4 illustrates a comparison of the suspension seat acceleration transmissibility measured with subject J under sine sweep excitation with the response characteristics computed for the seat with rigid mass and the four-DOF driver model. Both models provide an effective mass of 55.2 kg on the seat, compared with 55.6 kg for subject J. Although the two seat load representations yield seat transmissibility characteristics within relatively close bounds, the combined suspension seat-human driver model provides results in closer agreement with the measured data. While the largest deviations between the models and the measurements are observed in the resonant frequency region and at frequencies above 3 Hz, a close agreement with the measured results is observed in the 2 to 3 Hz frequency range, more particularly for the four-DOF driver model. While the resonant frequencies of the two models (1.3 Hz) correlate very well with the measured results, the four-DOF and rigid mass driver models yield an underestimation of the resonant transmissibility by 13.5% and 16.5%, respectively. At frequencies above 3 Hz, the rigid driver mass representation provides an overestimation of the measured seat transmissibility magnitude by as much as 125% at 5 Hz, while the

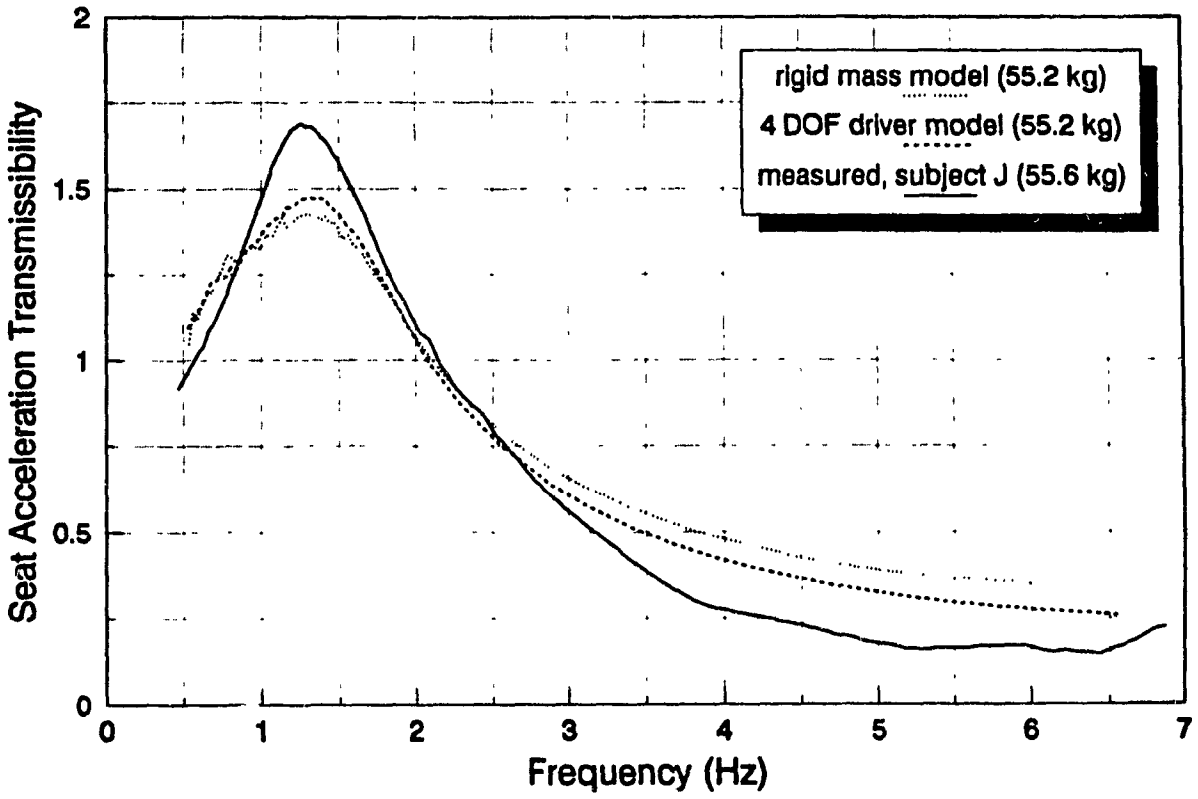

Figure 7.4 Seat vertical acceleration transmissibility characteristics measured with subject J and comparison with the response computed using the combined suspension seat-human driver model and the suspension seat-rigid mass model under sinusoidal excitation.

difference is slightly lower when the four-DOF driver model is used. The underestimation of transmissibility magnitude at resonance and the overestimation at frequencies above resonance by the analytical models may be attributed to relatively large damping considered in the suspension seat model and to the averaging associated with the measurements. A similar behaviour was also observed in Figure 3.5.

7.4.2 MODEL VALIDATION UNDER RANDOM EXCITATIONS

The rms acceleration response spectra computed using the combined suspension seat-human driver model and the rigid driver mass representation are compared with the data measured for subject J under ISO 2 random excitation class, as shown in Figure 7.5. The analytical response characteristics derived using the two different driver representations (rigid and four DOF of equal mass) are observed to be practically the same except for slight deviations around the predominant excitation frequency. The measured rms acceleration response, however, is observed to be 25% to 30% larger than those of the model response in the vicinity of the predominant excitation frequency. At the predominant excitation frequency, the rigid driver mass model yields an acceleration response slightly larger than that of the four-DOF driver model, which is consistent with the results obtained under sine sweep excitation (Figure 7.4). In contrast, the results obtained under ISO 1 random excitation reveal an

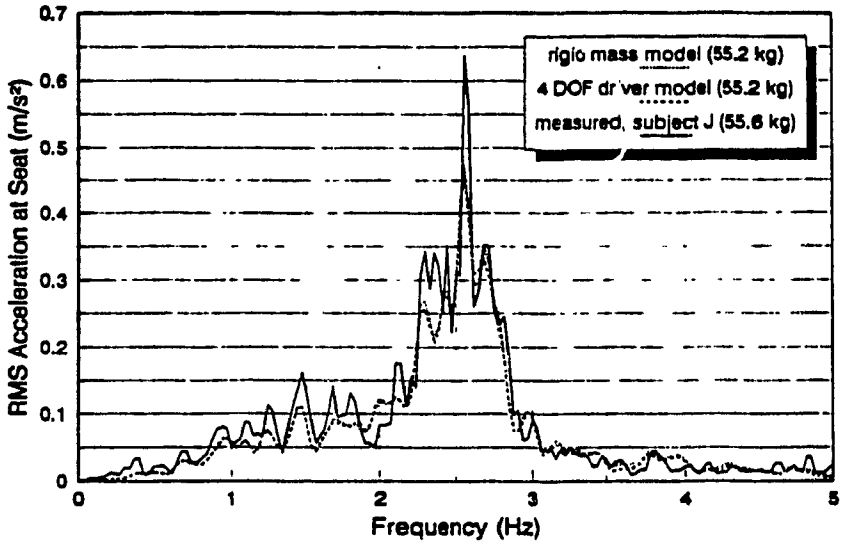

Figure 7.5 Seat rms acceleration response spectra measured with subject J and comparison with the response computed using the combined suspension seat-human driver model and the suspension seat-rigid mass model under ISO 2 random excitation class.

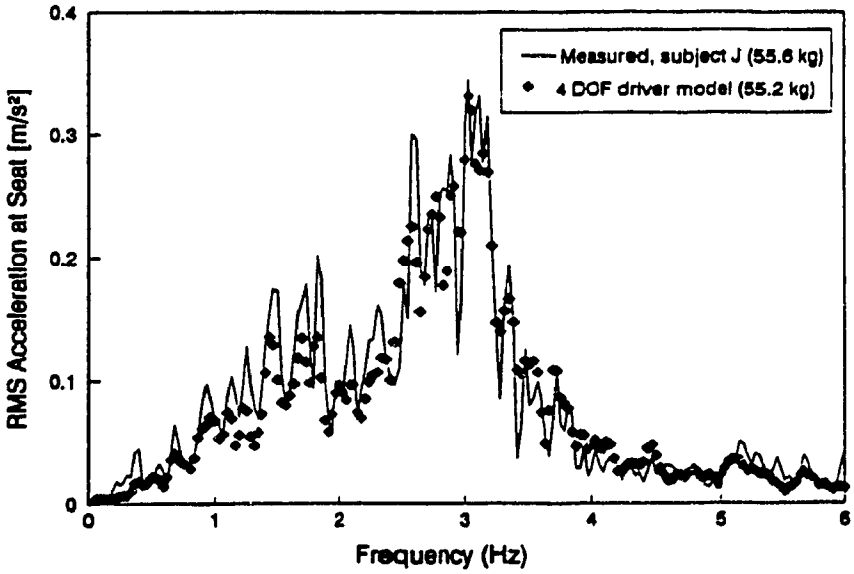

Figure 7.6 Seat rms acceleration response spectra measured with subject J and comparison with the response computed using the combined suspension seat-human driver model under ISO 1 random excitation class.

excellent agreement between the measured and the computed response characteristics of the combined suspension seat-human driver model, as shown in Figure 7.6.

7.4.3 MODEL VALIDATION UNDER SHOCK EXCITATIONS

The combined suspension seat-human driver model is further validated using the synthesized shock excitations derived using the response of a two-DOF vehicle model to a 75 mm peak displacement pulse input, as described in section 2.5.4. The acceleration responses measured and computed at the driver-seat interface are analyzed to derive the overall unweighted rms accelerations under excitations encountered at different vehicle speeds varying from 1 to 10 km/h. Figure 7.7 illustrates the comparison of the measured unweighted rms acceleration response with those computed using the suspension seat model with rigid mass and four-DOF driver models of equal mass. The results reveal an excellent agreement between the measured data and the response computed using the combined suspension seat-human driver model over the entire speed range. The rigid mass driver representation yields rms acceleration values slightly larger than the measured data, although the overestimation is below 10%. Figure 7.8 illustrates the excellent agreement between the measured and computed time histories of the acceleration response characteristics corresponding to a speed of 3 km/h. The computed response is derived using the combined

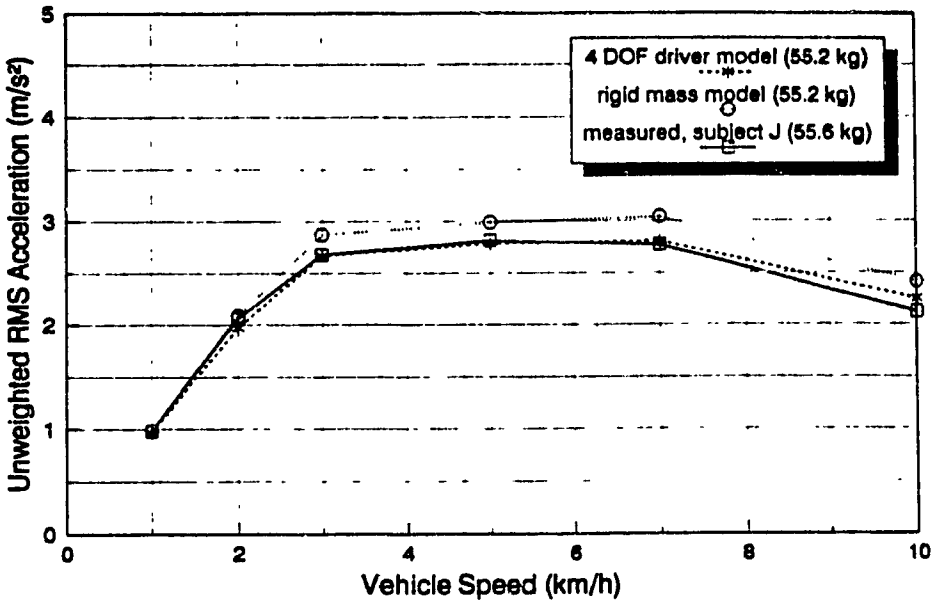

Figure 7.7 Seat unweighted rms acceleration response measured with subject J and comparison with the response computed using the combined suspension seat-human driver model and the suspension seat-rigid mass model under shock excitations.

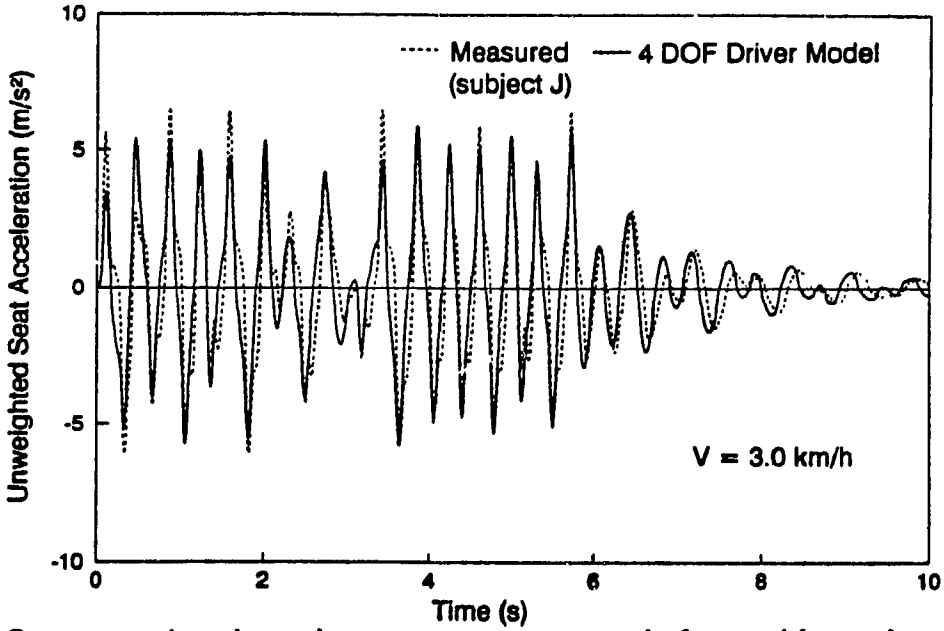

Figure 7.8 Seat acceleration time traces measured for subject J and computed using the combined suspension seat-human driver model under a 75 mm peak displacement shock input at a speed of 3 km/h.

suspension seat-human driver model. A comparison of the acceleration responses measured with the subject and the rigid mass (Figure 4.1) reveals that the seated subject yields a greater symmetry between the positive and negative peaks, indicating a better seat contact between the subject and the seat than was possible with a rigid mass load.

7.4.4 SUMMARY OF RESULTS ON MODEL VALIDATION

Although the vibration response characteristics of the combined suspension seat-human driver model are quite similar to those of the suspension seat-rigid mass model, the former exhibits slightly better correlation with the measured data under sine sweep and shock excitations. The similarities between the response characteristics of the suspension seat with rigid mass and four-DOF driver models under random excitations are attributed to the predominance of the off-road vehicle vibration at frequencies well below the primary whole-body resonant frequency. At such low frequencies, the influence of human body dynamics is less apparent. While the results of the study suggest that the combined suspension seat-human driver model provides an improved estimate of the response behaviour in an off-road vehicle environment, further refinements of the model are extremely desirable to accurately describe the response behaviour at higher frequencies.

7.5 Parametric Study of the Combined Suspension Seat-Human Driver Model

A parametric study is performed using the combined suspension seat-human driver model to study the influence of variations in the suspension seat design parameters on the whole-body vibration exposure levels. The parameter sensitivity analysis is performed in a manner analogous to that described in section 3.6 under ISO 2 excitation class and sections 4.4 and 4.5 under shock excitations. The results of the parametric sensitivity analysis are compared to those derived using the rigid driver mass to derive the influence of whole-body dynamics in defining near optimal suspension seat design parameters under random and shock excitations. The study is thus limited to an evaluation of the influence of variations in the suspension seat parameters, such as suspension stiffness K_S, suspension mass m_S, shock absorber damping coefficients C_H and C_L, and transition velocity V_S, cushion damping and stiffness coefficients C_c and K_c, Coulomb friction F_C, and compression and extension bump stop stiffnesses K_n^c and K_n^e. These parameters are varied to assume values ranging between 0.4 to 1.6 times the baseline values identified in Table 3.1.

7.5.1 PARAMETRIC SENSITIVITY ANALYSIS UNDER ISO 2 EXCITATION

Since the different performance indices identified in section 3.6.1 resulted in similar trends in the response characteristics, the parametric sensitivity

analysis is performed using the W_z-frequency-weighted rms acceleration at the driver-seat interface only. The differential equations of motion, (7.1) to (7.5), are solved in the time domain for varying suspension parameters to determine the unweighted acceleration response, $\ddot{z}_2(t)$, of mass m_4. The weighted rms acceleration is then computed using the procedure defined in section 4.3.3 with the weighting filter transfer functions given by equations (3.22), (3.23) and (3.25).

Figure 7.9 illustrates the influence of the suspension seat model parameters on W_z-frequency weighted rms acceleration response of mass m_4 of the combined suspension seat-human driver model under ISO 2 excitation class. The results obtained with the combined suspension seat-human driver model exhibit design trends similar to those observed with the rigid driver mass representation. The results, however, reveal two distinct design requirements: (i) the shock absorber high damping coefficient affects the exposure levels in a more significant manner when human body dynamics is incorporated; and (ii) a softer cushion yields a reduction in the exposure level with the human driver model, which is in contrast with the design requirements of a stiffer cushion derived from the rigid driver mass representation. The influence of cushion stiffness, however, yields only less than 5% variation in the exposure levels, as shown in Figure 7.9. Of the various suspension seat design parameters, a reduction in the low damping

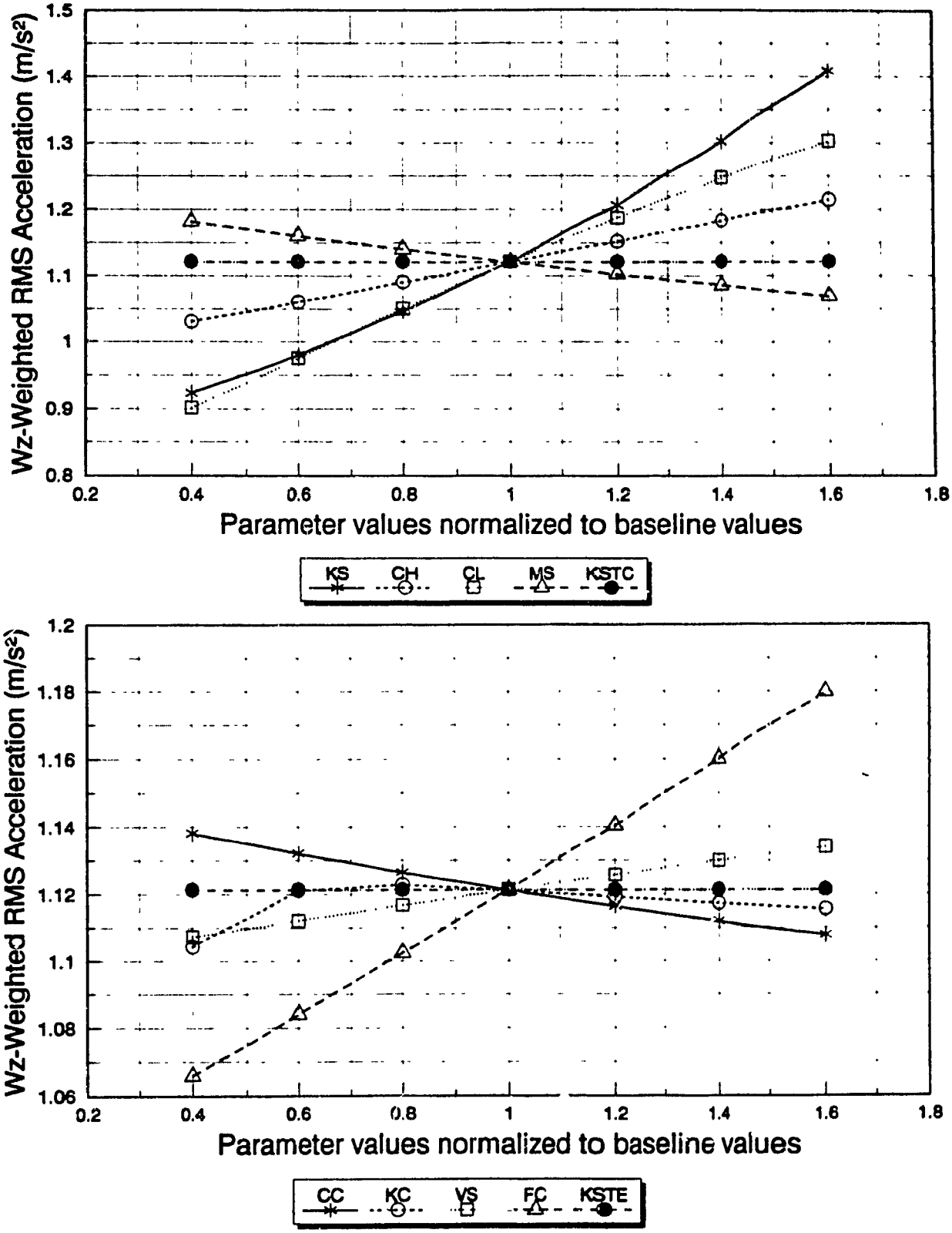

Figure 7.9 Influence of suspension seat model parameters on the overall W_z-weighted rms acceleration response of the combined suspension seat-human driver model under ISO 2 excitation.

coefficient of the shock absorber provides significant reduction (20%) in vibration exposure level. The vibration exposure levels computed from the combined suspension seat-human driver model with reduced C_L value are slightly higher than those computed from the rigid driver mass representation, although the difference is quite small. On the basis of the computed exposure levels, the seat estimated S.E.A.T. is 0.68 when the parameters are set at baseline, and 0.55 when modified to incorporate low C_L value. From the results of the parametric studies performed using the seat-driver and seat-rigid mass models, it is concluded that the selection of design parameters under ISO 2 random excitation is not affected by human body dynamics.

7.5.2 PARAMETRIC SENSITIVITY ANALYSIS UNDER SHOCK EXCITATIONS

The combined suspension seat-human driver model is coupled with the two-degree-of-freedom vehicle model, defined in section 2.5.4, to study the influence of the suspension seat design parameters on the whole-body vibration exposure levels under shock excitations. The equations of motion of the seven-DOF vehicle-suspension seat-human driver model, illustrated in Figure 7.10, are defined by equations (4.3) and (4.4) for the vehicle and (7.1) to (7.5) for the combined suspension seat-human driver models, with the relative displacement x_1 represented by equation (4.7). The parameters for the vehicle model are those defined in Table 2.3. In an effort to evaluate

the influence of the severity of the shock excitations on the driver's response, the differential equations are first solved with the model baseline parameters for different shock inputs. The shock response characteristics are derived for vehicle speeds ranging from 1 to 10 km/h and half-sine displacement inputs with peak amplitudes of 50, 100 and 150 mm, while the obstacle width is maintained at 200 mm. Since the performance index based upon the W_k-weighted rmq acceleration resulted in excellent agreement with the measured data, the results are presented in terms of W_k-weighted rmq acceleration only to assess the severity of the vibration exposure. For each shock input, the nonlinear differential equations of motion are solved in the time domain for the acceleration response $\ddot{z}_2(t)$ of mass m_4. The weighted rmq acceleration is then computed using the procedure defined in section 4.3.3 with the W_k filter transfer functions given by equations (3.22), (3.24) and (3.25).

The W_k-weighted rmq accelerations computed for mass m_4 and at the seat base for various obstacle heights and vehicle speeds are presented in Figure 7.11. The response characteristics are similar to those derived using the rigid driver mass model (Figure 4.9). The seat-driver model yields attenuation of the shock excitations over the entire range of vehicle speeds for a low obstacle height (50 mm). The interactions with the bump stops caused by large displacement obstacles, result in amplification of the shock

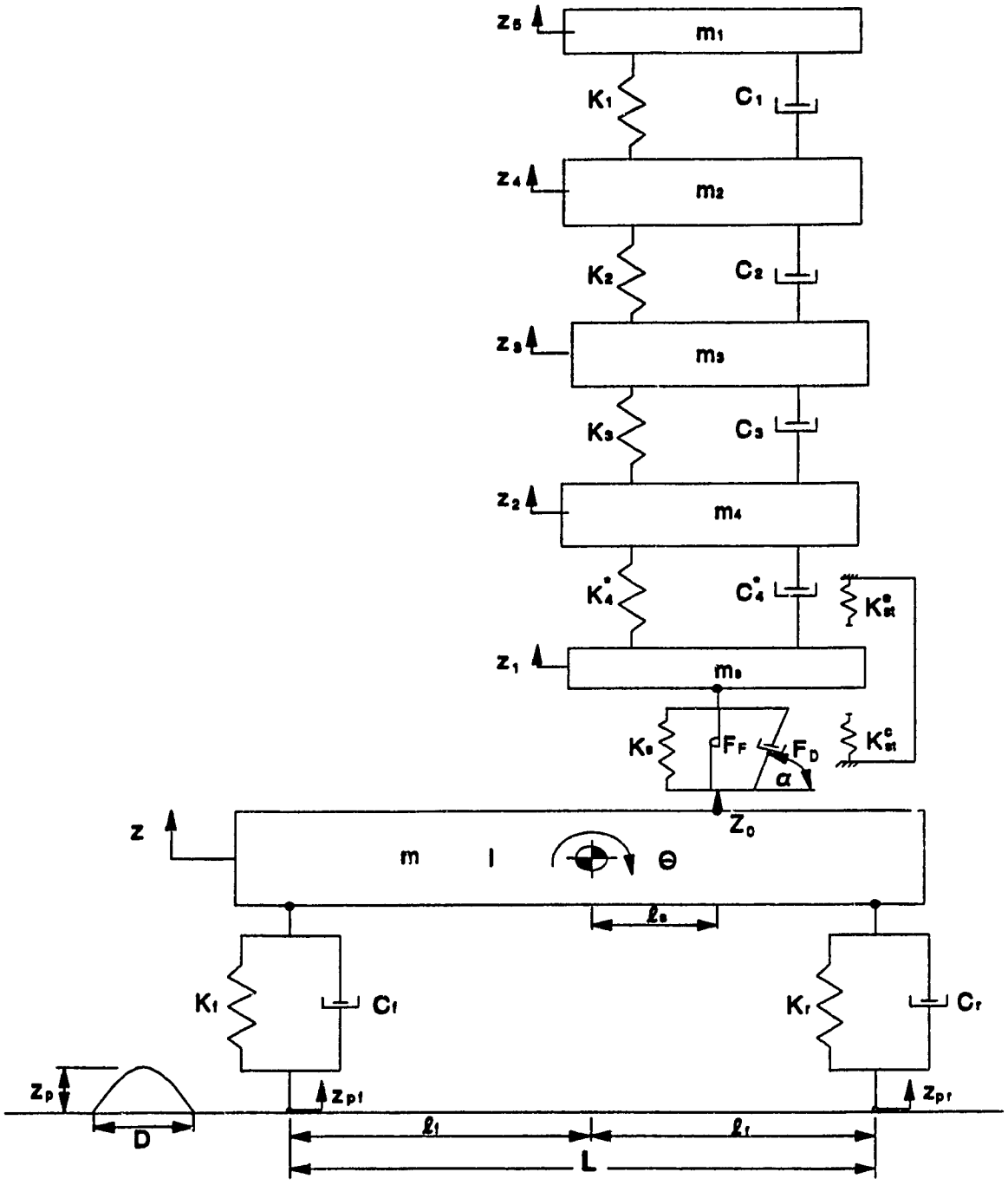

Figure 7.10 Seven-degree-of-freedom vehicle-suspension seat-human driver model representation under half-sine shock excitation input.

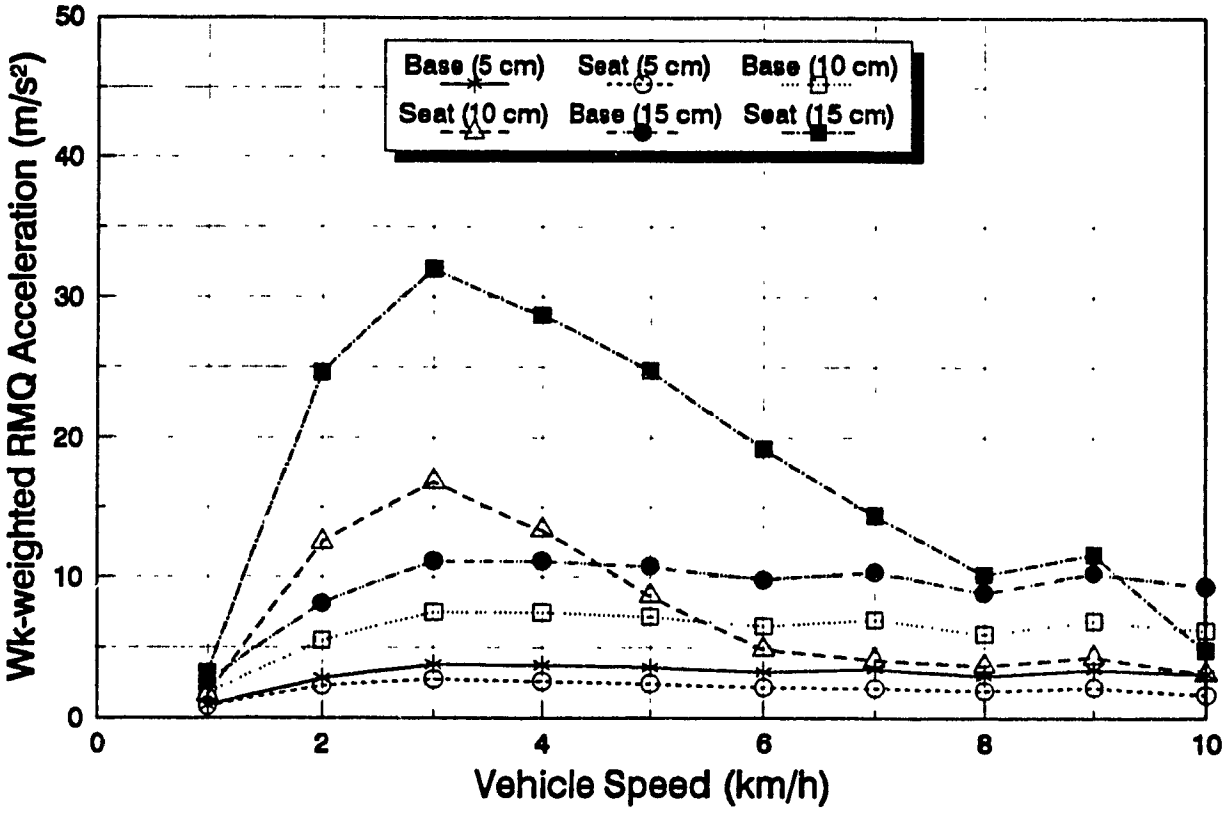

Figure 7.11 Influence of obstacle height and vehicle speed on W_k-weighted rmq accelerations derived at the base and for the combined suspension seat-human driver model subjected to vehicle shock motions.

excitations over a progressively larger speed range as the obstacle height is increased, as illustrated in Figure 7.11. At a vehicle speed of 3 km/h, the W_k-weighted rmq accelerations of mass m_4 are 2.8 ms^{-2}, 16.7 ms^{-2}, and 31.9 ms^{-2} corresponding to obstacle displacements of 50 mm, 100 mm and 150 mm, respectively. While the results are quite similar to those observed with the rigid driver model under a 50 mm shock input, the human body model yields significantly lower values of rmq acceleration under high pulse excitations when the bump stop interactions occur. The corresponding S.E.A.T. values are computed as 0.71, 2.23 and 2.87, for the three pulse displacements considered in this study. Although the human body dynamics do not affect the seat performance under low level shocks, the effect is quite noticeable when the shock excitations involve bump stop interactions. In such cases, the relative ability of the seat to attenuate the vibration appears to be significantly better than that observed with the rigid driver mass representation.

The parametric sensitivity analysis is performed to evaluate the influence of suspension seat design parameters on whole-body vibration exposure under shock inputs involving bump stop interactions (obstacle height of 100 mm) and low level shocks implying no such interactions (obstacle height of 50 mm) for a vehicle speed of 3 km/h. Figures 7.12 and 7.13 present the results of the parametric study under shock inputs of 50 mm and 100 mm

peak displacement, respectively. For a 50 mm shock input, the relative influence of the various suspension seat design parameters follows exactly the same trend as derived under ISO 2 random excitation, with the exception that the C_L damping coefficient provides lower vibration exposure levels when set at 80% of its initial value. The design guidelines are also observed to be very similar to those established using a rigid driver mass representation with the exception that a softer cushion stiffness appears beneficial when the combined suspension seat-human driver model is considered. The influence of K_c, however, is relatively small as observed earlier under ISO 2 excitation. Of the various design parameters considered, a reduction in the suspension stiffness provides the lowest exposure level, resulting in 20% lower rmq acceleration when compared to the baseline value. Almost insignificant differences are observed in the exposure levels computed using the human and rigid mass driver models under excitations arising from a 50 mm obstacle.

Under excitations arising from a 100 mm obstacle, the influence of variations in the suspension parameters on the W_k-weighted rmq acceleration response of the combined seat-driver model is quite similar to that observed with the seat-rigid mass model. The influence of the suspension parameters is almost opposite to that observed for a 50 mm obstacle, with the exception of suspension and cushion stiffness

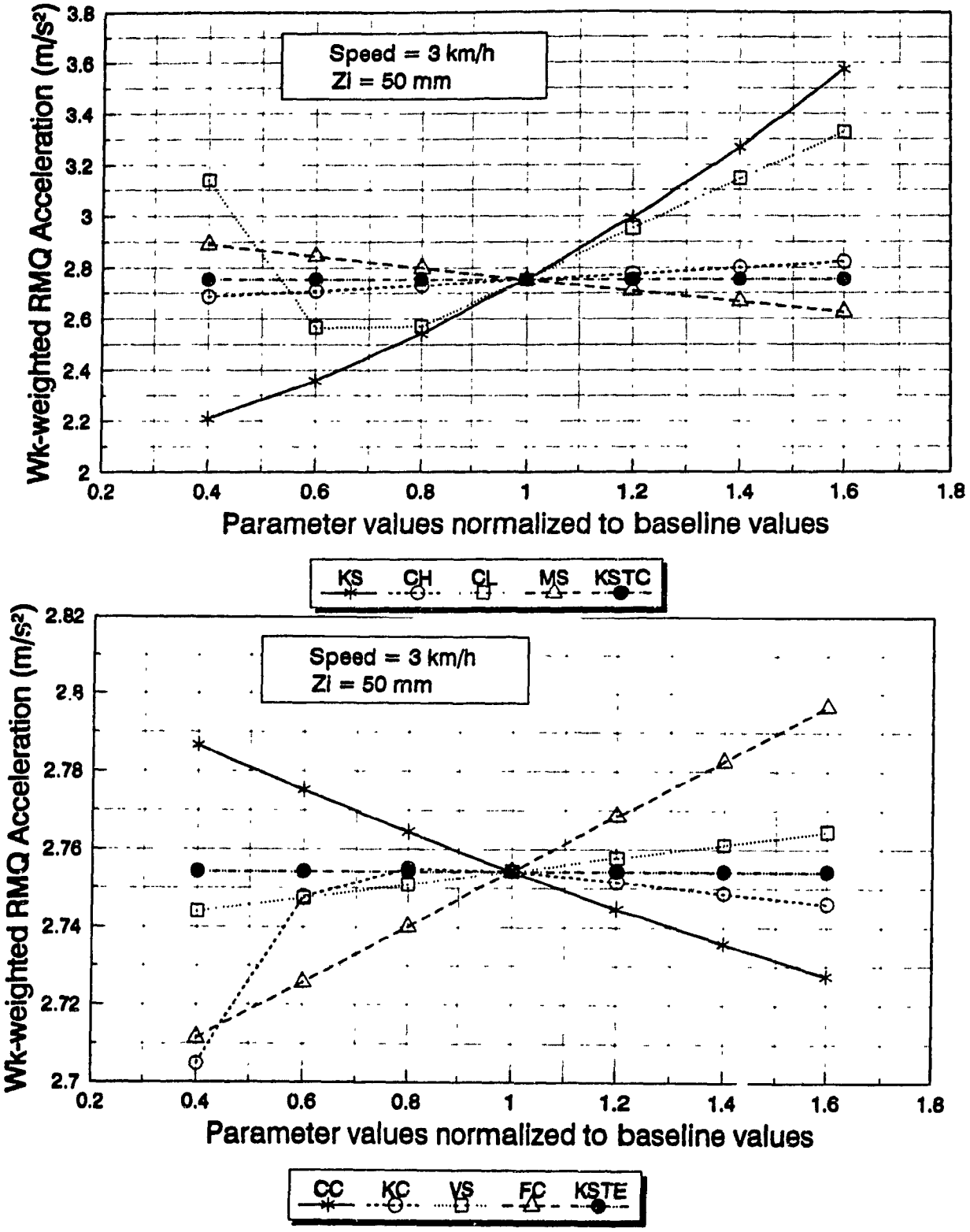

Figure 7.12 Suspension seat model parameters influence on the W_k-weighted rmq acceleration response of the combined suspension seat-human driver model for a 50 mm half-sine pulse input.

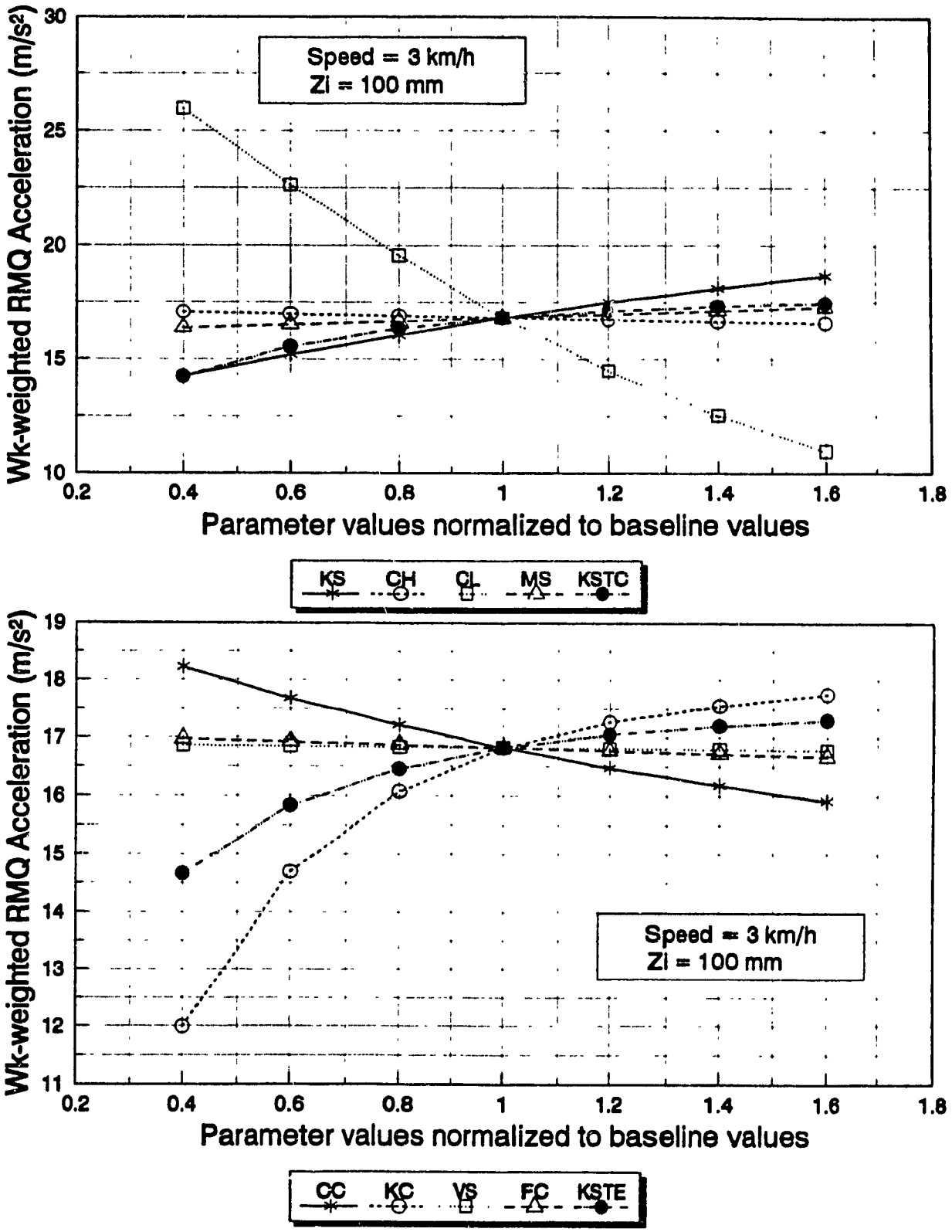

Figure 7.13 Suspension seat model parameters influence on the W_k-weighted rmq acceleration response of the combined suspension seat-human driver model for a 100 mm half-sine pulse input.

coefficients, and cushion damping coefficient. The low damping coefficient is observed to affect the exposure levels the most by providing a reduction of as much as 30% when set to a high value.

The influence of whole-body dynamics under excitations arising from a 100 mm obstacle is best seen by the fact that the exposure levels computed using the combined suspension seat-human driver model are considerably lower than those derived using the rigid driver mass representation. With suspension parameters set equal to their baseline values, the overall W_k-weighted rmq acceleration response of the seat-human driver model is almost 30% lower than that obtained with the seat-rigid mass model when high level shocks are involved. While insignificant differences in exposure levels between the two driver model representations are observed under ISO 2 and low level shocks, the difference is apparent under high level shocks. The exposure levels computed using the combined suspension seat-human driver model under a 100 mm shock input, however, remain significantly high with respect to the health criteria associated with the various assessment methods. As discussed earlier with the suspension seat-rigid mass model, the exposure to only a few single shock events of this nature within a workday would be sufficient to exceed the health criteria defined in the current and proposed revised ISO standards.

7.6 Summary

The influence of the whole-body dynamics of the driver on the vibration attenuation performance of a suspension seat is evaluated through laboratory measurements of the seat response characteristics when loaded with a rigid mass and with a human subject. A combined suspension seat-human driver model is developed and validated using the data acquired from laboratory measurements performed with a suspension seat loaded with a human subject exposed to sine sweep, random and shock excitations. The combined suspension seat-human driver model in general provides a closer agreement with the measured data, although important differences are observed within particular frequency ranges. A parametric sensitivity analysis is performed to estimate the influence of whole-body dynamics on suspension seat design parameters. Human body dynamics is observed to have a negligible contribution on the selection of suspension parameters under random vibration and low level shock excitations. The exposure levels computed under high level shock excitations, however, are strongly affected by the dynamics associated with the seated human driver.

CHAPTER 8

CAB SUSPENSION ANALYSIS

8.1 Introduction

Suspension seats, when adequately tuned for the vehicle vibration environment, provide effective attenuation of vertical vibration. The vibration attenuation performance of passive suspension seats, however, is limited by the various design constraints and the relative travel of the suspension. Alternatively, a suspension system for vehicle cab may be considered to enhance the vehicle ride quality, not only in the vertical direction, but also along the roll and pitch coordinates. Although several cab suspension designs have been proposed for heavy highway vehicles, the developments in off-road vehicle cab suspensions have been primarily limited to agricultural vehicles. Various studies on suspended cabs for tractors with dominant vibration frequency of 2.5 Hz have reported reductions in rms vibration levels of as high as 70% in the vertical direction, and 25 to 40% in the pitch mode [99]. The combined suspension seat-human driver model, presented in Chapter 7, yields a vertical unweighted rms acceleration transmissibility magnitude of 0.72 under ISO 2 excitation, representing a 28% reduction in vibration for the seat alone. A further reduction in transmitted vibration could perhaps be realized through a combined cab-seat suspension system. Apart from the attenuation of vertical vibration, a suspension at the cab offers considerable potentials to reduce the

pitch and roll components of ride vibration, which are almost equally significant.

Longitudinal and, more particularly, the lateral components of vibration encountered in wheeled off-road vehicles have been found to be most significant at the driver-seat interface [29]. While a few suspension seats incorporating a longitudinal isolator have been developed, the attenuation of lateral vibration predominant at frequencies around 1 Hz, has not yet been attempted. Isolation of such low frequency lateral vibration by passive means would undoubtedly involve excessive motion of the driver, interference with the tasks, and safety hazards. Alternatively, a suspension at the cab may result in reduction in the lateral and longitudinal vibration through attenuation of the roll and pitch components of ride vibration, while improving the vertical attenuation offered by the suspension seat alone. The design of a cab-seat suspension, however, necessitates the selection of adequate cab and seat suspension parameters. The natural frequencies of the cab suspension associated with various modes should ideally be much lower than the dominant excitation frequencies and the natural frequency of the suspension seat in the bounce mode. A low natural frequency cab suspension is thus highly desirable, implying that a compromise be made between increased attenuation of vibration and excessive relative displacement of the suspension.

In this chapter, a mathematical model of an off-road vehicle suspended cab

supported at the four corners is developed and validated experimentally along with the suspension seat model defined previously. A prototype cab suspension system is developed in the laboratory and measurements are performed under sinusoidal bounce and roll, and bounce and pitch excitations. Upon validation, a parametric study is carried out to select appropriate cab suspension design parameters to better protect the driver from excessive vibration.

3.2 Suspended Cab and Seat Model Development

The cab suspension is idealized as a combination of four linear springs and nonlinear dampers installed at the corners of a log skidder cab, manufactured by Timberjack. Figure 8.1 illustrates a schematic representation of the cab-seat suspension model. Each cab suspension unit is represented by a parallel combination of a linear spring K_i (K_1, K_2, K_3, and K_4), and nonlinear damping coefficients C_i (C_1, C_2, C_3, and C_4). The suspension seat model with rigid driver mass, developed in Chapters 3 and 4, is integrated to the cab suspension model, as shown in the figure. The nonlinear damping coefficients, C_i, assume high and low values, C_{Hi} and C_{Li}, depending upon the relative velocities, V_{Ri}, across the dampers. The location of the cab center of gravity with respect to the suspension elements is represented by the distances a_3 and a_2 in the pitch plane, and by b_1 and b_2, in the roll plane. Similarly, the location of the suspension seat with respect to the line passing through the cab center

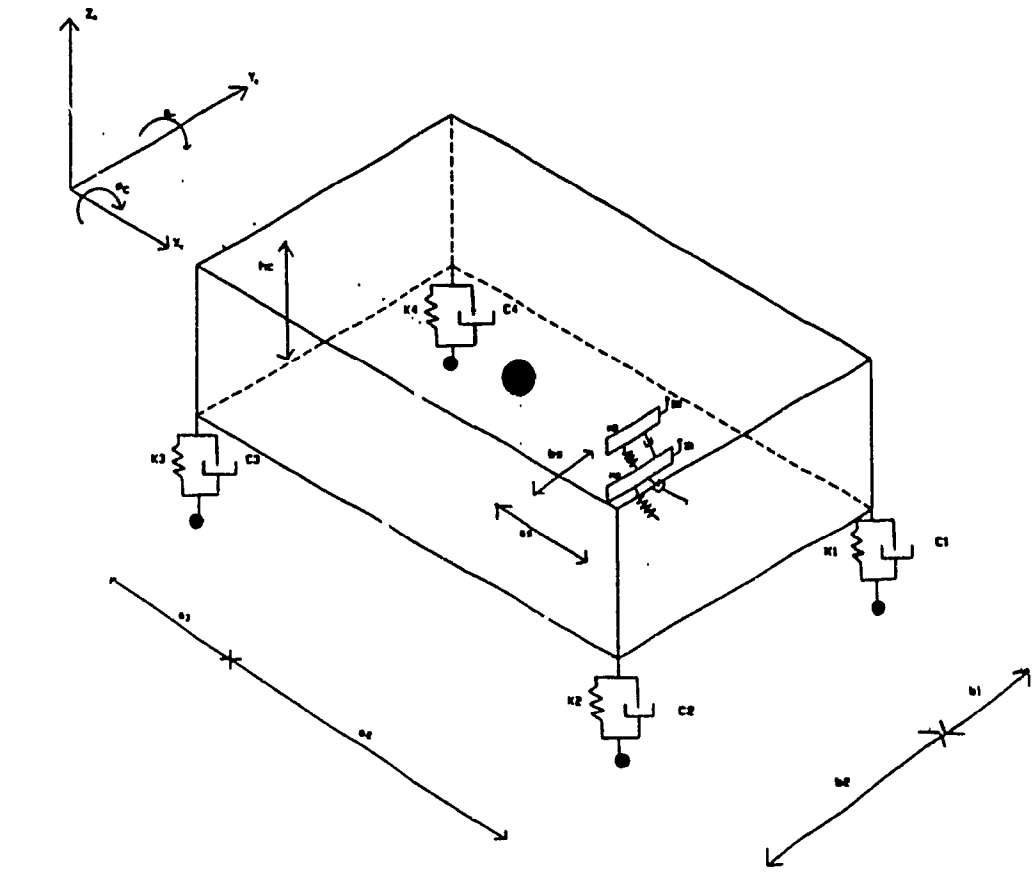

a) Pitch Plane

b) Roll Plane

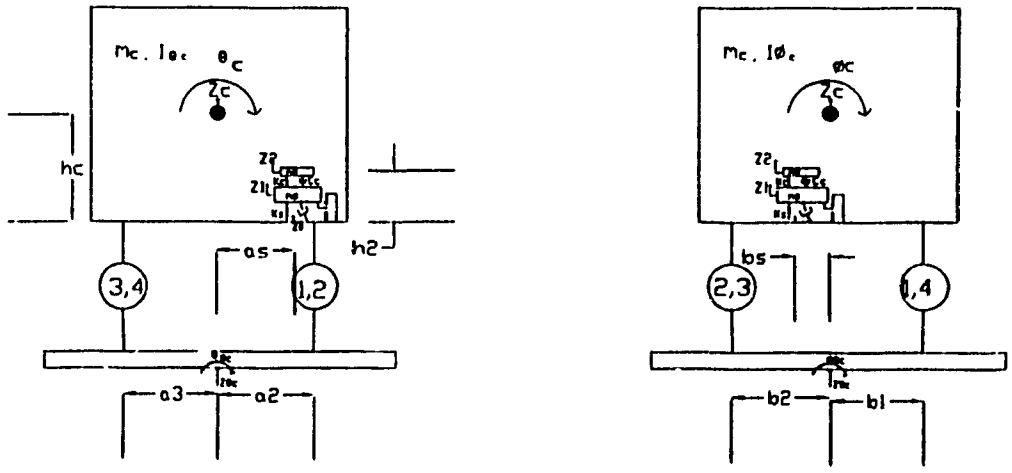

Figure 8.1 Schematic of a suspended cab supported on four corner mounts and equipped with a suspension seat. a) pitch-plane, and b) roll plane representations.

of gravity is represented by a_s in the pitch plane, and by b_s in the roll plane. The height of the cab center of gravity with respect to the cab floor is represented by h_c, while that of the driver mass on the suspension seat is denoted by h_2. z_{0c}, θ_{0c} and ϕ_{0c} represent the vibration excitations encountered at the chassis along the vertical, pitch and roll coordinates, respectively. z_c, θ_c, and ϕ_c are the corresponding response coordinates at the cab c.g. The vertical input to the suspension seat is represented by z_0, while z_1 and z_2 denote the response coordinates of the seat suspension and driver mass, respectively. The differential equations of motion for the five-degree-of-freedom combined suspended cab and suspension seat, derived assuming small motion, are expressed as:

CAB BOUNCE:

$$m_c\ddot{z}_c+\sum_{i=1}^{4}F_{Ki}+\sum_{i=1}^{4}F_{di}-F_K(x_1)-F_F(\dot{x}_1)-F_S(x_1,\beta)-F_D(\dot{x}_1,\alpha)=0 \qquad (8.1)$$

CAB PITCH:

$$\begin{aligned}&I_{\theta c}\ddot{\theta}_c-a_2(F_{K1}+F_{K2}+F_{d1}+F_{d2})+a_3(F_{K3}+F_{K4}+F_{d3}+F_{d4})+\\&a_s\left[F_K(x_1)+F_F(\dot{x}_1)+F_S(x_1,\beta)+F_D(\dot{x}_1,\alpha)\right]=0\end{aligned} \qquad (8.2)$$

CAB ROLL:

$$\begin{aligned}&I_{\phi c}\ddot{\phi}_c-b_1(F_{K1}+F_{K4}+F_{d1}+F_{d4})+b_2(F_{K2}+F_{K3}+F_{d2}+F_{d3})+\\&b_s\left[F_K(x_1)+F_F(\dot{x}_1)+F_S(x_1,\beta)+F_D(\dot{x}_1,\alpha)\right]=0\end{aligned} \qquad (8.3)$$

SEAT SUSPENSION BOUNCE:

$$m_s\ddot{z}_1 + F_K(x_1) + F_F(\dot{x}_1) + F_S(x_1,\beta) + F_D(\dot{x}_1,\alpha) - F_c(x_2,\dot{x}_2) = 0 \qquad (8.4)$$

DRIVER MASS BOUNCE:

$$m_0\ddot{z}_2 + F_c(x_2,\dot{x}_2) = 0 \qquad (8.5)$$

where the relative displacements, x_1 and x_2, are given by:

$$\begin{aligned} x_1 &= z_1 - z_0 = z_1 - z_c + a_s\theta_c + b_s\phi_c \\ x_2 &= z_2 - z_1 \end{aligned} \qquad (8.6)$$

m_c, $I_{\theta c}$, and $I_{\phi c}$ are the cab mass, and pitch and roll mass moments of inertia of the cab about its c.g. F_{Ki} are the cab suspension forces due to the linear springs, given by:

$$\begin{aligned} F_{K1} &= K_1\left[(z_c - a_2\theta_c - b_1\phi_c) - (z_{0c} - a_2\theta_{0c} - b_1\phi_{0c})\right] \\ F_{K2} &= K_2\left[(z_c - a_2\theta_c + b_2\phi_c) - (z_{0c} - a_2\theta_{0c} + b_2\phi_{0c})\right] \\ F_{K3} &= K_3\left[(z_c + a_3\theta_c + b_2\phi_c) - (z_{0c} + a_3\theta_{0c} + b_2\phi_{0c})\right] \\ F_{K4} &= K_4\left[(z_c + a_3\theta_c - b_1\phi_c) - (z_{0c} + a_3\theta_{0c} - b_1\phi_{0c})\right] \end{aligned} \qquad (8.7)$$

The damping forces developed by the cab suspension shock absorbers, F_{di}, are given by:

$$F_{di} = \begin{cases} C_{Hi} V_{Ri} & |V_{Ri}| \le V_0 \\ C_{Hi} V_0 \operatorname{sgn}(V_{Ri}) + C_{Li}\left[V_{Ri} - V_0 \operatorname{sgn}(V_{Ri})\right] & |V_{Ri}| \ge V_0 \end{cases} \qquad i = 1,2,3,4 \qquad (8.8)$$

where V_0 is the preset velocity of the blow-off valves within the shock absorbers, and V_{Ri} is the relative velocity across damper i, given by:

$$\begin{aligned} V_{R1} &= \left(\dot{z}_c - a_2\dot{\theta}_c - b_1\dot{\phi}_c\right) - \left(\dot{z}_{0c} - a_2\dot{\theta}_{0c} - b_1\dot{\phi}_{0c}\right) \\ V_{R2} &= \left(\dot{z}_c - a_2\dot{\theta}_c + b_2\dot{\phi}_c\right) - \left(\dot{z}_{0c} - a_2\dot{\theta}_{0c} + b_2\dot{\phi}_{0c}\right) \\ V_{R3} &= \left(\dot{z}_c + a_3\dot{\theta}_c + b_2\dot{\phi}_c\right) - \left(\dot{z}_{0c} + a_3\dot{\theta}_{0c} + b_2\dot{\phi}_{0c}\right) \\ V_{R4} &= \left(\dot{z}_c + a_3\dot{\theta}_c - b_1\dot{\phi}_c\right) - \left(\dot{z}_{0c} + a_3\dot{\theta}_{0c} - b_1\dot{\phi}_{0c}\right) \end{aligned} \qquad (8.9)$$

The forces associated with the suspension seat are the same as given in Chapter 3, with x_1 described by equation (8.6). Equations (8.1) through (8.9), together with equations (3.2) to (3.7) describe the dynamics of the combined cab-seat suspension system.

8.3 Experimental Evaluation of the Combined Cab-Seat Suspension

A laboratory prototype, comprising a Timberjack log skidder cab supported on four corner-mounted suspension units, was fabricated to experimentally evaluate a cab-seat suspension system and to validate the analytical model. Each suspension unit consisted of an inclined hydraulic shock absorber

concentric about a coil spring. The SIFRA suspension seat loaded with sandbags was installed in the cab at a specific location. Appropriate test fixtures were constructed to mount the suspended cab on two vertical electro-hydraulic vibration exciters capable of providing pure vertical motion when set in phase, and vertical and roll or pitch motions when a phase difference was introduced between the exciters.

8.3.1 DETERMINATION OF THE CAB INERTIAL CHARACTERISTICS

Figure 8.2 illustrates the geometry of the Timberjack log skidder cab. The investigation of the ride performance potentials via analytical means necessitates the identification of cab parameters, such as cab mass (m_c), location of c.g., and roll and pitch mass moments of inertia ($I_{\phi c}$, and $I_{\theta c}$).

The centre of gravity of the cab was determined by suspending the cab from various edges and by identifying the point of convergence of the various lines of action of the vertical weight component. The roll and pitch mass moments of inertia of the cab were determined experimentally from natural oscillations of the cab supported on cylindrical edges and soft springs. For determining the pitch mass moment of inertia, the rear part of the cab was supported on two cylindrical edges, while the front was supported on two soft springs, as shown in Figure 8.3. An accelerometer was mounted on the cab floor to measure the oscillations of the cab caused by a transient excitation induced through a

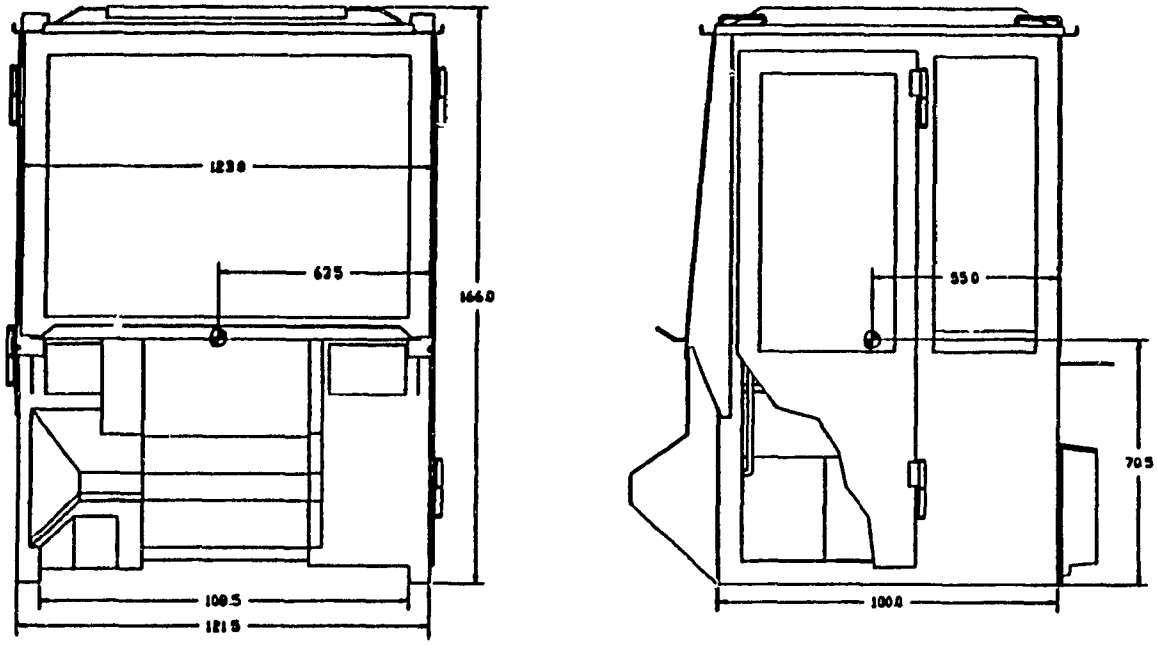

Figure 8.2 Schematic of the Timberjack log skidder cab considered in the study.

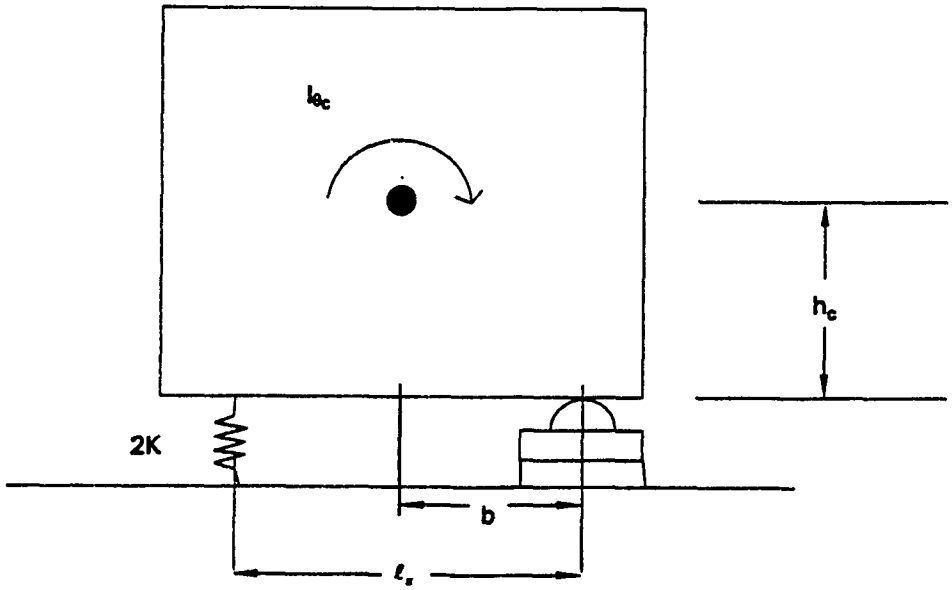

Figure 8.3 Schematic of the set-up used to determine the cab pitch mass moment of inertia.

hammer. The pitch mass moment of inertia was then derived from the measured natural period of pitch oscillations ($\tau_{n\theta}$) and the cab geometry:

$$I_{\theta c} = \frac{2K\ell_x^2}{(2\pi)^2}\tau_{n\theta}^2 - m_c(h_c + b)^2 \qquad (8.10)$$

where K is the spring rate of each supporting springs, ℓ_x is the longitudinal distance between the edge and the springs, b is the longitudinal distance between the c.g. and the edge supports, and h_c is the height of the cab c.g.

When performing the measurements, the following parameter values were used: K = 64.08 kN/m, ℓ_x = 0.915 m, h_c = 0.64 m, b = 0.5175 m, and m_c = 531.8 kg. The natural period of pitch oscillation, $\tau_{n\theta}$, was estimated as 0.667 s. The pitch mass moment of inertia was thus computed as 496.6 kg m^2.

In a similar manner, the roll mass moment of inertia was determined by supporting the left-hand side of the cab on the same two springs, while the right-hand rested on cylindrical edge supports. The roll mass moment of inertia was derived from the natural period of oscillation in the roll mode ($\tau_{n\phi}$) and the cab geometry, in the following manner:

$$I_{\phi c} = \frac{2K\ell_y^2}{(2\pi)^2}\tau_{n\phi}^2 - m_c(h_c + d)^2 \qquad (8.11)$$

where the lateral distance between the edge and the spring supports, ℓ_y, was fixed at 0.723 m, and the lateral distance between the edges and the cab centre of mass, d, was determined as 0.5925 m. The measured period of roll oscillations was found to be 0.875 s, yielding a roll mass moment of inertia of 491.4 kg m^2. Table 8.1 summarizes the inertial properties of the cab.

TABLE 8.1

Inertial Properties and Dimensions of the Cab

CHARACTERISTICS	SYMBOL	VALUE
Cab mass (kg)	m_c	531.8
CAB DIMENSIONS		
Height (m)	-	1.66
Length (m)	-	1.0
Width (m)	-	1.085
MASS MOMENT OF INERTIA		
Pitch (kg m^2)	$I_{\theta c}$	496.6
Roll (kg m^2)	$I_{\phi c}$	491.4
CENTRE OF MASS COORDINATES		
Height (m)	h	0.64
Pitch plane front (m)	a_3	0.44
Pitch plane rear (m)	a_2	0.33
Roll plane left (m)	b_2	0.51
Roll plane right (m)	b_1	0.46

8.3.2 CHARACTERIZATION OF THE CAB SUSPENSION COMPONENTS

Each corner-mounted suspension unit used for supporting the cab consisted of

a slightly inclined parallel combination of hydraulic shock absorber and coil spring. The coil springs were selected such that the uncoupled bounce natural frequency of the cab, f_{nc}, would occur well below the dominant excitation frequency, f, of a typical off-road vehicle. Assuming small inclination, the uncoupled vertical mode natural frequency of the cab may be estimated from:

$$f_{nc} = \frac{1}{2\pi}\sqrt{\frac{4K_i}{m_c}} \tag{8.12}$$

The uncoupled bounce mode natural frequency can be further related to the static deflection of the suspension springs, δ:

$$f_{nc} = \frac{1}{2\pi}\sqrt{\frac{g}{\delta}} \tag{8.13}$$

where g is the acceleration due to gravity.

Since the vertical vibration of a wheeled off-road vehicle predominates in the neighbourhood of 2.5 Hz [29], the cab suspension parameters thus need to be selected to yield vertical natural frequency lower than 1.8 Hz in order to achieve vibration isolation. However, a relative travel of 100 mm has often been considered as the upper tolerable limit on vertical displacement to provide

a stable floor for the driver [40]. Considering the relative travel to be equal to the static deflection, equation (8.13) reveals that the cab natural frequency should not be lower than 1.6 Hz. The cab suspension design parameters must then be established based on a suitable compromise between increased vibration attenuation and acceptable suspension travel.

The coil spring stiffness of the suspension units used for validating the model was estimated from the force-displacement characteristics of individual springs. Their spring rate was estimated as 23.454 kN/m. The corresponding bounce uncoupled natural frequency of the cab and the static suspension deflection were thus derived as 2.1 Hz and 55.6 mm, respectively. Although the prototype suspension springs do not conform with the design requirements stipulated above, these were considered acceptable for the purpose of model validation.

The cab suspension shock absorbers were selected and modified to achieve high damping coefficient due to bleed circuit at low piston velocities, and low damping coefficient at higher velocities due to multi-stage blow-off valve, as shown previously in Figure 3.2. The shock absorbers, manufactured by Fox Racing Shox, were designed such that the transition velocity, V_0, and damping coefficients , C_{Hi} and C_{Lo} , during bleed and blow-off stages respectively, could be tuned using interchangeable bleed shaft and blow-off springs. The shock

absorbers were tested in the laboratory to establish their force-velocity characteristics. The tests were performed for sinusoidal excitations in the 0.5 to 8 Hz frequency range, with peak displacement amplitudes of 0.635 and 1.27 cm. Figure 8.4 illustrates the force-velocity characteristics of the damper measured under 0.635 cm peak excitation amplitude. From the measured data, the following shock absorber design characteristics were derived: C_H = 1875 Ns/m, C_L = 660 Ns/m, and V_0 = 0.07 m/s.

8.3.3 EXPERIMENTAL SET-UP

The cab supported on four inclined corner-mounted coil springs and shock absorbers was fixed on two vibration exciters, as shown in Figure 8.5. The preload of each spring was adjusted in order to account for the varying load distribution of the cab. Although the electro-hydraulic vibration exciters could only generate pure vertical motions, rotational roll and pitch motions were realized by introducing a phase between the two exciters, using a multi-channel phase synthesizer. The two vibration exciters could provide vertical motions up to ±7.5 cm in the 0 - 50 Hz frequency range, and forces up to 16.6 kN.

A cab support chassis was designed and fabricated, and the cab was mounted on the chassis through the suspension units. The chassis was supported on the two vibration exciters using spherical bearings and a pair of slider mechanisms, as shown in Figure 8.6. The SIFRA suspension seat loaded with

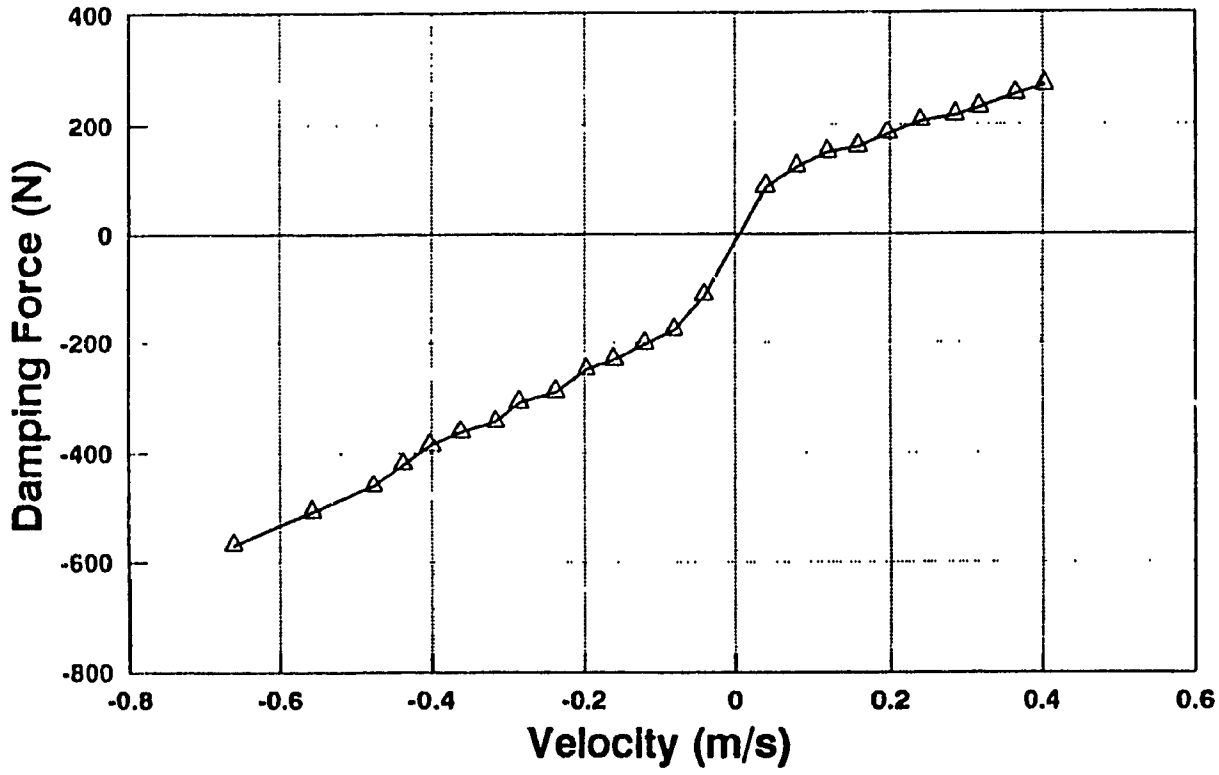

Figure 8.4 Force-velocity characteristics of the shock absorbers used as part of the cab suspension units measured under 0.635 cm peak displacement sinusoidal excitations.

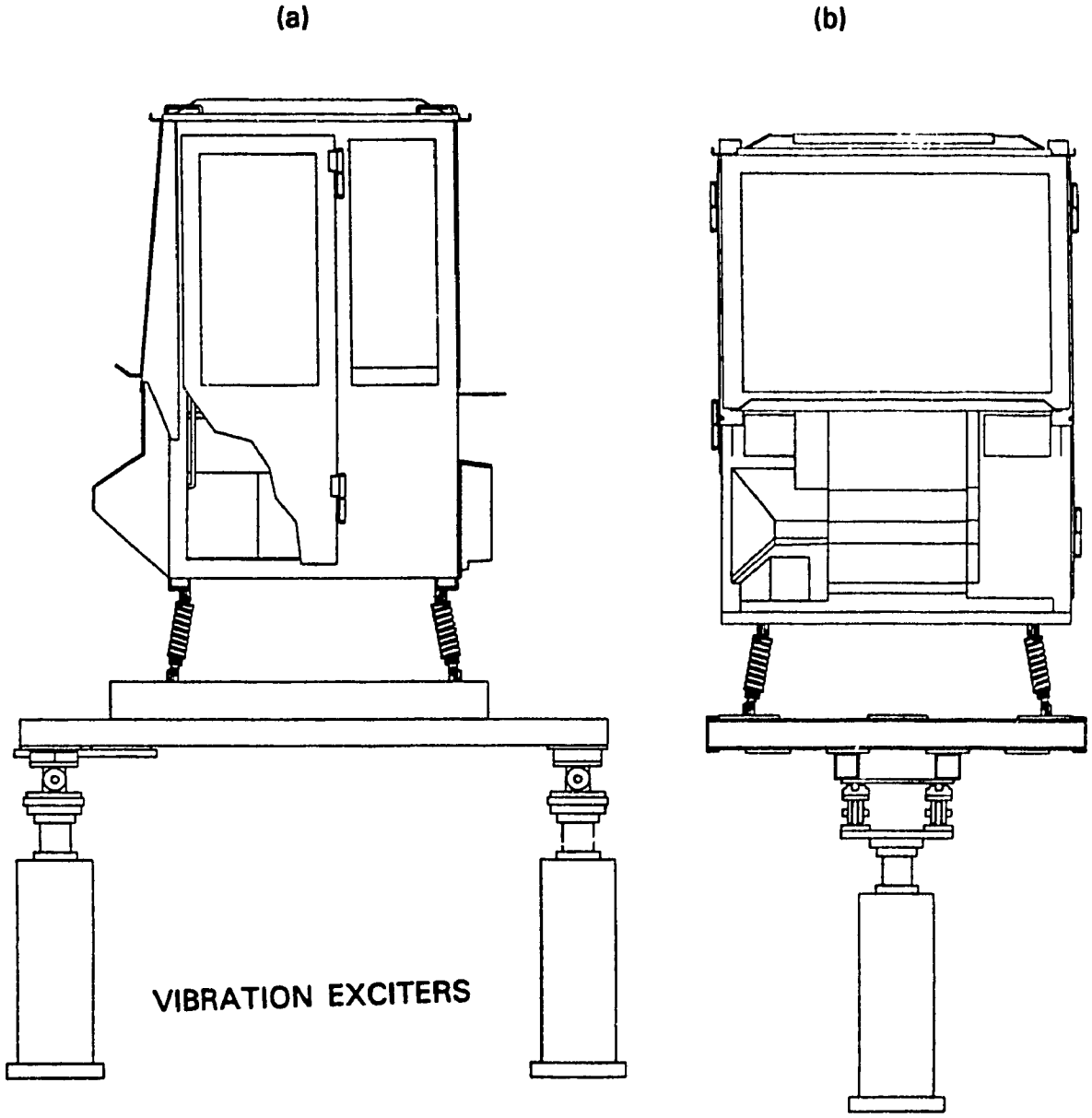

Figure 8.5 Schematic diagram of the suspended cab supported on two electro-hydraulic exciters: a) Side view (pitch plane); b)Front view (pitch plane).

(a)

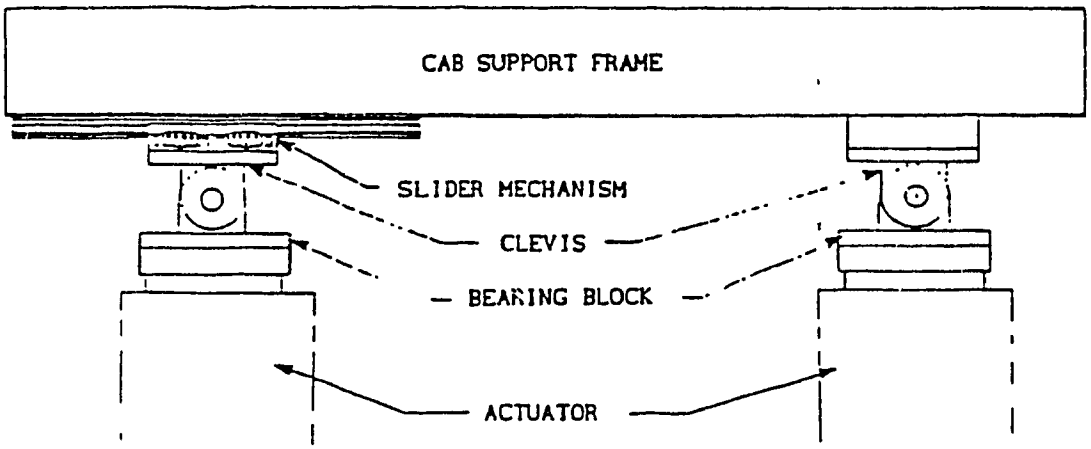

(b)

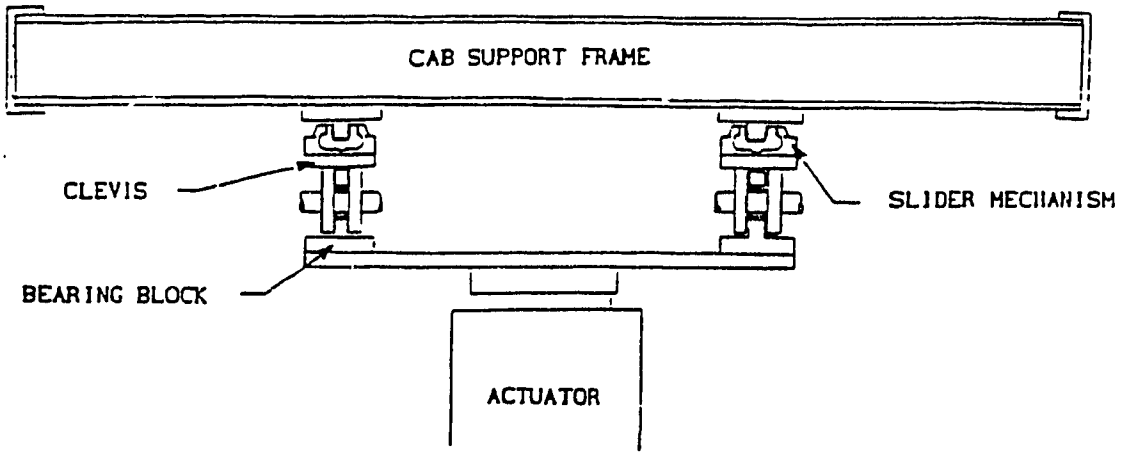

Figure 8.6 Schematic of the cab-chassis supported on two electro-hydraulic vibration exciters: a) Front view (roll plane); b) Side view (roll plane).

sandbags of total mass of 63.6 kg was installed in the cab at a location defined in Figure 8.1, close to the cab c.g. (a_s =0.02 m, and b_s = 0.04 m).

The tests were performed separately in two-planes: vertical-longitudinal or pitch plane, and vertical-lateral or roll plane, by appropriately orienting the cab on the two exciters. Five linear accelerometers and a triaxial seat accelerometer were used to measure the vertical and rotational excitations and the corresponding responses at the cab floor and at the seat-mass interface. Two accelerometers were mounted at the chassis of the cab, one at each exciter support separated by a distance d_o, to monitor the cab input excitations along the vertical axis, given by the accelerations $\ddot{x}_{01}$ and $\ddot{x}_{02}$, respectively. An accelerometer was fixed on the cab floor at a position in line with the centre of mass to monitor the cab vertical acceleration response, $\ddot{z}_c$. Two additional accelerometers were fixed on the cab floor to measure the pitch rotational motion by placing the accelerometers at a fixed distance apart ($d_{3\theta}$) on each side of the cab centre of gravity along the longitudinal cab axis. The corresponding accelerations measured by the two accelerometers were referred to as $\ddot{x}_{3\theta}$ and $\ddot{x}_{4\theta}$. The same two accelerometers were also used to measure the roll acceleration by placing the accelerometers on the lateral axis during tests performed in the roll plane, separated by a distance $d_{3\phi}$. The accelerations measured in the roll plane were referred to as $\ddot{x}_{3\phi}$ and $\ddot{x}_{4\phi}$. Finally, only the vertical axis acceleration, $\ddot{z}_2$, at the mass-seat interface was monitored, at a distance h_2 above the cab floor.

The rotational cab excitation and response motions in pitch and roll were estimated from linear vertical accelerations measured at different locations on the cab floor. Pure bounce excitation, $\ddot{z}_{0c}$, was realized by driving the vibration exciters with constant amplitude harmonic motions (0.625 cm peak) in the 0.5 to 7.0 Hz frequency range, without any phase difference between them. Pitch and roll excitations were realized by introducing a 30° phase difference between the exciters, in their respective planes. From the measured linear vertical accelerations, the roll and pitch excitation and cab response accelerations were computed using a differential analog circuit performing the following computations:

PITCH PLANE: $$\ddot{\theta}_{0c} = \frac{\ddot{x}_{01} - \ddot{x}_{02}}{d_0} \quad ; \quad \ddot{\theta}_c = \frac{\ddot{x}_{3\theta} - \ddot{x}_{4\theta}}{d_{3\theta}} \tag{8.14}$$

ROLL PLANE: $$\ddot{\phi}_{0c} = \frac{\ddot{x}_{01} - \ddot{x}_{02}}{d_0} \quad ; \quad \ddot{\phi}_c = \frac{\ddot{x}_{3\phi} - \ddot{x}_{4\phi}}{d_{3\phi}} \tag{8.15}$$

PURE BOUNCE: $$\ddot{z}_{0c} = \ddot{x}_{01} = \ddot{x}_{02} \tag{8.16}$$

8.4 Validation of the Cab-Seat Suspension Model

The combined cab-seat suspension model developed in section 8.2 is validated by comparing its response characteristics with those derived from the experiments performed on the prototype suspension. The response characteristics of the analytical model are derived through numerical integration

of the coupled differential equations of motion, under pure bounce excitation, and under combined bounce and pitch, and bounce and roll excitations. The model validation is performed with respect to performance indices defined on the basis of translational and rotational acceleration transmissibility functions, expressed as the ratio of the peak acceleration amplitude response to the peak excitation acceleration amplitude at specific frequencies. Four performance indices are defined based on:

- the cab vertical acceleration transmissibility, $T_{zc}(f)$;
- the driver mass vertical acceleration transmissibility, $T_{zs}(f)$;
- the cab pitch acceleration transmissibility, $T_{\theta c}(f)$;
- the cab roll acceleration transmissibility, $T_{\phi c}(f)$.

These transmissibility functions are defined as:

$$T_{zc}(f)=\frac{|\ddot{z}_c(f)|}{|\ddot{z}_0(f)|} \qquad T_{zs}(f)=\frac{|\ddot{z}_2(f)|}{|\ddot{z}_0(f)|}$$
$$T_{\theta c}(f)=\frac{|\ddot{\theta}_c(f)|}{|\ddot{\theta}_0(f)|} \qquad T_{\phi c}(f)=\frac{|\ddot{\phi}_c(f)|}{|\ddot{\phi}_0(f)|} \tag{8.17}$$

The vertical and rotational excitations for the analytical model, z_{0c}, θ_{0c}, and ϕ_{0c},

are computed using the measured linear accelerations and the kinematic relationships.

Under pure bounce, both exciters were driven in phase with the same amplitude of sinusoidal excitation. The vertical displacement excitation acting at the suspended cab center of gravity could then be expressed as:

$$z_{0c} = |z_{0c}| \sin \omega t \tag{8.18}$$

where $|z_{0c}|$ represents the peak displacement amplitude at angular frequency ω, corresponding to the peak excitation amplitude $|x_{01}|$ and $|x_{02}|$ at the two exciters. Since there was no phase difference between the two vibration exciters for generating pure bounce, the peak displacement amplitude at the cab centre of gravity was the same as that applied at the exciters.

In order to incorporate roll and pitch excitations, a phase difference was introduced between the two vibration exciters. In the roll plane, the bounce and roll excitations in line with the cab centre of gravity are represented by:

$$\begin{aligned} z_{0c} &= |z_{0c}| \sin(\omega t - \psi_1) \\ \phi_{0c} &= |\phi_{0c}| \sin(\omega t - \psi_2) \end{aligned} \tag{8.19}$$

where the peak excitation amplitudes and phases at frequency ω are a direct function of the phase difference between the two vibration exciters and the horizontal distances between the exciters and the cab centre of gravity. In the pitch plane, the excitations in line with the cab centre of gravity are represented as:

$$z_{0c} = |z_{0c}| \sin(\omega t - \psi_1)$$
$$\theta_{0c} = |\theta_{0c}| \sin(\omega t - \psi_2) \qquad (8.20)$$

On the basis of a 30° phase difference between the exciters, and on a vertical peak displacement amplitude of 0.625 cm at the exciter supports, corresponding values of amplitude and phase characteristics of the excitations in line with the cab centre of gravity are computed. These are derived for the three types of input, and their values are listed in Table 8.2.

TABLE 8.2

Peak Excitation Amplitude and Phase under Bounce, Roll and Pitch.

Excitation	$\lvert z_{0c} \rvert$ (mm)	ψ_1 (degrees)	$\lvert \theta_{0c} \rvert$ (x 10^{-4}rad)	ψ_2 (degrees)	$\lvert \phi_{0c} \rvert$ (x 10^{-4}rad)	ψ_2 (degrees)
Pure Bounce	6.25	0	-	-	-	-
Roll Plane	6.04	14.70	-	-	17.98	285
Pitch Plane	6.04	14.15	17.98	285	-	-

From the computed time response motions at each excitation frequency, the transmissibility functions defined by equations (8.17) are calculated by dividing the peak acceleration response amplitude by the peak excitation at each frequency.

8.4.1 MODEL VALIDATION UNDER PURE BOUNCE EXCITATION

Figures 8.7 and 8.8 present a comparison of the measured and analytical vertical vibration transmissibility of the cab and the driver mass, respectively, under a pure bounce excitation of 6.25 mm peak displacement. The results show reasonable agreement between the analytical and the measured response characteristics, specifically at excitation frequencies greater than the vertical mode natural frequency. The model response, however, differs from the measured response at low excitation frequencies. The discrepancies at low frequencies are attributed to Coulomb friction due to the cab suspension, which was assumed negligible in the model. The measured acceleration transmissibility of the cab mass reveals near lock-up of the suspension at frequencies below 1.4 Hz.

The analytical and measured transmissibility characteristics illustrated in Figures 8.7 and 8.8 reveal a vertical mode cab natural frequency in the neighbourhood of 1.7 Hz, while that of the combined cab and seat is computed as 1.5 Hz. The measured and computed transmissibility at the cab floor are found to be

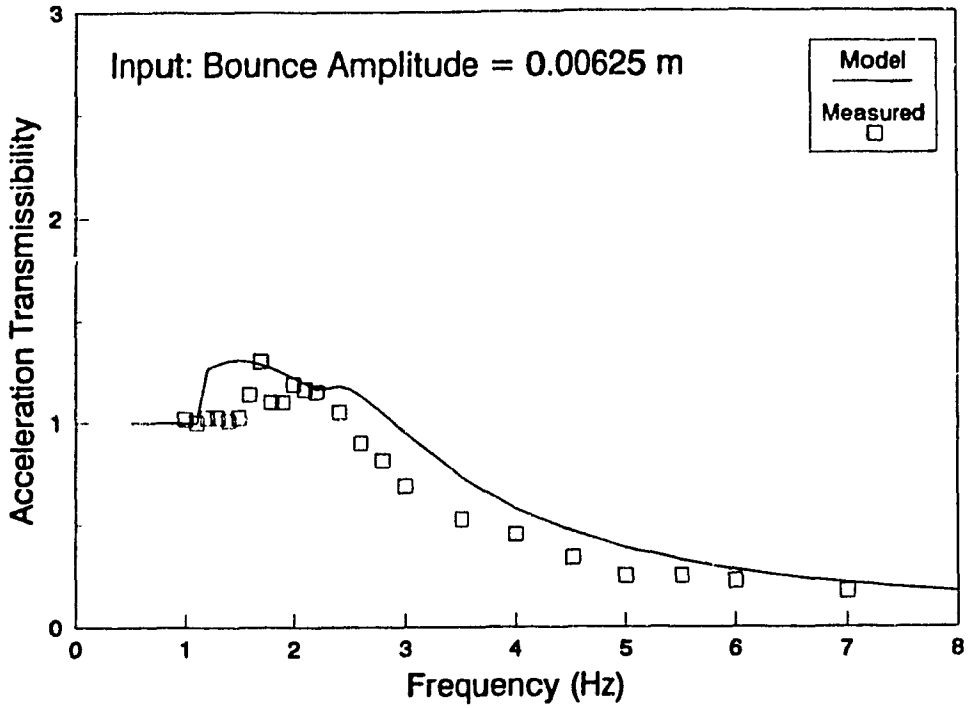

Figure 8.7 Comparison of measured and model computed vertical acceleration transmissibility at the cab floor under pure bounce.

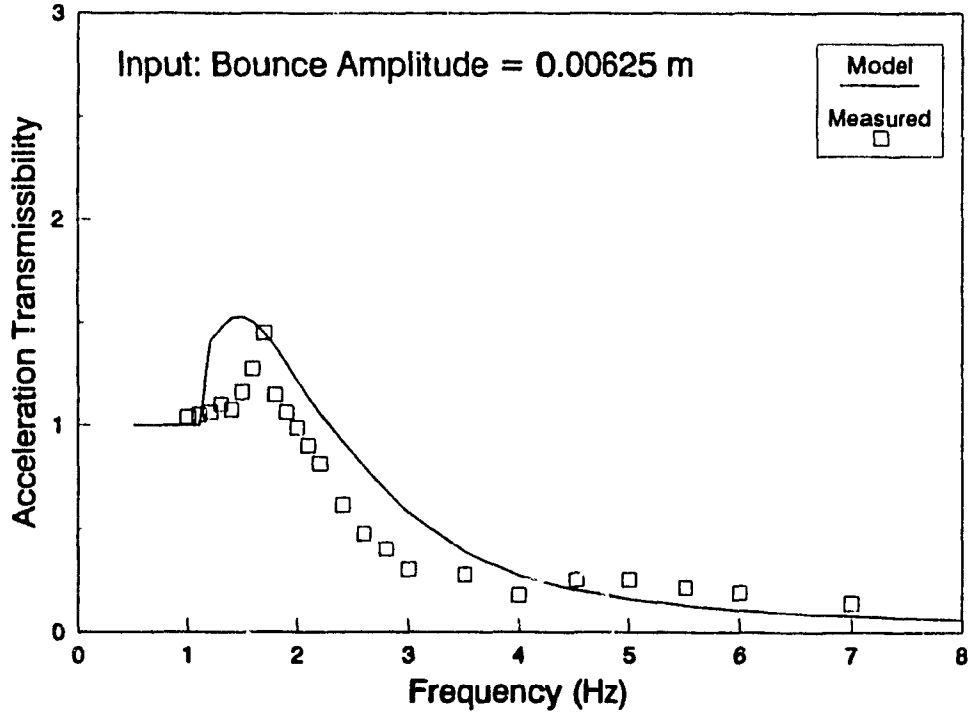

Figure 8.8 Comparison of measured and model computed vertical acceleration transmissibility at the driver mass under pure bounce.

within 40 % at frequencies above resonance, while differences as large as 100% are noted at specific frequencies at the driver mass level. The transmissibility computed from the model at the driver mass tends to be larger than measured in the 1.7 to 4.5 Hz frequency range, indicating that too large a damping coefficient might have been assumed for the cab suspension.

Figure 8.9 presents a comparison of the analytical vertical acceleration transmissibility response characteristics of the cab and cab-seat suspensions. At frequencies above 2 Hz, the combined cab-seat suspension provides superior vibration attenuation. The suspension seat resonance at lower frequencies, however, yields poor performance. The combined cab and seat yield an acceleration transmissibility of 0.83 at the predominant excitation frequency of 2.5 Hz, compared to 0.76 for the seat suspension alone. An improved attenuation performance of the cab-seat suspension can be realized only by selecting either lower natural frequency or significantly lower cab suspension damping.

8.4.2 MODEL VALIDATION UNDER BOUNCE AND ROLL EXCITATIONS

Figures 8.10 and 8.11 provide a comparison of measured and model response in terms of vertical acceleration transmissibility under bounce and roll excitations. The results are observed to be almost identical to those obtained under pure bounce excitation, indicating negligible contributions due to roll.

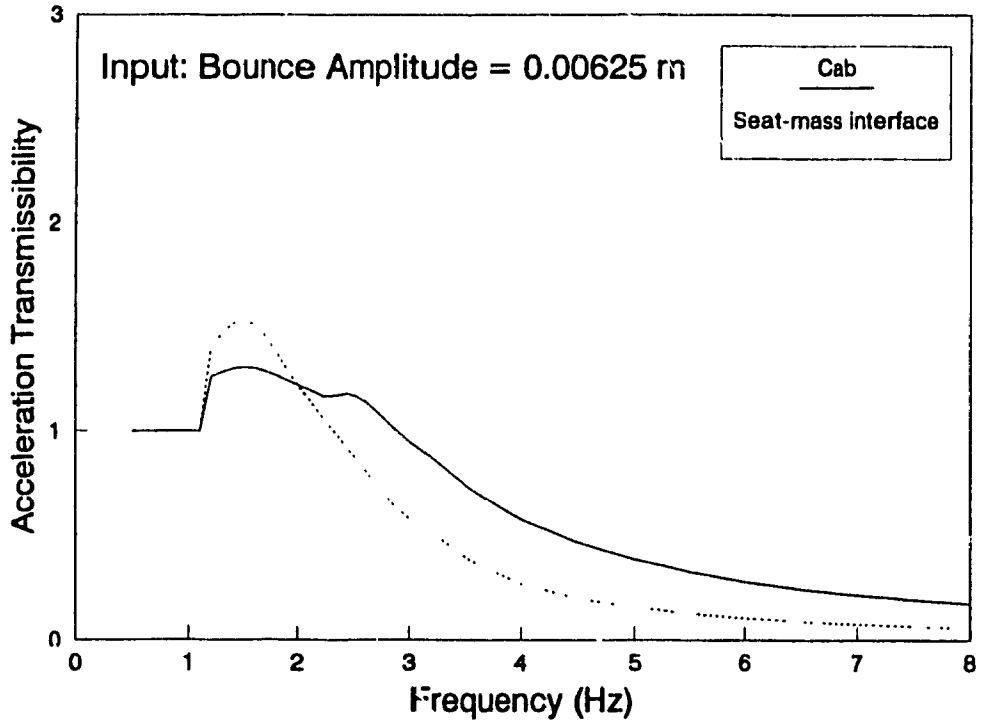

Figure 8.9 Comparison of model computed vertical acceleration transmissibility at the cab floor and at the driver mass under pure bounce.

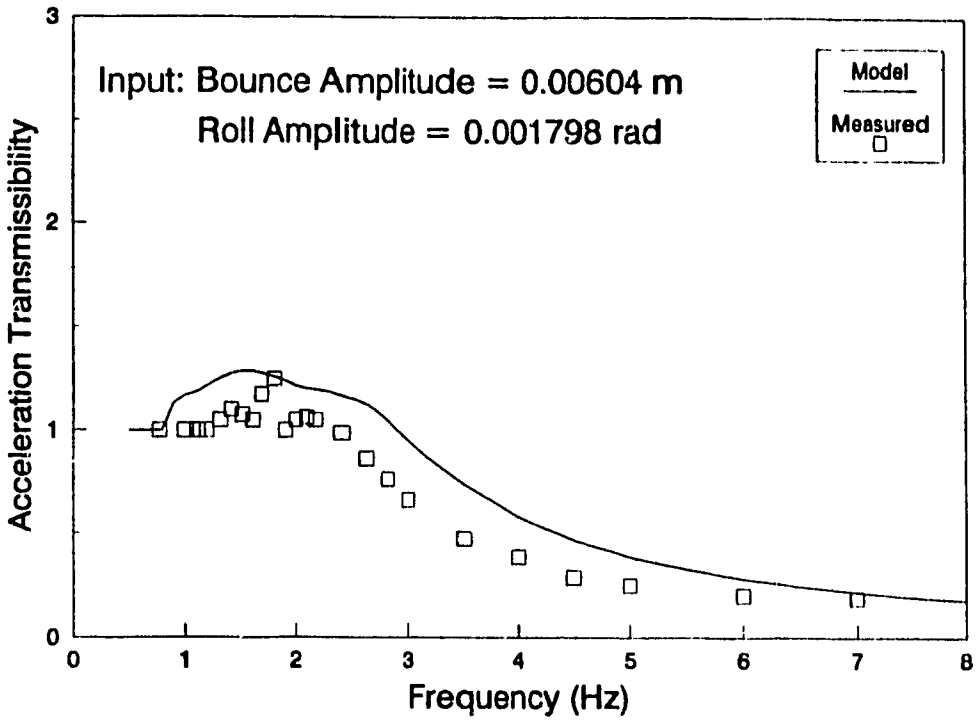

Figure 8.10 Comparison of measured and model computed vertical acceleration transmissibility at the cab floor under a combination of bounce and roll.

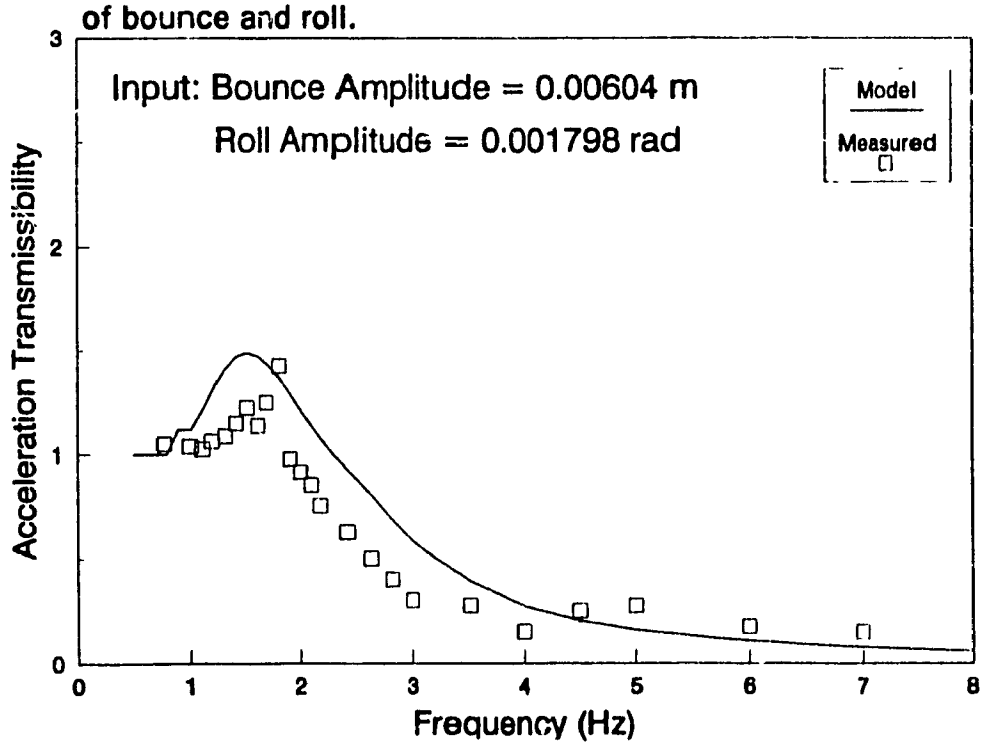

Figure 8.11 Comparison of measured and model computed vertical acceleration transmissibility at the driver mass under a combination of bounce and roll.

Figure 8.12 illustrates a comparison of measured and analytical roll acceleration transmissibility characteristics, $T_{\ddot{\phi}c}(f)$. The experimental results exhibit a peak around 4.5 Hz, which was attributed to excessive yawing of the cab caused by the fixture design and unequal preloads of the different suspension units. The measured and analytical roll natural frequencies of the combined cab and seat suspension are observed near 1.3 Hz and 1.1 Hz, respectively. Apart from important differences between the computed and measured roll acceleration transmissibility in the neighbourhood of the resonant frequency and within the 3-6 Hz frequency range, the model response correlates reasonably well with the measured results.

8.4.3 MODEL VALIDATION UNDER BOUNCE AND PITCH EXCITATIONS

Figure 8.13 provides a comparison of the measured and the computed model response in terms of vertical acceleration transmissibility at the cab floor under combined bounce and pitch excitations. While the results are very similar to those obtained under bounce and roll excitations, the model response correlates quite well with the measured results. The analytical pitch natural frequency of the combined cab and seat is observed to be approximately 1.0 Hz as shown by the pitch acceleration transmissibility in Figure 8.14, although no experimental data was available to validate the pitch transmissibility response.

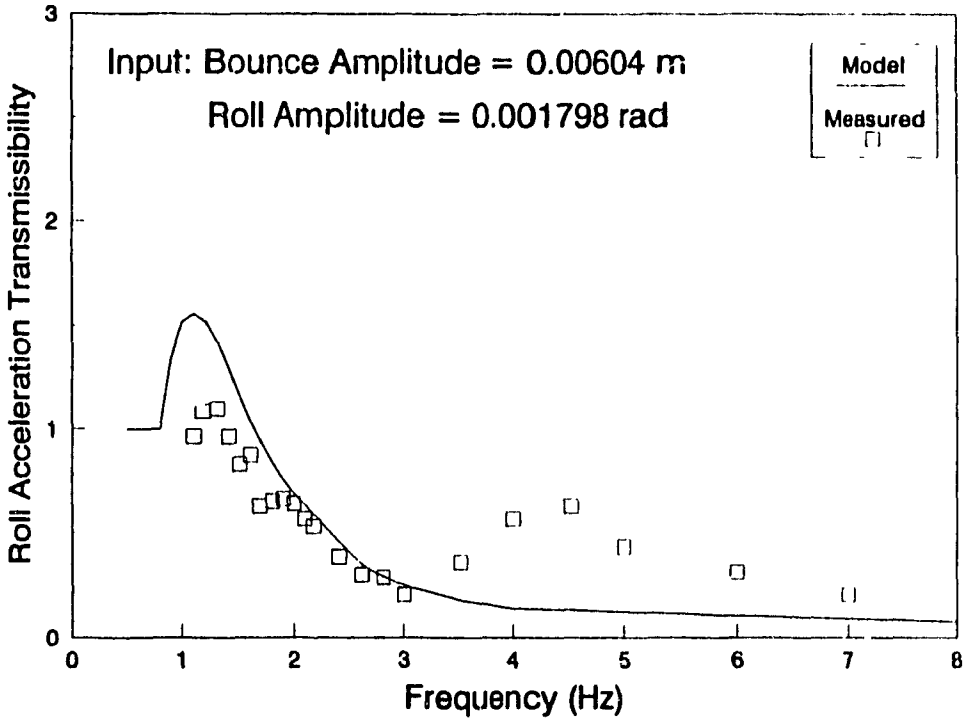

Figure 8.12 Comparison of measured and model computed roll acceleration transmissibility at the cab under a combination of bounce and roll.

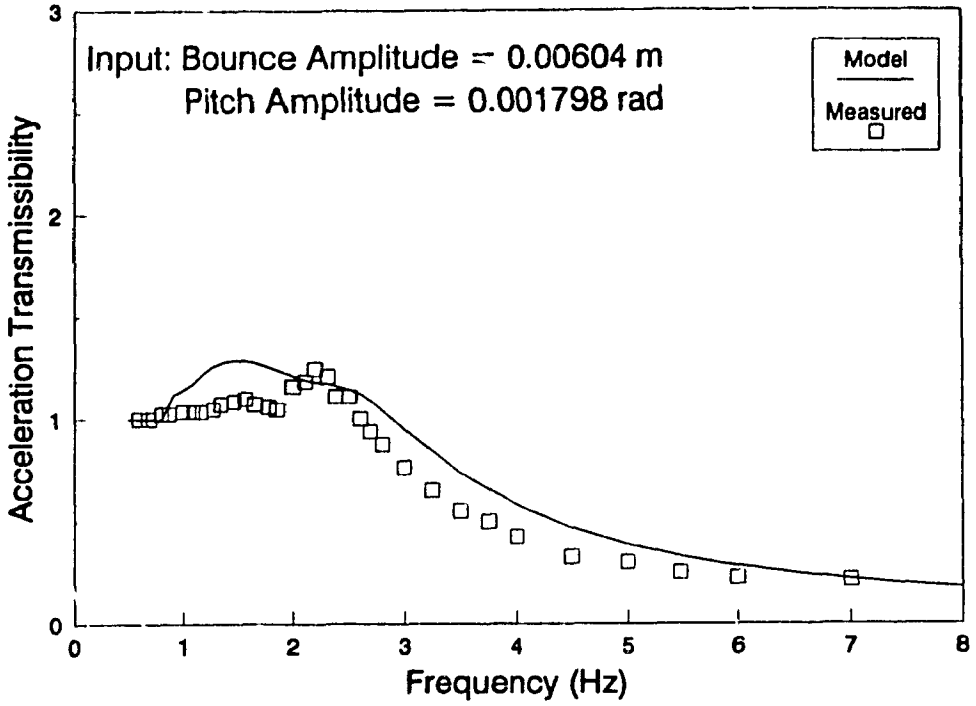

Figure 8.13 Comparison of measured and model computed vertical acceleration transmissibility at the cab floor under a combination of bounce and pitch.

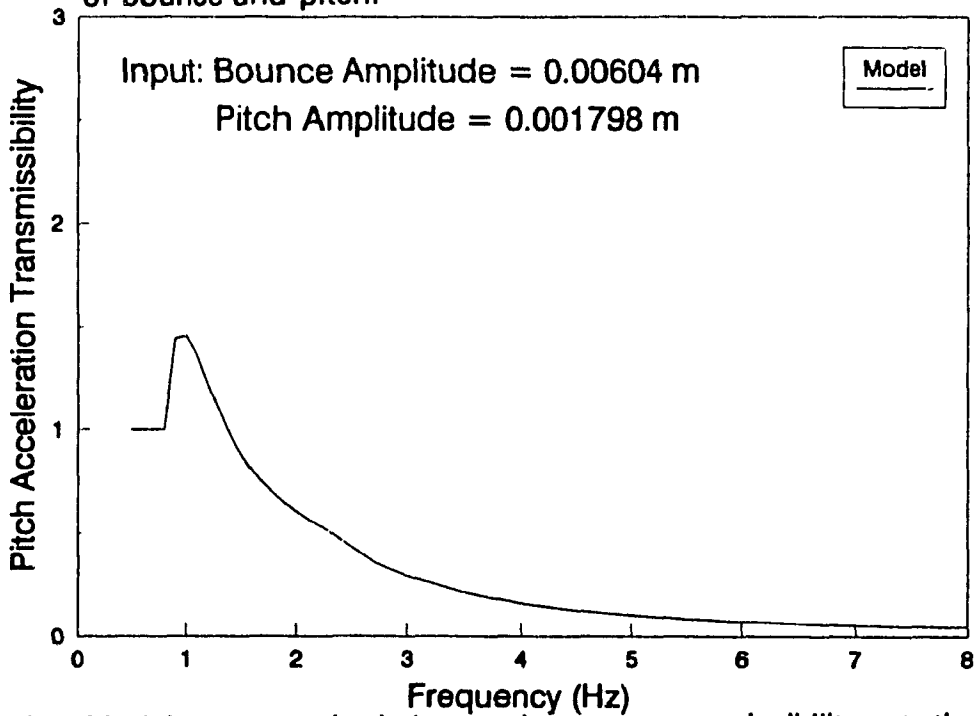

Figure 8.14 Model computed pitch acceleration transmissibility at the cab under a combination of bounce and pitch.

In view of the relatively small distance between the exciters and the cab center of gravity location, the magnitude of roll and pitch excitations was thus quite small. This explains the insignificant effect on vertical acceleration transmissibility resulting from the combined vertical and rotatory motions, as shown in Figures 8.15 and 8.16 for the cab and the driver mass, respectively. Except at very low frequency (near 1 Hz), pitch and roll do not add any significant contributions to the computed vertical acceleration transmissibility.

8.5 Cab-Seat Suspension Response to Random Excitations

The combined cab-seat suspension model validated under pure sinusoidal excitations is used to determine the driver and cab response under random excitations encountered in off-road forestry vehicles. The typical random excitations are derived from field measurements performed on log skidder vehicles. The vertical acceleration levels measured at the front and rear axles on both sides of the vehicle and at the chassis are analyzed to determine the vertical, roll and pitch components of the vibration transmitted to the cabin. The acceleration PSD spectra of the excitations revealed dominant vertical vibration near 1.8 Hz, roll vibration near 1.4 Hz and pitch vibration near 0.9 Hz. The corresponding magnitudes of rms excitation acceleration were observed as 1.32 ms^{-2} in bounce, 0.74 rad/s^2 in pitch and 1.135 rad/s^2 in roll.

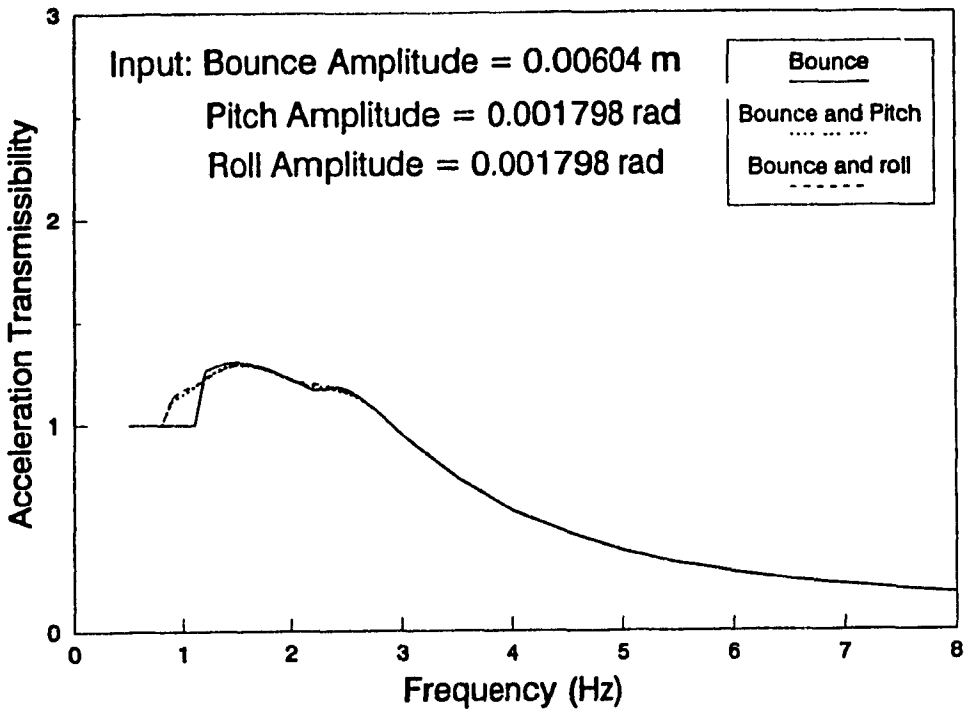

Figure 8.15 Comparison of model computed vertical acceleration transmissibility at the cab floor under pure bounce, and under a combination of bounce and pitch and bounce and roll.

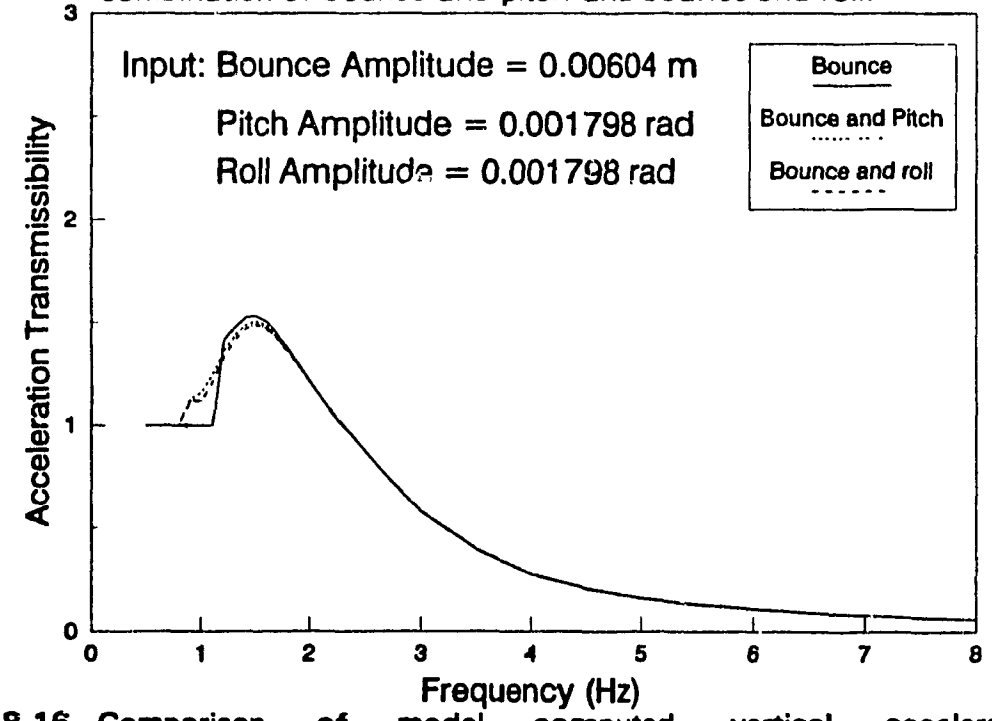

Figure 8.16 Comparison of model computed vertical acceleration transmissibility at the driver mass under pure bounce, and under a combination of bounce and pitch and bounce and roll.

The coupled differential equations of motion for the cab-seat suspension model are solved in the time domain using the field measured vertical, roll and pitch excitations. The cab model parameters are selected as those used for the model validation under sinusoidal excitations. The resulting driver mass and cab centre of gravity acceleration response are expressed in terms of acceleration PSD using the FFT algorithm. The PSD response characteristics along with the excitations are shown in Figures 8.17 to 8.20 for a suspended cab with baseline parameter values. From the figures, it is apparent that the baseline cab suspension yields significant amplification of the cab chassis excitations, implying that the suspension tuning must be performed to effectively attenuate the skidder vibration, which predominates at relatively low frequency. The rms acceleration corresponding to the PSD responses shown in the figures are 3.29 ms^{-2} for the driver mass bounce, 2.15 ms^{-2} for the cab c.g. bounce, 1.12 and 2.18 rad/s^2 for cab pitch and cab roll, respectively. These represent significant amplification of the rms accelerations of the measured excitations at the chassis. The amplification of the cab chassis vertical excitation is observed to be larger at the driver mass than at the cab centre of gravity indicating that a rigid seat would perhaps be more appropriate in a suspended cab with baseline parameters. With the cab suspension baseline parameters, the cab natural frequencies for the various modes of vibration coincide with the frequencies at which the excitation is dominant, thus creating amplification. A parametric study is thus carried out to select appropriate cab

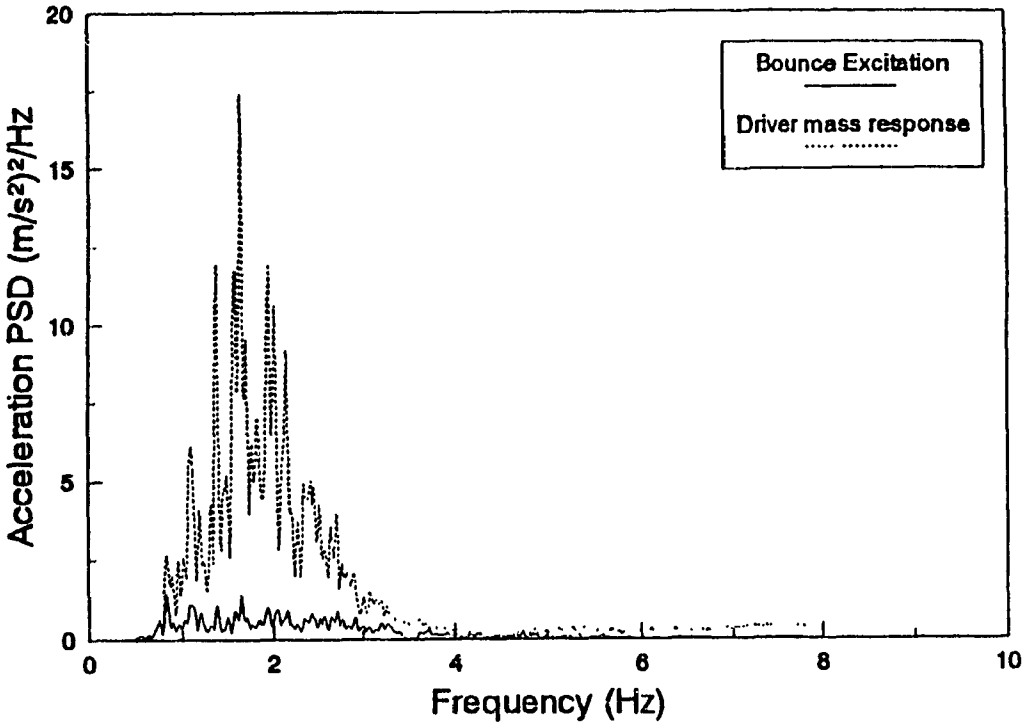

Figure 8.17 PSD of driver mass acceleration response to the bounce excitation shown for a cab with baseline suspension parameters.

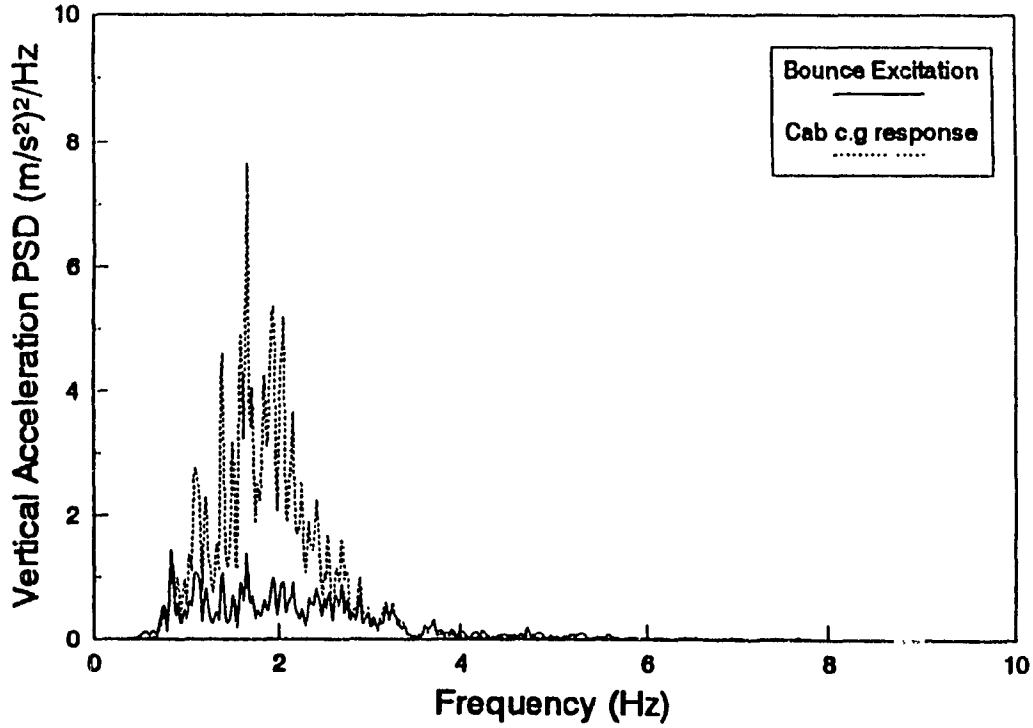

Figure 8.18 PSD of cab centre of gravity acceleration response to the bounce excitation shown for a cab with baseline suspension parameters.

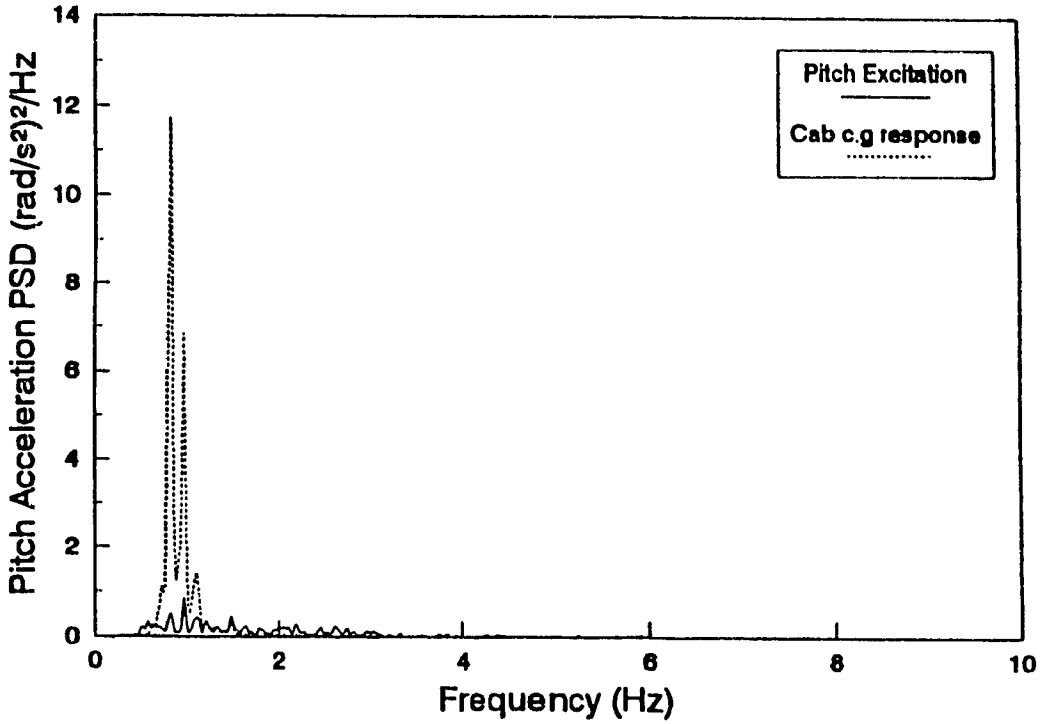

Figure 8.19 PSD of cab centre of gravity pitch acceleration response to the pitch excitation shown for a cab with baseline suspension parameters.

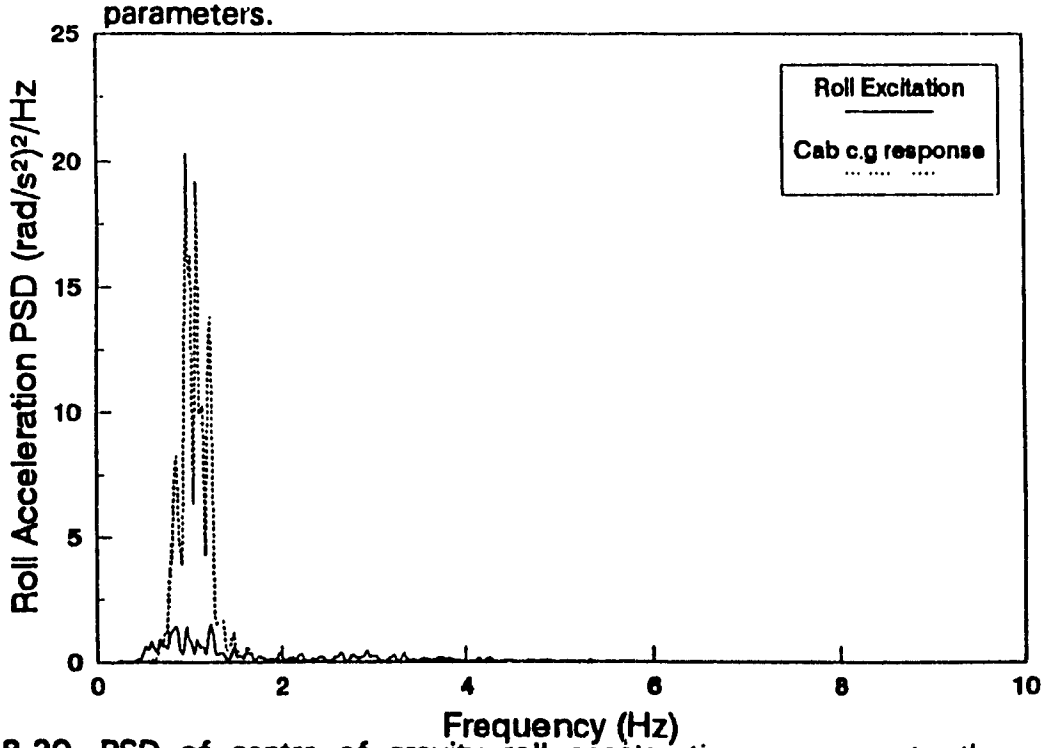

Figure 8.20 PSD of centre of gravity roll acceleration response to the roll excitation shown for a cab with baseline suspension parameters.

suspension parameters under representative off-road vehicle excitations.

8.6 Parametric Sensitivity Analysis of the Combined Cab and Seat Model

The influence of various cab suspension parameters on the vibration transmitted to the driver mass is investigated to realize an adequately tuned cab suspension. The parametric study is performed by varying the cab-suspension parameters only, while the seat suspension parameters are held fixed. The variations in the cab suspension parameters include the suspension spring rate, the shock absorber damping coefficients corresponding to bleed and blow-off stages, and the shock absorber transition velocity. The spring rates of the front (K_3 and K_4) and rear (K_1 and K_2) suspension units are modified to achieve specific uncoupled bounce mode resonant frequency, while maintaining identical static deflections at the front and rear. The changes in weight distribution caused by variations in the c.g. location along the longitudinal axis of the cab are incorporated in selecting the spring rates. Considering the pitch plane shown in Figure 8.1, the spring rates corresponding to equal static deflection may be expressed as a function of the uncoupled vertical angular natural frequency, ω_n, and the centre of gravity location characterized by a_2 and a_3 along the longitudinal axis, and by b_1 and b_2 along the lateral axis. Letting $\ell = (a_2 + a_3)$, and $w = (b_1 + b_2)$, the spring rates are derived from the following expressions:

$$K_1 = m_c\omega_n^2\left(\frac{b_2}{w}\right)\left(\frac{a_3}{\ell}\right) \qquad K_2 = m_c\omega_n^2\left(\frac{b_1}{w}\right)\left(\frac{a_3}{\ell}\right)$$
$$K_3 = m_c\omega_n^2\left(\frac{b_1}{w}\right)\left(1-\frac{a_3}{\ell}\right) \qquad K_4 = m_c\omega_n^2\left(\frac{b_2}{w}\right)\left(1-\frac{a_3}{\ell}\right) \tag{8.21}$$

Thus, by fixing the cab uncoupled bounce natural frequency, the suspension spring rates may be computed for different values of the c.g. coordinates along the longitudinal axis, a_3/ℓ, while maintaining the c.g. coordinates on the lateral axis (b_1 and b_2) as constants. The longitudinal position of the seat, a_s, with respect to the cab centre of gravity is also varied to study the influence of seat location on the transmitted vibration. The parametric study is performed for variations in suspension parameters corresponding to cab natural frequencies of 0.8, 1.0, 1.2, 1.5, and 2.0 Hz, and the ratio a_3/ℓ ranging from 0.1 to 0.9. The computations are performed by maintaining the point of excitation identical to that considered for the baseline cab suspension and by neglecting the effect of the mass due to the seat and the driver on the cab response. The influence of shock absorber design parameters on the vibration response is investigated by varying the damping coefficients from 0.4 to 1.6 times their baseline values.

The influence of variations in the suspension parameters on the ride performance characteristics is investigated using the following performance indices:

- the vertical rms acceleration of the cab c.g.;

- the vertical rms acceleration of the driver-mass;
- the pitch rms acceleration of the cab c.g.;
- the roll rms acceleration of the cab c.g.;
- the peak relative vertical displacement of the cab;
- the peak relative vertical displacement of the driver mass with respect to the cab floor.

8.6.1 INFLUENCE OF CAB SUSPENSION SPRING RATES

Figures 8.21 to 8.26 present the influence of variations in the suspension spring rates on the rms acceleration of vibration transmitted to the cab and the driver mass, and the peak relative displacements. The results of the study are presented for variations of the uncoupled bounce mode natural frequency of the cab, cab c.g. location, and seat location, while the damping parameters are held equal to their baseline values. The results clearly illustrate the significant influence of cab natural frequency on all the performance indices, while the influence of variations in the c.g. location appears to be minimal. A low natural frequency cab suspension yields superior attenuation of the bounce, pitch and roll vibration at the driver mass and cab c.g. location, as shown in Figures 8.21 to 8.24. A low natural frequency cab suspension further reduces the peak relative displacement between the driver mass and the cab floor, as shown in Figure 8.25. The influence of cab c.g. location on the relative displacement of the driver mass is also observed to be insignificant. The low natural frequency

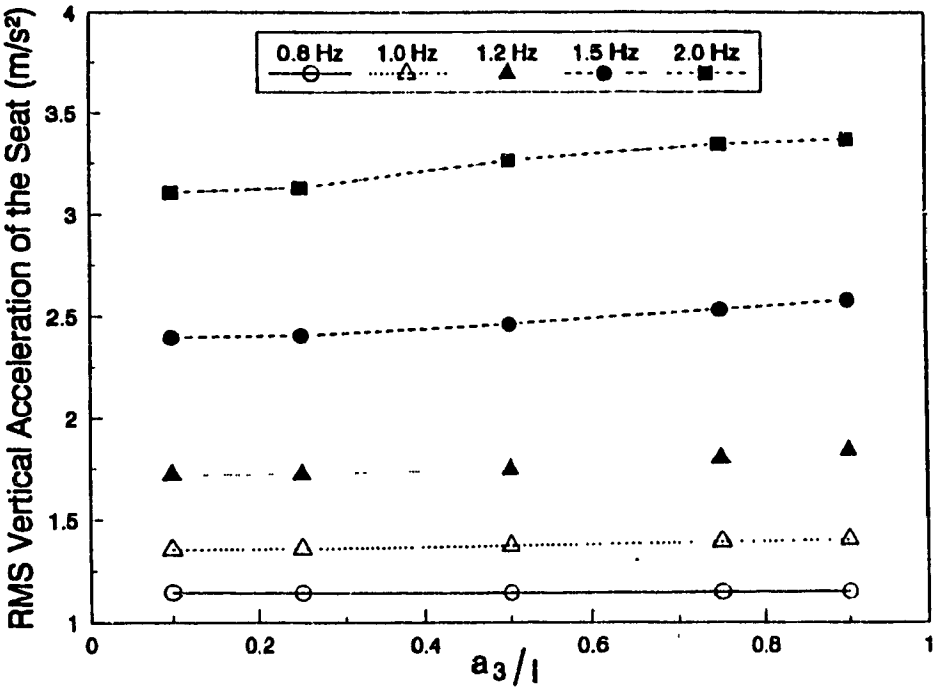

Figure 8.21 Influence of cab natural frequency and centre of gravity location on the rms vertical acceleration response of the driver mass.

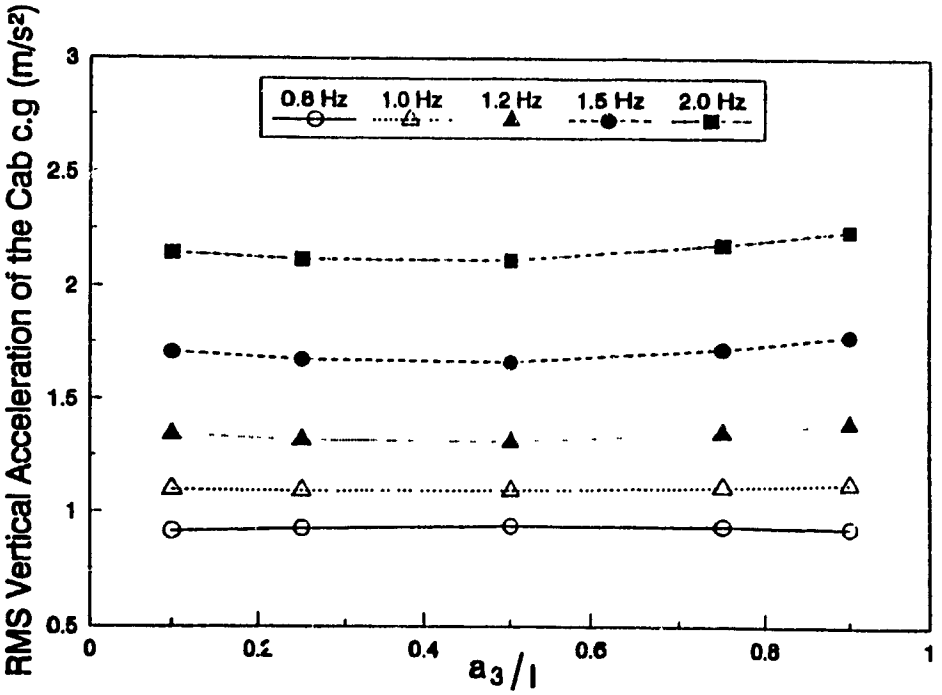

Figure 8.22 Influence of cab natural frequency and centre of gravity location on the rms vertical acceleration response of the cab centre of gravity.

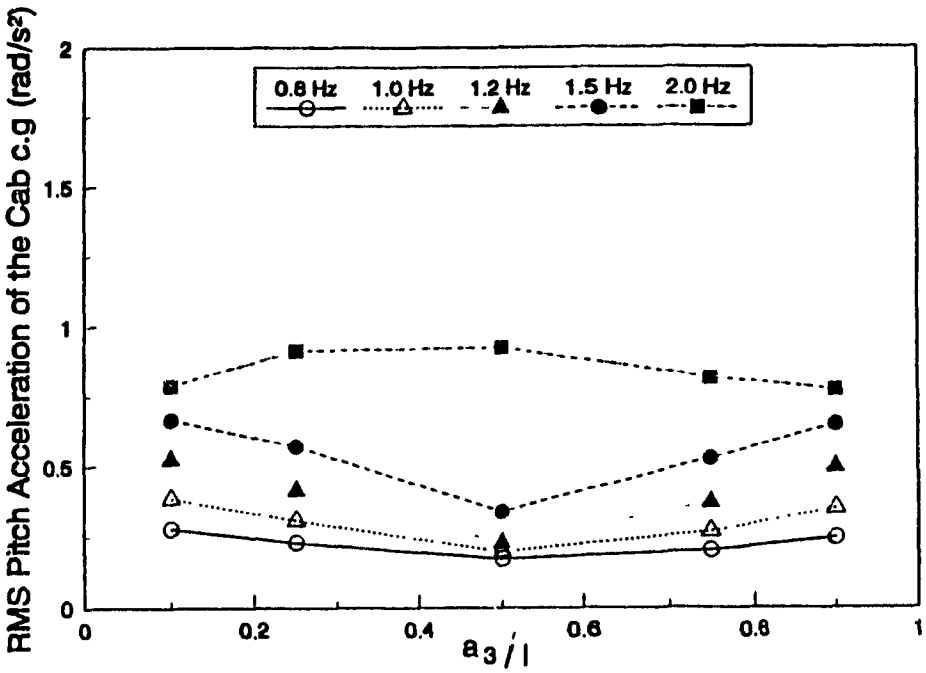

Figure 8.23 Influence of cab natural frequency and centre of gravity location on the rms pitch acceleration response of the cab centre of gravity.

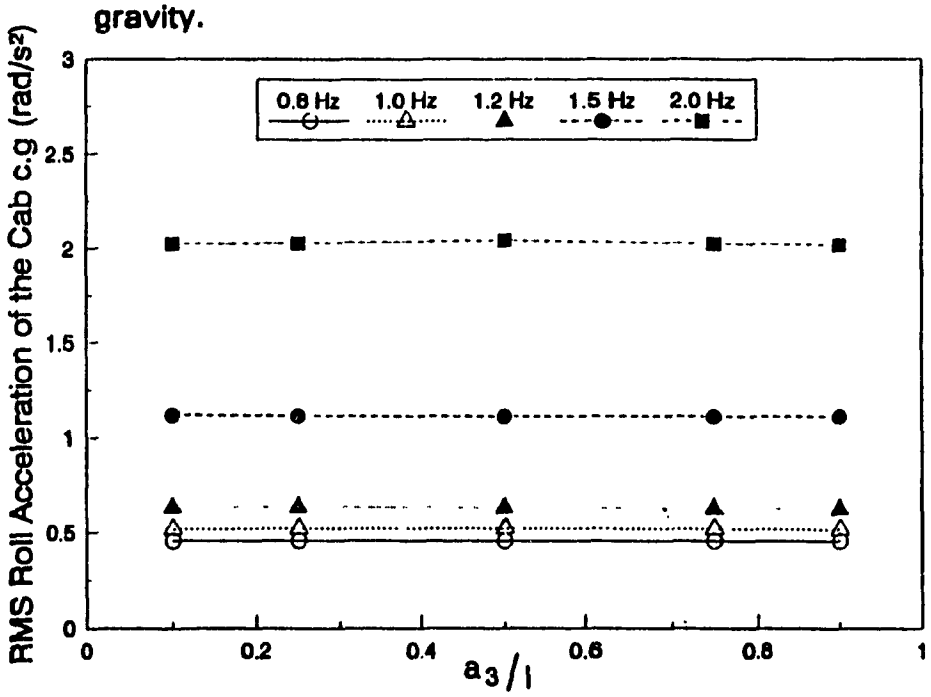

Figure 8.24 Influence of cab natural frequency and centre of gravity location on the rms roll acceleration response of the cab centre of gravity.

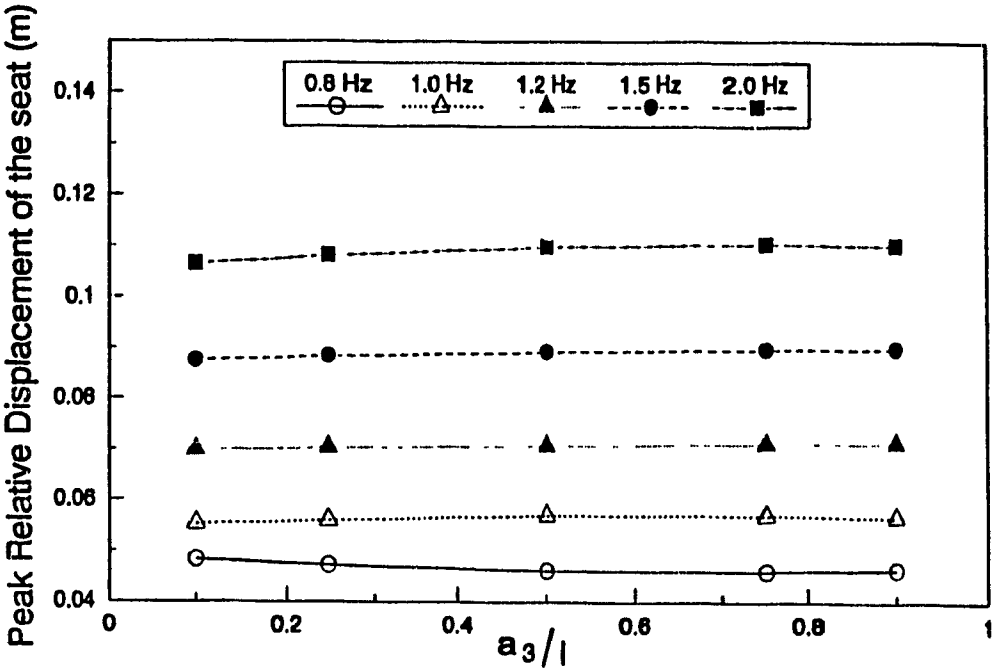

Figure 8.25 Influence of cab natural frequency and centre of gravity location on the peak relative displacement of the driver mass.

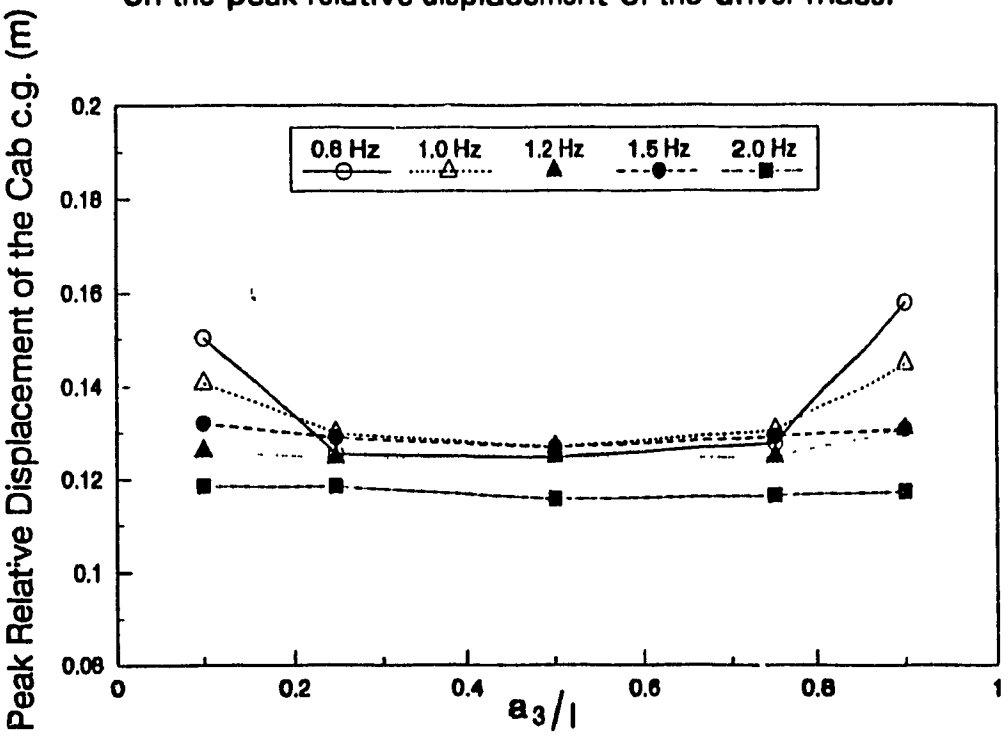

Figure 8.26 Influence of cab natural frequency and centre of gravity location on the peak relative displacement of the cab.

cab suspension, however, yields increased peak relative deflections of the cab with respect to the chassis, as shown in Figure 8.26. The peak relative deflection of the cab corresponding to low natural frequencies (0.8 and 1.0 Hz) is further influenced by the c.g. location. The c.g. location closer to the front or rear suspension units yields excessive relative displacement of the cab, which is attributed to the location of pitch oscillation center near the front or rear of the cab. Furthermore, the rms acceleration due to vertical vibration transmitted to the driver mass through the suspension seat is found to be considerably larger than that at the cab c.g., suggesting that a rigid seat may be desirable when the cab is suspended.

Since the bounce, roll and pitch excitations are predominant near 1.8, 1.4, and 0.9 Hz, respectively, a low natural frequency cab suspension (near 0.8 Hz) is highly desirable to achieve best attenuation of the low frequency excitations. Although the vibration transmitted to the cab floor can be effectively attenuated using the low natural frequency cab suspension, the cab floor vibration transmitted to the driver tends to be amplified by the low natural frequency suspension seat (near 1.3 Hz). While a further reduction in seat natural frequency may yield improved vibration isolation, the corresponding increase in relative deflections between the driver and the cab floor prohibits the use of a lower natural frequency suspension seat.

From the results of the parametric study, it is apparent that the peak relative deflection of the cab exceeds the limiting value of 100 mm, irrespective of the uncoupled bounce mode natural frequency of the cab suspension. A compromise between the vibration attenuation performance and the peak relative displacement of the cab thus needs to be realized. The cab natural frequency of 0.8 Hz together with a_3/ℓ of 0.5 perhaps yields the best compromise between the vibration isolation and the peak relative displacement of the cab. Such a cab suspension design yields the peak relative displacement of the cab and driver mass as 125 mm and 50 mm, respectively. The corresponding ratios of the rms accelera on at the cab centre of gravity to that of the excitation at the chassis are ap roximately 0.71 for bounce, 0.27 for pitch and 0.40 for roll. A significant reduction of the roll and pitch components of vibration is thus achieved via cab suspension, while attenuation of the vertical vibration is only slightly improved when compared to that of the suspension seat alone, which was computed as 0.76. The ratio of rms acceleration of the driver mass to that of the cab chassis or excitation, however, is approximately 0.87, which is larger than that for the suspension seat alone, thus less effecti.e than the cab or seat alone. Under these conditions, a suspended cab with rigid seat would appear to provide better vibration isolation for the driver.

Using the relations expressed by equation (8.21), the following values of cab

suspension spring rates are selected to achieve a compromise between the vibration isolation and the peak relative deflection (uncoupled bounce natural frequency of 0.8 Hz, $a_3/\ell = 0.5$):

$$K_1 = K_4 = 3532 \text{ N/m} \qquad K_2 = K_3 = 3186 \text{ N/m}$$

8.6.2 INFLUENCE OF CAB SUSPENSION DAMPING PARAMETERS

The influence of variations in the cab suspension high and low damping coefficients C_{Hi} and C_{Lo}, and transition velocity, V_o, on the suspension performance is investigated by selecting the spring rates defined in the preceeding section. Figure 8.27 illustrates the influence of the high damping coefficient corresponding to bleed flows on the cab and driver mass vertical rms acceleration, while Figure 8.28 shows the influence on roll and pitch rms accelerations of the cab. The influence of variations in the damping coefficient on the peak relative displacement response is shown in Figure 8.29. The results clearly illustrate that a reduced value of high damping coefficient yields lower rms acceleration of vertical, pitch and roll vibration of the cab and driver mass. The influence of high damping parameter on the peak relative displacement is almost insignificant, as shown in Figure 8.29.

The influence of variations in the low damping coefficient corresponding to blow-off stage on the vertical rms accelerations and peak relative displacements of the driver mass and cab centre of gravity was found to be almost identical to

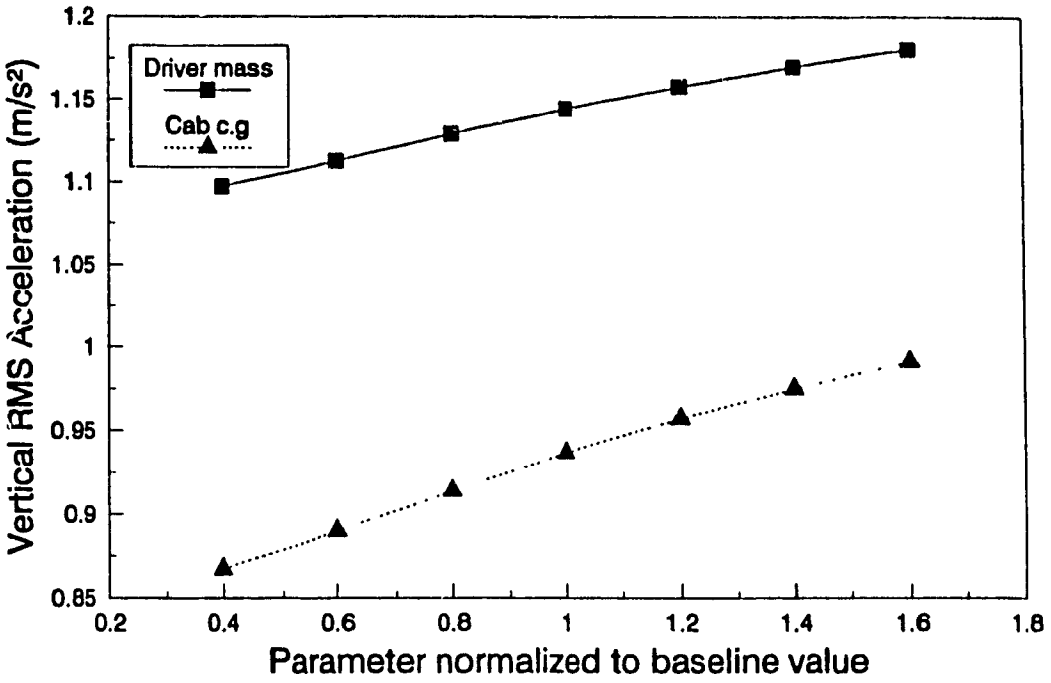

Figure 8.27 Influence of the shock absorber high damping coefficient on the vertical rms acceleration of the driver mass and the cab centre of gravity.

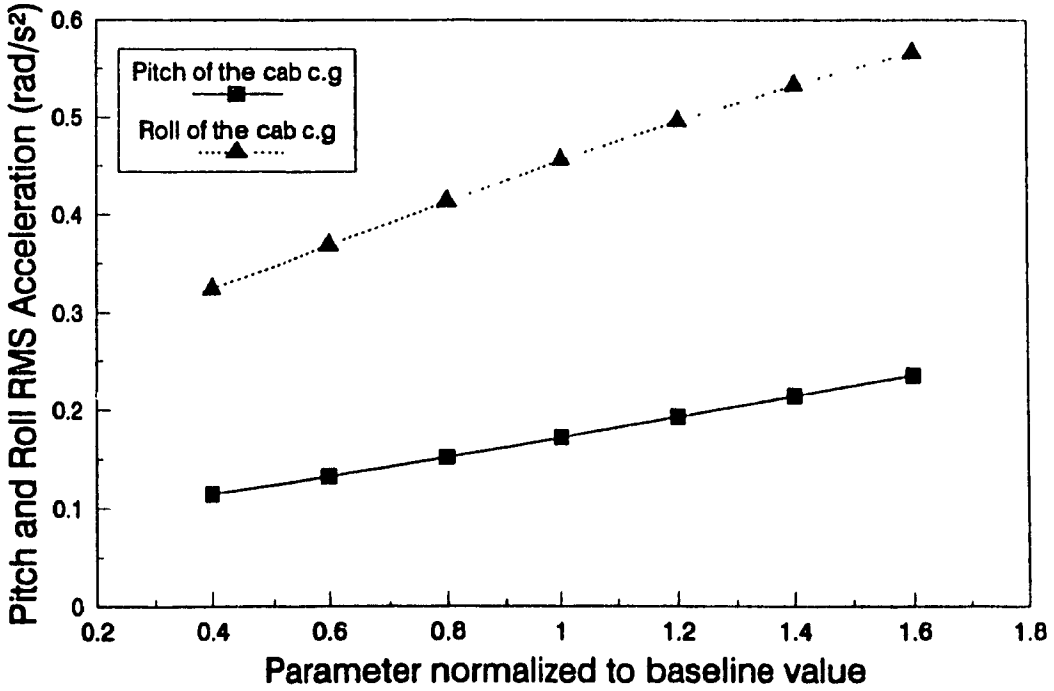

Figure 8.28 Influence of the shock absorber high damping coefficient on the pitch and roll rms accelerations of the cab centre of gravity.

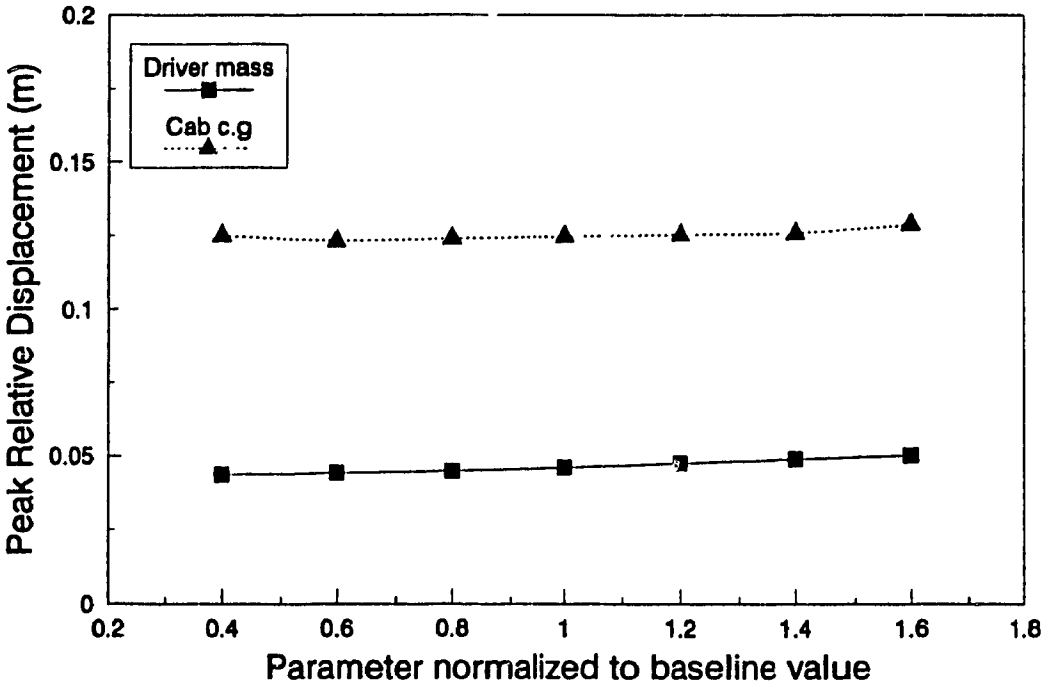

Figure 8.29 Influence of the shock absorber high damping coefficient on the vertical peak relative displacement of the driver mass and the cab centre of gravity.

that established for the high damping coefficient. However, its influence on pitch and roll rms accelerations of the cab was found to be slightly less than that observed for the high damping coefficient. In all cases, a low damping coefficient value leads to the lower rms acceleration and peak relative displacement response. The shock absorber transition velocity was found to have a negligible effect on the different performance indices. From the results of the parametric study on the shock absorber design characteristics, it may be concluded that a reduction of the high and low damping coefficients to 40% of their baseline values can provide considerable improvement in the ride performance of the cab suspension.

8.7 Response Characteristics of the Selected Cab-Seat Suspension

The cab-seat suspension model with parameters identified in the previous section is analyzed to determine its response characteristics in terms of acceleration PSD and frequency contents. The acceleration PSD response characteristics of vertical excitation, and vertical response of the driver mass and cab c.g. are illustrated in Figures 8.30 and 8.31, respectively. The proposed cab suspension design parameters yield significant attenuation of vertical vibration at frequencies greater than 1.6 Hz. The suspended cab, however, yields considerable amplification of chassis vertical vibration transmitted to the cab and driver mass in the 0.6 to 1.1 Hz frequency range. The roll and pitch vibration of the chassis are significantly attenuated in the

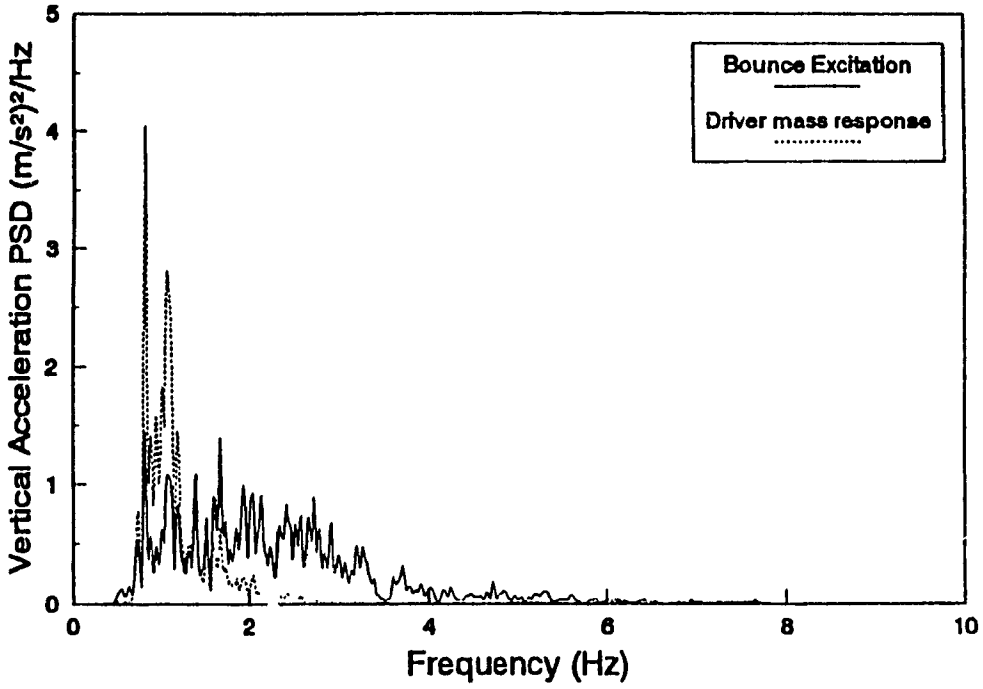

Figure 8.30 PSD of bounce excitation and vertical driver mass acceleration response of the cab-seat suspension.

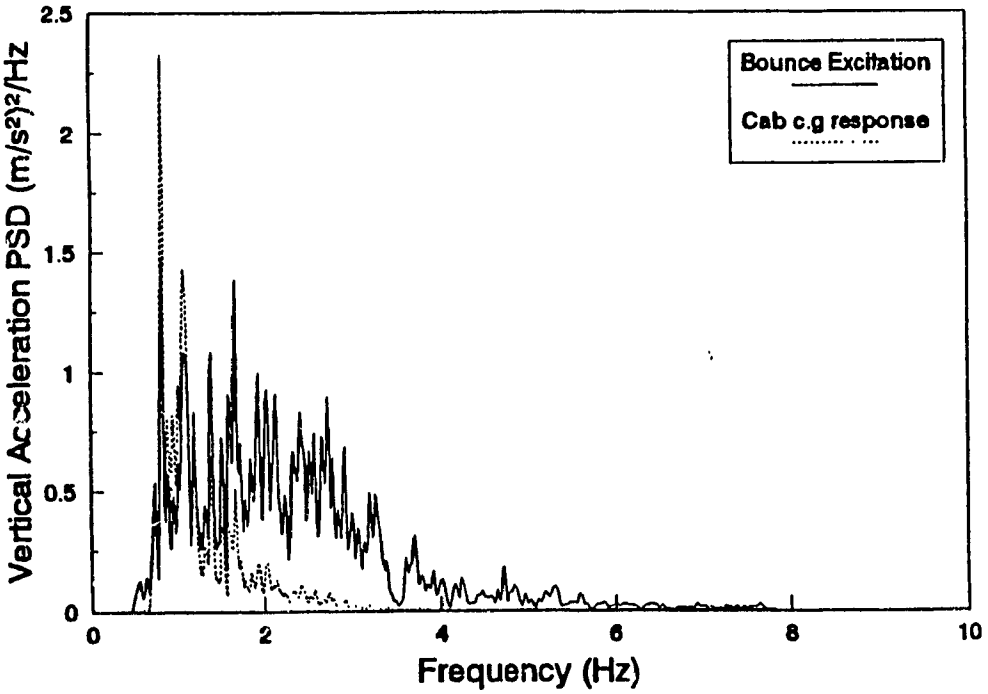

Figure 8.31 PSD of bounce excitation and vertical cab centre of gravity acceleration response of the cab-seat suspension.

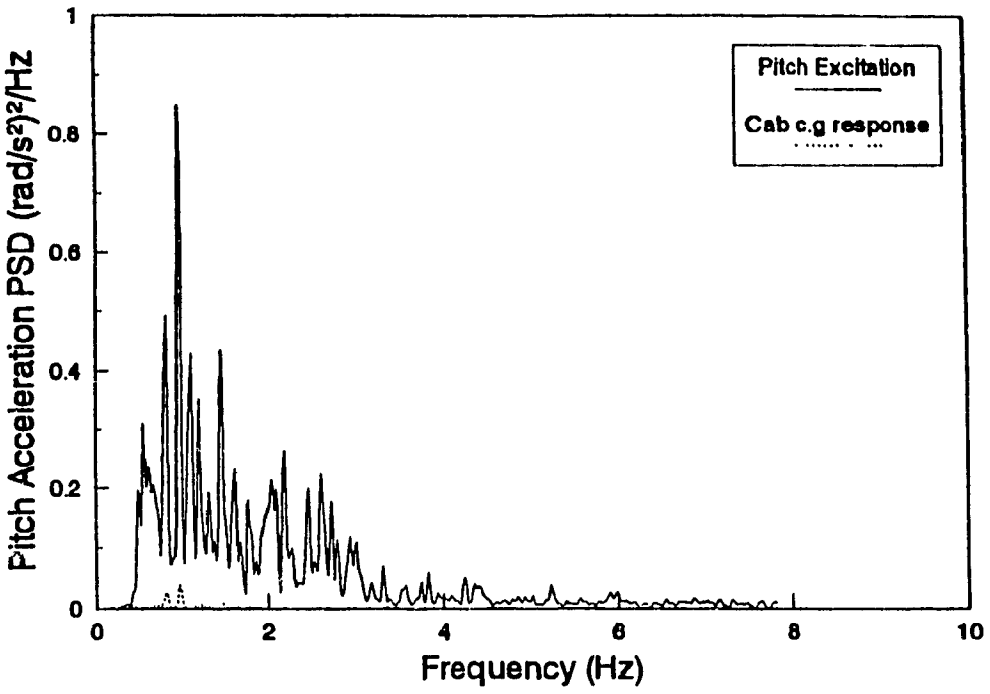

Figure 8.32 PSD of pitch excitation and cab centre of gravity pitch acceleration response of the cab-seat suspension.

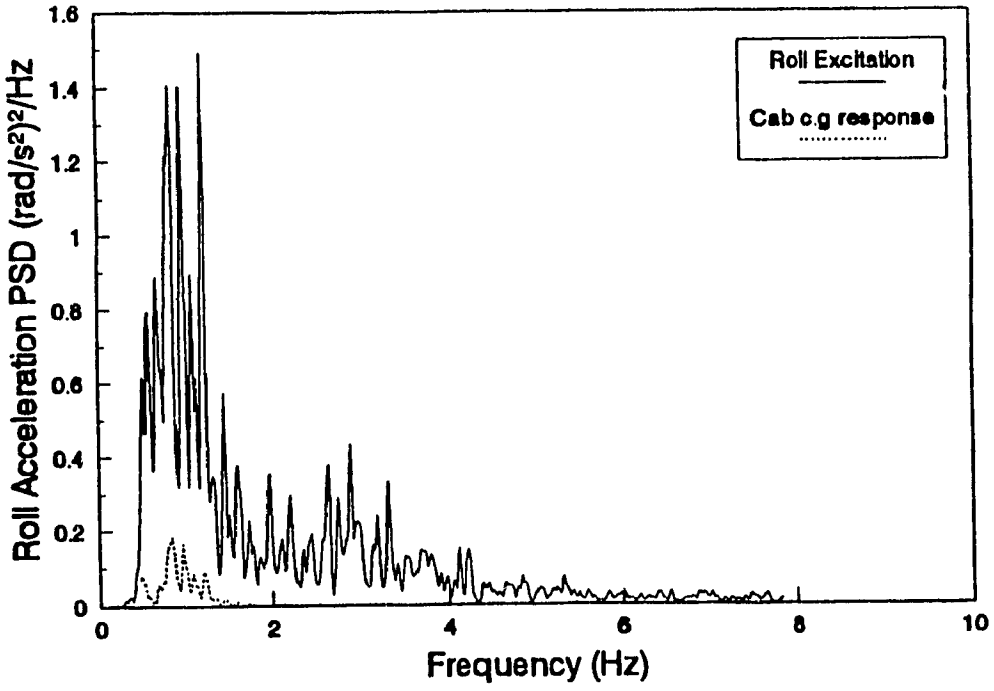

Figure 8.33 PSD of roll excitation and cab centre of gravity roll acceleration response of the cab-seat suspension.

entire frequency range, as shown in Figures 8.32 and 8.33. With optimized cab suspension parameters, the computed vertical rms acceleration is found to be 1.04 ms^{-2} and 0.81 ms^{-2} at the driver mass and at the cab c.g., respectively, compared with 1.32 ms^{-2} at the cab chassis. The cab angular acceleration response is computed as 0.09 rad/s^2 and 0.26 rad/s^2 for pitch and roll, respectively, as compared to 0.74 and 1.13 rad/s^2 at the cab chassis. Thus significant attenuation (more than 75%) of the pitch and roll components of vibration is achieved via the tuned suspended cab. Cab bounce is reduced by close to 40%, while the driver's unweighted rms acceleration is reduced by only 20%. These results thus suggest that a properly tuned suspended cab used in conjunction with a rigid seat would provide the same degree of attenuation of the bounce component of vibration transmitted to the driver as a low natural frequency tuned suspension seat alone.

8.8 Summary

A five-degree-of-freedom nonlinear cab-seat suspension model is developed by integrating the two-degree-of-freedom nonlinear suspension seat model with rigid driver mass to a three-degree-of-freedom cab suspension model. The inertial properties of an off-road forestry vehicle cab are evaluated, and a four corner-mounted coil spring/shock absorber suspension is configured. A prototype cab-seat suspension system is fabricated and tested in the laboratory using sinusoidal excitations representing pure bounce motion, and combined

bounce and roll, and bounce and pitch motions. The test results are used to validate the analytical model. A parametric study is performed to select appropriate cab suspension parameters to achieve attenuation of bounce, roll and pitch vibration with minimal peak relative displacement response of the driver mass and the cab. The results of the parametric study indicate that a cab suspension with low natural frequency of 0.8 Hz and centre of gravity located at the centre of the pitch axis provides a desirable compromise between the vibration attenuation performance and peak relative displacement response of the cab under vibration excitations representative of those encountered by off-road vehicles.

CHAPTER 9

CONCLUSIONS AND RECOMMENDATIONS FOR FUTURE WORK

9.1 General

Prolonged exposure to whole-body vibration and shock is known to contribute significantly to the degradation of health and comfort of seated individuals. Off-road vehicle drivers are particularly at risk in view of the severe nature of shocks and vibration provoked by the vehicle motion over rough terrains. Protection of the driver against the ill-effects of shock and vibration may be accomplished through effective design of suspension seats and vehicle cab suspensions. Current guidelines associated with the assessment of the potential health effects resulting from shock and vibration exposure must be appropriately considered in the design and analyses of the suspension systems. The thesis research was formulated to develop analytical and experimental tools to effectively analyze the secondary suspension systems and to provide design guidelines to enhance driver protection under representative off-road wheeled vehicle vibration environment.

9.2 Highlights of the Study

The major highlights of this investigation are summarized below:

WHOLE-BODY VEHICULAR VIBRATION SIMULATOR (WBVVS)

A dedicated whole-body vehicular vibration simulator with enhanced safety control loops was developed to study the response characteristics of suspension seats and the seated human body under various types of sine, random and shock excitations. While the servo-actuators were configured to simulate vertical vibration alone, in-plane rotational vibration could also be generated. The WBVVS was designed to simulate a driver's workstation by providing a stable floor and a steering column, while the closed-loop feedback control of the forces and motions of the platform provided the necessary safety features, along with emergency safety switches. In this study, various vibration excitation signals were synthesized to evaluate suspension seat and seated human responses to deterministic and random vehicular vibration and shocks. Sinusoidal motions swept in the 0.625 to 10 Hz frequency range, four different classes of random excitations (ISO 1, ISO 2, Class I, Class II) representing the vibration environment of different off-road vehicles, and the shock motions idealized by the passage of a vehicle over a half-sine pulse at different speeds, were synthesized and used to drive the WBVVS.

BIODYNAMIC RESPONSE CHARACTERISTICS OF SEATED DRIVERS

The driving-point mechanical impedance (or apparent mass) and the seat-to-head transmissibility biodynamic response functions have been extensively

used to characterize whole-body dynamic response to vibration. The reported data, however, differ considerably in magnitude and phase response in view of the significant variations in experimental conditions, subject population and posture, and amplitude and types of excitations used in deriving these functions.

In this study, a synthesis of selected published data grouped under similar test conditions was performed, reducing the extent of the variations amongst the data, while revealing a strong dependence of vibration type and levels, and the subjects' posture and hands position on the magnitude and phase characteristics, particularly in the vicinity of the whole-body resonant frequency. While none of the reported data was derived under conditions likely to prevail during off-road vehicle driving, measurements of the driving-point mechanical impedance of seated subjects maintaining a driving position, with and without backrest support, were performed using the WBVVS under sine and random excitations in the 1.0 to 2.0 ms^{-2} amplitude range. Analysis of the measured data revealed that posture and seat backrest angle are the two most important variables that affect the whole-body mechanical impedance characteristics. On that basis, most probable or target values of driving-point mechanical impedance in the 1.0 to 10 Hz frequency range were derived for three different seated postures: "erect back supported" (EBS); "erect back not supported" (ENS); and

"slouched" (SLO). Although the seat-to-head transmissibility function was not measured, the synthesis of selected published data was used to define applicable target values for both ENS and EBS postures in the 1.0 to 10 Hz frequency range.

Considerable differences were observed between the driving-point mechanical impedance characteristics derived from the measurements and the synthesis, and those proposed by ISO relying on data measured under various experimental conditions. The ISO standardized seat-to-head transmissibility, however, correlated reasonably well with the synthesized data derived for subjects maintaining an ENS posture.

DEVELOPMENT OF A HUMAN DRIVER MODEL

Although a number of biodynamic models have been proposed in the literature to account for whole-body vibration response, the methodology used for estimating the model parameters has often relied on data measured under various conditions. While the driving-point mechanical impedance and seat-to-head transmissibility characteristics have been most widely used to estimate the model parameters, none of the proposed models have attempted to match both the magnitude and phase response under representative off-road vehicle driving conditions.

This study proposes a four-degree-of-freedom linear human driver model and a methodology is developed to identify the model parameters using the target values of driving-point mechanical impedance and seat-to-head transmissibility magnitude and phase for seated drivers maintaining an ENS posture. Based on anthropometric and biomechanical data, limit constraints are imposed on the model parameters, while a nonlinear programming based optimization technique is applied to minimize the sum of squared magnitude and phase errors associated with mechanical impedance and seat-to-head transmissiblity target values.

The derived driver model provides a reasonable estimate of the driving-point mechanical impedance characteristics with peak magnitude error approaching 20% at frequencies above 5 Hz, while the phase response is in close agreement at frequencies below 6 Hz. Although the seat-to-head transmissiblity characteristics deviate considerably more, the peak magnitude error approaches 30% at frequencies below 7 Hz, while the phase response is in relatively good agreement below 6 Hz. The whole-body resonant frequency established from both response functions agrees well with the measured results, although the peak resonant transmissiblity magnitude is overestimated by the model. For off-road vehicle drivers subjected to vibration predominant below 5 Hz, the model is considered to be quite adequate to account for whole-body dynamics.

INFLUENCE OF BODY DYNAMICS ON SUSPENSION SEAT VIBRATION ATTENUATION PERFORMANCE

The assessment of the vibration attenuation performance of suspension seats is often carried out by loading the seat with a rigid mass, while neglecting the contributions of the driver. In this investigation, the measurements conducted using a low natural frequency suspension seat have shown that, by replacing a subject with a rigid load, the vibration attenuation performance is overestimated by as much as 25% in the 2 to 3 Hz frequency range under sine sweep excitation, and by as much as 30% at the predominant excitation frequency of ISO 2 random excitation. The influence of body dynamics on suspension seat performance was reasonably well accounted for by the combined suspension seat-human driver model developed in this study. The combined model provided better correlations with the measured response under sine and shock excitations. The degree of correlation with the measured responses, however, was observed to be highly dependent on the type and intensity of the excitation and the frequency range considered.

RESPONSE ANALYSIS UNDER SHOCK EXCITATIONS

Shock excitations are frequently encountered in off-road vehicles operating in the forestry, construction and mining sectors. The response analysis of the combined suspension seat-human driver model was investigated under

two types of shock inputs: (i) high level shocks causing excessive relative motions and interactions with the seat travel limiting bump stops; and (ii) low level shocks causing no such interactions. For the low natural frequency suspension seat considered in this study, the influence of the various suspension seat design parameters on driver's exposure levels showed a similar behaviour both under continuous random vibration (ISO 2) and low level shocks for which the predominant excitation frequencies lie above the seat resonant frequency. The vibration exposure levels computed using the various assessment methods, however, were considerably larger (≈70%) for a single low level shock event than those derived under continuous random vibration. Although a reduction of the shock absorber low damping coefficient provided the most significant improvement in seat attenuation performance under both ISO 2 and low level shock excitations, the reduction in exposure level provoked by such a change did not contribute to lower the health hazard rating significantly under low level shocks in comparison with that estimated under ISO 2 excitation when applying the various proposed health criteria.

Under high level shock excitations, the various suspension seat design parameters, with the exception of suspension and cushion stiffnesses, affect the exposure levels in a manner opposite to that observed for both ISO 2 and low level shock excitations. This was attributed to the bump

stop interactions creating self-excited motions closer to the seat resonant frequency. Although increased shock absorber damping is a most desirable feature under high level shocks, the vibration exposure levels resulting from single shock events of this nature were observed to constitute a significant health hazard with respect to the various proposed health criteria defined in the standards.

SIGNIFICANCE OF VARIOUS EXPOSURE ASSESSMENT METHODS AND HEALTH CRITERIA

In this study, various whole-body vibration exposure assessment methods and the associated health criteria defined in the current ISO standard and its proposed revision were applied to compute the driver's response under random and shock excitations. The overall frequency-weighted rms acceleration response using the W_z weighting was computed and compared with the "exposure limit", representing the assessment method defined in the current standard. The exposure assessment method defined in the proposed revision involves the computation of the W_k-frequency-weighted rms acceleration response and its comparison with a defined "health guidance caution zone". In addition, the proposed revision defines a procedure for evaluating the shock response, involving the computation of W_k-frequency-weighted rmq acceleration.

A methodology was developed in this study to compute the frequency-weighted rms and rmq accelerations in the frequency domain using the weighting filter transfer functions. The propose method provided the assessments in a highly efficient manner. Under random and shock excitations, the W_k weighting consistently resulted in rms accelerations being approximately 15% lower than those computed using the W_z weighting. These values, however, led to a similar estimate of the health hazard under ISO 2 random excitation. While the "exposure limit" based on the W_z-weighted rms values was reached after 4 to 6 hours of exposure, the corresponding W_k-weighted rms values were observed to lie within the "health guidance caution zone" defined for daily exposure durations between 4 and 8 hours. Under shock excitations, however, the guidance provided in the revised version was observed to be considerably more restrictive on tolerable exposure duration than with the current standard, particularly when the rmq procedure was applied. This was further emphasized by the magnitudes of rmq values being 1.7 to 2.0 times the corresponding magnitudes of rms values computed under similar shock excitations.

COMBINED SUSPENDED CAB-SUSPENSION SEAT ANALYSIS

Although adequately tuned suspension seats can provide significant attenuation of vertical terrain-induced vibration, it has often been argued

whether any further improvement could be achieved by incorporating such a seat within a suspended cab. In this study, a prototype suspended cab equipped with a low natural frequency suspension seat was developed and its bounce, roll and pitch vibration response characteristics were evaluated in the laboratory. A suspended cab-suspension seat model was developed and validated, while neglecting the human body dynamics. This model was further used to estimate the driver and the cab response in the vertical, pitch and roll modes under field-measured random excitations. A parametric study was performed to develop cab suspension design guidelines to optimize its performance under the corresponding excitations.

The tuned cab suspension resulted in significant attenuation of the pitch and roll components by more than 75%, while cab bounce was reduced by close to 40%. The driver unweighted vertical rms acceleration for the combined suspended cab-suspension seat, however, was reduced by only 20% with respect to the vehicle chassis. In comparison, a low natural frequency tuned suspension seat with minimal damping could provide by itself a 40% attenuation under ISO 2 random excitation. The study concluded that the use of a soft suspension seat within the suspended cab would impair the effectiveness of the seat or the cab alone for reducing the driver's exposure levels.

9.3 Conclusions

On the basis of the studies conducted in this thesis, the following conclusions are drawn:

- The whole-body vehicular vibration simulator (WBVVS) provides a convenient tool to assess the vibration attenuation performance of suspension seats and the human body response under deterministic, random and shock motions.
- Off-road vehicle random vibration excitation classes defined in ISO Standards can be effectively synthesized and reproduced on the WBVVS platform with a high degree of accord with the specified characteristics.
- The suspension seat model with rigid mass representation generally tends to overestimate the response measured with a rigid load at excitation frequencies above resonance.
- Human body dynamics affect the estimated suspension seat vibration attenuation performance to varying degrees depending on the frequency and type of excitation, and the properties of the suspension seat.
- The vibration attenuation performance of a low natural frequency suspension seat is overestimated at frequencies above the seat resonance when human body dynamics is neglected.
- The combined seat-driver response computed using the four-degree-of-freedom linear human driver model developed in this study is in closer agreement with the measured seat-person response than that computed

by simply using a rigid driver mass representation. The degree of correlation depends on the type and frequency characteristics of the excitations.

- The resonant frequency and resonant transmissibility magnitude of a low natural frequency suspension seat can be effectively determined using a rigid mass representation of the driver. Such representation would result in significant errors when applied to seats with a higher natural frequency in view of the non negligible influence of body dynamics at higher excitation frequencies.
- The whole-body driving-point mechanical impedance and seat-to-head transmissibility magnitude and phase characteristics published in the literature present large variations due to the wide range of experimental conditions used in deriving the data and the strong dependence of the response on the excitation type and amplitude, the sitting posture (with and without backrest support) and the hand position.
- The published data on seat-to-head transmissibility of seated individuals indicate a dependence of the magnitude and phase characteristics on the backrest support.
- Whole-body driving-point mechanical impedance magnitude and phase characteristics of seated subjects maintaining specific driving postures can be measured accurately, with a high degree of repeatability, using either deterministic or random excitations.

- The driving-point mechanical impedance magnitude and phase characteristics of seated individuals are affected considerably by the mass of the subjects. Heavier subjects tend to show larger impedance magnitude and lower phase than low weight subjects in the vicinity of the resonant frequency.
- The sitting posture and the backrest angle constitute the two most influential factors affecting the driving-point mechanical impedance characteristics for seated subjects maintaining a driving position with their feet supported, subjected to sine and random vibration with amplitudes of W_z frequency-weighted rms acceleration within the range 1.0 to 2.0 ms^{-2}.
- The influence of posture is most apparent on impedance magnitude within the resonant frequency region where the magnitude is largest for subjects maintaining an ENS posture, lowest for an EBS posture, while that for SLO posture is in-between. Backrest inclination tends to smoothen the resonant peak, while increasing the impedance magnitude above resonance.
- The magnitude of the idealized driving-point mechanical impedance of seated vehicle drivers increases with frequency up to the resonant frequency (4.75 to 4.875 Hz), where the peak magnitude is within the 2500 to 2900 Ns/m range, depending upon the posture. Beyond resonance, the magnitude decreases with increasing frequency and

increases again above 6 Hz. The phase response decreases from close to 90° at low frequency to almost 45° at resonance, beyond which it tends to stabilize.

- The magnitude of the idealized seat-to-head transmissibility is significantly influenced by the sitting posture, while the phase only slightly. The resonant frequency estimated from this function is 5.0 Hz and 7.0 Hz, respectively for ENS and EBS postures, while the corresponding resonant magnitudes are 1.45 and 1.79.
- The idealized driving-point mechanical impedance characteristics are within the envelope of values derived from the synthesis of selected data sets obtained by restraining the range of experimental conditions.
- The ISO standardized mean driving-point mechanical impedance magnitude is considerably larger than that of the idealized data, with differences as large as 50% occurring at frequencies below 7.5 Hz. The phase response, however, is in reasonable agreement.
- The idealized seat-to-head transmissibility characteristics for subjects maintaining an ENS posture are in relatively close agreement with the standardized data defined by ISO, while significant discrepancies occur with the idealized data defined for an EBS posture.
- The four-degree-of-freedom linear driver model derived for a seated subject of mass 75.4 kg maintaining an ENS posture and a driving position provides reasonable agreement with the idealized driving-point

mechanical impedance and seat-to-head transmissibility characteristics defined for such posture. Peak impedance magnitude error of 20% occurs at frequencies above 5 Hz, while that on transmissibility magnitude is within 30% below 7 Hz. The phase response of both functions is in good agreement below 6 Hz, while the main body resonant frequency computed from the model agrees well with the idealized data. The model, however, tends to overestimate the transmissibility magnitude at resonance.

- The response behaviour of suspension seats under low and high level impacts can be conveniently analyzed through simulations involving shock excitation signals resulting from the response of a simple vehicle model to half-sine pulse inputs of different heights.
- The various exposure assessment methods proposed in the standards can be effectively integrated with the response computations of the suspension seat-driver model to estimate the driver vibration exposure levels under various types of random and shock excitations.
- Under ISO 2 and low level shock excitations, a rigid driver mass representation provides similar estimates of the vibration exposure levels than the four-DOF human driver model developed in this study.
- Under high level shocks involving suspension seat bump stop interactions, differences in exposure levels as large as 30% are observed between rigid driver and four-DOF driver models.

- The suspension seat design guidelines required to minimize the driver's degree of vibration exposure are highly dependent on the characteristics of the excitation. Under ISO 2 and low level shock excitations, the attenuation of vibration at an excitation frequency well above the seat resonant frequency requires low values of suspension stiffness, shock absorber damping coefficients and transition velocity, and Coulomb friction, while large values of suspension mass, cushion stiffness and damping coefficients.
- The suspension seat design guidelines under high level shocks involving interactions with the bump stops are those for attenuating vibration at an excitation frequency occurring at or near the seat resonant frequency. Thus high values of shock absorber damping coefficients, cushion damping and Coulomb friction are highly desirable features, while low values of suspension and cushion stiffness, bump stop stiffness, and suspension mass are required.
- The suspension seat shock absorber low damping coefficient has the greatest influence on the vibration exposure levels. Reductions of the order of 20% could be expected when the damping is set according to the design requirements established for the different types of excitations.
- The degree of attenuation in vibration exposure level achievable for a low natural frequency suspension seat is 30% under ISO 2 and low level

shock excitations, while an amplification of 30% occurs under the influence of high level shocks.

- The health hazard caused by exposure to shocks is considerably greater than that caused by random vibration, and results in tolerable daily exposure durations being significantly lower than under continuous vibration when applying the health criteria associated with the various assessment methods.
- Under random vibration exposure, the new proposed health criterion based on the evaluation of the overall W_k frequency-weighted rms acceleration provides a similar estimate of the risk as that defined in the current ISO standard, based on the W_z frequency-weighted rms acceleration, even though the W_k weighting provides consistently lower exposure levels than the W_z.
- Under shock excitations, the criterion based on the W_k frequency-weighted rms acceleration provides a considerably more severe assessment of the health hazard represented by such exposure than that based on the W_z weighted values (current standard). This is particularly the case when high level shocks are involved and when the assessment is based on rmq accelerations, which are 1.7 to 2.0 times larger than their corresponding rms values.
- The dynamics of a combined suspended cab-suspension seat in bounce, pitch and roll can reasonably well be represented by a three-degree-of-

freedom nonlinear suspended cab model and a two-degree-of-freedom nonlinear suspension seat model, while neglecting human body dynamics.

- Under realistic field-measured random excitation, a prototype suspended cab can provide significant attenuation of the bounce, pitch and roll acceleration components within the cab, provided the suspension is designed with low damping and low vertical natural frequency.
- The use of a low natural frequency suspension seat within a suspended cab can impair the degree of attenuation of the vertical component of chassis vibration transmitted to the driver. A rigid seat or a significantly higher natural frequency seat would perhaps be more beneficial for use within a suspended cab designed for off-road vehicle vibration environments.
- Although the degree of vertical vibration attenuation achievable by a properly tuned suspended cab may be similar to that estimated by a tuned suspension seat (≈40%) under random excitation, significant attenuation of the pitch and roll acceleration components (>75%) can only be realized with a suspended cab.

9.4 Recommendations for Future Studies

The following specific studies are recommended for future research:

- The development of a human driver model comprising fewer degrees of

freedom should be attempted since the seated body exhibits only few secondary resonant peaks below 10 Hz.

- The four-DOF human driver model parameters should be modified to characterize the biodynamic response functions derived for the "erect back supported"(EBS) and the "slouched"(SLO) postures. The seat-to-head transmissibility characteristics, however, need to be defined for the SLO posture.
- The response of the combined suspension seat-human driver model using several of the biodynamic models proposed in the literature should be investigated under random and shock excitations, and compared with the response computed using the four-DOF driver model developed in this study and with that measured with a human subject.
- Measurement of the seat-to-head transmissibility characteristics of seated subjects under the conditions defined in this study should be considered. These could be used, in conjunction with the idealized driving-point mechanical impedance, to derive a human driver model, while ensuring that both functions were measured under identical conditions.
- In view of the severe nature of the exposure levels caused by suspension seat bump stop interactions under high level shocks, the performance potentials of soft travel limiting bump stops with progressively hardening properties should be investigated.

- In an effort to better characterize the driver vibration exposure levels and suspension seat performance in environments involving many shocks, the analyses need to be performed under combined random and shock excitations by varying the proportion of shocks and continuous random vibration.
- Effective attenuation of whole-body random vibration and shock excitations should be explored using variable damping mechanisms involving semi-active and active control systems.
- While the parametric sensitivity analysis conducted in this study involved changing one parameter at a time, constrained nonlinear programming techniques could be considered to refine the seat and cab suspension design guidelines to provide minimum acceleration exposure levels, while also limiting the relative displacements.
- The combined suspended cab-suspension seat model could be further investigated involving variations of both cab and seat suspension parameters to determine the optimal characteristics of the combined system under the influence of low frequency off-road vehicle vibration.

REFERENCES

[1] Dupuis, H. and Zerlett, G. "The Effects of Whole-Body Vibration", Springer-Verlag, New York, (1986), 162 pp.

[2] Seidel, H. and Heide, R. "Long-term effects of whole-body vibration: a critical survey of the literature" *Int Arch Occup Environ Health*, Vol 58, (1986), 1-26.

[3] Institut National de Recherche et de Sécurité (INRS). "Vibration At Work" Paris, France, (1989), 48pp.

[4] Su, H., et al. "Response of a Nonlinear Vehicle Suspension with Tunable Shock Absorber to Random Road Excitation", ASME Pub. DE-Vol.18-5, Proc. of the 12th Biennial ASME Conference on Mechanical Noise and Vibration, Montréal, (1989), 185-193.

[5] Foster, A. "A Heavy Truck Cab Suspension for Improved Ride", SAE Technical Paper Series 780408, (1978), 1899-1916.

[6] Griffin, M.J. "Handbook of Human Vibration", Academic Press, London, (1990), pp.333-385.

[7] Griffin, M.J. "Vertical Vibration of Seated Subjects: Effects of Posture, Vibration Level and Frequency", *Aviation, Space and Env. Med.*, Vol.46, (1975), 269-276.

[8] Oborne, D.J., and Boarer, P.A. "Subjective Response to Whole-Body Vibration. The Effects of Posture", *Ergonomics*, Vol.25, (1982), 673-681.

[9] Ashley, C. "Equal Annoyance Contours for the Effect of Sinusoidal Vibration on Man", *The Shock and Vibration Bulletin*, Vol.41, (1970), 13-20.

[10] Oborne, D.J., and Clarke, M.J. "The Determination of Equal Comfort Zones for Whole-Body Vibration", *Ergonomics*, Vol.17, (1974), 769-782.

[11] Fothergill, L.C., and Griffin, M.J. "The Subjective Magnitude of Whole-Body Vibration", *Ergonomics*, Vol.20, (1977), 521-533.

[12] Draft International Standard ISO/DIS 2631-1. "Mechanical Vibration and Shock- Evaluation of Human Exposure to Whole-body Vibration- Part 1: General Requirements", (1994), 33pp.

[13] Bongers, P., and Boshuizen, H. "Back Disorders and Whole-Body Vibration at Work", Ph.D. Thesis, University of Amsterdam, The Netherlands, (1990), 317pp.

[14] Aantaa, E., Virolainen, E., and Karskela, V. "Permanent Effects of Low Frequency Vibration on the Vestibular System", *Acta Otolaryngolica*, Vol.83, (1977), 470-474.

[15] Frymoyer, J.W., Pope, J.W., et al. "Epidemiologic Studies of Low Back Pain", *Spine*, Vol.5, (1980), 419-423.

[16] Sandover, J. "Behaviour of the Spine under Shock and Vibration: A Review", *Clin. Biomech.*, Vol.3, (1988), 249-256.

[17] Rosegger, R., and Rosegger, S. "Health Effects of Tractor Driving", *J. Agr Eng Res*, Vol.5, (1960), 241-275.

[18] International Standard ISO 2631/1. "Evaluation of Human exposure to Whole-Body Vibration-Part 1: General Requirements", First edition, (1985), 17pp.

[19] Lines, J.A. "Description of Time Domain Simulation of Tractor Ride Vibration", National Institute of Agricultural Engineering, Ergonomics Dept. File, No.42, (1983).

[20] Claar II, P., Buchele, W.F., Marley, S.J., and Seth, P.N. "Off-Road Vehicle Ride: Review of Concepts and Design Evaluation with Computer Simulation", SAE Paper No. 801023, (1980).

[21] Matthews, J. "Ride Comfort for Tractor Operators III. Investigation of Tractor Dynamics by Analog Computer Simulation", *J. of Agric. Engng. Res.*, Vol.10, (1965), 93-108.

[22] Patil, M.K., et al. "Response of Human Body to Tractor Vibration and its Minimization by Provisions of Relaxation Suspension to Both Wheels and Seat at the Plane of Centre of Gravity", *Med. & Biol. Eng. and Comput.*, Vol.18, (1980), 554-562.

[23] Haack, M. "On the Suspension at the Front Axle of Pneumatic-Tyred Farm Tractors with Unsprung Rear Axle", Vol.4, Lantech Forsch, (1954).

[24] Cadou, P.B., and Bowser, F.J. "The Development of a Scraper Suspension System", SAE Paper No. 780462, (1962).

[25] Foster, A. "A Heavy Truck Cab Suspension for Improved Ride", SAE Technical Paper Series 780408, (1978), 1899-1916.

[26] Wild, R. "A Practical Approach to Cab Suspensions", SAE Technical Series 780407, (1978).

[27] Rakheja, S., Afework, Y., et al. "An Analytical and Experimental Investigation of the Driver-Seat Suspension System", *Vehicle System Dynamics*, Vol.23, (1994), 24pp.

[28] Troup, J.D.G. "Clinical Effects of Shock and Vibration on the Spine", *Clin. Biomech.*, Vol.3, (1988), 227-231.

[29] Boileau, P.-E, and Scory, H. "Les lombalgies chez les conducteurs de débusqueuses: étude des vibrations appliquées au corps entier dans les chantiers forestiers du Québec", *Archives des maladies professionnelles*, Vol.49, (1988), 305-314.

[30] Wong, J. "Theory of Ground Vehicles", Wiley Interscience, New York, (1978), 330pp.

[31] International Standard ISO 5007. "Agricultural Wheeled Tractors - Operator's Seat - Laboratory Measurement of Transmitted Vibration", First edition, (1990), 13pp.

[32] International Standard ISO 7096. "Earth-Moving Machinery - Operator Seat - Transmitted Vibration", First edition, (1982), 14pp.

[33] Griffin, M.J. "Biodynamic Response to Whole-Body Vibration" *Shock and Vibration Digest*, Vol.13, (1981), 3-12.

[34] Suggs, C.W., Stikeleather, L.F., et al. "Application of a Dynamic Simulator in Seat Testing" *Trans. of ASAE*, Vol.13, (1970), 378-381.

[35] ISO Technical Report 5007. "Agricultural Wheeled Tractors - Operator Seat - Measurement of Transmitted Vibration", ISO/TR 5007-1980(E), (1980), 29pp.

[36] Boileau, P.-E. et al. "Vibration Exposure of Skidder Operators in the Quebec Forestry Sector", Proceedings of 12th International Congress in Acoustics, Toronto, Canada, (1986), F2-8.

[37] Young, R.E. and Suggs, C.W. "Seat Suspension System for Isolation of Roll and Pitch in Off-Road Vehicles" *Trans. of ASAE*, Vol.16, (1973), 873.

[38] Thomson, W.T. "Theory of Vibration with Applications", 4th edition, Prentice-Hall Inc., New Jersey, (1993), 546pp.

[39] Stikeleather, L.F. "Operator Seats for Agricultural Equipment", ASAE Distinguished Lecture Series, No. 7, (1981).

[40] Boileau, P.-E. and Rakheja, S. "Vibration Attenuation Performance of Suspension Seats for Off-Road Forestry Vehicles", *International Journal of Industrial Ergonomics*, Vol.5, (1990), 275-291.

[41] Coermann, R.R., and Whittwer, A.L. "The Passive Dynamic Mechanical Properties of the Human Abdomen Thorax System and of the Whole-Body System", *Aerospace Medicine*, Vol.31, (1960), 443.

[42] Rakheja, S. "Computer-Aided Dynamic Analysis and Optimal Design of Suspension Systems for Off-Road Tractors", Ph.D. Thesis, Concordia University, Montréal, Canada, (1983), 354pp.

[43] Rakheja, S., Ahmed, A.K.W., et al. "Ride Performance Characteristics of Seat-Suspension Systems and Influence of the Seated Driver", ASAE Paper No. 917569, Chicago, Illinois, (1991), 26pp.

[44] Ahmed, A.K.W., and Rakheja, S. "An Equivalent Linearization Technique for the Frequency Response Analysis of Asymmetric Dampers", *Journal of Sound and Vibration*, Vol.153, (1992), 537-542.

[45] Rakheja, S., Sankar, S., and Afework, Y. "Vibration Transmission Performance of Vertical Seat Suspension Systems", Report submitted to IRSST, CONCAVE, (1989), 114pp.

[46] Roberts, J.B. "Response of Non-Linear Mechanical Systems to Random Excitations. Part 2: Equivalent Linearization and Other Methods", *Shock and Vibration Digest*, Vol.13, (1981), 15-29.

[47] Scanlan, R.H. "Linear Damping Models and Causality in Vibration", *Journal of Sound and Vibration*, Vol.13, (1970), 499-503.

[48] Meirovitch, L. "Elements of Vibration Analysis", Second edition, Mc Graw Hill, New York, (1986).

[49] Rakheja, S., Van Vliet, M., et al. "A Discrete Harmonic Linearization Technique for Simulating Non-Linear Mechanical Systems", *Journal of Sound and Vibration*, Vol.100, (1985), 511-526.

[50] Meister, A., Brauer, D., et al. "Evaluation of Responses to Broad-Band Whole-Body Vibration", *Ergonomics*, Vol.27, (1984), 959-980.

[51] Parsons, K.C., and Griffin, M.J. "Method for Predicting Passenger Vibration Discomfort,", Society of Automotive Engineers Technical Paper Series 831029, (1983).

[52] ISO Document 108/4 N 239. Report on "Shock Discomfort - A Comparison of Approaches", by P.R. Payne, J.W. Brinkley, and J. Sandover. ISO Secretariat, Berlin, Germany (1994), 50 pp.

[53] Palanichamy, M.S., Patil, M.K and Ghista, D.N. Minimization of the Vertical Vibrations Sustained by a Tractor Operator by Provision of a Standard-Type Tractor Seat Suspension", *Annals of Biomedical Engineering*, Vol.6, (1978), 138-153.

[54] Patil, M.K., Palanichamy, M.S., and Ghista, D.N. Man-Tractor System Dynamics: Towards a Better Suspension System for Human Ride Comfort", *J. Biomechanics*, Vol.11, (1978), 397-406.

[55] Hrovat, D., and Hubbard, M. "Optimum Vehicle Suspensions Minimizing RMS Rattlespace, Sprung-Mass Acceleration and Jerk", *Transactions of the ASME*, Vol.103, (1981), 228-236.

[56] Hrovat, D., and Hubbard, M. "A Comparison between Jerk Optimal and Acceleration Optimal Vibration Isolation", *J. Sound and Vibration*, Vol.112, (1987), 201-210.

[57] Allen, G.R. "Human Tolerance of Repeated Shocks", Proc. European Symp. Life Sciences Research in Space, Cologne, Germany. 24-26 May 1977. 343-349.

[58] Bluthner, R., Hinz, B., et al. "Back Muscle Response to Transient Whole-Body Vibration". *International Journal of Industrial Ergonomics*, Vol.12, 1993, 49-59.

[59] Sandover, J. "Dynamic Loading as a Possible Source of Low-Back Disorders". *Spine*, Vol.8, 1983, 652-658.

[60] Collins, J.J., Whittle, M.W. "Impulsive Forces During Walking and their Clinical Implications", *Clin. Biomech.*, Vol.4, 1989, 179-187.

[61] Wilder, D.G. "The Biomechanics of Vibration and Low Back Pain", *American Journal of Industrial Medicine*, Vol.23, 1993, 577-588.

[62] Wikstrom, B.-O., Kjellberg, A., Orelius, M. "Whole-Body Vibration: A Test of Different Methods for the Asessment of Shocks". UK Informal Group Meeting on Human Response to Vibration, Royal Military College of Science, Shrivenham, 21-22 September 1987, 11p.

[63] Kjellberg, A., Wikstrom, B.-O. "Subjective Reactions to Whole-Body Vibration of Short Duration". *J. Sound and Vibration*, Vol.99, 1985, 415-424.

[64] Griffin, M.J., Whitham, E.M. "Discomfort Produced by Impulsive Whole-Body Vibration". *J. Acoust Soc. Am.*, Vol.68, 1980, 1277-1284.

[65] Monsees, N., Whyte, R.T., et al. "Relationship Between Subjective Assessment and Objective Measurements of Tractor Ride Vibration (RMS and RMQ)". UK and French joint Meeting on Human Response to Vibration, 26-28 September 1988, INRS, Vandoeuvre, France.

[66] Donati, P., Mistrot, P., et al. "Vibration Discomfort Experienced by a Driver when a Lorry Runs over Obstacles (Preliminary Experiment)". UK-French Joint Meeting on Human Response to Vibration, 26-28 September 1988, INRS, Vandoeuvre, France.

[67] Broyde, F., Donati, P., Galmiche, J.P. "Assessing the Discomfort of Whole-Body Vibration Containing Transients: rms or rmq Method?" UK Informal Group Meeting on Human Response to Vibration, A.F.R.C. Institute of Engineering Research, Silsoe, 21-22 September 1989.

[68] Coermann, R.R. "The Mechanical Impedance of the Human Body in Sitting and Standing Position at Low Frequencies", *Human Factors*, (1962), pp.227-253.

[69] Suggs, C.W., Abrams, C.F. and Stikeleather, L.F. "Application of a Damped Spring-Mass Human Vibration Simulator in Vibration Testing of Vehicle Seats", *Ergonomics*, Vol. 12, (1969), pp.79-90.

[70] Fairley, T.E. and Griffin, M.J. "A Test Method for the Prediction of Seat Transmissibility", Society of Automotive Engineers International Congress and Exposition, Detroit, 24-28 February (1986), SAE Paper 860047

[71] Payne, P.R. "Method to Quantify Ride Comfort and Allowable Accelerations" *Aviation, Space, and Environmental Medicine*, (1978), pp.262-269.

[72] Griffin, M.J., Lewis, C.H., Parsons, K.C. and Whitham, E.M. "The Biodynamic Response of the Human Body and its Application to Standards", AGARD Conference Proceedings No. 253 "Models and Analogues for the Evaluation of Human Biodynamic Response, Performance and Protection" Paris, France, 6-10 November 1978, Paper A28, pp. 1-18.

[73] Fairley, T.E. and Griffin, M.J. "The Apparent Mass of the Seated Human Body: Vertical Vibration", *J. Biomechanics*, Vol.22, No. 2, (1989), pp.81-94.

[74] Wambold, J.C. and Park, W.H. "A Human Model for Measuring Objective Ride Quality" ASME Paper 75-DET-6, Design Engineering Technical Conference, Washington, D.C., September 17-19, 1975, 8pp.

[75] Allen, G. "A Critical Look at Biodynamic Modelling in Relation to Specifications for Human Tolerance of Vibration and Shock" Paper A25, AGARD Conference Proceedings No.253 "Models and Analogues for the Evaluation of Human Biodynamic Response, Performance and Protection", Paris, France, 6-10 November 1978, pp.A25-5 - A25-15.

[76] Demic, M. "Investigation of Human Body Oscillatory Parameters under the Action of Shock Excitations", ISO document TC 108/SC 4/WG 2 N 158, (1987), 15pp.

[77] Payne, P.R. and Band, E.G.U. "A Four-Degree-Of-Freedom Lumped Parameter Model of the Seated Human Body" Aerospace Medical Research Laboratories Report AMRL-TR-70-35, Wright-Patterson Air Force Base, Ohio, (1971), 111pp.

[78] Mertens, H. "Nonlinear Behaviour of Sitting Humans Under Increasing Gravity", *Aviation, Space, and Environmental Medicine*, (1978), pp.287-298.

[79] Mertens, H. and Vogt, L. "The Response of a Realistic Computer Model for Sitting Humans to Different Types of Shocks" Paper A26, AGARD Conference Proceedings No.253 "Models and Analogues for the Evaluation of Human Biodynamic Response, Performance and Protection", Paris, France, 6-10 November 1978, pp.A26-1 - A26-16.

[80] Smith, S.D. "Comparison of the Driving -Point Impedance and Transmissibility Techniques in Describing Human Response to Whole-Body Vibration" Proc. U.K. Informal Group on Human Response to Vibration, APRE, Farnborough, September 20-22 (1993), 12pp.

[81] Amirouche, F.M.L. and Ider, S.K. "Simulation and Analysis of a Biodynamic Human Model Subjected to Low Accelerations - A Correlation Study", *Journal of Sound and Vibration*, Vol. 123, No. 2, (1988), pp.281-292.

[82] Panjabi, M.M., Andersson, G.B.J., Torneus, L.L., Huet,E. and Maltson, L. "In Vivo Measurements of Spinal Column Vibrations" *Journal of Bone Surgery*, Vol. 68A, (1986), pp.695-702.

[83] Patil, M.K. and Palanichamy, M.S. "A Mathematical Model of Tractor-Occupant System with a New Seat Suspension for Minimization of Vibration Response" *Applied Mathematical Modelling*, Vol.12, (1988), pp.63-71.

[84] Muskian, R. and Nash, C.D.A. "A Model for the Response of Seated Humans to Sinusoidal Displacements of the Seat" *Journal of Biomechanics*, Vol.7, (1974), pp.209-215.

[85] ISO Committee Draft CD 5982. "Mechanical Driving Point Impedance and Transmissibility of the Human Body", Document ISO/TC 108/SC 4 N226, (1993), 21p.

[86] Harris, C.M. and Crede, C.E. "Shock and Vibration Handbook", McGraw-Hill Book Inc., New York, (1976), pp.10-1 - 10-46.

[87] Vogt, H.L., Coermann, R.R. and Fust, H.D. "Mechanical Impedance of the Sitting Human Under Sustained Acceleration", *Aerospace Medicine*, Vol. 39, No. 7, (1968), pp.675-679.

[88] Miwa, T. "Mechanical Impedance of Human Body in Various Postures", *Industrial Health*, Vol. 13, (1975), pp.1-22.

[89] Fairley, T.E. and Griffin, M.J. "Modelling a Seat-Person System in the Vertical and Fore-and-Aft Axes", Institute of Mechanical Engineers Conference, C149/84, (1984), pp.83-89.

[90] Hinz, B. and Seidel, H. "The Nonlinearity of the Human Body's Dynamic Response during Sinusoidal Whole Body Vibration", *Industrial Health*, Vol. 25, (1987), pp.169-181.

[91] Sandover, J. "Measurements of the Frequency Response Charateristics of Man Exposed to Vibration", Ph.D. Thesis, Loughborough University of Technology, (1982).

[92] Fairley, T.E. and Griffin, M.J. "Application of Mechanical Impedance Methods to Seat Transmissibility", International Conference on Noise Control Engineering, Edinburgh, (1983), pp.533-536.

[93] Magnusson, M., Pope, M., Rostedt, M. and Hansson, T. "Effect of Backrest Inclination on the Transmission of Vertical Vibrations through the Lumbar Spine", *Clinical Biomechanics*, Vol. 8, (1993), pp.5-12.

[94] Paddan, G.S. and Griffin, M.J. "The Transmission of Translational Seat Vibration to the Head - I. Vertical Seat Vibration" *J. Biomechanics,* Vol. 21, No. 3, (1988), pp.191-197.

[95] Fairley, T.E. "Predicting Seat Transmissibilities: The Effect of the Legs", U.K and French Joint Meeting on Human Response to Vibration, INRS, Vandoeuvre, France, (1988), 11pp.

[96] Pheasant, S. "Bodyspace - Anthropometry, Ergonomics and Design", Taylor & Francis, London and Philadelphia, (1986), 275 pp.

[97] IMSL 1988: IMSL is a trade mark of IMSL Inc., Texas, USA.

[98] Kazarian, L. "Dynamic Response Characteristics of the Human Vertebral Column", Stockholm: Trycheri Balder, (1972).

[99] Lines, J.A., Whyte, R.T., and Stayner, R.H. "Suspensions for Tractor Cabs", Proceedings Third International Symposium of AISS, Vienna, 19-21 April (1989).

APPENDIX A

Participant Consent Form

Experiments involving the Participation of Human Subjects

PARTICIPANT CONSENT FORM

CONCAVE RESEARCH CENTRE
DEPARTMENT OF MECHANICAL ENGINEERING
CONCORDIA UNIVERSITY

Name of the Participant:
Address:
Telephone Number:

PROJECT: Study of Driver's Response to Whole-Body Off-Road Vehicular Vibrations

PURPOSE OF THE EXPERIMENT:

The overall objective of the experiment is to contribute to reduction of health and safety risks posed by prolonged exposure to off-road vehicle vibrations. The specific objectives of this experiment are: (i) to establish an understanding of the biodynamic behaviour of seated drivers under vehicular vibration; (ii) to determine the magnitude and location of high dynamic forces on the driver's back and thighs; (iii) design seat cushion, back-rest and suspension to provide favorable posture, reduced concentration of dynamic forces, and reduced transmitted vibration.

BRIEF OUTLINE OF TEST PROCEDURE:

Participants are required to sit on a seat (rigid and/or suspended), mounted on a motion platform, in a typical driving posture with hands on the steering wheel. The seat is instrumented with miniature accelerometer and thin-film pressure sensors to measure the bio-dynamic response of the subject' under vibration. The motion platform is activated to generate vibration spectra of different classes of vehicles, as recommended by *International Standards Organization* and *Society of Automotive Engineers*. The participant is required to maintain the assumed posture during the vibration excitation, which lasts approximately 2 minutes and 30 seconds. One test will be performed for laboratory type sinusoidal excitations in the 0.625 - 10 Hz frequency range, which lasts approximately six minutes. In the event a discomfort is experienced, the participant may stop the experiment using the hand-held switch (tied to the steering wheel).

Please read the enclosed descriptiont of the proposed experiments.

CERTIFICATION

I fully understand the study in which I am participating and the tests which will be performed. I understand that I am participating in this study on my own free will and I am free to withdraw my consent and to discontinue my participation at any time without negative consequences. I have had adequate opportunities to ask questions and understand the program, I may, however, ask additional questions during the study.

This is to certify that I agree to participate in this study under the directions of investigators, Dr. Subhash Rakheja and M. Paul-Émile Boileau.

Date

Signature of the Participant

DESCRIPTION OF PROPOSED EXPERIMENTS

Research Project: Dynamic Human-Seat Interface Pressure Measurement System

The primary objective of the proposed study is to investigate effective means of controlling the whole-body vibration transmitted to the drivers of off-road vehicles through design of suspension seats with optimal postural control properties. The study involves determination of human response to vibration environment of a class of off-road vehicles. The study will be carried out in the laboratory under controlled conditions, using a motion simulator.

The Motion Simulator:
In order to carry out the proposed experiments in a controlled and safe manner, the researchers have designed and installed a unique vehicle vibration simulator. The simulator supported on two servo-controlled hydraulic actuators, installed in the CONCAVE laboratory, is equipped with following unique safety control loops:

a. FORCE-CONTROL LOOP: To limit the maximum compression and extension force to the simulator. The force limits ensure maximum true acceleration of the simulator less than or equal to 2 m/s^2 rms (root mean square), during an experiment. An acceleration level exceeding the preset limit will cause the shut down of the motion simulator.

b. POSITION-CONTROL LOOP: To limit the maximum displacement of the simulator. Two externally adjustable position control switches are installed to limit the maximum displacement during a test. During the experiments, the two limit switches are adjusted to yield ± 5.0 cm. A displacement input exceeding the set limits will shut the motion simulator.

c. SUBJECT AND OPERATOR CONTROL SWITCHES:
The subject and operators both are provided with a hand-held safety switch, which when activated will cause the shut-down of the motion base.

A rigid seat and a steering column is installed on the motion simulator. The seat is instrumented using a miniature accelerometer (5 mm diameter and 5 mm high) embedded in 20 cm diameter rubber pad. The rubber pad, as recommended by the *International Standards Organization* (ISO) forms the seating surface when placed on the seat surface. A flexible pressure sensing mat (0.3 mm thick) will be place on the seat and back-rest surface to measure the postural support and distribution of dynamic forces at the human-seat interface.

The performance characteristics of suspension seats will be measured by replacing the rigid seat by commercially available suspension-seats, commonly used in the industry. The mechanical and air-suspension seats supplied by ISRINGHAUSEN will be used.

...../2

DESCRIPTION OF PROPOSED EXPERIMENTS (Continued)

Test Methodology:

Each subject will be asked to sit on the seat (rigid and/or suspended), mounted on the motion simulator, in a typical driving posture with hands on the steering wheel. The motion simulator will be driven to generate low frequency vibration, similar to those experienced in a off-road vehicle. Each subject will be asked to maintain the posture during an experiment. A total of seven tests will be carried out, where each test will be associated with different vibration levels. The vibration levels corresponding to each test will be generated using the following:

a. Vibration spectra, recommended by ISO-5008 for class-I vehicles
b. Vibration spectra, recommended by ISO-5008 for class-II vehicles
c. Vibration spectra, recommended by SAE (Society of Automotive Engineers) for class-1 vehicles
d. Vibration spectra, recommended by SAE for class-2 vehicles
e Vibration spectra, measured on the floor of a skidder vehicle.
f Sinusoidal vibrations of 2 m/s^2 rms amplitude in the 0.625-10 Hz frequency range.
g Random vibrations of 2 m/s^2 rms amplitude in the 0.625-10 Hz frequency range.

The duration of tests *a*, *b*, *c*, *d*, *e* and *g* is approximately 150 seconds, and the test *f* lasts approximately 6 minutes. The pressure and acceleration data will be acquired during each test for later analyses.